A coral perspective on last interglacial tropical Atlantic temperature and hydroclimate variability

Dissertation for the Doctoral Degree in Natural Sciences

Dr. rer. nat.

Within the Faculty of Geosciences
at the University of Bremen

Submitted by

William M. Brocas
August, 2017

Universität Bremen

marum

GLOMAR
Bremen International Graduate School for Marine Sciences

Name / *Name*: William M. Brocas Date / *Date*:

Anschrift / *Address:* MARUM Raum 1340 Leobenerstr., D-28359 Bremen

Erklärung / *Affirmation*

Ich versichere, dass / *I affirm that*

1. die Dissertation ohne unerlaubte fremde Hilfe angefertigt wurde /
   I wrote the present thesis independently and without illicit assistance from third parties,

2. keine anderen als die von mir angegebenen Quellen und Hilfsmittel benutzt wurden und /
   I used no sources other than those indicated nor aids other than those permissible,

3. die den benutzten Werken wörtlich oder inhaltlich entnommenen Stellen als solche kenntlich gemacht wurden. /
   I appropriately referenced any text or content from other sources

_____, den / *on this day* _____

_____
(Unterschrift / *Signature*)

Tag des öffentlichen Kolloquiums

07.06.2017
Room 1550, FB5, 15.15.

Gutachter der Dissertation

Prof. Dr. Dr. dc Gerold Wefer

Prof. Dr. Gerrit Lohmann

Weitere Mitglieder des Prüfungsausschusses

Prof. Wolfgang Bach

Dr. Thomas Felis

Dr. Hendrick Lantzch

Maria Reimer

Table of contents

Table of Abbreviations and units

Abbreviation	Term
AD	Anno Domini
AMOC	Atlantic Meridional Overturning Circulation
AMO	Atlantic Multi-decadal Oscillation
AWP	Atlantic Warm Pool
Ca	Calcium
CH4	Methane
CO2	Carbon dioxide
CC	Caribbean Current
c.e.	Combined error
CLLJ	Caribbean Low Level Jet
COSMOS	An atmosphere-ocean circulation model
CSW	Caribbean Surface Water
$\delta^{18}O$	Stable isotopic oxygen composition
$\delta^{18}O_{seawater}$	Stable isotopic oxygen composition of $_{seawater}$
DJF	December-January-February
DFG	Deutsche Forschungsgemeinschaft
ENSO	El Niño-Southern Oscillation climate phenomena
ERSSTv3b	Extended Reconstructed Sea Surface Temperature
FC	Florida current
Fig.	Figure
Fossil	Describes the skeletal remains of all dead corals regardless of time
GIS	Greenland ice sheet
GISS	Goddard Institute for Space Studies
GC	Guyana Current
GOM	Gulf of Mexico
GS	Gulf Stream
HADISST	Hadley Centre Global Sea Ice and Sea Surface Temperature
ICOADS	International Comprehensive Ocean-Atmosphere Data Set
IPO	Interdecadal Pacific Oscillation climate phenomena
ITCZ	Intertropical Convergence Zone
INTERDYNAMIC	Special priority program of the DFG
JJA	June, July, August
Ka	Thousand years ago before present
LC	Loop current
LIG	Last interglacial
MAM	March, April, May
Mg	Magnesium

MIS	Marine Isotope Stage
MPI	Max Planck
NAO	North Atlantic Oscillation climate phenomena characterised by a positive (+) and negative phase (-)
NASA GISS	National Aeronautics and Space Administration Goddard Institute for Space Studies
NBC	North Brazil Current
NBCR	North Brazil Current Retroflection
NCAR	National Center for Atmospheric Research
NEC	North Equatorial Current
NOAA	National Oceanic and Atmospheric Administration
P.I.	Pre-industrial (before ^{18}50 AD)
P-E	Precipitation minus evaporation
U	Uranium
RSL	Relative Sea Level
SAMS	South American Monsoon System
s.d.	Standard deviation
s.e.	Standard error
SLP	Sea level pressure
SODA	Simple Ocean Data Assimilation
SUW	Subtropical Under Water
Sr	Strontium
Sr/Ca	Ratio of Strontium to Calcium
SSS	Sea surface salinity
SST	Sea surface temperature
Th	Thorium
TII	Termination II penultimate deglaciation event
VPDB	Vienna-Pee Bee Belemnite
VSMOW	Vienna Standard Ocean mean water
WOA	World Ocean Atlas
XRD	X-Ray diffraction analysis of powder samples
yr	Year(s)

Units	**Measurement**
°C	degree Celsius
‰	per mill
µm	micrometre
cm	centimetre
km	Kilometre

m	metre
mb	millibar
mm	millimetre
mmol	millimoll
moll	moll
m/s	metres per second
ng	nanogram
ppb	part per billion
ppm	part per million
psu	practical salinity unit
Sv	one Sverdrup = 10^6 m^3 s^{-1}
W/m^2	watts per square metre

List of figures

Manuscript II

Manuscript III

Manuscript III- Supporting information

List of plates

Introduction

List of tables

Introduction

Manuscript I

Abstract

The warming envisaged by future climate change scenarios contains a natural climate variability component that must be disentangled from the contribution of anthropogenic sources. Instrumental records of the natural variability inherent to climate systems also documents a period of sustained anthropogenic influence and are often too spatially limited and temporally short to capture variability that occurs on annual to millennial time-scales. Prior to instrumental records, centennial to millennial resolved sedimentary and ice archives are typically used to reconstruct natural climate variability. However, high resolution records are required in order to document societally relevant climate events, such as hurricanes, droughts and other climate phenomena that occur on sub-seasonal to multi-decadal time-scales. Such records can be obtained from large, long lived, *Diploria Strigosa* corals that deposit annually banded aragonitic skeletons that incorporate geochemical and isotopic records of the shallow seawater they inhabit. Well- preserved *D. Strigosa* colonies that grew during the last interglacial (LIG, MIS 5e, ~127-117 ka) can be found upon the uplifted fossil reef terraces of the southern Caribbean island of Bonaire (Caribbean Netherlands).

The LIG experienced warmer than modern globally temperatures that are within the range of future climate projections. This resulted from an orbital configuration that differed from modern, while greenhouse gas concentrations were stable at pre-industrial levels. Despite not being fully analogous for future climate change scenarios, the LIG offers the opportunity to quantify the effect of natural and well- constrained influences on climate. Consequently, palaeoclimate records obtained from LIG *D. Strigosa* document sub-seasonal to multi-decadal climate variability in the absence of anthropogenic influences.

This thesis discusses the background, techniques and approaches used to successfully obtain and interpret palaeoclimate records from delicate LIG *D. Strigosa* material. Results are presented in three manuscripts that explore distinct aspects of monthly resolved coral Sr/Ca and $\delta^{18}O$ records and provide insights into LIG tropical Atlantic climate variability. Coral Sr/Ca is a proxy for sea surface temperatures (SST), whereas coral $\delta^{18}O$ is a combined proxy for SST and $\delta^{18}O$ of seawater ($\delta^{18}O_{seawater}$). A total of 85 years of paired coral Sr/Ca and $\delta^{18}O$ records from seven *D. Strigosa* colonies are presented. These coral colonies are precisely $^{230}Th/U$ dated to between 120.5 and 129.7 ka with one coral colony representing the late and early LIG each, and five the mid-LIG. These form the first sub-seasonal to decadal assessment of tropical Atlantic climate variability throughout the LIG and are compared to available modern, mid- to late Holocene and early LIG *D. Strigosa* coral records.

The first manuscript describes Bonaire's LIG *D. Strigosa*, their preservation and the variability of the Sr/Ca-SST records contained within. Mid-LIG Sr/Ca-SST seasonality of 4.1 and 4.9 °C was reconstructed at 124 and 126 ka, respectively. This is significantly higher than reconstructed Sr/Ca-SST seasonality of ~2.9 °C during modern times, early and late LIG. Climate model simulations reveal coral Sr/Ca-SST seasonality to be representative of tropical Atlantic throughout the LIG. These findings reflect a relationship with orbital controls as both mid-LIG SST and insolation seasonality are higher than modern. The longest reconstructed Sr/Ca-SST record of 37 years at 124 ka reveals variability on quasi-biennial and decadal time-scales. Decadal SST variability is reconstructed for the first time during the LIG and, as with

modern instrumental records, demonstrates the close link between Atlantic climate phenomena and Bonaire coral palaeoclimate records.

The second manuscript focuses on coral $\delta^{18}O$ records that were paired with the Sr/Ca records of the first manuscript and allow the SST component of coral $\delta^{18}O$ to be removed and coral $\delta^{18}O_{seawater}$ isolated. Coral $\delta^{18}O_{seawater}$ variations are indicative of Bonaire hydroclimate which at present is distinct within the Caribbean Sea. For instance, sea surface salinity seasonality is comparatively small and influenced primarily by ocean advection, with the main rainy season occurring in winter. While coral $\delta^{18}O_{seawater}$ seasonality was indistinguishable from modern during the early and late LIG, during the mid-LIG, at 124 ka, it was higher. This record also reveals that the coral $\delta^{18}O$ record leads coral Sr/Ca by two months, demonstrating further that the mid-LIG hydroclimate of Bonaire differed from modern fully coupled climate modelling reveals increased mid-LIG Caribbean precipitation that depleted $\delta^{18}O_{seawater}$ during boreal summer. Together with the coral palaeoclimate records, these results provide the first direct marine evidence that the Intertropical Convergence Zone (ITCZ) migrated beyond the northern coastline of South America and into the southern Caribbean Sea during the LIG.

With monthly resolved coral Sr/Ca, $\delta^{18}O$ and $\delta^{18}O_{seawater}$ records established within the previous manuscripts, the third manuscript compiles these records to assess LIG mean annual tropical Atlantic SST and hydroclimate changes. Tropical Atlantic surface waters are characterised as ~2 °C colder and less saline than modern at 126 ka. Although seasonality of insolation was higher, local annual insolation was similar to modern, highlighting that orbital controls were not directly responsible. Therefore, enhanced advection of Atlantic waters into the Caribbean Sea is implicated in response to stimulated Atlantic meridional ocean circulation at that time. In spite of proxy specific uncertainties, this coral-based interpretation agrees with the few LIG sedimentary records within the mid-tropical Atlantic that document colder than modern SST. Coral Sr/Ca and $\delta^{18}O_{seawater}$ then transition rapidly to modern-like SST and salinities at 124 ka. This coincides with the arrival of the northward migrating summer ITCZ, which influenced a hydroclimate shift at Bonaire but is shown to have not altered mean annual $\delta^{18}O_{seawater}$. As the summer ITCZ retreated southward to its modern day position, the modern-like tropical Atlantic sea surface conditions were maintained into the late LIG.

Zusammenfassung

Die globale Erwärmung, die für zukünftige Klimaszenarien vorhergesagt wird, enthält eine natürliche und eine anthropogene Komponente und verfügbare instrumentelle Aufzeichnungen sind ebenfalls anthropogen beeinflusst. Um den Einfluss der natürlichen Variabilität zu erfassen, müssen also die natürlichen und anthropogenen Komponenten separiert werden. Als weitere Schwierigkeit kommt hinzu, dass verfügbare Aufzeichnungen der natürlichen Variabilität räumlich und zeitlich oft zu begrenzt sind, um Schwankungen zu erfassen, die auf jährlichen bis tausendjährigen Zeitskalen auftreten. Wenn instrumentelle Aufzeichnungen nicht verfügbar sind, werden so in der Regel hundertjährig bis tausendjährig aufgelöste Sediment- und Eis-Archive verwendet, die nicht in der Lage sind, kurzfristige, gesellschaftlich relevante Klimaereignisse (wie Hurrikane oder Dürrephasen) sowie andere Klimaphänomene zu dokumentieren, die auf sub-saisonalen bis multi-dekadischen Zeitskalen auftreten. Als Lösung dieser Problematik bieten sich großwüchsige, langlebige *Diploria strigosa* Korallen an, die im Jahresrhythmus gebänderte aragonitische Skelette ausbilden und auf diese Weise die geochemischen und isotopischen Signale des umgebenden Meerwassers aufzeichnen. Gut erhaltene *D. Strigosa* Kolonien des letzten Interglazials (LIG, MIS 5e, ~127-117 ka) sind auf der südlichen Karibikinsel Bonaire (Karibische Niederlande) zu finden, wo fossilen Riffterrassen subaerisch exponiert wurden.

Die globalen Durchschnittstemperaturen während des LIG waren wärmer als in der heutigen Situation und bewegen sich im Rahmen der Vorhersagen der zukünftigen Klimaentwicklung. Diese warmen Temperaturen waren das Ergebnis einer Orbitalkonfiguration, die sich deutlich von der modernen Situation unterschied, wobei die Treibhausgaskonzentrationen sich auf einem stabilen vorindustriellen Niveau bewegten. Trotz der Tatsache, dass zukünftige Klimawandelszenarien nicht völlig analog zur Situation im LIG sind, ergibt sich hier die Möglichkeit, die natürlichen Einflüsse auf das Klima zu quantifizieren. Hier bieten die auf *D. Strigosa* basierenden paläoklimatischen Datensätze des LIG die Chance, sub-saisonale bis multi-dekadische Klimaschwankungen in Abwesenheit anthropogener Einflüsse zu rekonstruieren.

Die vorliegende Arbeit diskutiert den Hintergrund, die Techniken und das Vorgehen, um Paläoklimadatensätze aus zerbrechlichem *D. Strigosa* Material des LIGs zu gewinnen und zu interpretieren. Die Ergebnisse werden in drei Manuskripten vorgestellt, die die verschiedenen Aspekte der monatlich aufgelösten Sr/Ca- und $\delta^{18}O$-Korallendatensätze diskutieren und Einblicke in die tropisch-atlantische Klimavariabilität des LIGs erlauben. Sr/Ca-Messungen an Korallen sind dabei ein Proxy für Meeresoberflächentemperaturen (SST), wohingegen $\delta^{18}O$-Messungen ein kombinierter Proxy aus SST und $\delta^{18}O$-Werten des Meerwassers ($\delta^{18}O_{seawater}$) sind. Die Sr/Ca- und $\delta^{18}O$-Korallendatensätze umfassen insgesamt 85 Jahre und stammen aus sieben *D. Strigosa*-Kolonien. $^{230}Th/U$ Messungen an diesen Korallenkolonien ergeben Alter zwischen 120.5 und 129.7 ka. Jeweils eine Korallenkolonie stammt aus dem späten und frühen LIG, fünf weitere aus dem mittleren LIG. Diese Ergebnisse erlauben erstmalig eine sub-saisonale bis multi-dekadische Beurteilung der tropisch-atlantischen Klimavariabilität während des gesamten LIGs und werden in der Arbeit mit bestehenden *D. Strigosa* Korallendatensätzen des frühen LIGs und des mittleren bis späten Holozäns verglichen.

Das erste Manuskript stellt die *D. Strigosa* Korallen von Bonaire vor, erörtert deren Erhaltungszustand und zeigt die Sr/Ca und SST-Daten des LIGs, die an diesen Korallen gemessen wurden. Im mittleren LIG (124 bzw. 126 ka) wurden Sr/Ca-SST Saisonalitäten von 4.1 und 4.9 °C rekonstruiert. Dies ist deutlich höher als die moderne Sr/Ca-SST Saisonalität von ~2,9 °C, ein Wert, der auch für das frühe und späte LIG rekonstruiert wurde. Klimamodell-Simulationen zeigen, dass die rekonstruierte Korallen-Sr/Ca-SST-Saisonalität während des gesamten LIGs repräsentativ für den tropischen Atlantik war. Diese Erkenntnisse zeigen eine orbitale Kopplung, da sowohl die SSTs als auch die Insolationssaisonalität des mittleren LIGs höher waren als heute. Die längste rekonstruierte Sr/Ca-SST-Aufzeichnung von 37 Jahren bei 124 ka zeigt eine Variabilität auf quasi-zweijährigen und dekadischen Zeitskalen. Zum ersten Mal wird somit eine dekadische SST-Variabilität während des LIG rekonstruiert und zeigt - wie auch bei modernen Instrumentalaufzeichnungen - die enge Verbindung zwischen den atlantischen Klimaphänomenen und den Paläoklimarekonstruktionen an den Korallen von Bonaire.

Das zweite Manuskript konzentriert sich auf $\delta^{18}O$-Messungen an Korallen, die anschließend mit den Sr/Ca-Daten des ersten Manuskripts kombiniert werden. Auf diese Weise ist es möglich, den SST-Einfluss aus den $\delta^{18}O$-Daten zu entfernen und somit die $\delta^{18}O$-Werte des Meerwassers ($\delta^{18}O_{seawater}$) isoliert zu betrachten. Die $\delta^{18}O_{seawater}$ -Variationen erlauben Rückschlüsse auf das Bonaire-Hydroklima, welches sich zumindest in der heutigen Situation wesentlich von dem des Karibischen Meeres unterscheidet. So ist zum Beispiel die Saisonalität der Meeresoberflächensalinität vergleichsweise gering und vor allem durch die Ozeanadvektion kontrolliert. Die Hauptregenzeit findet im Winter statt. Während die heutige Korallen-$\delta^{18}O_{seawater}$-Saisonalität von der des frühen und späten LIG nicht zu unterscheiden ist, war sie im mittleren LIG (bei 124 ka) höher. Dieser Datensatz zeigt außerdem, dass die $\delta^{18}O$-Kurve der Sr/Ca-Kurve um zwei Monate vorausläuft, welches ebenfalls bestätigt, dass sich das Hydroklima von Bonaire im mittleren LIG von der modernen Situation unterscheidet. Voll gekoppelte Klimamodellierungen des mittleren LIGs zeigen erhöhte Niederschläge in der Karibik, die das $\delta^{18}O_{seawater}$-Signal während des borealen Sommers abgeschwächt haben. Zusammen mit den Korallen-Paläoklimarekonstruktionen liefern diese Ergebnisse die ersten direkten Beweise, dass die Intertropische Konvergenzzone (ITCZ) während des LIG über die nördliche Küste Südamerikas in das südliche Karibische Meer vordrang.

Das dritte Manuskript kombiniert die monatlich aufgelösten Sr/Ca-, $\delta^{18}O$- und $\delta^{18}O_{seawater}$-Korallendatensätze, die in den vorherigen Manuskripte behandelt wurden, um Änderungen der mittleren jährlichen tropisch-atlantischen SST und des Hydroklimas während des LIGs zu beleuchten. Die tropisch-atlantischen Oberflächengewässer um 126 ka waren ~2 °C kälter und weniger salin als heute. Obwohl die Saisonalität der Sonneneinstrahlung zu dieser Zeit höher war, verhielt sich die lokale jährliche Einstrahlung ähnlich zur heutigen Situation, was zeigt, dass die orbitalen Kontrollfaktoren in diesem Fall keinen direkten Einfluss hatten. Diese Konfiguration impliziert eine verstärkte Advektion der atlantischen Gewässer in das Karibische Meer als Reaktion auf die verstärkte atlantische meridionale Ozeanzirkulation. Trotz proxyspezifischer Ungewissheiten stimmt diese korallenbasierte Interpretation mit den wenigen vorhandenen LIG-Rekonstruktionen an Sedimenten im mittleren tropischen Atlantik überein, die im Vergleich zur modernen Situation kältere SSTs dokumentieren. Bei 124 ka

zeigen dann die an Korallen gemessenen Sr/Ca- und $\delta^{18}O_{seawater}$-Daten einen schnellen Übergang hin zu modernen SSTs und Salinitäten. Dies weist auf eine nordwärts verlagerte Sommerposition der ITCZ hin, die zu einer Veränderung des Hydroklimas bei Bonaire geführt hat. Allerdings resultierte diese Konfiguration in keiner Änderung der durchschnittlichen jährlichen $\delta^{18}O_{seawater}$-Werte. Als sich die Sommer ITCZ nach Süden zurückzog, in eine Lage vergleichbar zur heutigen Position, herrschten bis ins späte LIG vergleichsweise moderne tropische Atlantische Meeresoberflächenbedingungen vor.

Personal acknowledgements

The work conducted to achieve this thesis was possible through the funding awarded by The Deutsche Forschungsgemeinschaft as part of the INTERDYNAMIK - Special Priority Program.

First of all I would like to thank Gerold Wefer for fulfilling his role as Doctor Vater, providing the comfortable working environment at MARUM and facilitating my supervision during the early stages of my PhD. By hosting my thesis committee meetings invaluable early discussion were held that provided much clarity. These were also attended by Thomas Felis, Jürgen Pätzold, Henning Kuhnert and Gerrit Lohmann and I extend my thanks for their contribution.

This PhD project was the brainchild of Thomas Felis and I am grateful to him for providing me the opportunity to work on this engaging and multi-faceted project. Thomas's approachability, advice, expertise, patients, scrutiny and experience were invaluable to the success of this project and I am thankful for sharing these with me.

My development as a PhD candidate was also aided by my membership of GLOMAR who provided a supporting research community of fellow PhD candidates and Post Docs. Importantly GLOMAR offered me the opportunity to take part in numerous workshops, courses, seminars and funded my research stay. I greatly appreciate these experiences that were invaluable to my career development.

The research stay at Louisiana State University was a unique opportunity to be immersed in another academic culture, exchange expertise and tested a number of coral sampling related hypotheses. I thankful for the hospitality and camaraderie of Kristine DeLong, Gil Ouellette, Robin Cobb and Clay Tucker during that time.

Martin Kölling, Silvana Pepe and Monika Segl are thanked for sharing their expertise and efforts to ensuring that this project was provided promptly with accurate and rigorous coral Sr/Ca and $\delta^{18}O$ measurements. I am also grateful to the support offered by the administrative and technical staff of MARUM and FB5 who eased my integration into the working environment of Bremen.

Occasional specialist advice was needed to better understand bespoke software and techniques. Thankfully MARUM Post Doctorates Aline Govin, Henry Wu, Mathieu Martinez, David De Vleeschouwer, Anna Joy Drury and Gema Martínez Méndez eagerly offered me their time and knowledge. I also appreciate their sense checking and contribution to discussions.

Growing up my mother, Eleanor Jackson, and father, Klaus Stoll, instilled in me the virtues of critical thinking, evidence based decision making and provided the initial inspiration to pursue an academic career. For this support and more I cannot express enough thanks.

My friends who form my world in and around the University of Bremen cannot be appreciated enough. Among those who have shared the joy of life and their patience with me are; Tina, Claudia, Hendrik, Yann, Caroline, James, Anna, Ivan, Domenico, Danni, Nick, Maria, Vince, Catarina, Marius, Sebastian, Aditya, Yancheng, Lottie, West, Malin and Amanda.

And finally I wish to acknowledge my dearest Mariem who has shared with me all the recent trials and tribulations of academic life, set me an example and supported me with such diligence. Only in adversity, elation and the pursuit of what we hold dear do we truly come to know ourselves.

“This is rather as if you imagine a puddle waking up one morning and thinking, 'This is an interesting world I find myself in — an interesting hole I find myself in — fits me rather neatly, doesn't it? In fact it fits me staggeringly well, must have been made to have me in it!' This is such a powerful idea that as the sun rises in the sky and the air heats up and as, gradually, the puddle gets smaller and smaller, frantically hanging on to the notion that everything's going to be alright, because this world was meant to have him in it, was built to have him in it; so the moment he disappears catches him rather by surprise. I think this may be something we need to be on the watch out for.”

- Douglas Adams speaking on global warming

1. Introduction

The variability climate documented by instrumental records is of continual relevance to societies, especially as awareness of the impacts of tropical cyclones, flooding, heat waves droughts and other extremes increases. However, these records are typically too short, spatial limited and concurrent with increased anthropogenic influences upon climate to fully quantify the range of variability exhibited on sub-seasonal to millennia time-scales. Palaeoclimate records offer insights beyond the instrumental period and are required to capture natural climate variability such time-scales. This aids the disentangling of natural variability and anthropogenic forcings required to ascertain the influences upon current and future climate trends. Internationally represented organisations such as the Intergovernmental Panel on Climate Change are tasked with informing stake holders and policy makers as to the risks of climate change (IPCC, 2013). As part of this on-going assessment, a number of modelled global climate projections have been proposed that envisage likely future climate scenarios and their consequences under a variety of anthropogenic forcings (Fig. 1.1). Pertinent to this task, this thesis discusses the reconstruction high frequency climate variability during a period of well-defined natural influence on climate. The approach utilises sub-seasonal to multi-decadal proxy records for sea surface temperatures (SST) and hydroclimate recorded within annual banded skeleton of tropical corals and comparable regional climate simulations. These corals records characterise tropical Atlantic surface waters that contribute significantly to the physical mechanism and processes that influence the behaviour of major climate phenomenon.

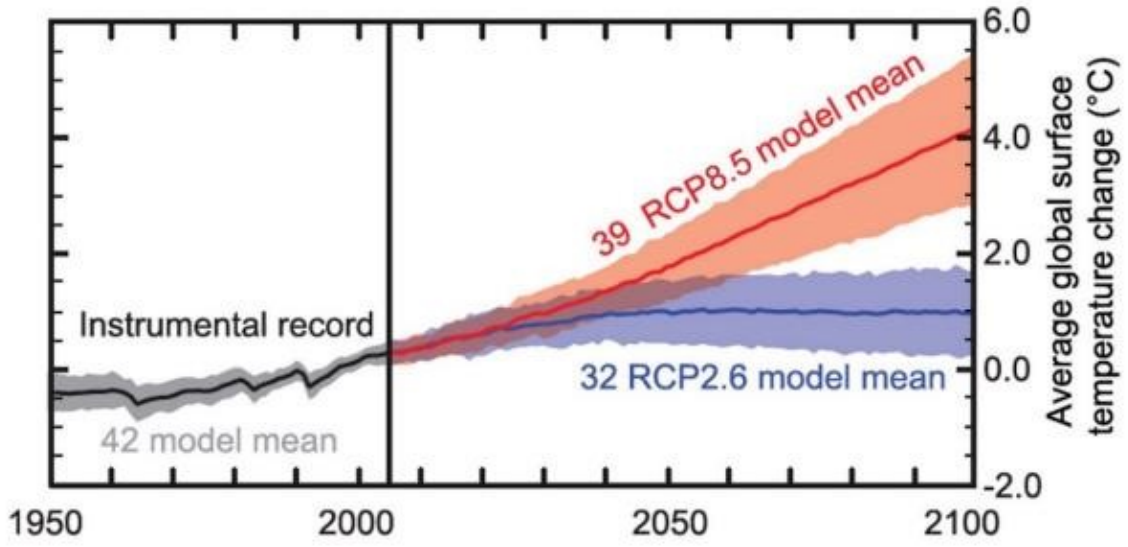

Figure 1.1: Mean projected future global surface temperature change using the multiple models based on the strictest (blue, RCP2.6) and none (red, RCP8.5) regulated anthropogenic greenhouse gas emission scenarios. Image adapted from IPCC, 2013.

1.1 The last interglacial

During the Quaternary (the past ~1.8 million years) glacial-interglacial cycles have dominated millennia scale climatic change. These cycles result from the culmination of the variable influence precession, obliquity and eccentricity (Milankovitch cycles) have upon the insolation the earth receives while orbiting the sun. The last interglacial (LIG, Marine Isotope Stage (MIS) 5e, 117-127 ka) is the most recent of these cycles beyond the current interglacial to have experienced warmer than modern day global SST (Otto-Bliesner et al., 2013) (Fig. 1.2a). This resulted from an orbital configurations that differed from the present interglacial, for example, the occurrence of the perihelion coincided with boreal summer, as opposed to today's boreal winter (Yin and Berger, 2010) (All seasons mentioned hereafter refer to boreal). This orbital configuration induced stronger seasonal insolation, and thus temperature, amplitudes in both hemispheres. Regional sensitivities dictated the affect this would have upon mean annual SST, for instance, through the process of polar amplification, higher than P.I. SST were primarily experienced in the extra-tropics (>45°N and 45°S) (Montoya et al., 2000). However, future climate change scenarios foresee warming due to increased anthropogenically emitted greenhouse gases (IPCC, 2013). Indeed, the principles three greenhouse gases carbon dioxide (CO_2) (Lüthi et al., 2008), methane (CH_4) (Loulergue et al., 2008) and nitrous oxide (Spahni et al., 2005) were stable at or slightly below P.I. levels during the LIG. Consequently, the LIG is considered semi-analogous to future climate change scenarios and an important test-bed for climate sensitivity studies within a warmer than present day earth system with well-constrained natural forcings on climate (Lunt et al., 2013).

Recently compilations of ocean-climate models have simulated a range of global average SST during the LIG from 0.4 °C colder (McKay et al., 2011) to 0.5 °C warmer (Pedersen et al., 2016) than P.I. However, these simulation typically underestimate multiple proxy compilations that reconstruct warmer than P.I. global SST of 1.9 (Turney and Jones, 2010), 0.7 ± 0.6 (McKay et al., 2011), ~1.0 (Otto-Bliesner et al., 2013) and 0.5 ± 0.3 °C (Hoffman et al., 2017). This disparity can be attributed to the spatial coverage of proxy records and climate simulations that do not incorporate dynamic vegetation models, misrepresent the effect of SST upon oceanic circulation and lack sensitivity to the climate influences on the LIG (Pedersen et al., 2016). Climate model and proxy studies do agree that significant regional differences occurred. For example, Greenland temperatures peaked at between ~5 and ~8 °C (Dahl-Jensen, 2013) whereas as Antarctic temperatures were ~3 to ~5 °C (Jouzel et al., 2007) warmer than P.I. However, poor data coverage prevents a more robust interpretation of tropical LIG temperatures. For instance ocean-climate simulation have been unable to consistently

replicate colder than P.I. SST reconstructed by tropical Atlantic SST proxy records. Similarly, within the eastern Pacific, sedimentary proxy SST records offers contradictory evidence (Otto-Bliesner et al., 2013), whereas there is agreement that cooling occurred within the African/Indian monsoonal region (Lunt et al., 2012; Hoffman et al., 2017; Pedersen et al., 2016). Such temperature changes are within the range of those projected by future climate change simulations and have implications for the sensitivity of continental ice volume and sea level change.

Global sea levels rose rapidly from ~135 ka during the termination II (TII) deglacial event that began the LIG with evidence suggesting this was interrupted by a pause/still-stand at ~130 ka, possible reflecting Heinrich Stadial 11 (Jiménez-Amat and Zahn, 2015). Global mean sea levels are widely cited to have peaked at between ~6 to ~9 m above present (Dutton et al., 2015) in accordance with a popular reconstruction of 95% probability that sea levels were 6.6 m above present (Kopp et al., 2009). However, regional variations occurred as demonstrated by LIG fossil coral material from Australian reefs revealing that higher that modern relative sea levels of ~3 - 4 m were stable between 127 and 119 ka and rose rapidly to ~9 m at 118 ka, reflecting fluctuations of LIG ice sheets (Fig. 1.2b) (O'Leary et al., 2013). Thus, the characteristics of LIG sea level is a focus of study with some authors evidencing the occurrence of one highstand (Stirling et al., 1998; Muhs et al., 2002; Speed and Cheng, 2004) while others suggest two highstands marked by a period of regression (Choukri et al., 2007; Rohling et al., 2008; Blanchon et al., 2009; Carr et al., 2010; Zazo et al., 2010; O'Leary et al., 2013). Further refinement of the spatiotemporal evolution of LIG sea levels is hindered until uncertainties regarding the viscosity of the Earth's mantle (Grant et al., 2013) and the configuration of ice sheets just prior to TII are addressed (Dendy et al., 2017).

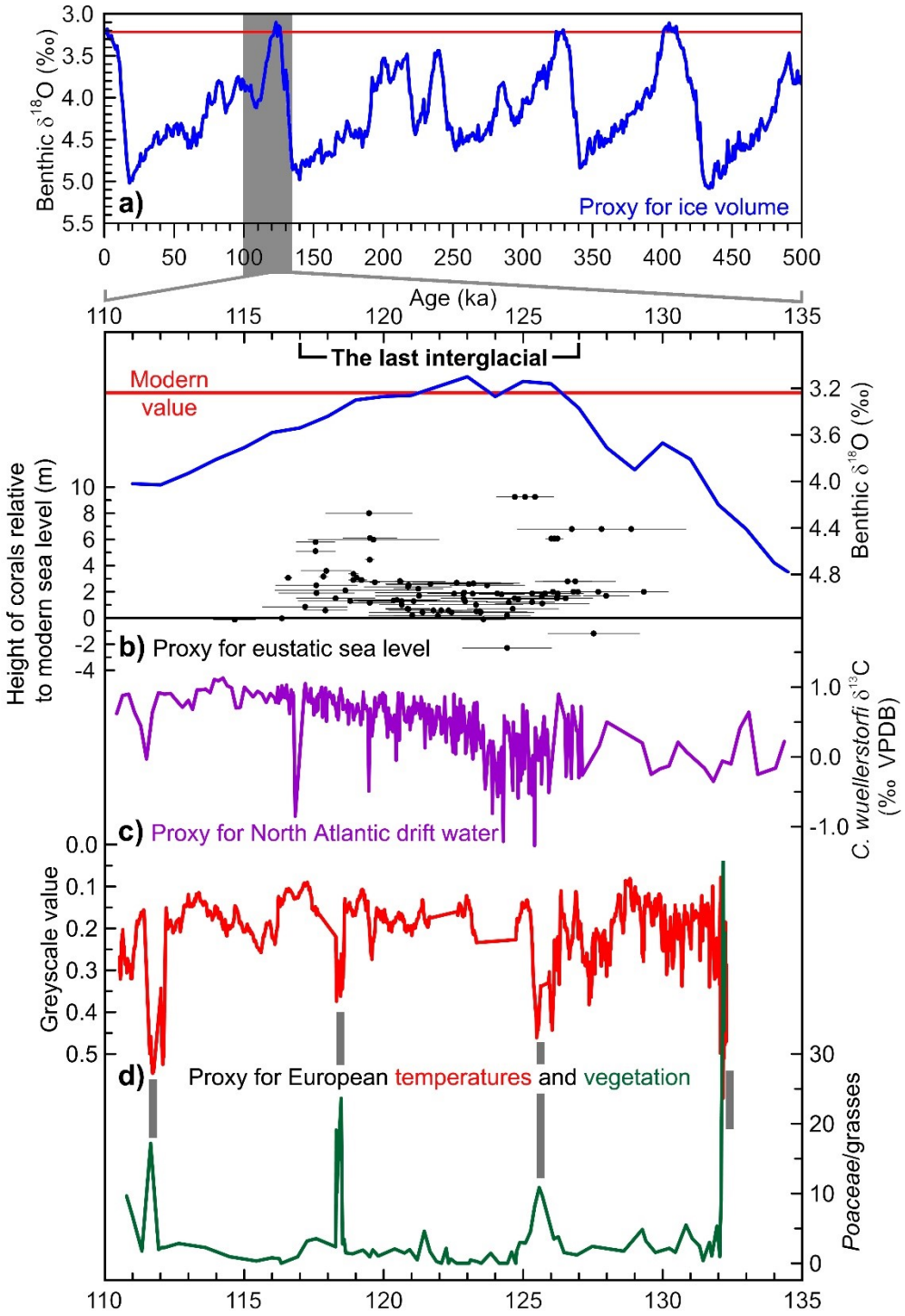

Figure 1.2: Climate instabilities during the last interglacial. a) Stack of 57 globally distributed benthic $\delta^{18}O$ records (Lisieki and Raymo, 2004) which are indicative of ice volume during the past 500 ka and throughout the last interglacial. The modern value is marked by a horizontal red line. b) Eustatic sea level as relative to modern of W. Australian fossil coral deposits (O'Leary et al., 2013). c) Dramatic reductions in North Atlantic deep water formation as indicated by more negative epibenthic foraminiferal $\delta^{13}C$ (Galaasen et al., 2014). d) Stack of grey scale values from the Eifel laminated sedimentary archive of maar lakes, Germany, indicated periods (denoted by grey bars) of cold and arid central European conditions that coincide with high abundances of grass pollen (Sirocko et al., 2005).

A primary characteristic of LIG temperature evolution is a bi-polar seesaw mechanisms, whereby higher than modern SST were reached within the southern ocean prior to the north Atlantic (Capron et al., 2014). As well as the globally desynchronised timing of LIG thermal optimum, Antarctic ice core records also reveal that multiple patterns of variability existed and multi-centennial climatic sub-events were found to occur more frequently and with greater amplitude than during the Holocene (Pol et al., 2014). Superimposed upon the climatic evolution of the LIG were notable changes and instabilities inherent to the global climate system (Kerr, 2014) (Fig. 1.2). These included monumental ice sheet loss (Blanchon et al., 2009), sea level rise (Fig. 1.2b) (O'Leary et al., 2013), rapid reorganization of oceanic currents (Fig. 1.2c) (Galaasen et al., 2014), cold events (Mokeddem et al., 2014) and abrupt European climatic shifts (Fig. 1.2d) (Sirocko et al., 2005). In the example of Galaasen et al. (2014) North Atlantic Deep Water formation was perturbed on centennial timescales, corresponded with maximum Greenland ice sheet (GIS) melting, and resulting in the reduction of Atlantic Meridional Overturning Circulation (AMOC) by up to 24% (Goñi et al., 2012).

Although the precise timing is still a topic of debate, the LIG is generally considered to have ended between 118.5 and 116 kyr (Cutler et al., 2003; Masson-Delmotte et al., 2011). While a chronological framework of major climatic events during the LIG has been proposed that considers inherent chronological uncertainties this focuses primarily on the extra-tropical northern and southern hemisphere (Govin et al., 2015a). How the tropical oceans responded and contributed to the feedback mechanisms that influenced global and regional LIG climate change, remains poorly defined.

1.2.1 State-of-the-art, tropical interglacial coral palaeoclimatology

Tropical corals have existed for millions of years and thrive in well-defined shallow warm water environments (Bradley, 2015). To survive within their preferred environments, healthy corals continually deposit an aragonitic skeleton of varying density that are the basis of large complex reef ecosystems. Over millennial timescales coral communities can from dominant geological structures such as reef terraces that typically represent a specific unit of time. The remnants of these reef systems and can be found elevated above present sea level due to a combination of tectonic uplift and the oscillations of glacial/interglacial sea levels. Dependant on the species, an individual coral colony deposits density growth bands that represent a consistent period of time (e.g. a year). During this skeletal deposition, a broad spectrum of geochemical and isotopic properties are incorporated into the corals aragonite skeleton and have been demonstrated to reflect cycles of key environmental parameters

(Knutson et al., 1972). Thus, fossil corals contain a geochemical and isotopic record of the environment in which they lived. These records can be extracted by micro-sampling techniques appropriate to the study species and employed parallel to the corals growth axis. With a potential life span on the order of hundreds of years and continually growth rates near to or greater than 1 cm/yr, corals can potentially, yield long sub-seasonally resolved records of tropical climate. However, after death, erosional forces and bioturbation may perturb a corals internal structure, this is especially pertinent to LIG dated coral material (Bradley, 2015). Therefore, techniques that assess in detail the aragonitic preservation of coral material such as X-radiography, X-ray fluorescence and scanning electron microscopy are complementary to the study of LIG tropical palaeoclimate records.

Intrinsic to the study of tropical coral palaeoclimatology is the availability of well-defined modern coral records for a similar region which can be used to contextualise findings. Within the tropical Atlantic robust multi-decadal, sub-seasonal reconstructions of SST and hydroclimate variability have been generated from the massive brain coral *Diploria strigosa* (*D. strigosa*). Monthly resolved, 41- year long (1958-1999 AD), coral Sr/Ca and $\delta^{18}O$ *D. strigosa* records were calibrated to local SST at Guadeloupe, Lesser Antilles (Hetzinger et al., 2006). These records later reconstructed hurricane activity (Hetzinger et al., 2008) and extended to 104 year record (1895-1999 AD) to capture modern multi-decadal climate variability (Hetzinger et al., 2010). Similar corals records from coastal Venezuela have also assessed the impact of modern coral stressors such as extreme El Niño-Southern Oscillation (ENSO) related warming events (Hetzinger et al., 2016). The dense skeletal wall elements of Bonaire (Caribbean Netherlands) *D. strigosa* have been established as a good source of palaeoclimate records. Coral Sr/Ca records from three modern *D. strigosa* colonies, representing a period from 1910-2000 AD, were used to accurately reconstruct modern SST seasonality at Bonaire (Giry et al., 2010). Fossil *D. strigosa* coral Sr/Ca and $\delta^{18}O$ records were subsequently generated, characterised the influences upon past tropical Atlantic temperatures and hydroclimate variability for multiple occasions throughout the mid- to late Holocene (Giry et al., 2012, 2013). This provides a contemporary framework for which tropical Atlantic palaeoclimatic records from prior to the present interglacial can be compared.

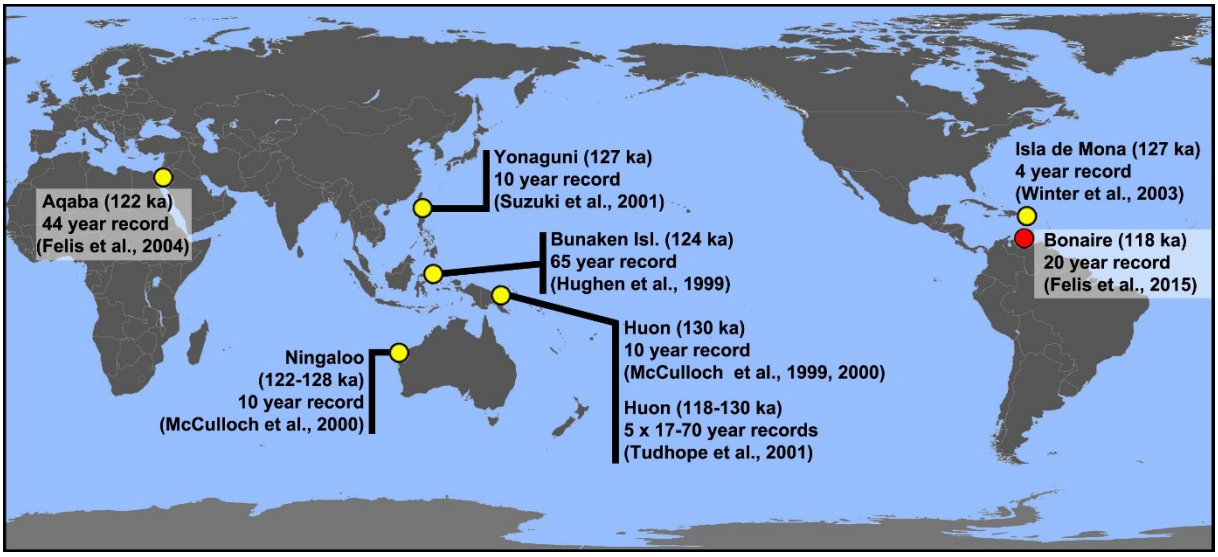

Figure 1.3: Global distribution of published last interglacial (LIG) coral data (yellow dots). The studies presented in this thesis expand upon a 20 year coral Sr/Ca and $\delta^{18}O$ record from a single coral colony at Bonaire dated to 117.7 ka (red dot) by reconstructing SST and hydroclimate variability throughout the LIG.

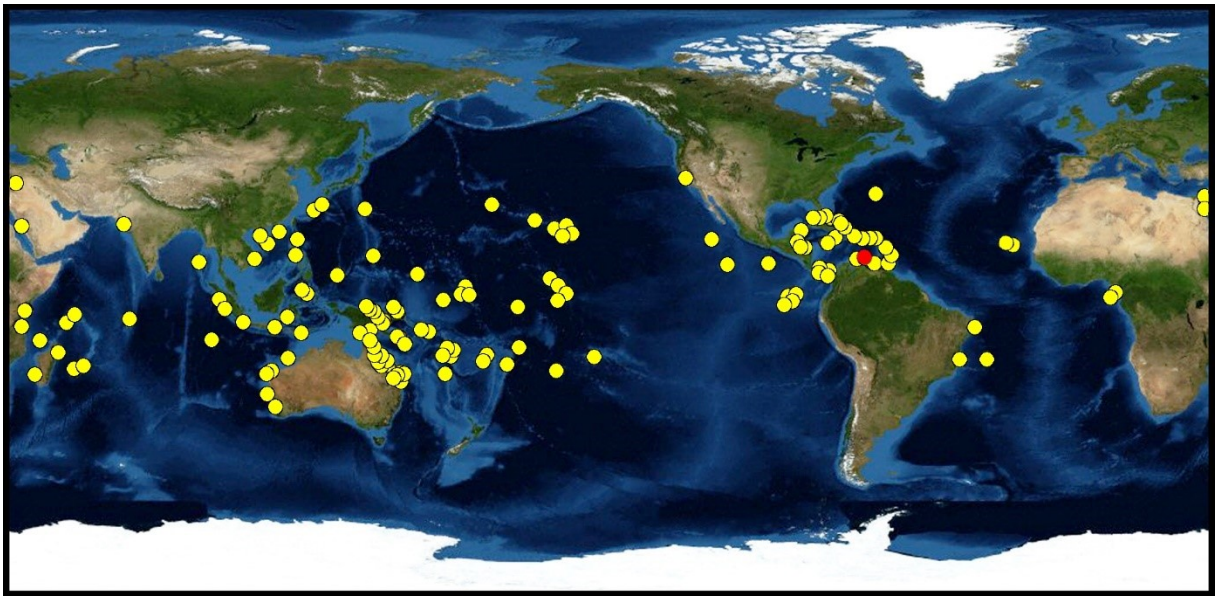

Figure 1.4: Global distribution of published coral and sclerosponge data (yellow dots) representing the past 15 ka according to the NCDC palaeoclimatology website, August 2017. The studies presented in this thesis extend the temporal coverage from the modern and mid- to late Holocene period into the last interglacial of multi-decadal long, sub seasonal coral records at Bonaire (red dot).

There is a comparative lack of coral palaeoclimatic investigation for the LIG (Fig. 1.3) when compared to the present interglacial (Fig. 1.4). For both interglacial periods, *Porites* spp. corals from the tropical west Pacific form the bulk of published coral research. Early LIG findings from the Huon peninsula, characterised the TII LIG inception event of ~135 ka as experiencing a rapid rise in relative sea level (RSL) of 30-50 m in 1000 years (McCulloch et

al., 1999) as well as a seasonality of, and annual mean, SST that was similar to present (McCulloch et al., 2000). Also within the western equatorial Pacific, the LIG was found to have been warmer and saltier than present. ENSO induced variability that was akin to the natural variability defined by the NINO3, 1856-1976 AD index, implying that modern (1960-1998 AD) ENSO behaviour is anomalously intense by comparison (Hughen et al., 1999). Indeed, ENSO type behaviour was found to have existed throughout the past 130 ka and was comparable to, or weaker than, modern times during LIG (Tudhope et al., 2001). This study also characterised LIG surface waters as warmer, and more saline, than present in response orbital forcings that enhanced south East Asian monsoon activity. Representing a region at the lowest thermal limit of *Porites* spp., a 10 year $\delta^{18}O$ record attributed enhanced seasonality of insolation during the LIG to enhanced evaporation of surface waters. This, combined with model simulations, demonstrated the intensification of the subtropical wind fields that drove increased volume fluxes of warmer waters from the Kuroshio Current (Suzuki et al., 2001). Of significance to the Atlantic and European climate system, higher than modern SST seasonality was reported in a 121.9 ka dated *Porites* spp. coral from the gulf of Aquba (Middle East) and attributed to variable winter cooling as a result of a tendency towards a more positive North Atlantic Oscillation (NAO) index (Felis et al., 2004).

Until recently, the LIG tropical Atlantic was only represented by relatively short, four year *Montastraea faveolata* coral Sr/Ca and $\delta^{18}O$ records from a coral dated to 127.5 ka, which recorded SST seasonality 1 - 2 °C higher than present (Winter et al., 2003). However, a more robust 20 year Sr/Ca and $\delta^{18}O$ record from 117.7 ka, at the end of the LIG, placed late-LIG Bonaire SST seasonality within the modern day range (Felis et al., 2015). Many of the above described studies suggest a sensitivity of tropical SST seasonality to the orbitally induced seasonality of insolation during their respective time windows. Moreover, a paucity of knowledge is highlighted regarding how tropical Atlantic SST and hydroclimate evolved throughout the LIG.

1.2.2 Coral Sr/Ca

1.2.2.1 A sea surface temperature proxy

Among the most widely studied environmental properties, SST are vital to modulating regional and global climate patterns. Through a process of bio-mineralisation coral colonies incorporate trace elements from the seawaters they inhabit into their aragonitic skeletons. These trace elements, such as Strontium (Sr), Magnesium (Mg) and Uranium (U), have been demonstrably used as palaeothermometers when measured as a ratio to Calcium (trace

element/Ca). For example, Sr^{2+} shares many of the chemical properties as Ca^{2+} and thus substitutes with Ca^{2+} within the corals crystal lattice (Kinsman and Holland, 1969). Therefore, large reef building corals, especially those that form brain/boulder like structures, are extremely useful to palaeoclimatic study due to their longevity and well-defined growth structure. The temperature dependant distribution coefficient and the initial trace elemental concentration of seawater determines the ratio of trace element/Ca. However, each trace elements has a different relationships with SST. For instance, as SST increases, Mg/Ca also increases, whereas Sr/Ca and U/Ca ratios decrease. Over the past decades of coral palaeoclimatology research, Sr/Ca has emerged as the most widely used and reliable trace element for the reconstruction of palaeotemperatures (McCulloch et al., 1994; Druffel et al., 1997; Gagan et al., 1998; Hughen et al., 1999; Swart et al., 2002; Winter et al., 2003; Cohen et al., 2004; Corrège et al., 2004,2006; Felis et al., 2003, 2004, 2009, 2012, 2014, 2015; Smith et al., 2006; Goodkin et al., 2007; Kilbourne et al., 2004, 2008; Abram et al., 2009; Hetzinger et al., 2010; DeLong et al., 2011; Giry et al., 2012; Xu et al., 2015; von Reumont et al., 2016).

This body of work builds on the ground breaking exploration of coral Sr/Ca as a palaeothermometer by Smith et al. (1979) that was later expanded on and applied to fossil corals by Beck et al. (1992). With the advent of the Inductively Coupled Plasma Atomic Emission Spectrophotometer, new high precision measurements could be made that compared coral samples with a reference material of known geochemical composition (Schrag, 1999). Efforts to address inter-laboratory bias have resulted in common best practices and the use of an agreed reference material, such as JCP-1 (Hathorne et al., 2013). A higher measurement precision accompanies sampling technique improvements of *D. strigosa* coral material, ensuring more accurate micro-sampling, less contamination leading to the generation of more reliable records (DeLong et al., 2012; Giry et al., 2010). Recently combined SST proxy studies have sort to understand biological uncertainties associated with bio-mineralisation to achieve a greater analytical precision. For example, Sr/U thermometry with the implementation of the boron isotope ($\delta^{11}B$) pH proxy (DeCarlo et al., 2016).

1.2.2.2 Interpreting Sr/Ca palaeothermometry

Although many advances in multi-collector mass spectrometry (Galy et al., 2001) have facilitated the routine measurement of this SST proxy, researchers must address certain considerations in order to be confident of Sr/Ca based palaeothermometers. “Vital effects” refer to poorly defined biological influences upon the uptake of geochemical proxies into a corals

aragonite skeleton. Such vital effects are attributed to the differences found between slopes and intercept values that describe modern coral Sr/Ca-instrumental SST relationships (Table 1.1).

Table 1.1: Published sub-seasonal Sr/Ca-SST relationships for the tropical Atlantic region. Sr/Ca = m*SST+ b, whereby m demotes the slope and b the intercept.

Authors	Year	Location	Species	Length (yr)	SST source	Slope	Intercept
Cardinal	2001	Bermuda	*Diploria labyrinthiformis*	49	COADS	-0.045	10.030
Swart	2002	Florida	*Montastrea annualaris*	2	Local SST	-0.038	9.994
Goodkin	2005	Bermuda	*Diploria labyrinthiformis*	30	Local SST	-0.036	10.100
Hetzinger	2006	Guadeloupe	*Diploria strigosa*	41	SODA SST	-0.042	9.986
Smith	2006	Florida	*Montastrea faveolata*	41	Local SST	-0.032	10.054
		Florida	*Montastrea faveolata*	41	Local SST	-0.032	10.083
Goodkin	2007	Bermuda	*Diploria labyrinthiformis*	20	Local SST	-0.037	10.100
		Bermuda	*Diploria labyrinthiformis*	21	Local SST	-0.044	10.300
		Bermuda	*Diploria labyrinthiformis*	20	Local SST	-0.043	10.300
Maupin	2008	Florida	*Siderastrea sidereal*	20	Local SST	-0.039	10.008
Giry	2012	Bonaire	*Diploria strigosa*	16	Satellite SST	-0.034	10.150
Xu	2015	Anegada	*Diploria strigosa*	28	ERSSTv3b	-0.046	N/A
Reumont	2016	Little Cayman	*Diploria strigosa*	42	HadISST	-0.040	10.235
All coral mean						-0.039	10.101
Diploria strigosa mean						-0.041	10.124
Diploria labyrinthiformis mean						-0.041	10.166

A dependence of Sr/Ca ratios on growth has been demonstrated in species of relative low growth rates and/or specific regions of low growth within a *D. strigosa* colony (DeLong et al., 2013). Studies such as Goodkin et al. (2007) demonstrated that by combining Sr/Ca data with the growth rates from multiple slow growing *D. labyrinthiformis* colonies, a universally robust SST calibration could be achieved and reliably applied to multiple tropical Atlantic sites.

These authors provided a minimum growth rate benchmark for palaeoclimate study of corals within this genera by reporting growth related Sr/Ca fractionation occurred in colonies growing at less than 0.35 cm/yr. No growth related correlation with Sr/Ca was documented within faster growing colonies of *D. strigosa* (Giry et al., 2010). Growth rates also serve as an indicator of the palaeo-reef environment inhabited by fossil corals. This is an important to consider as often fossil corals are assumed to have all originated from similar reef-habitats when in fact differing SST relationship are found between fore and back reef inhabiting corals (von Reumont et al., 2016). Furthermore, higher resolutions of micro-sampling, aided by larger growth rates, were found to lower the impact of growth related bio-smoothing (Gagan et al., 2012). These authors also concluded from micro-profiling the skeletal mass accumulation within the tissue layer of *Porites* spp. that coral palaeothermometry requires two types of calibration scales. The first, is an attenuated species specific thermometer sufficiently sensitivity to the study of seasonal to inter-annual SST variability. The second, a rescaled SST relationship applicable to the investigation of trends in mean SST on longer, millennial-scale, time frames. To further minimise uncertainties, five *D. strigosa* colonies from different sites upon the British Virgin Islands were used to assess Sr/Ca-SST calibration techniques and recommended the use of weighted least squares in the establishment of unbiased SST relationships (Xu et al., 2015). As demonstrated by recent tropical Atlantic studies, *D. strigosa* possess a close range of Sr/Ca-SST calibration slopes, supporting the palaeoclimatic application of this species (Table 1).

1.2.2.3 Pleistocene Sr/Ca seawater changes

The accurate reconstruction of absolute SST relies on the assurance that measured Sr/Ca is unaffected by fluctuations in the seawater content of either element. The residence time of Sr and Ca in seawater is ~2.5 million years (Hodell et al., 1990; 2001) and ~1 million years (De La Rocha and DePaolo, 2000), respectively. These residence times are much greater than the ocean mixing time and thus sea surface water content of these elements can generally be considered spatially uniform. This makes Sr/Ca an attractive geochemical proxy for the exploration of past SST, especially on glacial/interglacial timescales of concern to the manuscripts present in this thesis. However, a number of foraminifera based studies (Stoll et al., 1999; Hodell et al., 2001, Lear et al., 2003) suggests that seawater Sr is enriched on glacial/interglacial timescales as a result of dissolution of shelf carbonates shortly after glacial sea level low stands. Quantifying this affect has resulted in discrepancies between modelling and foraminifera studies that published a broad range of estimated enrichment from 0.5 to 2.0 % (Stoll and Schrag, 1999), 3% (Lear et al., 2003) and 12% (Stoll et al., 1999) of the modern day Sr value. In accordance with foraminifera Mg/Ca, another SST proxy, estimates >2% are

likely to be an overestimation (Asami et al., 2009). Nonetheless, such estimates have been incorporated into the Sr/Ca based reconstructions of absolute SST changes relative to present day (Kilbourne et al., 2004; Asami et al., 2009; 2013). A recent study by Yu et al. (2014) utilised Boron/Calcium ratios as a proxy for benthic carbonate ion saturation which were highly correlated with down core Sr/Ca records. These authors concluded that the observed variance in seawater Sr results from partitioning of Sr into foraminifera tests as a consequence of past changes to benthic carbonate ion saturation and supported minimal Sr variations occurring on glacial/interglacial timescales. For LIG time intervals represented by the ^{230}Th/U dated corals that comprise this thesis, relative sea level was between 1.9 and 4.1 m higher than present (O'Leary et al., 2013). Using the popular Sr variance estimate of 1.1% (Stoll and Schrag, 1999), this equates to a miniscule enrichment of mean coral Sr/Ca values by 0.0007 mmol/mol per m RSL fall. Seawater Sr does not occur on seasonal time-scales and so the reconstruction of Sr/Ca-SST seasonality as presented by the manuscripts that comprise this thesis avoids the above uncertainties.

The studies presented in this section illustrate the prudent strategies required to ensure the choice of Sr/Ca-SST calibration is justified and that uncertainties are considered. Additionally, the inter-colony offsets between modern corals that result from such uncertainties can be incorporated into error estimations when three or more modern coral from a similar species and locality are available. As demonstrated by Giry et al. (2012) and Felis et al. (2015), *D. strigosa* coral Sr/Ca-SST seasonality findings are often significant irrespective of the choice of calibration when a relativistic approach is taken that quantifies anomalies rather than absolute SST. Such approaches restore confidence in the interpretation of coral palaeoclimate records after it was revealed that coral Sr/Ca-SST reconstructions overestimated the glacial-Holocene shift in tropical SST derived from foraminiferal Mg/Ca-SST, 4 - 6 °C compared to 2 - 4 °C, respectively (Lough, 2001)

1.2.3 Coral $\delta^{18}O$

1.2.3.1 A mixed sea surface temperature and salinity proxy

The two most abundant isotopes of oxygen within seawater are ^{18}O and ^{16}O. While these two isotopes exhibit similar properties, the relative difference between their masses results in stronger bonds being found within ^{18}O. This results in a temperature dependant fractionation affect that reflects the different stages of the hydrological cycle, and ultimately determines the ratio of these isotopes within seawater (Rohling, 2013). The oxygen isotopic signature of seawater ($\delta^{18}O_{seawater}$) is incorporated into the aragonite skeletons of corals and has long been

established as temperature dependant (Epstein et al., 1953). Building upon the work of Emiliani et al. (1978), Fairbanks and Dodge (1979) were amongst the first to document the seasonal variations of $\delta^{18}O$ along the growth axis of tropical Atlantic corals and attribute this to SST variations. Typically, measurements are referenced to either the Vienna-Pee Bee Belemnite (VPDB) or Vienna Standard Ocean mean water (VSMOW) standards of known isotopic compositions. However, the $\delta^{18}O$ that is precipitated within the skeleton of corals in not in isotopic equilibrium with the seawater they inhabit. This disequilibria is caused by vital effects that describe the biological influences upon the mechanisms controlling calcification of a corals skeleton (McConnaughey, 1989), that can be on the order of 0.2 to 0.4 ‰ for coral $\delta^{18}O$, the equivalent of 1 - 2 °C (Linsley et al., 2000). Although, within a coral genus, such isotopic disequilibria can be consistent (Weber and Woodhead, 1972). Kinetic isotopic disequilibrium effects (McConnaughey, 1989) are growth rate dependant, although *Porites* spp. growing at more than 0.6 cm/yr have been demonstrably unaffected (Felis et al., 2003). Coral $\delta^{18}O$ can provide a proxy for SST, but should be interpreted with caution when attempting to assess mean tropical climatic conditions and in regions with a distinct hydroclimate.

As well as SST, coral $\delta^{18}O$ also reflects the oxygen content of the surrounding seawater ($\delta^{18}O_{seawater}$) which in turn is influenced by precipitation, evaporation, freshwater discharge and the expansion and contraction of ice sheets on hydroclimate. By isolating the $\delta^{18}O_{seawater}$ component within a coral $\delta^{18}O$ records past behaviours of the hydroclimate cycle can be reconstructed. A successful method to achieve this is to quantify the SST component via coral Sr/Ca and separate it from the coral $\delta^{18}O$ measured simultaneously on the same sample, as demonstrated by McCulloch et al. (1994) and Gagan et al. (1998, 2000). Using univariate linear regression equations, these authors first established the respective relationship of Sr/Ca and $\delta^{18}O$ to SST, represented by their proxy-SST regression slopes, β_1 and $\gamma 1$, respectively. Once both proxies were converted to temperature the component of coral $\delta^{18}O$ ($\delta^{18}O_{SST}$) was isolated using the following equations;

$$\delta^{18}O_{coral} = \delta^{18}O_{SST} + \delta^{18}O_{seawater}$$

Whereby, $$\delta^{18}O_{SST} = \gamma_1 / \beta_1 \, (Sr/Ca_{coral})$$

Thus, $$\delta^{18}O_{seawater} = \delta^{18}O_{coral} - \gamma_1 / \beta_1 \, (Sr/Ca_{coral})$$

Due to the previously described uncertainties surrounding the quantification of absolute coral Sr/Ca and $\delta^{18}O$, Ren et al, (2003) demonstrated that by calculating the first derivatives of these two proxies it is worthwhile to disregard the intercept values of coral $\delta^{18}O$ and Sr/Ca-SST regressions. This approach was later refined by Cahyarini et al, (2008) who established that by removing the mean coral proxy value it is possible to target the first order variability within each coral proxy record. Consequently;

$$\delta^{18}O_{seawater} = (\delta^{18}O_{coral} - \delta^{18}O_{coral\ mean}) - \gamma_1 / \beta_1 \, (Sr/Ca_{coral} - Sr/Ca_{coral\ mean})$$

1.2.3.2 Coral $\delta^{18}O_{seawater}$ and hydroclimate change

Coral $\delta^{18}O_{seawater}$ is a critical oceanographic parameter in the study of the world's oceans due to its positive relationship and covariance with sea surface salinity (SSS) (Urey, 1947). This quantification of seawater density is of importance to the understanding of the dynamics that underpin mechanisms such as the AMOC which modulates Atlantic Ocean circulation critical to Northern European climate. Fluctuation within coral $\delta^{18}O_{seawater}$ records occur on seasonal to centennial time-scales indicating changes in seasonal rainfall patterns and variability induced by climate phenomena. Higher (enriched) $\delta^{18}O_{seawater}$ and SSS values typically denote regions characterised by the dominance of evaporation over precipitation, ocean advection and periods of prolonged heat and drought. Conversely, lower coral $\delta^{18}O_{seawater}$ occurs due to the influence of heavy rains, runoff and river discharge which all deplete the isotopic composition of the surface waters corals inhabit. This is especially significant to consider in topical environments where a relatively diminished annual SST cycle coexists with a strong seasonal SSS cycle. To reliably distinguish the predominant influence on coral $\delta^{18}O$, locations are preferred which exhibit large cycles of annual rainfall or SST vs. diminished SSS cycles, and/or locations whereby these two criteria have a convergent effect on coral $\delta^{18}O$ such that they experience warm-wet and cold-dry seasons (Cahyarini et al, 2008; Bradley, 2015). Consequently, coral $\delta^{18}O_{seawater}$ records can document the historical sensitivity of regions exposed to extreme SST and/or SSS variations that result from ENSO and Intertropical Convergence Zone (ITCZ) induced variability (Dunbar et al., 1994; Linsley et al., 1994).

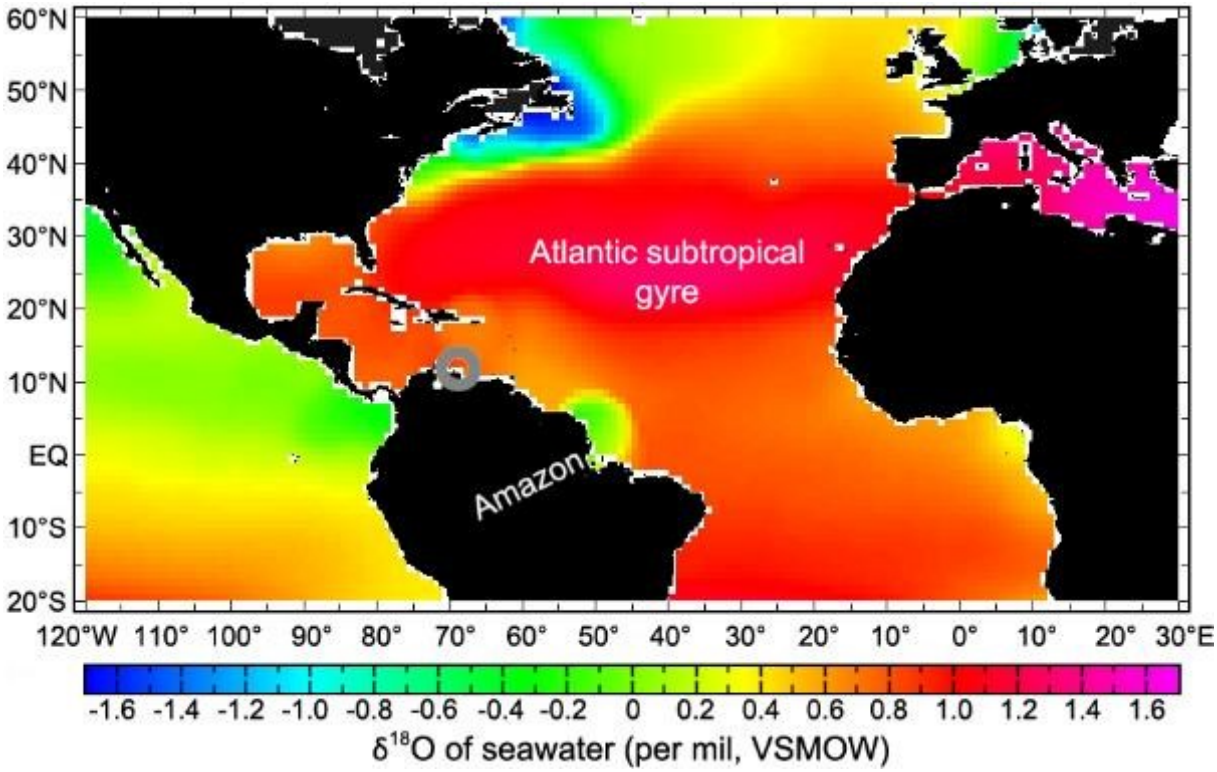

Figure 1.5: Annual mean oxygen isotopic competition of seawater ($\delta^{18}O_{seawater}$) within the modern tropical Atlantic. Gridded instrumental data supplied at 1°x1° resolution by NASA GISS Legrande_Schmidt2006v1p1 d18o (Legrande and Schmidt, 2006). Freshwater discharge from the Amazon River is highlighted as a major regional source of the depleted $\delta^{18}O_{seawater}$. Whereas, excessive evaporation within the Atlantic subtropical gyre results in a source of more positive $\delta^{18}O_{seawater}$ values. The south Caribbean island of Bonaire can be found within the grey circle.

Amazonian river freshwater discharge depletes $\delta^{18}O_{seawater}$ resulting in a visible plume that mixes with tropical Atlantic waters (Fig. 1.5) and varies seasonally, with peak discharge occurring between August and November, 3 - 4 after peak South American monsoon system (SAMS) rainfall. The resultant freshwater plume can be seen to move north westward across the Caribbean, diverting away from the south Caribbean Sea, and so does not directly influencing coral $\delta^{18}O_{seawater}$ records from Bonaire. On longer, centennial to millennia, time-scales $\delta^{18}O_{seawater}$ is affected by the exchange of lighter ^{16}O with sinks such as ice sheets, and to a lesser extent, aquifers. During glacial periods the resultant cooler temperatures allow higher latitude precipitation to freeze and form ice sheets more readily. Consequently, ice sheets grow and aquifers swell locking water depleted in ^{18}O within terrestrial based sinks. Global sea levels drop in response and become enriched in ^{18}O, leading to higher $\delta^{18}O_{seawater}$ values (Fig. 1.2). The converse occurs during warmer interglacial periods leading to the estimation that $\delta^{18}O_{seawater}$ is enriched or depleted by ~0.01‰ per meter sea level change (Rohling, 2013). Consequently, mean annual coral $\delta^{18}O_{seawater}$ reconstructions apply a correction for periods, such as the LIG, influenced by sea levels that differed from present.

1.2.3.3 Climate influences upon interglacial coral $\delta^{18}O_{seawater}$

Unlike SST, for which instrumental records typically exist for the past 150 years, SSS records prior to 1950 AD are scarce, especially within the tropics. Once the modern hydroclimate regime governing coral $\delta^{18}O_{seawater}$ has been established, paired coral Sr/Ca and $\delta^{18}O$ records can reconstruct past $\delta^{18}O_{seawater}$ changes and proxy SSS beyond instrumental records. Insights from the past decade of tropical coral $\delta^{18}O_{seawater}$ reconstructions are here highlighted that demonstrate the utility of this research. A 336-year coral Sr/Ca and $\delta^{18}O$ record from Madagascar (1658-1995 AD) demonstrates the impact of regional ENSO teleconnections with Indian di-pole events on local hydroclimate variability. Notably, a shift occurred throughout this period highlighting the variable nature of the relationship between SST and the hydroclimate balance of the Greater Agulhas Current region (Zinke et al., 2004). Similarly, paired Sr/Ca and $\delta^{18}O$ records spanning between 1726 to 1997 and 1780 to 1997 AD have been generated from the south Pacific islands of Rarotonga and Fiji, respectively. These records illustrate past variations within the Interdecadal Pacific Oscillation (IPO) phenomenon on regional SST and the South Pacific Convergence Zone upon coral $\delta^{18}O_{seawater}$ (Linsley et al., 2004). These authors reported spatial variability of the IPO within the south Pacific which resulted in a distinct collapse of the IPO and SST relationship in the region during the mid-1800s when compared to modern. Within the tropical Indian Ocean (Chagos Archipelago) paired Sr/Ca and $\delta^{18}O$ records, for a period 1950 - 1995 AD, established that a SST threshold of 28.5°C was exceeded during the 1970's AD and as a consequence, $\delta^{18}O$ and Sr/Ca-SST become linearly related (Pfeiffer et al., 2006). This result demonstrated the care required in interpretation of these paired Sr/Ca and $\delta^{18}O$ records as the relationship between SST and precipitation can be complex and exhibit threshold behaviour. Coupled coral Sr/Ca and $\delta^{18}O$ records (1873 -1995 AD) from the Ogasawara Islands within the North West Pacific Ocean document a shift toward fresher sea surface conditions between 1905 and 1910 AD (Felis et al., 2009). This was attributed to a weakening of the Kuroshio Current system as a result of diminished surface winds, a key component of the Pacific subtropical gyre circulation.

Modern coral based reconstructions from paired Sr/Ca and $\delta^{18}O$ records (1895-1999 AD) of the hydroclimate variability at Guadeloupe (northern Caribbean) reveal an inverse relationship between surface air temperatures and SSS, with warmer and drier conditions reconstructed since the 1950s AD (Hetzinger et al., 2010). These records detected inter-annual to decadal variability, further substantiating the role of ENSO and NAO on these timescales, respectively. Additional evidence for Caribbean hydroclimate change comes from Watanabe et al. (2001) who found that compared to recent times the Caribbean Sea experienced and enhanced annual SSS cycle and a 2°C drop in SST during the Little Ice Age (15th to late 19th century AD).

As well as reconstructing $\delta^{18}O_{seawater}$, paired Sr/Ca and $\delta^{18}O$ coral records can be assessed using spectral analysis to determine the phase relationship between these records as an indicator of hydroclimate change. This has been used within the South China Sea to constrain the rainy season experienced in this region for modern and Mid-Holocene (~6.45 ka) time periods (Deng et al., 2009). A shift in the hydroclimate regime is reported from the modern setting dominated by May to October rainfall to one during the Holocene whereby peak rainfall occurred between December and April. This temporal shift in the hydroclimate regime indicates the changing interplay between the East Asian subtropical summer monsoon and western North Pacific summer monsoon on regional precipitation patterns (Guo et al., 2016). Although not statistically significant, a similar transition in phase relationship between coral Sr/Ca and $\delta^{18}O$ records and decreasing annual mean coral $\delta^{18}O_{seawater}$, suggests a more northerly positioned ITCZ at Bonaire during the mid- Holocene (Giry et al., 2013). These changes from modern hydroclimate occurred in unrelated regions during a time of increased insolation seasonality, highlighting the sensitivity of the monsoon dynamics to orbital controls, a finding supported by a recent stalagmite study from Central America (Pollock et al., 2016).

The only example of tropical Atlantic reconstructed coral $\delta^{18}O_{seawater}$ during the LIG is provided by Felis et al. (2015). These authors report from a single fossil coral specimen dated to 117.7 ka that coral $\delta^{18}O_{seawater}$ seasonality, an indicator of hydroclimate, was similar to modern during the late LIG despite documented Atlantic climatic instabilities (Fig. 1.2). Cumulatively, these studies illustrate the potential wealth of information obtainable through the judicious application of paired coral Sr/Ca and $\delta^{18}O$ records. Furthermore, the requirement for multi-colony studies representing various snapshots across a period of time likely subject to $\delta^{18}O_{seawater}$ variability and hydroclimate changes is also emphasised.

1.3 The significance of Bonaire

1.3.1 Geographic and geological setting

The island of Bonaire is located within the sub-oceanic basin that comprises the Caribbean Sea. Together with the Gulf of Mexico (GOM) and the Atlantic Ocean between 30°N and 30°S, the Caribbean Sea forms an integral part of the tropical Atlantic Ocean. Since the Isthmus of Panama rose to close the Central America sea way, ~15 million years ago, the Caribbean Sea has been isolated from the Pacific Ocean. This event peaked ~4.6 million years ago, uniting the continents of North and South America, leading to a reorganisation of ocean currents and the formation of the Gulf Stream (GS). Consequently, surface water masses of the Caribbean Sea ultimately feed into the GS, diverting warm water and moist air masses. northward to influence northern hemisphere climate. Counter-intuitively it is suggested that this promoted north hemisphere glaciation, leading to the current ice age which is modulated by orbital forcings (Haug and Tiedemann, 1998).

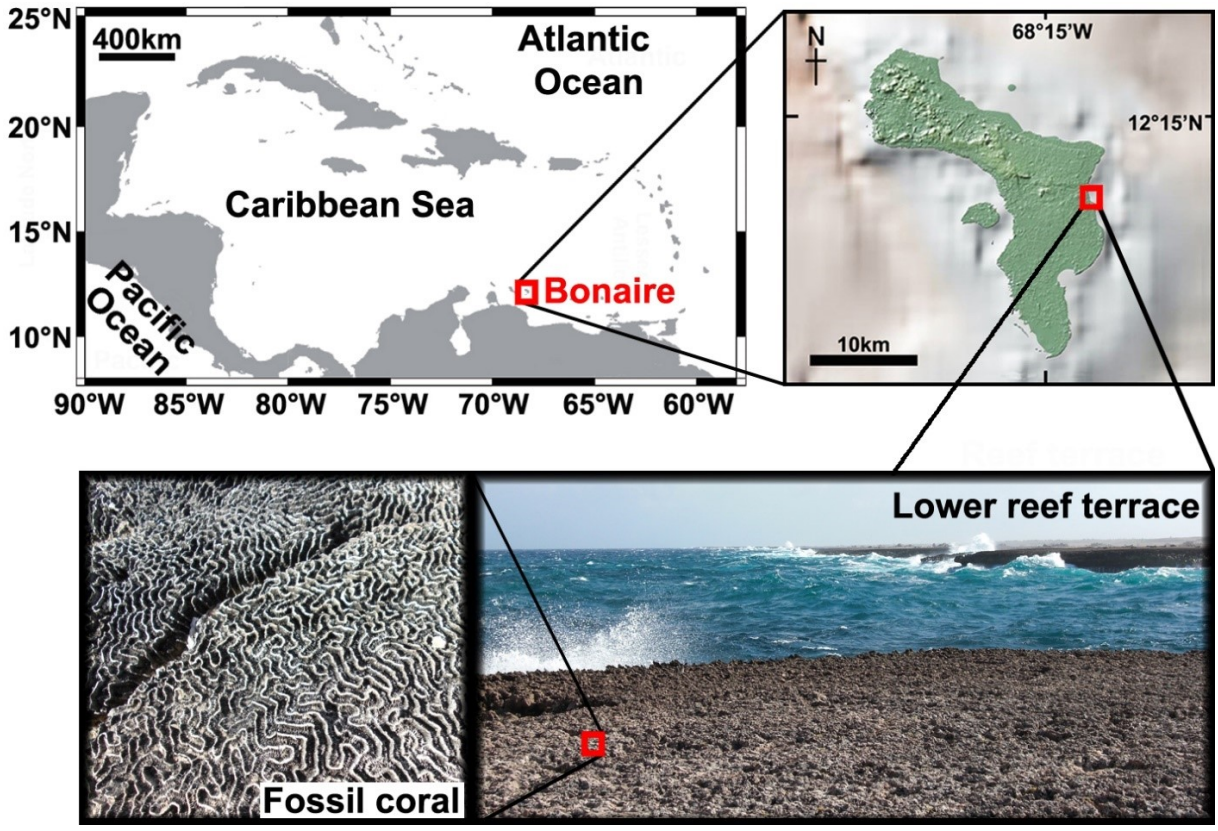

Figure 1.6: Map illustrating the location of the island of Bonaire (Caribbean Netherlands) within the Caribbean Sea (upper panels). Bonaire is fringed by elevated fossil reef terraces on which fossil corals may be preserved (lower panels). Photos curtesy of Thomas Felis.

Within the southern Caribbean Sea, ~100 km north of the coast of Venezuela, the island of Bonaire (12°10'N, 68°15'W) is found alongside Aruba and Curaçao, that comprise the ABC islands (Fig. 1.6, upper panels). However, politically, since the dissolution of the Netherlands Antilles in 2010, Bonaire is considered a special municipality of the Netherlands in conjunction with St. Eustatius and Saba. The ABC Island and are separated from one another by ~2000 m of water depth to form a discontinuous ridge of tertiary submarine volcanoes that have been subsequently uplifted and coated in Plio-Pleistocene reef limestone. This volcanic island arc is located on the southern edge of the Caribbean tectonic plate that slowly moves eastwards as it shares a conservative plate boundary with the South American plate. Bonaire itself is geologically complex but essentially comprises of two main geological features. A volcanic core is exposed in the middle and north west of the island and comprises of silica-rich sediments that formed during the upper Cretaceous (~120 Million years ago) that have since been folded and faulted to form the Washikemba formation. This core has subsequently been overlain in the central and southern parts of the island by quaternary limestone. Fringing the coast, a series of fossil reefs that form terraces can be found (de Buisonje, 1974). As a result of continuous slow uplift and tilting the lower most of these Pleistocene fossil reef terraces are found 8 - 12 metres above and submerged below modern sea level in the north and south of the island, respectively (Engel et al., 2010). In accordance with Kim and Lee (1999), coral material from these uplifted reef terraces grew during sea-level highstands and should correspond to interglacial periods. This inference has recently been supported for the lower terrace by multiple ^{230}Th/U dates of eight *D. strigosa* colonies from the lower most terrace (Fig. 1.6, lower panels) that ranged between ~117.7 and 129.7 ka (Fig. 1.7) (Felis et al., 2015; Obert et al., 2016).

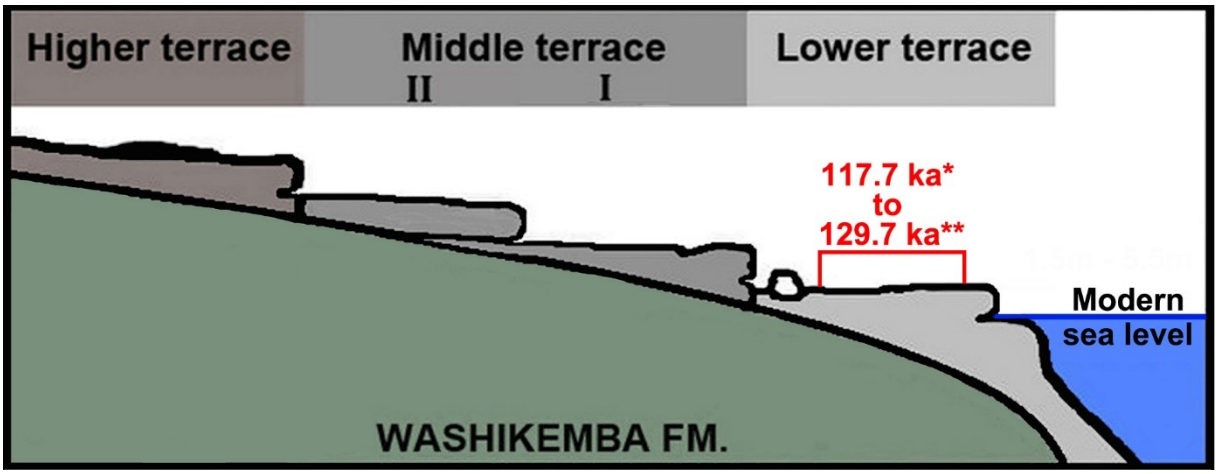

Figure 1.7: Geological schematic of Bonaire reef terraces. Quaternary reef limestone terraces coat Upper Cretaceous volcanic rocks referred to as the Washikemba formation. Eight coral colonies cemented to the lower terrace have been assigned ^{230}Th/U ages between 117.7 and 129.7 ka (*Felis et al., 2015; ** Obert et al., 2016)

1.3.2 Oceanographic setting

Bonaire is exposed to strong winds and wave action that prevail along the northern and eastern coastline. Upon the more sheltered southern and western shore, diverse living coral communities are found. Holocene coastal coral deposits and debris are found scattered upon the lower terrace, the source of which remains controversial due to the fact they exhibit depositional features indicative of either high energy storm or Tsunami events (Engel et al, 2012; Scheffers et al., 2014). These deposits have been used for reconstructions of Bonaire climate during the Holocene and revealed that Bonaire was sensitive to, and so representative of, tropical Atlantic climate (Giry et al., 2010, 2012, 2013).

The Caribbean Sea is semi- enclosed with connections to the Atlantic Ocean through two main pathways within the island arc of Lesser Antilles to the east, and one to the north between the Greater Antilles. Therefore, Bonaire can we found in the midst of water masses that contain a diverse set of physical characteristics that are intrinsically linked to tropical and sub-tropical climates. The oceanography of the Caribbean Sea is typified by three water masses with distinguished salinity and temperature properties. Within the upper water column (0-220 m) two separate water masses exist, the first contains comparatively fresh surface waters known as the Caribbean Surface Water (CSW). The second forms in the Atlantic subtropical gyre as a result of evaporative processes dominating over precipitation. This creates a high salinity water mass that sinks beneath the CSW at an approximate 100 m water depth, known as the Subtropical Under Water (SUW) (Wüst, 1964). Beneath the SUW at a depth of 1000 m lies the colder and fresher water mass of the Antarctic Intermediate Water. Freshwater discharged from the Amazon and Orinoco Rivers mix with the equatorial Atlantic surface waters and are brought into the Caribbean Sea by the North Brazil Current (NBC) and Guyana Current (GC) (Fig. 1.8). However, the SUW enters the Caribbean Sea as an extension of the North Equatorial Current (NEC). The CSW and SUW merge into the Caribbean Current (CC) that transports warm water north-westwards into the GOM as part of the Loop Current (LC) (Fig. 1.8). This ultimately influences the formation of the Florida current (FC) before flowing northward as the GS that is integral to AMOC and northern European climate.

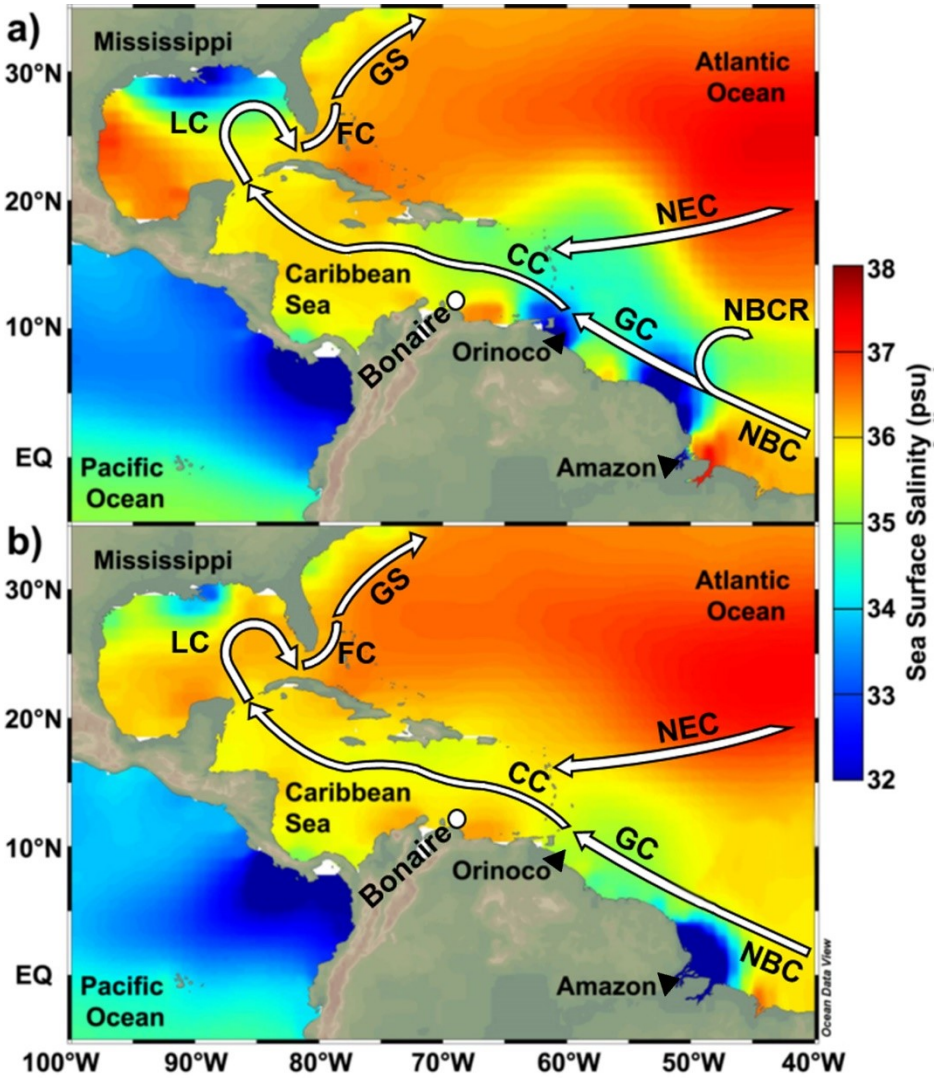

Figure 1.8: A comparison of summer (a, July-August-September) and winter (b, January-February-March tropical Atlantic average sea surface sanity between 1955 and 2012 AD. Data available from the World Ocean Atlas 2013 (Zweng et al., 2013) and illustrated using Ocean Data View v4.7.9 (Schlitzer et al., 2015). The river mouths of major sources of less saline water from the Amazon, Orinoco and Mississippi rivers are labelled. Bonaire is denoted by a white circle. White arrows illustrate the major ocean currents of the Gulf Stream (GS), Florida Current (FC), Loop Current (LC), Caribbean Current (CC), Guiana Current (GC), North Equatorial Current (NEC), North Brazil Current (NBC) and its July to December retroflection (NBCR).

The oceanography of the Caribbean Sea is influenced primarily by the mixing of surface waters derived from the mid- Atlantic (via the NEC) and equatorial Atlantic (via the NBC). The combined inflow of these water masses is measured at ~28 Sverdrup (Sv) and enters the Caribbean Sea through three approximately equal pathways of ~8 - 10 Sv at the Windward, Leeward and Greater Antilles Island Passages. In response to AMOC circulation and the dominance of trade winds, this inflow varies seasonal by 4 Sv between a maximum in April to July and minimum in October (Johns et al., 2002). While the mid- Atlantic waters that enter at >15°N are wind driven, the water masses to the south through Grenada Passage, via the GC,

are drawn in due to AMOC processes. GC water masses contain a seasonal freshwater component derived from Orinoco and Amazon River discharge. This reaches a peak from August to November, 3 - 4 months after maximum precipitation in north-eastern South America, and extends north-westward into the Caribbean Sea. During the latter half of the year this freshwater plume is increasingly diverted from entering the Caribbean Sea by the eastward retroflection of the NBC (NBCR) (Fig. 1.8a) (Ffield, 2005). Just north of the ABC island arc, the fastest CC current velocities (130 cm s^{-1}) are found (at ~13°N, 68°W) (Hernández-Guerra and Joyce, 2000).

An additional oceanographic factor that potentially influences Bonaire SSS seasonality is the well-documented region of Venezuelan upwelling that occurs between December and May as a result of Ekman transport promoted by easterly trade winds (Taylor et al., 2012). This induces more saline waters originating from the Subtropical Underwater (Wüst, 1964) to penetrate surface waters and have been implicated in a *D. strigosa* mortality study at Bonaire and Curaçao (Bak et al., 2005). However, these events occur within the range of days to weeks and therefore unlikely to be recorded by monthly resolved coral records. Additionally, anomalous winter SST that accompany increased winter SSS are not observed at Bonaire, whereas they are in the vicinity of the Gulf of Venezuela and the Cariaco Basin, ~300 km to the south-west and east of the island, respectively. An eastward flow between Bonaire and the northern coast of Venezuela further inhibits prolonged upwelling at Bonaire (Andrade et al., 2003). As will be discussed in the next section these oceanographic influences upon Bonaire are interconnected with broader tropical Atlantic climatic phenomena resulting in the ABC islands occupying a region of niche sensitivity within the Caribbean Sea.

1.3.3 Climate setting

Bonaire experiences a semi-arid climate due to it receiving ~550 mm/yr of rainfall, average air temperatures of ~27 °C and its location just outside of the traditional Caribbean hurricane belt. Annual SST exhibit a distinct seasonality of ~2.9 °C that ranges from between 25.7 and 28.6 °C in February-March and September-October, respectively (Smith et al., 2008) (Fig. 1.9a). Year-long easterly trade winds prevail but diminish between July and October (ICOADSv2.5, Woodruff et al., 2011). This coincides with decreased sea level pressure (SLP) (Kaplan et al., 2000) (Fig. 1.9b) and heat loss to the atmosphere at the ocean surface. Generally, these trade winds promote high rates of net evaporation of moisture throughout the year that is not compensates for by freshwater influxes (Etter et al., 1987) (NCAR, Kalnay et al., 1996) (Fig. 1.9c).

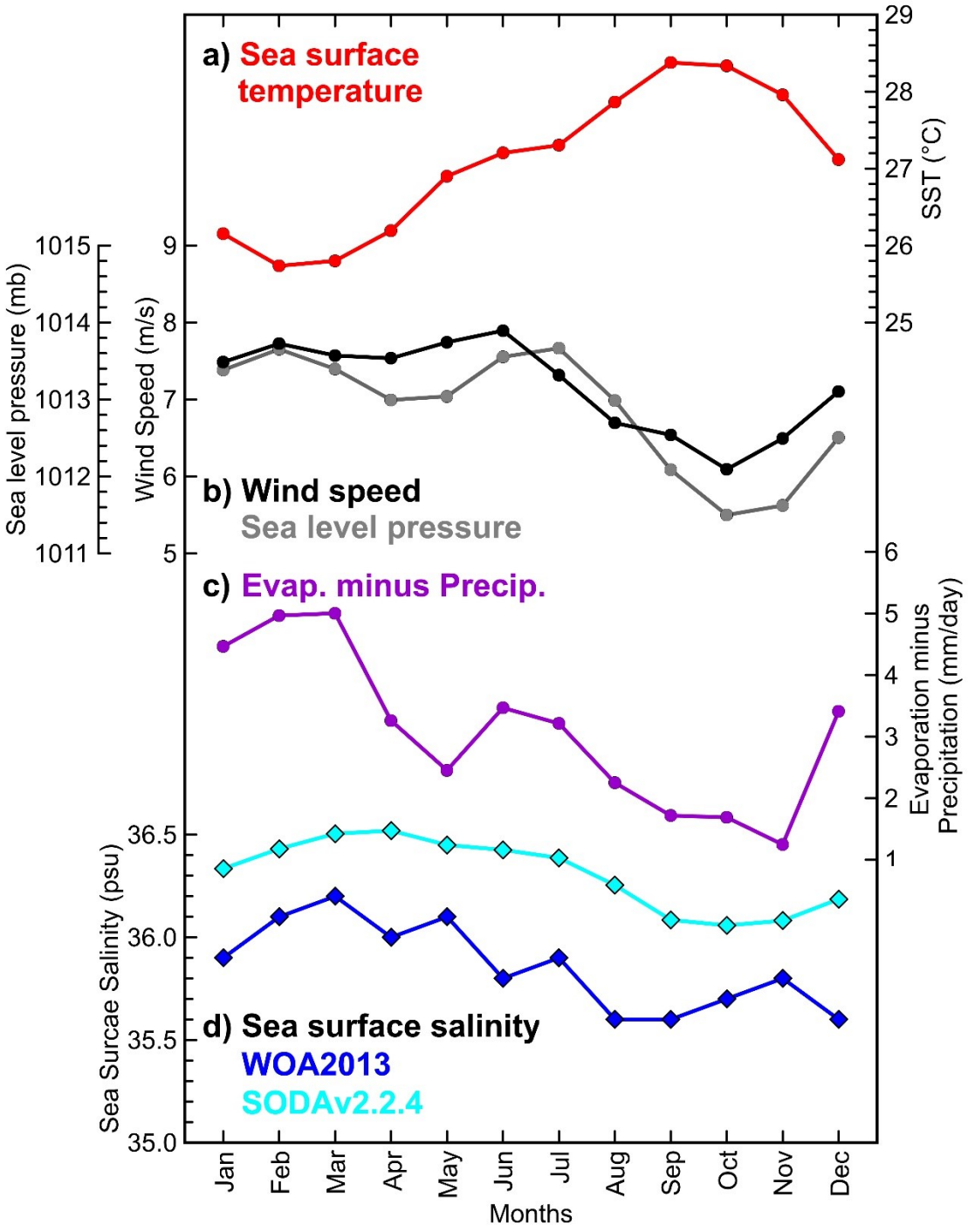

Figure 1.9: Instrumental gridded monthly mean annual cycles of significant environmental properties at Bonaire. **a**) Sea surface temperatures for a 2° x 2° gridbox from 1910 - 2000 AD (ERSSTv3b, Smith et al., 2008). **b**) Wind speed within a 2° x 2° gridbox centred at 12°N, 67°W from 1947 - 2015 AD (ICOADSv2.5, Woodruff et al., 2011) and sea level pressure for a 4° x 4° gridbox centred on 12°N, 68°W from 1958 - 1999 AD (KAPLAN COADS_SLPclim slp, Kaplan et al., 2000). **c**) Evaporation minus precipitation for a 2.8° x 2.8° gridbox centred at 67.5°W, 12.5°N for 1950 - 2000 AD (NCAR, Kalnay et al., 1996). Positive values denote net evaporation at Bonaire. **d**) Sea surface salinity from 1955-2012 AD for a gridbox 1° x 1° gridbox centred on 12°N, 68°W available from the Simple Ocean Data Assimilation Reanalysis v2.2.4 (light blue, Carton and Giese, 2008) and World Ocean Atlas 2013 (dark blue, Zweng et al., 2013).

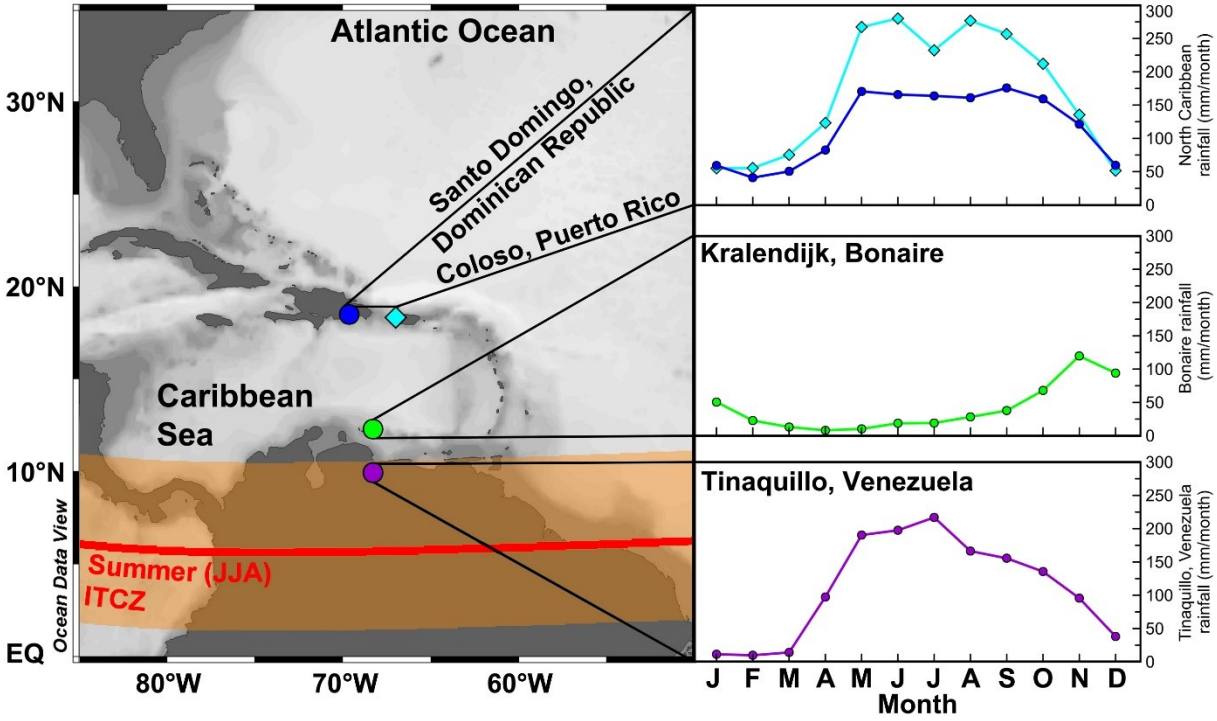

Figure 1.10: Monthly instrumental rainfall data series (Lawrimore et al., 2011) demonstrating Bonaire rainfall compared to that typical for the north Caribbean (Santo Domingo and Coloso) and northern South America (Tinaquillo). An approximate position of the most northerly summer (June-July-August) position of the modern Intertropical Convergence Zone (ITCZ) is illustrated based on rainfall data of Waliser and Gautier (1993).

The main rainy season at Bonaire begins in October and ends at the start of January due to a sea-continent breeze indirectly induced by wind fields associated with the southerly position of the winter ITZC (Hastenrath, 1984). A secondary season of "small rains" can occur between July and August as a result of spatially sporadic convective events (Martis et al., 2002). Bonaire's pattern of annual precipitation, and its relative dryness, is in contrast to much of the Caribbean region. This is illustrated by the land masses to the north and south of Bonaire exhibiting rainfall patterns typical of the influence of the North Atlantic subtropical high and the ITCZ, receptively (Jury et al., 2007) (Fig. 1.10). Consequently, Bonaire is surrounded by precipitation regimes characterised by a summer (JJA; June-July-August) rainfall season that can be occasionally interrupted by a relative drought in July (Giannini et al., 2000). This demonstrates that the modern hydroclimate of Bonaire is primarily influenced by the seasonal advection of oceanic waters rather than precipitation. Although ITCZ induced SAMS precipitation discharged from the Orinoco and Amazon Rivers does contribute indirectly to ocean advection at Bonaire by strengthening the NBC, GC and CC during summer. Importantly for Bonaire, this freshwater plume deviates north westward and does not directly influence SSS (Chérubin and Richardson, 2007). The spring SSS maxima at Bonaire is attributed to weaker

GC and CC currents and increased evaporation. Consequently, SSS instrumental records demonstrate an annual average SSS seasonality of ~0.6 psu, which coincides with the annual cycle of SST. This is in contrast to regional SSS seasonality which is typically 2.8 psu at the Grenada passageway and ~1.6 psu upon mixing with mid- Atlantic water masses within the Caribbean Sea (SODAv2p2p4, Carton and Giese, 2008; WOA13, Zweng et al., 2013) (Fig. 1.9d). In summary, modern SST at Bonaire exhibit behaviour closely related to the Atlantic Warm Pool (AWP) typical of the tropical Atlantic, whereas its hydroclimate occupies a spatially unique region neither directly influenced by freshwater riverine discharge (Fig. 1.8b) nor summer ITCZ rains (Fig. 1.10). While currently within the shadow of the ITCZ coral Sr/Ca-SST and $\delta^{18}O$ records from Bonaire have the potential to demonstrate significant sensitivity to these competing influence that surround the island. On inter-annual to multi-decadal timescales Bonaire can be found at the confluence of influences from climate phenomena that originate in the Pacific and Atlantic oceans which compete to modulate SST and hydroclimate.

1.3.4 Tropical Atlantic climate variability

Tropical Atlantic climate exhibits variability influenced by both the tropical and extra-tropical oceans (Czaja, 2004) that modulate the regions dominant trade winds, currents and an upwelling systems (Jury, 2009). Tropical Atlantic SST are modulated seasonally by the AWP which migrates north during summer. However, the extent to which the AWP penetrates the Caribbean Sea in any given year is variable due to the influence North Atlantic SLP has upon surface winds. Characterised by surface waters warmer than 28.5 °C, the AWP is a feature of the tropical Atlantic that fluctuates on seasonal, inter-annual and multi-decadal time-scales (Wang et al., 2008). The influence of the AWP on tropical Atlantic climate phenomena can manifest in fluctuations to Caribbean hurricane activity and rainfall within the Nordeste (Brazil) and Sahel regions. The variability of these dramatic events, SST and regional rainfall patterns are of importance to the inhabitants of the region, as demonstrated by decadal shifts in Caribbean socio-economic output (Jury, 2009). Alongside the association with the tropical Atlantic, the Caribbean Sea is also host to influences from the Pacific basin through the intertwined nature of ocean/atmosphere interactions. For instance, the AWP also fluctuates on inter-annual and decadal timescales in response to eastern pacific ENSO and the Atlantic Multi-decadal Oscillation (AMO), respectively. At present, it is unclear from palaeoclimatic records and modelling studies what influence projected climate change scenarios will have on such modes of SST and rainfall variability. Natural climatic variability has recently been implicated in the observation of a hiatus in the rise of global temperatures (Dai et al., 2015), and disputed (Karl et al., 2015; Robson et al., 2016). This debate brings into renewed focus the importance

of assessing the dynamics that underpin natural climate variability and reiterates the need for sub-seasonal palaeoclimate records to confidently capture inter-annual to multi-decadal climate variability and extend available instrumental records

1.3.4.1 Inter-annual to quasi-biennial variability

Inter-annual tropical Atlantic SST variability results from the coupled ocean/atmosphere interactions between the tropical Pacific and the extra-tropical north Atlantic. Within these regions, ENSO (Fig. 1.11a) and the NAO (Fig. 1.11b) phenomenon dominate variability, respectively (Kushnir et al., 2006).

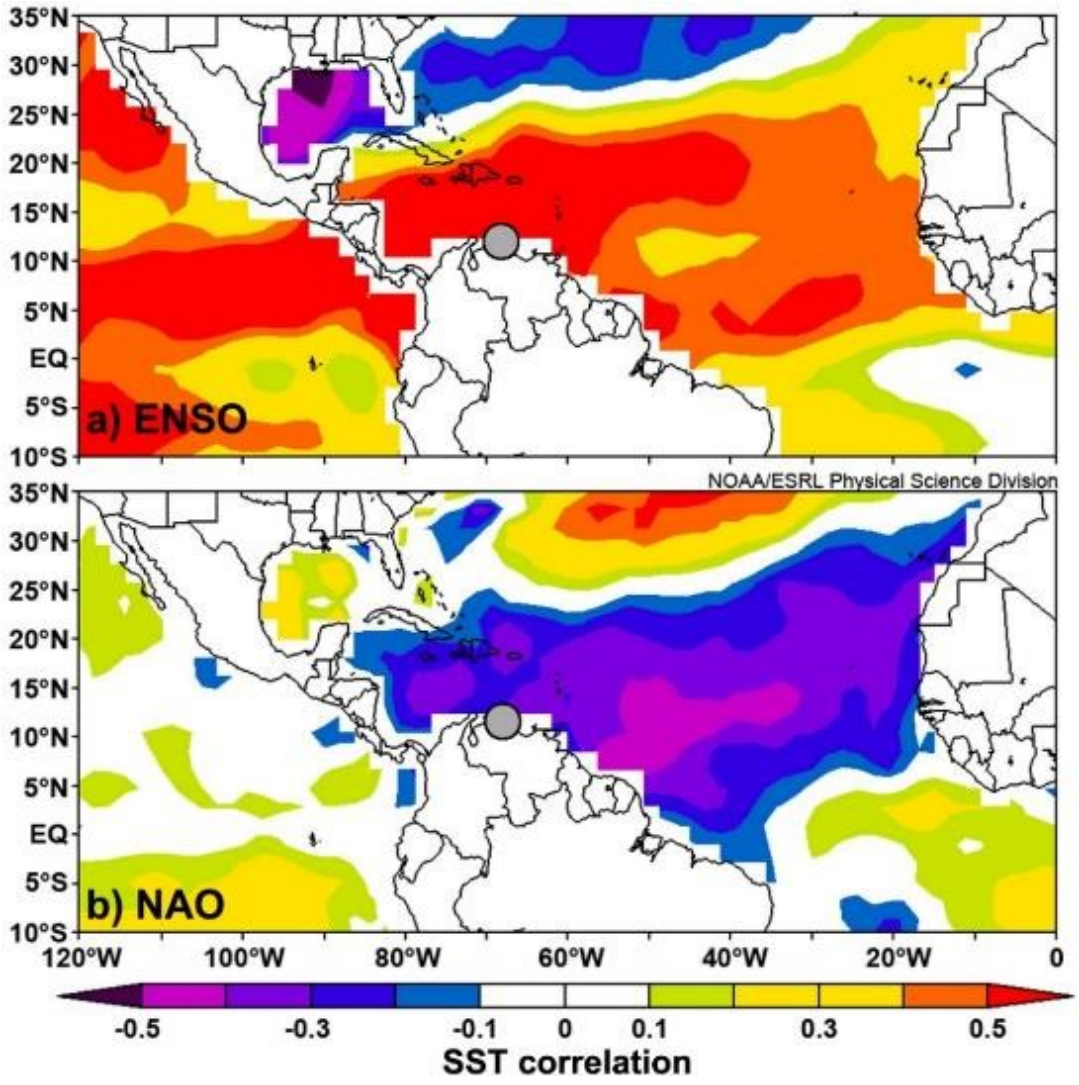

Figure 1.11: Surface ocean correlation map between March-May tropical Atlantic sea surface temperatures (Smith et al., 2008) vs. (a) December to January El Niño 3.4 index (Climate Prediction Center) and (b) December to January North Atlantic Oscillation index (Hurrel, 1995) during a period from 1947 - 2013 AD. Grey circles indicate the location of the island of Bonaire. Image adapted from the Physical Sciences Division at NOAA-ESRL, Boulder Colorado from their web site at http://www.esrl.noaa.gov/psd/.

Due to anomalies within the Walker circulation, north-easterly trade winds weaken and the latent and sensible heat loss of the tropical Atlantic decreases leading to a warm Atlantic ocean (Enfield and Mayer, 1997; Chiang et al., 2002). Through air-sea teleconnections, 50 - 80% of anomalous SST variability can be attributed to the influence of ENSO, whereby Atlantic SST warm ~4 - 5 months after the peak Pacific SST warmth (Enfield and Mayer, 1997; Sutton et al., 2000). Typically during an El Niño year the Caribbean experiences a drier summer that is followed the next year by a wetter than average spring (Giannini et al., 2001). Atlantic hurricane activity has been demonstrably linked to ENSO behaviour, whereby it reduces and increases during El Niño and La Niña years, respectively (Smith et al., 2010).

Defined by the winter sea level pressure anomaly measured between Reykjavik, Iceland and Ponta Delgada, Azores, the NAO predominately influences the strength of Atlantic westerly trade winds during winter (DJF). As with ENSO, the NAO modulates the sensible and latent heat capacity of the tropical Atlantic, which in turn modulates the position of the ITCZ (Xie and Carton, 2004). Varying positive (NAO+) and negative (NAO-) phases of a non-periodic nature characterise the NAO and results in a strengthening and weakening of Caribbean easterly trade winds, respectively. Phases of NAO+ are associated with cooling of the ocean surface as heat loss to the atmosphere is enhanced and precipitation is diminished, whereas the opposite occurs during NAO-. An example of the societal importance of NAO phases is demonstrated by its influences upon the path of tropical Atlantic hurricanes which are more likely to make landfall within the GOM during NAO- years (Elsner et al., 2000). The tropical Atlantic is at its most variable when the influences of ENSO and NAO constructively interfere (Giannini et al., 2001). The strength of surface winds that comprise the Caribbean Low Level Jet (CLLJ) are in phase with the NAO (Wang, 2007) and exhibit a inter-annual component (1.25 and 2.3 year) that supresses Caribbean SST by increasing winter/spring easterly trade winds.

This quasi-biennial variability also occurs within Atlantic SST (Barnett, 1991; Dima and Lohmann, 2004) and is influential to similar quasi-biennial variance seen in hurricane activity (Gray, 1984). Quasi-biennial Atlantic SST variability derives from the interactions of the more fundamentally stable annual cycle with the multi-decadal variability that arises from the Atlantic tri-pole (Dima and Lohmann, 2004). Consequently, colder sub- surface waters that are upwelled in the equatorial Atlantic are brought to the south Caribbean Sea and modulated by the equatorial node to induce variations in the slope of the equatorial Atlantic thermocline (Servain, 1991). Modern corals from Guadeloupe, east Caribbean Sea, have reconstructed quasi-biennial SST variability and attributed this to the observed variance to quasi-biennial modulation of the NAO (Hetzinger et al., 2006). Similarly, quasi-biennial SST variability has

also been detected in modern and fossil corals from Bonaire for snapshots throughout past 6.2 ka (Giry et al., 2012). Defining a precise source of these mechanisms is still problematic with evidence indicates air-sea interactions derived from both the Atlantic (Chang et al., 2006) and Pacific Oceans (Tourre et al., 1999).

The behaviour of ENSO under future climate change projections is largely uncertain (Huang and Xie, 2015; Huang, 2016) although it has been suggested that ENSO related variability since 1970 AD is anomalous high, might typify future climate change until 2040 (Kim et al., 2014) and originated in the North Atlantic (Dima et al., 2015). In particular it is unknown what influence a warm than modern world would have upon ENSO and NAO induced inter-annual tropical Atlantic variability. In order to address such uncertainties. Tropical Atlantic coral palaeoclimatic records could potentially reveal if the relationship between ENSO and NAO persisted beyond the current interglacial period. Indeed, coral palaeoclimatic records could test evidence from climate simulations that suggest La Niña type ENSO conditions may have been more common during the LIG due to the orbital configuration that differed from present (Clement et al., 1999; Kukla et al., 2002).

1.3.4.2 Decadal variability

On greater than inter-annual timescales tropical Atlantic variability continues to be influenced by NOA and ENSO climate phenomena, but with differing significance. A decadal SST variability has been shown by a spectral peak at ~13-15 years within modern instrumental data compilations (Deser and Blackmon, 1993; Chang et al., 1997) and Cariaco sedimentary records spanning the past 825 year (Black et al., 1999). The winter expression of this decadal mode promotes SST and wind speed anomalies on either side of the mean ITCZ position (~5 °N) and is indicative of the north Atlantic di-pole that influences basin wide air-sea heat fluxes and climatic patterns. With a lag of ~8 months this mode propagates downstream to form a tri-pole signal with the equatorial Atlantic (Fig. 1.12) (Moron et al., 1998). Fluctuation in the western Atlantic basin zonal wind fields that feed into the CLLJ serve to promote winter upwelling and link the north and equatorial Atlantic to the Caribbean Sea (Servain et al., 2003). The annual cycle interacts with the thermodynamic properties and ocean-climate feedback mechanism of the decadal mode to influence quasi-biennial variability (Dima and Lohmann, 2004), with the relative spectral significance of the latter two modes being modulated by the NAO (Tourre et al., 1999). Uncertainty remains regarding the subsurface expression of the decadal mode, although a growing consensus attributes decadal variability to underlying behaviours of AMOC (Latif et al., 2006a; and reference therein).

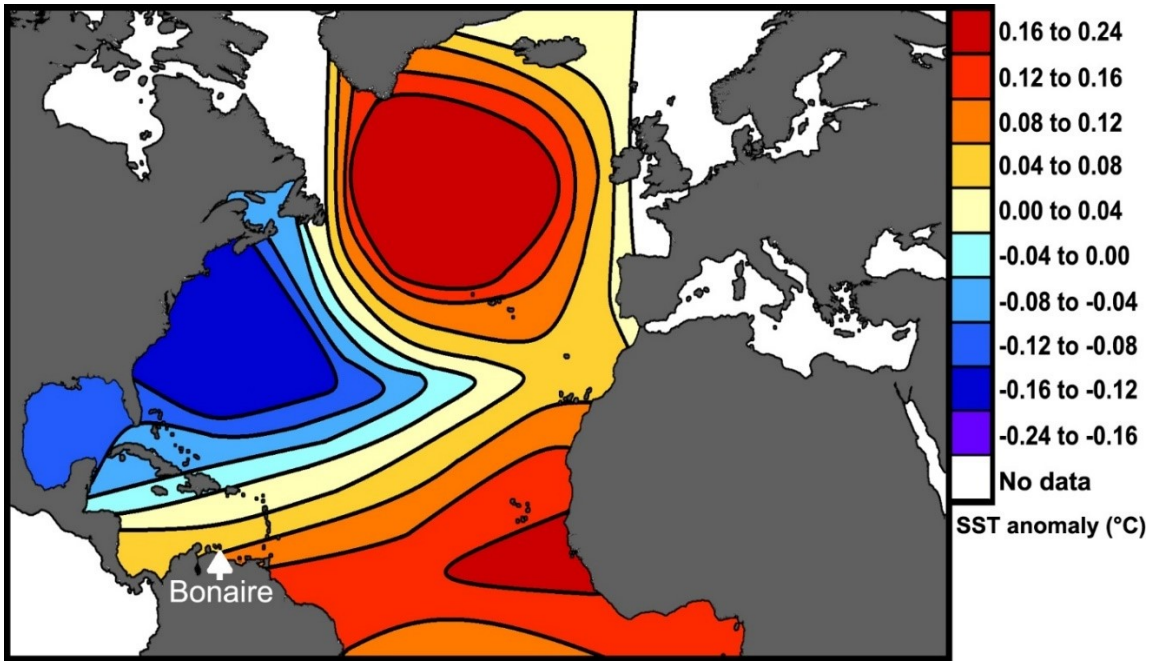

Figure 1.12: Sea surface temperature anomaly during the seventh phase composite of the North Atlantic decadal mode. Reimaged from Moron et al. (1998) to better illustrate the tri-pole influences on Atlantic SST.

1.3.4.3 Multi-decadal variability

With a typical period of between 60 - 90 years, the AMO (Kerr, 2000) predominantly influences climate patterns on multi-decadal timescales within the tropical and north Atlantic (Fig. 1.13), inducing variability in North Eastern Brazilian and African Sahel rainfall, Atlantic hurricanes and North American and European summer climate (Knight et al., 2006). Due to instrumental records insufficient length to confidently capture the drivers and impacts of AMO, this phenomena is largely investigated through climate simulations (Latif et al., 2006b). A lagged response of AMOC to NAO variability has been identified in simulations as a results of modulation to Labrador Sea convection, influencing Atlantic SST anomalies. It is also suggested that weakening of AMOC since the 1980's AD is within the natural variability of this system on multi-decadal time-scales and therefore not solely anthropogenically induced (Latif et al., 2006a). The variability of AMO since 1956 AD highly correlates with that of the NBC that feeds surface waters into the Caribbean Sea (Zhang et al., 2011) highlighting the requirement for study of oceanographic influences on AMO within this region (Zhang et al., 2017).

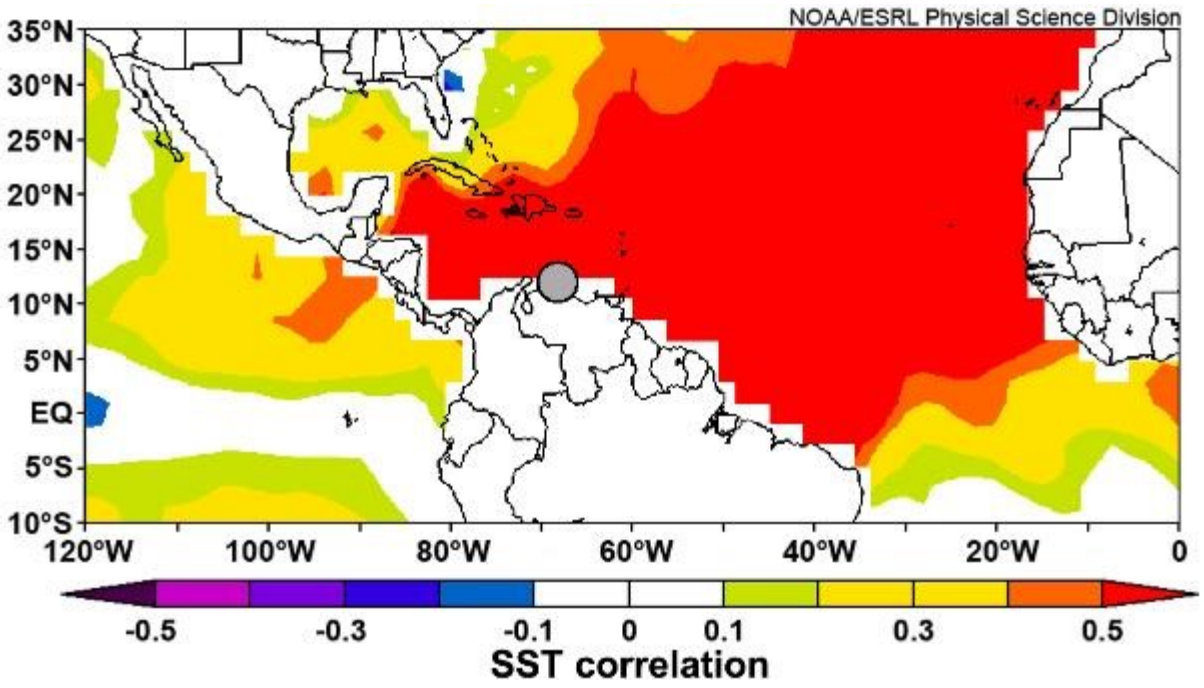

Figure 1.13: Surface ocean correlation map between December to January sea surface temperatures (Smith et al., 2008) and Atlantic Multi-decadal Oscillation index (Enfield et al., 2001) during a period from 1947 - 2013 AD. Grey circles indicate the location of the island of Bonaire. Image adapted from the Physical Sciences Division at NOAA-ESRL, Boulder Colorado from their website at http://www.esrl.noaa.gov/psd/.

Sub-seasonal *Montastraea faveolata* coral Sr/Ca- SST and $\delta^{18}O$ records spanning 1751 - 2004 have been used to extend available instrumental records from Puerto Rico (Kilbourne et al., 2008). These authors reported multi-decadal spectral peaks at ~60 year providing a unique assessment of AMO associated climate variability within the Caribbean. This variability was attributed to strengthening of the north easterly trade winds that promotes upwelling within the region and the northward Ekman transport of surface waters of a lower salinity. However, although salinity changes are implicated the underlying mechanisms remain unsubstantiated (Kilbourne et al., 2014). South east of Bonaire at Los Roques, Venezuela, a *D. strigosa* coral $\delta^{18}O$ record (1923 - 2004 AD) detected similar ~60 year variability owing to the influence of the AMO on Caribbean SST and rainfall (Hetzinger et al., 2012). Furthermore, a correlation between the August-October component of this record and tropical Atlantic hurricane activity has been demonstrated highlighting the societal importance of coral-based AMO reconstructions.

1.4 The palaeoclimatic utility of fossil coral records

1.4.1 Sampling of *Diploria strigosa* colonies

Diploria strigosa (Dana, 1846) is increasingly becoming the coral of choice for palaeoclimatic study within the Atlantic realm. Typically found in shallow waters of coastal GOM, southern Florida, Bahamas, North West Caribbean, Puerto Rico, Lesser Antilles and Bermuda, *D. strigosa* forms notable large hemispherical brain-like structures. Upon tropical Atlantic islands, such as Bonaire, *D. strigosa* constitutes an integral part of the modern and fossil reefs (Plate 1.1). However, *D. strigosa* (Plate 1.1a) is also commonly found amongst other similar *Diploria sp.* such as *Diploria labyrinthiformis* (Plate 1.1b) and *Diploria clivosa* (Plate 1.1d). Fortunately, *D. strigosa* can be differentiated by their internal skeletal architecture and its occasionally subtle external expression. For instance, the surface structure of *D. strigosa is* described as more uniform, possess wider thecae, under developed coenostreum, 15-20 speta per cm and valley widths of ~5 mm (Budd et al., 2012). These distinctions are important to note as the skeletal structure of *D. strigosa* is a more suitable source of palaeoclimatic records, due to its distinctive and less fragile thecae walls, which are more resilient to diagenetic processes. Easily identifiable, a theca can be extracted by using a handheld circular drill from the surrounding porous skeletal elements of the septa and columellae (Plate 1.2). This thesis adopts the coral structure naming convention of Budd et al. (2012).

The paleoclimate utility of *D. strigosa* species and the preference for measuring along the thecae wall skeletal element has been convincingly demonstrated by Giry et al. (2010). Geochemical and isotopic measurements sampled perpendicular to growth, across multiple skeletal types, were found to significantly differ with the most reliable and consistent measurements extracted from the theca material. For example, Sr/Ca measurements from the skeletal elements that surround the thecae typically record higher Sr/Ca values, and thus lower SST. Therefore, delicate sampling techniques are required to ensure that precision micro-drilling has occurred along these dense skeletal elements. *D. strigosa* at Bonaire exhibits continuous growth and annual density bands which are more and less dense in summer (JJA) and winter (DJF), respectively (Giry et al., 2010). This reliable growth pattern is vital for the construction of absolute internal chronologies (age models) that accompany the interpretation of geochemical and isotopic measurements.

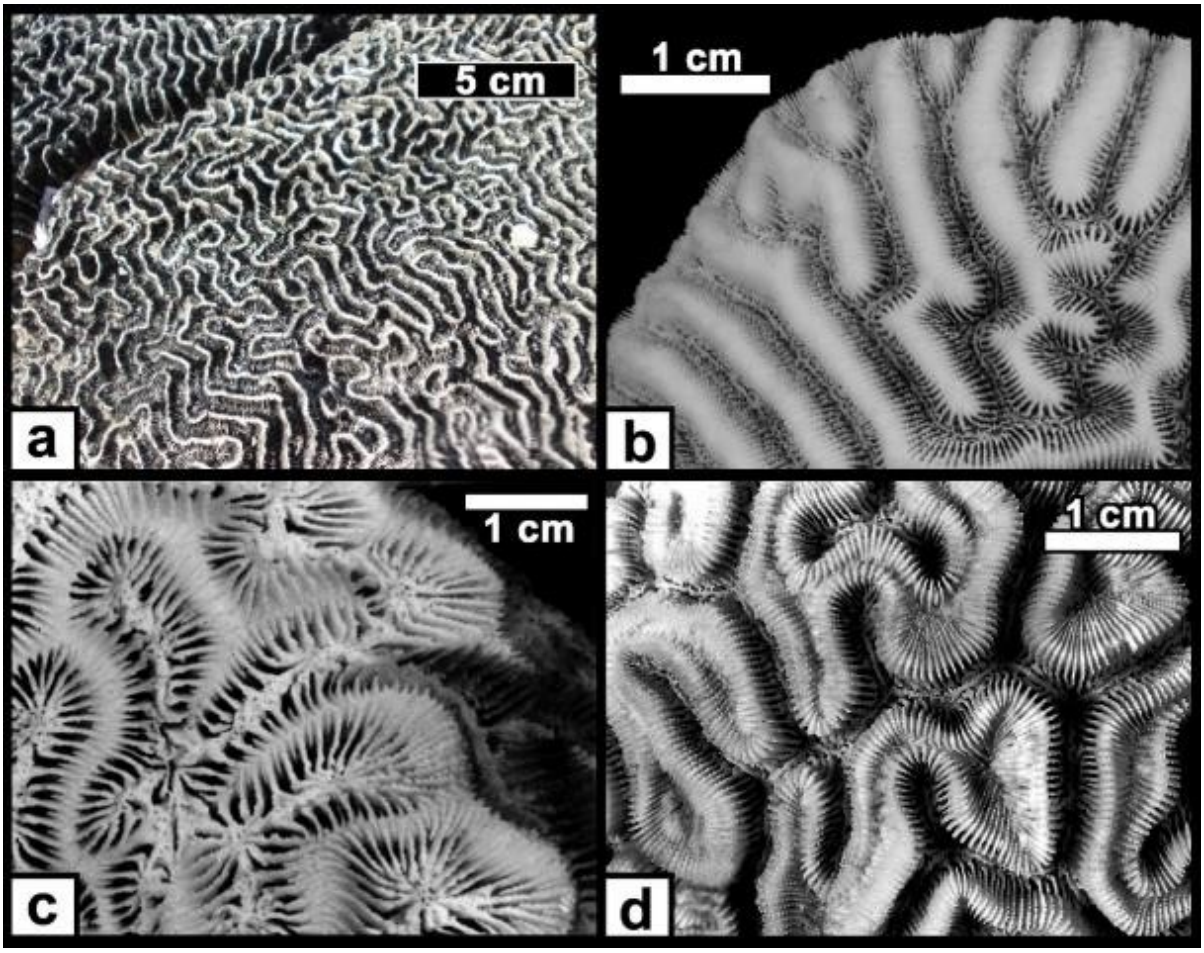

Plate 1.1: Comparison of the external structure of (a) a fossil (dead) *Diploria strigosa* cemented to an uplifted Bonaire reef terrace, (b) *D. strigosa*, (c) *Diploria clivosa* and (d) *Diploria labyrinthiformis*. Note the more uniform meandering growth (thick white) and thicker thecae skeletal element of (b) in comparison to (c) and (d). Image (a) provided by T. Felis, while (b), (c) and (d) are available from Australian institute for marine science (http://coral.aims.gov.au)

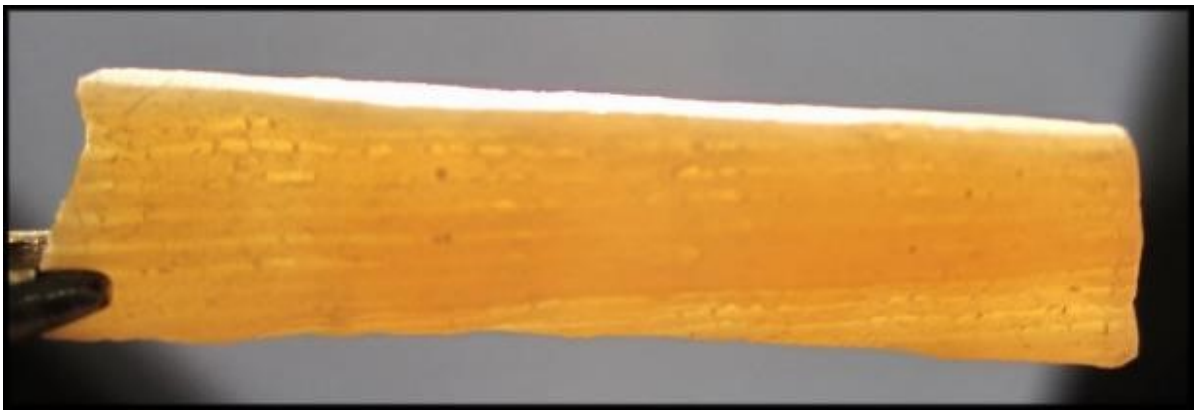

Plate 1.2: A theca extracted from a *Diploria strigosa* colony using a diamond tipped micro-grinder to test a hypothesis regarding the age reliability ^{230}Th/U ages using different skeletal types (Obert et al., 2016).

The interpretation of fossil coral palaeoclimate records is complicated by the observation that fossil coral material from a similar locality may have inhabited different palaeo-reef environments as a result of changes in water depth and sea level rise. This uncertainty is difficult to address without intensive palaeo-reef studies of the micro-topography of a elevated reef terraces, although abnormal growth rates provide an indicator. Another indicator is to ensure that a fossil coral is retrieved from an elevation (corrected for uplift) above sea level that is less than the common documented depth range of the species. In the example from the lower terrace of Bonaire, *D. strigosa* are found between ~1.5 and 4.0 m above sea level which is less than the modern documented water depth of 0 - 10 m for this species (Sommer et al., 2011). This range remains likely inhabited when one considers that LIG sea levels were ~6 to ~9 m above present (Dutton et al., 2015). This is an important consideration as demonstrated by the difference observed between palaeoclimate records obtained from similar corals inhabiting the differing water depths of the fore and back reef (von Reumont et al., 2016). In light of these considerations, Bonaire fossil *D. strigosa* colonies are likely recorders of LIG ambient water properties of the sea surface.

1.4.2 Dating of coral material

The aragonite skeleton precipitated out of seawater by corals provides an excellent material for dating methods. The relatively precise dating of coral material is vital to the interpretation of coral based sea level reconstructions (Dutton and Lambeck, 2012; Muhs et al., 2012; O'Leary et al., 2013) and palaeoclimatic studies (Tudhope et al., 2001; Corrège et al., 2004; Ayling et al., 2006; Asami et al., 2009; Felis et al., 2004, 2012, 2015). The annual density banding inherent to most corals allows internal chronologies to be built with absolute certainty, such that modern material with a known date of death can count years back from the top (youngest) coral growth increment. These internal chronologies when established within fossil material are consider "floating" with no fixed start of end date for their records. However, key to the utility of coral derived climate records is the relative certainty that can be obtained from dating fossil material. Typically, coral material is subject to either the radiocarbon or the ^{230}Th/U dating method. Both methods have be demonstrated to be highly reproducible for material that grew up to ~30,000 years ago, the temporal limit that radiocarbon dating can be applied (Reimer et al., 2013). ^{230}Th/U dating relies on the geochemical fractionation of Uranium (U) and Thorium (Th) in seawater and the steady radioactive decay of ^{238}U and ^{234}U to ^{230}Th isotopes, to reliably date material as old as 600 ka (Scholz and Hoffman, 2008). ^{230}Th/U dating also possess the added advantages of being considered absolute due its non-reliance on ^{14}C variations in the atmosphere and the influence of ocean reservoir effects. Furthermore, coral

^{230}Th/U dating is not dependent on orbital tuning methods intrinsic to the age models that typically define sedimentary palaeoclimatic records. The reliability of ^{230}Th/U dating is predicated on the assumption that 1) no extra ^{230}Th becomes integrated into the coral after growth and 2) any changes to the activity ratios that follow are a consequence of radioactive decay. The first of these closed system assumptions has been demonstrably shown to not apply to other fossil marine carbonate material derived from molluscs and foraminifera (Scholz and Hoffman, 2008). The second, however, may not always be applicable to fossil coral and speleothem material (Gallup et al., 1994; Stirling and Andersen, 2009). In essence, this describes a coral that experienced "closed system behaviour" and is another metric by which fossil coral preservation can be assessed. Furthermore, this technique assumes that past (^{234}U/^{238}U) ratios of seawater have remained unchanged from present and consequently that observed deviations from the expected activity ratio result from open-system behaviour (Stirling and Andersen, 2009).

Testing these dating assumptions results in number of costly and time consuming reliability criterion that need to be considered when ^{230}Th/U ages are generated from fossil coral material (Scholz and Mangini, 2007). The dense thecae wall skeletal element that characterises species such as *D. strigosa*, has been shown to aid the determination of reliable age estimates (Stirling, 1995; Andersen et al., 2010; Obert et al., 2016). Compared to the conventionally used bulk material, the thecae is comprised of higher density skeletal material and is thus less susceptible to post-depositional/open system behaviour. This hypothesis was recently examined and demonstrated the improved utility of *D. strigosa* thecae when compared to bulk material. For instance, all *D. strigosa* thecae from the lower reef terrace of Bonaire yielded LIG ages, whereas bulk material samples were found to be significantly older or younger than this period. Although strictly reliable ages are possible from bulk material, thecae from *D. strigosa* and corals of a similar skeletal architecture are more suitable for ^{230}Th/U dating methods (Obert et al., 2016).

1.4.3 Micro-sampling LIG corals; challenges and improvements

Traditional building materials for development are scarce upon islands such as Bonaire and so uplifted reef terraces are increasingly being mined. The availability of usable coral material is further hindered by its exposure to erosional forces that influences the preservation of the material and the ability to reconstruct continuous climate records (Hendy et al., 2007). Once extracted, these rare coral colonies are easily damaged during transport and sectioning of coral colonies creates brittle slabs. Therefore, before drilling on a reef terrace, experience is

required to best judge the likely preservation and surface expression of the targeted coral colony's growth orientation. However, it is only latter in the laboratory, with the aid of visual inspection and X-radiography, that preservation and growth orientation can be confirmed. In order to maximise the potential of exposed internal corallites to micro-sampling, an accurate assessment of the external growth orientation is required prior to sectioning a colony core into slabs. Within the retrieved Bonaire collection, one coral colony core (BON-23-AI) was 51 cm long and thus had the potential to yield exceptional long records. This colony was fractured into five separate pieces, but nonetheless, given a parallel growth orientation, it is possible to splice geochemical and isotopic records together to create a continuous palaeoclimate record. However, this coral cores external corallites did not give a clear indication of the growth direction and so computer tomography scanning was used to none-destructively visualise its interior. This resulted in 550, 1 mm slices, that were augmented into a single 3D image of the entire internal structure of the colony using the software Amira©. Tools such as these allow the internal growth structures to be visualised, resulting in the observation that this colony's growth was orientated 45° to the drilled core direction (Fig. 1.14). Consequently, as only short, non-continuous records would have been obtained, further study of this colony was avoided. Such techniques ensure no relatively time consuming and costly analyses are performed.

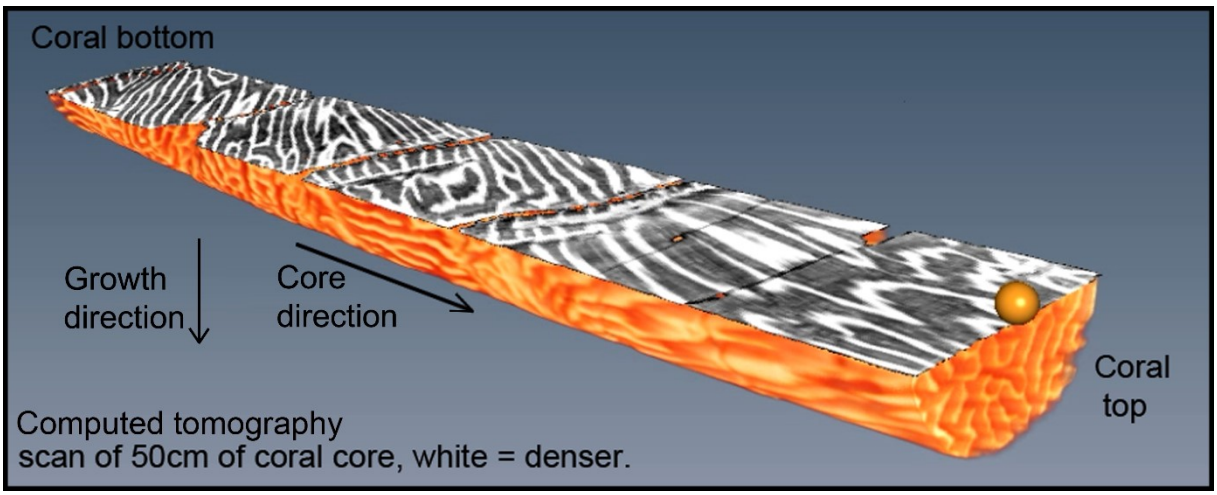

Figure 1.14: 3D computer tomography scan of a *Diploria strigosa* colony comprised of 550 1 mm scan slices. Light colours denote denser regions. Note the orientation of thecae wall structures (white lines) indicate a growth direction different to that of the core. Many fractures are also present.

To expose internal coralites, 6 - 7 mm thick slabs were created by sectioning coral colony cores parallel to their growth. This allowed the identification of suitable skeletal paths to be made that is vital to the generation of long continual palaeoclimate records. X-radiography reveals the density structure of the coral slabs and highlights the dense thecae skeletal elements which are the most suitable target for micro-drilling (Giry et al., 2010). On occasion, the growth direction of LIG corals differed from that observed during extractions from the reef terrace. Therefore, the possibility exists that the coral colonies were not retrieved in-situ and instead were moved within the lower reef terrace before being affixed to it. This uncertainty hinders the application of the LIG coral collection from Bonaire in the accurate reconstruction of relative sea level changes. Importantly, X-radiography illustrates when a theca being sampled starts to "shoal" and continued micro-drilling begins to incorporate powder from surrounding skeletal types. Additionally, manual operating of a micro-drill can allow an investigator to detect the shoaling of their targeted theca through the reduction of vibrations that results when less resistant skeletal elements are met. This contingency against the incorporation of none theca skeletal elements into a sample is not possible with pre-programmed automated micro-drills. Should a theca shoal, *D. strigosa* slabs typically contain another suitable adjacent theca within the same annual density band that can be cross-matched to ensure the resultant record is uninterrupted.

Although fossil *D. strigosa* colonies from Bonaire have been successfully used to reconstruct SST and hydroclimate during the mid- to late Holocene (Giry et al., 2010; 2012; 2013) the LIG collection presents new challenges. As a consequence of the processes governing preservation, the majority of suitable LIG thecae are on the order of 0.8 - 1.0 mm thick, whereas those of the mid- to late Holocene are between 1.0 - 1.5 mm. This observation highlights the care required for precision micro-drilling that avoids contamination from other skeletal elements while ensure sufficient coral powder is retrieved (Plate 1.3). Furthermore, in order to obtain monthly resolved geochemical and isotopic records annual growth rates need to be sufficient for ~12 samples to be taken per annual density band. This presents a greater challenge with LIG corals that possess annual growth rates typically less than those of modern and mid- to late Holocene colonies, ranging between 0.48 - 0.84 cm and 0.46 - 1.1 cm, respectively.

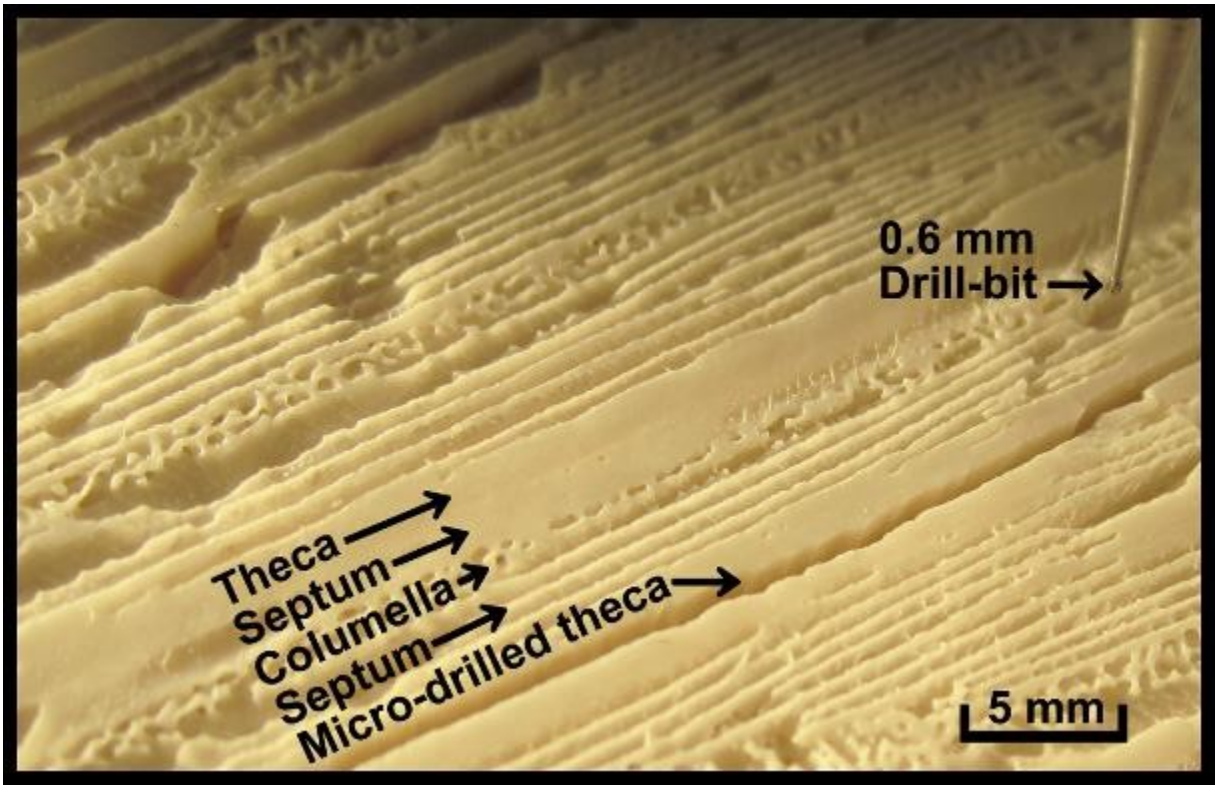

Plate 1.3: A micro-drilled path along the theca of a *Diploria strigosa* colony. Other skeletal elements are highlighted and should be avoided during micro-sampling to avoid contamination of geochemical or isotopic samples.

For a variety of sampling and growth related reasons the apparent orientation of the targeted theca might shift from the parallel ideal, relative to the drill-bit. The drill required for micro-drilling often is in a fixed vertical position, therefore the mounting of the coral on the drill stage requires modification (Plate 1.4a). This increases the likelihood of fracturing slabs of brittle fossil corals. It is the authors experience that coral slabs can be mounted within a block of polystyrene of the appropriate length to serve as a splint that cushions the coral slab, allowing the slab to be more easily handled and secured to the drill stage (Plate 1.4b). Once secured the orientation of the coral slab within the split can be altered with additional polystyrene props and secured in place using elastic bands to achieve the desired orientation of the theca relative to the drill-bit (Plate 1.5). Such techniques ensure micro-drilling maximises the powder yield and prevents sample contamination that results when the drill-bit penetrates the surrounding septum or columellae skeletal elements.

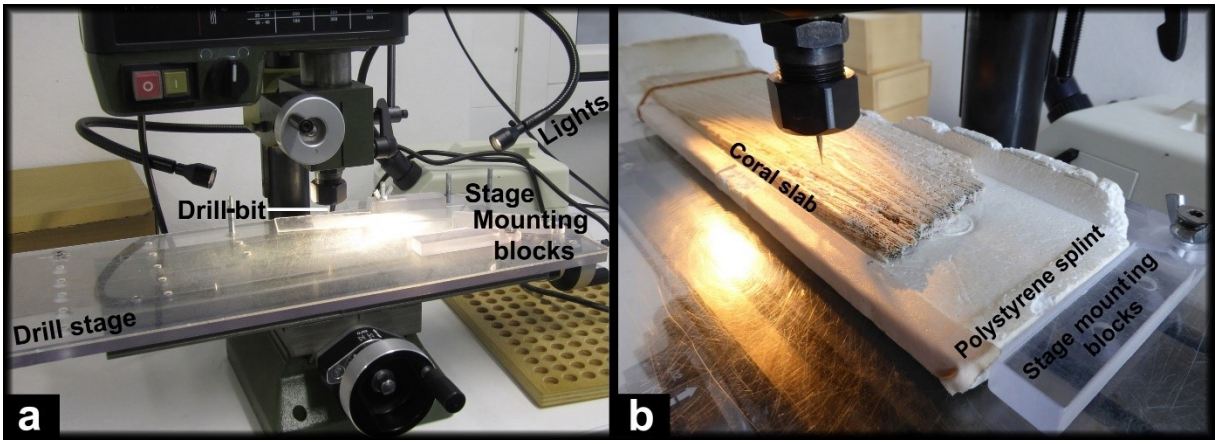

Plate 1.4: a) Micro-drill station setup and b) coral *Diploria strigosa* slab mounted on the drill stage via the use of a Polystyrene splint. This aids the durability of delicate last interglacial *D. strigosa* slabs.

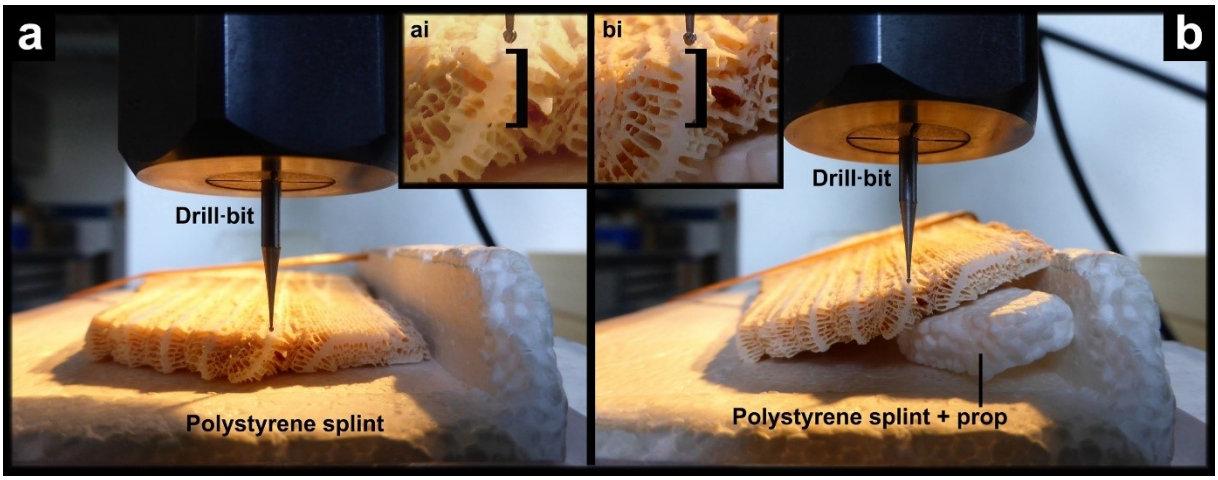

Plate 1.5: A slab of *Diploria strigosa* mounted on a polystyrene splint, without (A) and with (B) additional polystyrene props positioned under the slab to alter the drill-bits angle of approach. Note the drill-bit will excavate more of the theca (Bi) and avoid contamination from other skeletal elements (Ai).

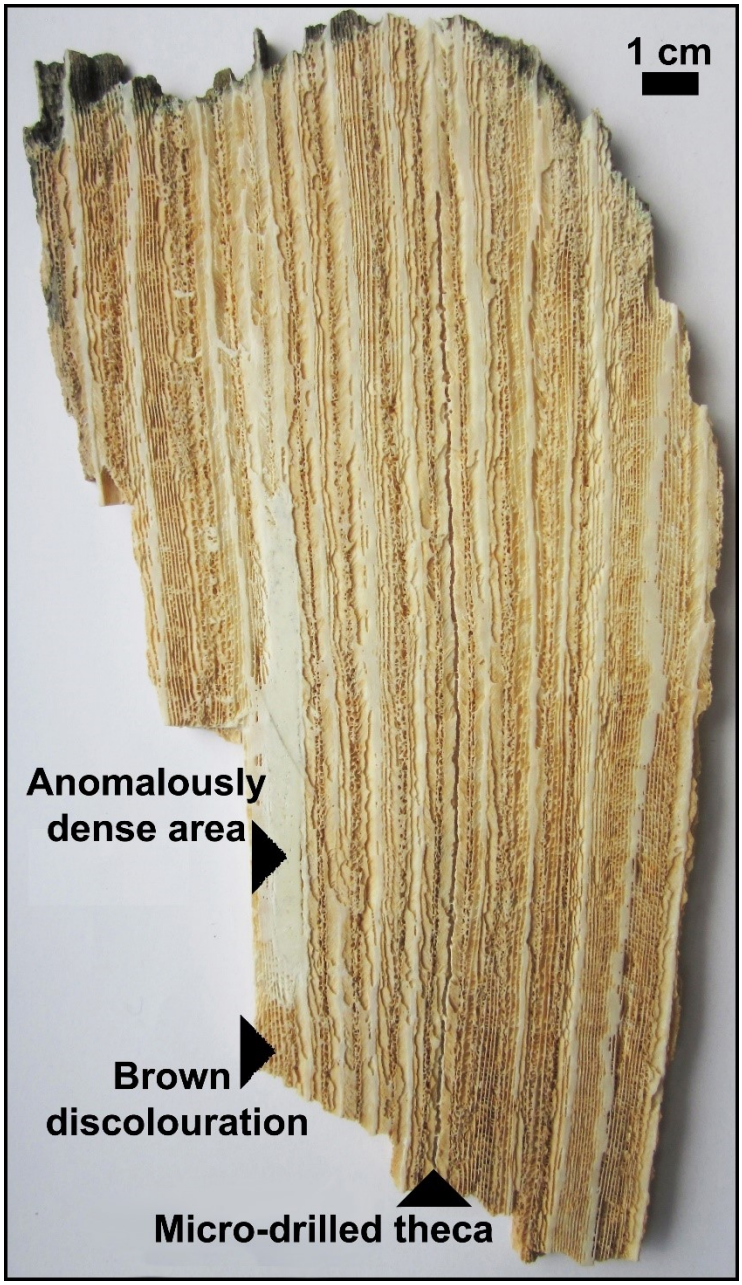

Plate 1.6: *Diploria strigosa* colony BON-17-AI dates to 121.7 ± 0.9 ka (Obert et al., 2016) but despite containing long thin thecae walls, the septum and columellae skeletal elements are noticeably discoloured.

Upon sectioning coral colony BON-17-AI (121.7 ± 0.9 ka), visual discolouration of porous skeletal elements (Plate 1.6) was observed and later found to result from secondary aragonite/calcite infillings when subjected to thin section analysis (Plate 1.7). This colony also differed by being obtained as a costal deposit that was fragmented, rather than drilled, from the reef terrace (Plate 1.8). Consistent with these early indicators of diagenetic alteration, bulk material samples ^{230}Th/U dated significantly younger than those dates obtained from thecae material, more so than other LIG dated coral records (Obert et al., 2016). However, the thecae was potentially unaltered and X-radiography of this colony suggested that, although thin,

geochemical sampling of the thecae elements would be possible. Unfortunately sampling resulted in a 21 year record that reconstructed an unrealistic Sr/Ca-SST seasonality of 7.1 ±0.6 °C (± 1 standard error, s.e) and very erratic Mg/Ca and $\delta^{13}C$ records that are indicative of diagenetic alteration. Despite the more reasonable $\delta^{18}O$-SST seasonality reconstruction of 4.1 ±0.2 °C, the combination of these factor justified the exclusion of this colony from further study. Nonetheless, the examining this colony serves as a good demonstration of assessing LIG *D. strigosa* potential to contain reliable palaeoclimatic records.

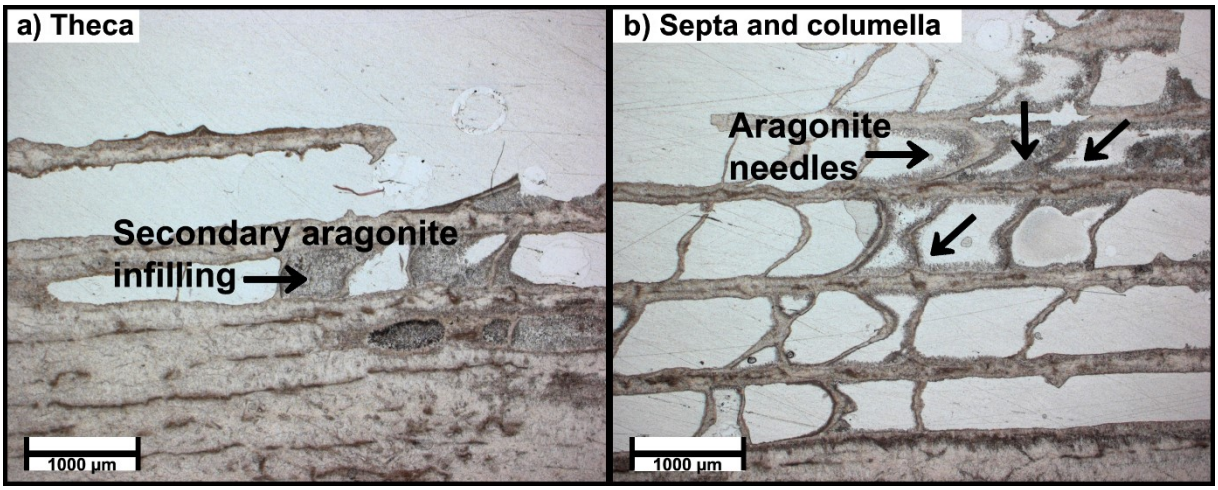

Plate 1.7: Thin section analysis of *Diploria strigosa* colony BON-17-AI, which dates to 121.7 ± 0.9 ka (Obert et al., 2016), reveals diagenetic alteration from secondary aragonite infilling near the theca and needles within the septa and columella skeletal elements.

Plate 1.8: *Diploria strigosa* colony BON-17-AI, which dates to 121.7 ± 0.9 ka (Obert et al., 2016), retrieved as a fragment cleaved off the lower reef terrace at Bonaire while drilling another colony. Green algae surface layer indicates exposure. Photographed coral supplied by Thomas Felis.

1.5 Motivations

One of the primary goals that motivates palaeoclimate study is the opportunity to extend instrumental climate records beyond the period of reliable observations. This is especially significant within the tropics which are typically represented geographically sparse instrumental records that rarely extend beyond 1950 AD. This limited coverage hinders the understanding of natural inter-annual to multi-decadal climate variability, which in the tropics, is associated with extreme climate events such as hurricanes and floods that hamper economic development (Gray, 1984; Wang et al., 2008, Jury et al., 2009). Moreover, the period documented by instrumental records is subject to anthropogenic influences, and so palaeoclimate records are required to capture natural variability. With palaeoclimate records, the contribution of natural climate variability to the largely anthropogenic induced global warming envisaged within the next century by multiple climate modelling assessments can be assessed (IPCC, 2013). Indeed, evidence suggests global warming will lead to increased climate sensitivity (Shaffer et al., 2016). The reliability of these ocean and climate models can be tested using palaeoclimatic records, which themselves benefit from the larger spatial coverage offered by simulations. Therefore, a holistic understanding of climate trends requires studies that implement complementary model/proxy assessments.

The well-known background climate forcings of insolation and greenhouse gases during the LIG offers a test-bed conducive to palaeoclimatic study of warmer than modern global temperatures. Climate proxy records contained within sediment and ice cores form the basis for characterising the LIG climate and the LIG is often used to test climate simulations. However, sediment and ice records typically constrain multi-decadal to millennial scale natural climate variability (Schmidt et al., 2006; Black et al 2007; Richey et al., 2009) providing a broad understanding of LIG climate evolution. These records also typically derive from the extra-tropics which experiences high amplitudes of change compared to modern. However, a tropical perspective is also required to further understand the mechanisms and consequences of natural climate variability. The temperature and hydroclimate of the tropical Atlantic plays an important role in modulating the behaviour of global climate phenomena, such as the ITCZ and AMOC (Leduc et al., 2007; Montaggioni and Braithwaite, 2009).

The large hemispheric structures built by the *D. strigosa* have proven valuable to palaeoclimatic study of natural climate variability. This is due to their skeletal structure forming annual density bands suitable for the generation of sub-seasonally resolved records (Giry et al., 2010) and their resilience to diagenetic disturbance. Within the tropical Atlantic *D. strigosa* are

more versatile to palaeoclimatic study than other tropical Atlantic coral species (Helmle et al., 2000). These attributes, alongside the ability of *D. strigosa* to accurately incorporate within their skeletal structure the properties of the waters they inhabit, ultimately motivates their study. By measuring paired Sr/Ca and $\delta^{18}O$ within the skeletal structures of *D. strigosa* (Kuhnert et al., 2005) the SST and hydroclimate variability of the tropical Atlantic can be quantified at sub-seasonal to multi-decadal time-scales. This has been done for modern times (Hetzinger et al., 2006; 2010; 2016; von Reumont et al., 2016), mid- to late Holocene (Giry et al., 2012; 2013) the late LIG (Felis et al., 2015). These studies provide the temporal context that motivates the first time use of *D. strigosa* within this thesis to study natural variability throughout multiple LIG time windows.

Within the tropical Atlantic live and fossil *D. strigosa* are found upon the south Caribbean island of Bonaire and are uniquely situated at the crossroad of a several climate phenomena that induce variability. While the modern SST regime at Bonaire is typical of the Caribbean Sea, its hydroclimate is not. This observation motivates the study of whether these regimes were altered in response to the variable behaviour of regional climate phenomena such as the AWP, ITCZ, ENSO and NAO on a variety of time-scales. During the LIG these phenomena were influenced by differing orbital parameters that increased the seasonality of insolation compared to modern, the flux of ice sheet discharge, cold events, oceanographic disruptions, ITCZ migration and periods of rapid sea level change. Bonaire fossil *D. strigosa* corals are potential recorders of these influences and ideal for multi-disciplinary assessments of natural climate variability and change during the LIG. With well-defined sub-seasonal resolved internal chronologies these rare coral records can also be averaged to provide an independent assessment of the spatiotemporal evolution of mean climatic conditions. This represents the next step in constraining natural climate variability that can be directly compared with the findings from sedimentary records and modelling assessments (Wendel, 2014).

1.6 Research hypothesise and objectives

Following the background and motivations outlined previously, here follows a summary of the main research questions (bold) and objectives this thesis aims to address;

If *D. strigosa* coral colonies from the lower reef terrace of Bonaire are sufficiently preserved then robust sub-seasonally resolved Sr/Ca and $\delta^{18}O$ records can be successfully generated for LIG palaeoclimatic reconstructions. The first aim is to assess the potential of massive *D. strigosa* colonies from Bonaire to generate robust sub-seasonally resolved Sr/Ca and $\delta^{18}O$ records during the LIG. Accordingly, prudent sampling strategies are devised that accommodate the complex skeletal architecture and its preservation within LIG $^{230}Th/U$ dated fossil corals. Such strategies aim to provide the ≥12 samples required to reliable capture seasonal cycles while also obtaining sufficient coral powder per sample to allow paired coral Sr/Ca and $\delta^{18}O$ measurements required for the simultaneous assessment of SST and hydroclimate (coral $\delta^{18}O_{seawater}$) variability.

If the LIG experienced an orbital configuration that promoted higher seasonality of insolation than modern, then tropical Atlantic SST and $\delta^{18}O_{seawater}$ seasonality should also be higher than modern. By achieving the objective of generating monthly resolved coral palaeoclimate records the seasonality of coral Sr/Ca and $\delta^{18}O$, $\delta^{18}O_{seawater}$ can be accurately quantified for the LIG. Such changes are likely to be indicative of orbital controls upon LIG climate evolution and phenomena as suggested by mid- to late Holocene, MIS 7 and 9 coral palaeoclimate records. Furthermore, provided records are of sufficient length, natural modes of variability can also be detected on inter-annual to multi-decadal timescales that, by modern analogy, are characteristic of the sources of LIG climate variability at Bonaire.

If modern *D. strigosa* Sr/Ca-SST, $\delta^{18}O$, $\delta^{18}O_{seawater}$ records are available from Bonaire, then how significant are SST and hydroclimate changes during the LIG? Modern *D. strigosa* records are available from Bonaire and can be utilised to incorporate potential uncertainties in the interpretation of LIG coral Sr/Ca-SST and $\delta^{18}O$ records. These modern records display inter-colony offsets that potentially reflect the unknown influences of differing inhabited water depths, locations and time intervals of fossil coral material. Incorporating these uncertainties is an aim of the error calculation applied to LIG coral material. Furthermore, similar mid- to late Holocene and early LIG coral palaeoclimate records are available from Bonaire that allow reconstructions from throughout the LIG to be put in context of the climate influences upon these times.

If Bonaire is influenced by tropical Atlantic climate phenomena, then to what extent do LIG coral Sr/Ca-SST, $\delta^{18}O$, $\delta^{18}O_{seawater}$ records characterise this region? Coral palaeoclimate records can be assessed alongside coupled ocean and climate LIG time-slice model simulations that can more easily establish regional climate patterns. These simulations can also be used to test assumptions made during the construction of coral palaeoclimate records, such as the similar timing of modern and LIG annual SST cycle. A combined coral and model approach can aim to identify the causal mechanics underpinning reconstructed SST and hydroclimate changes by identifying patterns associated with climate phenomena such as the AWP and ITCZ. Conversely, coral palaeoclimate records can test the ability of climate simulations to capture regional responses to the well-defined climate forcings of the LIG.

If Bonaire coral Sr/Ca-SST, $\delta^{18}O$, $\delta^{18}O_{seawater}$ records exhibit variability in response to tropical Atlantic climate phenomena and LIG climate drivers, was this sufficient to alter annual sea surface conditions from modern? In addition to the sub-seasonal to multi-decadal insights into climate variability, coral palaeoclimate records can aim to identify whether seasonal influences were sufficiently perturbed to alter mean tropical Atlantic sea surface conditions. Such changes are likely to reflect the influence of LIG climate drivers upon oceanic (AMOC) and climate phenomena (ITCZ). This approach also aims to supplement the few sedimentary records that are available for the tropical Atlantic that typically resolve millennia scales SST and hydroclimate change. Such an approach offers an assessment independent of potential uncertainties that some sedimentary derived palaeoclimate records are associated with, such as seasonal dependency.

1.7 Thesis outline

This PhD thesis is comprised of four chapters which are briefly described below. A single bibliography containing the all references can be found at the end.

Chapter 1 places the presented manuscripts within their scientific context by outlining the study areas regional significance, relevance to recent literature, approaches taken to address uncertainties and answer the scientific questions posed. With this background it is possible to understand the motivation and aims that underpin the presented studies.

Chapter 2 contains the three manuscripts which have either been prepared for, submitted to, or published in internationally recognised peer-reviewed journals. Each manuscript expands upon chapter one and details the relevant methodology.

Chapter 2.1 provides the first multi-coral reconstruction of SST seasonality within the tropical Atlantic during the LIG. Fossil *D. strigosa* coral Sr/Ca from 7 ^{230}Th/U dated colonies are described and diagenetically assessed. At total of 85 years of monthly revolved Sr/Ca-SST records are generated representing multiple time windows from throughout the LIG. The LIG evolution of coral Sr/Ca-SST is quantified and reflects orbital controls upon seasonality of insolation during that period. The natural range of SST seasonality is reconstructed and compared alongside coupled ocean and climate time-slice simulations, illustrating that the coral findings are indicative of SST seasonality within the wider tropical Atlantic realm. Distinct quasi-biennial and decadal modes of SST variability are documented within the LIG for the first time and demonstrate the close link between Atlantic climate patterns and Bonaire coral Sr/Ca-SST.

Chapter 2.2 expands upon the coral Sr/Ca records and findings of chapter 2.1 by presenting paired coral $\delta^{18}O$ records that allow LIG time windows of coral $\delta^{18}O_{seawater}$, a proxy for SSS and hydroclimate, to be constructed. Higher than modern mid-LIG seasonality of $\delta^{18}O_{seawater}$ is reconstructed alongside a distinct shift in the phase timing of paired coral Sr/Ca and $\delta^{18}O$ records. This indicates a hydroclimate regime change occurred during the LIG within the south Caribbean Sea, presently controlled by ocean advection with a small winter rain peak. Contemporaneous timeslice coupled ocean and climate simulations reveal that these coral finding reflect an increase in ITCZ induced precipitation that depleted summer $\delta^{18}O_{seawater}$. These model and coral findings offer the first evidence of the LIG northward expansion of the ITCZ from the north South American coastline into the southern Caribbean Sea.

Chapter 2.3 investigates the implications of chapters 2.1 and 2.2 coral findings upon the mean annual SST and hydroclimate at Bonaire. Mean annual coral Sr/Ca and $\delta^{18}O_{seawater}$ values are reconstructed for seven time windows throughout the LIG and reveal a transition from colder and fresher than modern SST at 125.8 ka toward comparably warm and saline sea surface properties at 123.7 ka that are maintained into the late LIG. This transition reflects the gradual northward progression of the ITCZ into the south Caribbean Sea which coincided with less ocean advection of colder and less saline tropical Atlantic surface waters which lead to a more precipitation influence hydroclimate. LIG coral Sr/Ca-SST findings are discussed in light of the uncertainties posed by current SST proxies that comprise recent mid-LIG tropical Atlantic SST compilations. Colder than modern mid-LIG mean annual coral Sr/Ca-SST supports tropical Atlantic annual mean sedimentary SST records derived from foraminifera transfer functions. Cumulatively, these findings have implications upon the variable strength of AMOC circulation during the LIG.

Chapter 3.0 summarises and draws parallels between the findings discussed in the manuscripts of chapter two to arrive at conclusions pertinent to the aims of this thesis.

Chapter 4.0 provides an overall outlook and suggests paths for future research based on the findings and conclusion of the manuscripts presented within this thesis.

All monthly interpolated coral Sr/Ca and $\delta^{18}O$ records have been made publically available to the PANGAEA database at;

Brocas, William M; Felis, Thomas; Obert, J Christina; Gierz, Paul; Lohmann, Gerrit; Scholz, Denis; Kölling, Martin; Scheffers, Sander R (2016): Monthly Bonaire coral Sr/Ca from the last interglacial, 120.5 -129.7 ka ago. PANGAEA, doi:10.1594/PANGAEA.862148

Brocas, William M**;** Felis, Thomas; Gierz, Paul; Lohmann, Gerrit**;** Werner, Martin**;** Obert, J Christina**;** Scholz, Denis**;** Kölling, Martin**;** Scheffers, Sander R (2017): Monthly Bonaire coral d18O and d18Oseawater from the last interglacial, 120.5 -129.7 ka ago. PANGAEA, doi:10.1594/PANGAEA.877852

2. Manuscripts

Manuscript I

Last interglacial temperature seasonality reconstructed from tropical Atlantic corals

Authors: **William M. Brocas**, Thomas Felis, J. Christina Obert, Paul Gierz, Gerrit Lohmann, Denis Scholz, Martin Kölling, Sander R. Scheffers

Status: Published in "Earth and Planetary Science Letters"

Citation: Brocas, W. M., T. Felis, J. C. Obert, P. Gierz, G. Lohmann, D. Scholz, M. Kölling and S. R. Scheffers (2016), Last interglacial temperature seasonality reconstructed from tropical Atlantic corals, Earth Planet. Sci. Lett. 449, 418-429, doi:10.1016/j.epsl.2016.06.005.

Manuscript II

Last interglacial hydroclimate seasonality reconstructed from tropical Atlantic corals

Authors: **William M. Brocas**, Thomas Felis, Paul Gierz, Gerrit Lohmann, Martin Werner, J. Christina Obert, Denis Scholz, Martin Kölling, Sander R. Scheffers

Status: Submitted to "Paleoceanography and Paleoclimatology"

Manuscript III

Corals evidence mid- last interglacial tropical Atlantic cooling and freshening

Authors: **William M. Brocas** and Thomas Felis

Status: Drafted and ready for submission to "Geophysical Research Letters"

Contribution of doctoral candidate to manuscripts

Manuscript I

a) Physical assessment of coral collections retrieved from Bonaire
b) Prepared coral material for diagenetic analysis and ^{230}Th/U dating
c) Micro-drilling and preparation ~3000 powder samples for geochemical analysis
d) Constructed reliable monthly coral Sr/Ca records, interpreted SST seasonality and performed multi-taper spectral analysis
e) Collaborated with modelling coauthors on the experimental design of LIG temperatures and interpreted findings.
f) Wrote the manuscript and led the successful publication process to "Earth and Planetary Science Letters"

Manuscript II

a) Micro-drilled ~3000 samples and prepared them for isotopic analysis
b) Interpreted $\delta^{18}O$ seasonality data and performed the required analysis
c) Used available coral Sr/Ca data to convert coral $\delta^{18}O$ into coral $\delta^{18}O_{sewater}$, and performed spectral analysis on records.
d) Assessed and interpreted coral $\delta^{18}O_{sewater}$ data
e) Collaborated with modelling coauthors on the experimental design of LIG precipitation and interpreted findings.
f) Wrote the manuscript and leads the submission process to "Paleoceanography and Paleoclimatology"

Manuscript III

a) Complied LIG coral Sr/Ca, $\delta^{18}O$ and $\delta^{18}O_{seawater}$ data into mean annual averages
b) Compiled available mid-LIG tropical Atlantic mean annual sedimentary records
c) Interpreted coral and sedimentary records for temperature and hydroclimate anomalies from present
d) Prepared the manuscript for submission to "Geophysical Research Letters" and will lead this process

2.1 Last interglacial temperature seasonality reconstructed from tropical Atlantic corals

Authors: William M. Brocas[1], Thomas Felis[1], J. Christina Obert[2], Paul Gierz[3], Gerrit Lohmann[3], Denis Scholz[2], Martin Kölling[1] and Sander R. Scheffers[4]

[1]MARUM - Center for Marine Environmental Sciences, University of Bremen, 28359 Bremen, Germany

[2]Institute for Geosciences, Johannes Gutenberg University Mainz, 55099 Mainz, Germany and Biogeochemistry Department, Max Planck Institute for Chemistry, 55020 Mainz, Germany

[3]Alfred Wegener Institute, Helmholtz Centre for Polar and Marine Research (AWI), 27570 Bremerhaven, Germany

[4]National Marine Science Centre, Southern Cross University, Coffs Harbour, NSW 2480, Australia

Corresponding author:
William M. Brocas, MARUM - Center for Marine Environmental Sciences, University of Bremen, 28359 Bremen, Germany (wbrocas@marum.de) (tel: +4942121865665)

Highlights

- Tropical Atlantic coral Sr/Ca reveals last interglacial temperature variability
- Coral and climate model results show increased temperature seasonality at ~125 ka
- Early and late last interglacial temperature seasonality was similar to modern
- Last interglacial temperature seasonality co-varies with insolation seasonality
- Mid last interglacial tropical Atlantic decadal temperature variability is hinted

Keywords

Coral Sr/Ca, the last interglacial, Caribbean climate, sea surface temperature,
Quasi-biennial to decadal variability

2.1.1 Abstract

Reconstructions of last interglacial (LIG, MIS 5e, ~127-117 ka) climate offer insights into the natural response and variability of the climate system during a period partially analogous to future climate change scenarios. We present well-preserved fossil corals (*Diploria strigosa*) recovered from the southern Caribbean island of Bonaire (Caribbean Netherlands). These have been precisely dated by the ^{230}Th/U-method to between 130 and 120 ka ago. Annual banding of the coral skeleton enabled construction of time windows of monthly resolved strontium/calcium (Sr/Ca) temperature proxy records. In conjunction with a previously published 118 ka coral record, our eight records of up to 37 years in length, cover a total of 105 years within the LIG period. From these, sea surface temperature (SST) seasonality and variability in the tropical North Atlantic Ocean is reconstructed. We detect similar to modern SST seasonality of ~2.9 °C during the early (130 ka) and the late LIG (120 - 118 ka). However, within the mid-LIG, a significantly higher than modern SST seasonality of 4.9 °C (at 126 ka) and 4.1 °C (at 124 ka) is observed. These findings are supported by climate model simulations and are consistent with the evolving amplitude of orbitally induced changes in seasonality of insolation throughout the LIG, irrespective of wider climatic instabilities that characterised this period. The climate model simulations suggest that the SST seasonality changes documented in our LIG coral Sr/Ca records are representative of larger regions within the tropical North Atlantic. These simulations also suggest that the reconstructed SST seasonality increase during the mid-LIG is caused primarily by summer warming. A 124 ka old coral documents, for the first time, evidence of decadal SST variability in the tropical North Atlantic during the LIG, akin to that observed in modern instrumental records.

2.1.2 Introduction

Reliable assessments of past natural climate variability are required to further evaluate the strength of modelled future climate projections, which often underestimate the extent of regional impacts (Braconnot et al., 2012). The last interglacial (LIG, Marine Isotope Stage (MIS) 5e, 127-117 ka) is often regarded as semi-analogous to, and thus a test-bed for, future climate change scenarios. However, warmer than present global temperatures during the LIG resulted from differing orbital configurations as opposed to increased anthropogenic emissions in recent climate change scenarios (Yin and Berger, 2010). Although the primary driver of climatic change differs, the LIG remains an important test-bed for climate sensitivity studies within a warmer than present day earth system (Lunt et al., 2013). The LIG was punctuated by profound changes and instabilities. However, as demonstrated by a water hosing experiment performed on model simulations of LIG climate and a coral proxy record (Felis et al., 2015), temperature seasonality in the tropical Atlantic was relatively insensitive to the influences of monumental ice sheet loss (Blanchon et al., 2009), sea level rise (O'Leary et al., 2013), rapid reorganization of oceanic currents (Galaasen et al., 2014), cold events (Mokeddem et al., 2014) and abrupt climatic shifts (Sirocko et al., 2005).

Tropical Atlantic climate variability plays a significant role in large-scale climate patterns and although much is known of its modern variability, the implication of past changes to this system requires further study. In the Caribbean basin, sea surface temperature (SST) variability is a result of variations in North Atlantic sea level pressure that modulates surface winds and induces fluctuation to the Atlantic Warm Pool (AWP). The AWP is characterised by surface waters warmer than 28.5 °C located in the tropical Atlantic (Fig. 2.1) and experiences fluctuations on seasonal, inter-annual and multi-decadal time-scales (Wang et al., 2008). On these latter two time-scales, the ENSO and AMO perturb the AWP, respectively. The climate of the tropical Atlantic is determined by the maximum extent to which the AWP penetrates during boreal summer. Fluctuations in hurricane activity and Nordeste (Brazil) and Sahel rainfall originate from within the tropical Atlantic region. This region is at the crossroads of multiple modes of variability that derive from the tropical and extra-tropical oceans (Czaja, 2004) where a dominant upwelling system, trade winds and currents preside (Jury, 2009). SST and regional rainfall patterns therefore express behaviours related to these influences and are of broad interest due to their association with decadal shifts in Caribbean socio-economic output (Jury, 2009). However, the effect of projected climate change on such modes/trends in SST variability remains uncertain.

Coral archives, when supplemented by reliable ^{230}Th/U ages, can contribute seasonally resolved time windows for the assessment of past tropical climate variability. LIG Pacific *Porites* corals have characterised ENSO variability (Hughen et al., 1999; Tudhope et al., 2001) TII (McCulloch et al., 1999) and modulations to the Kuroshio Current (Suzuki et al., 2001). The latter two studies reported similar to and increased western Pacific SST seasonality, respectively, compared with modern for their periods of study within the LIG. Increased LIG SST seasonality has been reported in the northern Red Sea from a 122 ka coral and accredited primarily to enhanced winter cooling as a result of a tendency towards a more positive state of the North Atlantic Oscillation (NAO) at that time (Felis et al., 2004). Representation of tropical Atlantic SST seasonality during the LIG is so far limited to two coral studies from the Caribbean. A 4-year strontium/calcium (Sr/Ca) *Montastraea faveolata* record from 127 ka recorded SST seasonality 1 °C higher than present (Winter et al., 2003), while a 20-year *Diploria strigosa* Sr/Ca record at the end of the LIG (118 ka) reconstructed SST seasonality within the present-day range (Felis et al., 2015). Prior to the LIG, three *Porites* sp. coral studies explored SST seasonality during interglacial periods at different South Pacific islands. During MIS 7 at 197 ka, SST seasonality was reported as identical to modern (Asami et al., 2013). Likewise, during MIS 9 (337 - 374 ka), SST seasonality was found to be similar to modern (Kilbourne et al., 2004) and enhanced by up to 15% (Ayling et al., 2006), respectively. These studies attribute orbital configuration influencing regional insolation as the primary mechanism behind the observed tropical SST variability. However, all these studies draw their conclusions from a single coral based time window during their respective interglacials.

Here we assess past tropical Atlantic climate variability by quantifying the range of SST seasonality and identifying modes of SST variability during several coral-based time windows throughout the LIG. We implement Sr/Ca palaeothermometry on precisely dated fossil specimens of *D. strigosa* corals that inhabited the shallow tropical waters of the southern Caribbean island of Bonaire (Caribbean Netherlands). The annually banded aragonite skeleton of *D. strigosa* is suitable for precision micro-sampling techniques (Hetzinger et al., 2006, 2010; Giry et al., 2010, Giry et al., 2012, 2013; Felis et al 2015). Coral Sr/Ca variations are a well-established proxy for SST variability on seasonal (Gagan et al., 1998), inter-annual (Felis et al., 2009) and multi-decadal time-scales (Linsley et al., 2000). The reconstruction of Sr/Ca-based SST seasonality is not affected by glacial/interglacial changes in the Sr content of seawater as a result of dissolution of shelf carbonates during glacial sea level low stands nor its residence time, which is on the order of millions of years (Stoll et al., 1999). These concerns typically affect reconstructions of absolute SST on these time-scales (Kilbourne et al., 2004; Asami et

al., 2013; Felis et al., 2012, 2014). Sr/Ca variations within *D. strigosa* have been successfully demonstrated to replicate Caribbean instrumental temperature trends during the past century (Hetzinger et al., 2006, 2010), highlighting the importance of site specific modern day records for the interpretation of palaeoclimatic reconstructions. Our study benefits from being able to assess SST variability based on *D. strigosa* coral Sr/Ca records from Bonaire (southern Caribbean) in the context of the modern day, the mid- to late Holocene (Giry et al., 2012, Giry et al., 2013) and the end of LIG (Felis et al., 2015). Our well-preserved coral material allows further explorations of the factors affecting tropical Atlantic SST variability for multiple occasions throughout the LIG.

2.1.3 Material and methods

2.1.3.1 Study area and environmental setting

The island of Bonaire (~12°10'N, 68°18'W) is situated ~100 km off the north coast of Venezuela in the open ocean setting of the Lesser Antilles island arc, southern Caribbean Sea (Fig. 2.1). Bonaire is characterised by a semi-arid climate, receiving less than ~550 mm/yr, while easterly trade winds predominate. These trade winds are commonly referred to as the Caribbean low level jet and vary in close connection with the North Atlantic subtropical high. Seasonal SST varies between a mean winter (February-March) minimum of 25.8 ± 0.6 and a mean summer (September-October) maximum of 28.3 ± 0.5 °C (± 1 standard deviation) throughout the years 1910 - 2000 AD (ERSSTv3b, Smith et al., 2008).

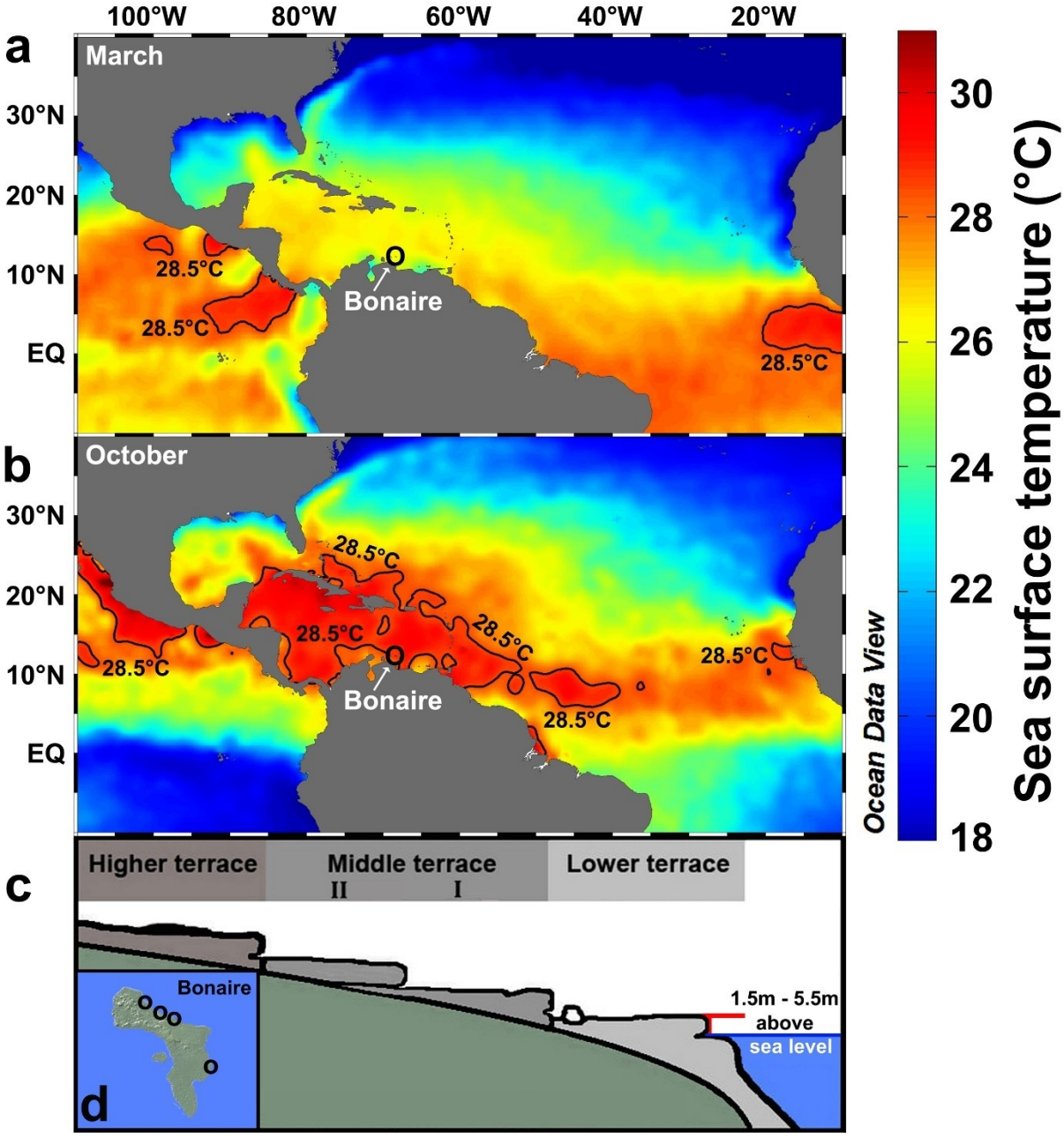

Figure 2.1: Environmental setting of fossil Bonaire corals (circle). Tropical Atlantic sea surface temperatures (Locarnini et al., 2013) representing the coolest month, March (a), and the warmest, October (b), at Bonaire. The Atlantic warm pool, is denoted by SST contours of greater than 28.5 °C. (c) Adapted geological schematic of elevated reef terraces along the coastline of Bonaire (Kim and Lee, 1999). The corals used in this study were recovered from four sites on the lower terrace (d) that formed during the last interglacial period (Felis et al., 2015, Obert et al., 2016).

2.1.3.2 Coral material

Cores from 32 fossil *Diploria strigosa* colonies were drilled during expeditions in 2006 and 2009 on top of an elevated reef terrace along the north-eastern and eastern coast of Bonaire (Caribbean Netherlands, Fig. 2.1d). Coral material was obtained between ~1.5 to ~5.5 m above present sea level and between ~20 to ~88 m from the present-day sea cliff edge. This conforms to the lower terrace described by Kim and Lee (1999) (Fig. 2.1c), which formed during the LIG (Felis et al., 2015; Obert et al., 2016). This feature typifies much of the northern and eastern coastline of Bonaire. Drilled coral cores were visually inspected and sectioned parallel to growth direction, as determined from the orientation of corallites. Thin cross sections (slabs) of 6 - 7 mm were sliced, which exposed the internal structures of each colony. Thus, it was possible to target the path of micro-sampling directly parallel to growth. Seven colonies were selected based on their suitability to produce the longest and most reliable geochemical records, while reflecting the broad geographical range of material retrieved from Bonaire. This study followed established procedures outlined by Felis et al. (2009), Giry et al. (2010) and Giry et al. (2012).

2.1.3.3 Screening for diagenesis

Coral slabs were initially subjected to X-radiography in order to establish the presence of clearly identifiable density banding. This also acts as a preliminary indicator of preservation and aids the assessment of skeletal theca elements suitable for directing micro-sampling paths. X-radiography also serves to highlight regions within the coral slab to be avoided due to abnormally high or low density that likely results from diagenetic alteration. The dense theca skeletal element has been previously identified as the most suitable target source within *D. strigosa* for yielding Sr/Ca records (Hetzinger et al., 2006; Giry et al., 2010). Once the target theca was identified within each of the seven selected colonies, parallel sections of mixed coralline skeletal elements were screened for preservation. Firstly, to quantify the calcite content of the aragonite skeleton, samples were finely ground and subjected to powder X-Ray diffraction analysis (powder XRD). Petrographic thin sections assessed under transmitted and cross/polarised light visualised any secondary aragonite or calcite cements.

2.1.3.4 Micro-sampling, Sr/Ca analysis, chronology building and spectral analyses

Visual slab surface inspection and indications from X-radiographs of coralline density allowed for the identification of theca skeletal wall elements that had suitable orientation to maximise the yield of coral powder micro-sampling. An estimate of average coral growth rates was made with further reference to the annual density bands seen in the X-radiographs. Based on these rates, continuous micro-sampling paths of either 0.4 or 0.5 mm interval spacing along the theca were used to ensure that approximately twelve samples were obtained per year, in

accordance with established procedures (Giry et al., 2010, 2012; Felis et al., 2015). These sampling paths were created using a 0.6 mm diameter drill-bit along the centre of the theca, to a depth of 2 mm. Subsequent geochemical analysis, visual inspection and additional X-radiographs confirmed that the sampling path had been precise. This ensured that the targeted theca has been milled and contamination from adjacent skeletal elements had been avoided. Approximately 0.30 - 0.35 mg of the milled coral powder was collected, weighed and dissolved in 4.0 ml of 2% suprapure HNO_3 containing 1 ppm Scandium. Coral Sr/Ca measurements were performed using an ICP-OES at MARUM (University of Bremen). Offline corrections for instrumental drift were accounted for after each sample using a laboratory coral standard. Analysed identically to our samples, 74 sub-samples of coral powder reference material JCp-1 (Hathorne et al., 2013) were measured, and the average Sr/Ca value was 8.902 ± 0.020 mmol/mol. Only Sr/Ca measurements with ≤ 0.2% relative standard deviation were assessed further.

Sr/Ca records were assigned age models based on X-radiograph inferred annual density banding and annual cycling of Sr/Ca seen in the records themselves. With the support of our climate modelling simulations, we determined that the timing of the maximum (September-October) and minimum (February-March) annual SST cycle did not change during the last interglacial (LIG) from that seen in present day SST records (Smith et al., 2008). Annual maximum and minimum Sr/Ca values were therefore assigned as tie-points to the coldest (February-March) and warmest (September-October) months, respectively. Monthly time series were generated by following the established procedures of Felis et al. (2009) and Giry et al. (2010). Thereby, a monthly time series of Sr/Ca results from linear interpolation between these tie-points and subsequent interpolation to monthly resolution. Annual skeletal growth rates were determined by taking the distance between the maximum Sr/Ca values of each individual year, to that of the next. The average of all years on record resulted in the mean coral growth rate. Within any given year, the Sr/Ca seasonality was calculated by subtracting the maximum (coldest) from the minimum (warmest) monthly value, from the oldest toward the youngest part of the record. The average of all years on record resulted in the mean Sr/Ca seasonality value, which was then converted to SST seasonality using the seasonal Sr/Ca-SST relationship of -0.042 mmol/mol per ^{o}C for *D. strigosa* (Hetzinger et al., 2006). Recent studies have supported the close range of Caribbean *D. strigosa* monthly Sr/Ca-SST calibration slopes, reporting values of -0.040 (von Reumont et al., 2016) and -0.046 (Xu et al., 2015) mmol/mol/°C. We employed the Hetzinger et al. (2006) calibration because it derives from amongst the longest modern *D. strigosa* record and its use closely replicates the instrumental SST seasonality at Bonaire

(ERSSTv3b; Smith et al., 2008), as demonstrated by Giry et al. (2012) using three modern *D. strigosa* colonies. Multi-taper method spectral analysis (Ghil et al., 2002) was applied to the detrended and normalised monthly interpolated (with the mean annual cycle removed) and seasonally collated (winter: December to February; spring: March to May; summer: June to July; autumn: September to November) coral Sr/Ca records. Significance relative to a red noise null hypothesis was established using a robust method of noise background estimation (Mann and Lees, 1996) (three tapers; bandwidth parameter two).

2.1.3.5 Coral ^{230}Th/U dating

^{230}Th/U-ages of our coral colonies were determined using precise ^{230}Th/U-dating at the Max Planck Institute for Chemistry, Mainz, Germany. (Obert et al., 2016). Here, we only briefly summarise this study. Several sub-samples of each coral were taken for ^{230}Th/U-dating using a Nu Plasma multi-collector inductively coupled plasma mass spectrometer (MC-ICPMS). Some sub-samples were comprised of mixed coralline structures, which is typical for this type of analysis, while others consisted only of the dense theca element. These dense theca wall samples are generally better preserved, show less evidence for post-depositional diagenetic alteration and provide more reliable ages (Obert et al., 2016). Here, the following six criteria were used to assess the reliability of coral ages.

- The existence of primary aragonitic textures
- Calcite content ≤ 2%
- ^{238}U concentration within the range of the respective modern coral species
- <1 ng g^{-1} ^{232}Th content
- $(^{234}U/^{238}U)_i = 1.1468 \pm 0.004$
- Different sub-samples of the same coral have ^{230}Th/U-ages and activity ratios in agreement within error

^{230}Th/U-ages are considered as "strictly reliable" if all criteria are fulfilled, "less strictly reliable" if the initial ($^{234}U/^{238}U$) activity ratio is within 1.1468 ± 0.008, as opposed to ± 0.004, and "moderately reliable" if the ^{232}Th content was also larger than 1 ng g^{-1} (Obert et al., 2016). For multiple determinations of an individual coral, we use the weighted mean and weighted standard error of the sub-samples to calculate the age (Table 2.1). All ages are presented as thousand years ago (ka) before the year of measurement (AD 2014). Uncertainties are quoted at the 2σ-level.

Sample I.D	No. of ages [a] (Bulk + Theca)	Age [a] (ka)	Standard deviation/error [a] (± 2 s.d./s.e.) (ka)	Calcite content [b] (%)	Annual growth rate (cm/yr) (± 1 s.d.)	Sampling resolution (samples/yr) (± 1 s.d.)	Record length (yr)	Sr/Ca seasonality (mmol/mol) (± 1 s.e.)	Sr/Ca-SST [c] seasonality (°C) (± 1 s.e.) (± 1 c.e.)
BON-5-D*	1 (1+0)	117.7	0.8	<1%	0.68 (0.15)	11 (2)	20	0.109 (0.003)	2.6 (0.1) (0.8)
BON-5-A	6 (2+4)	120.5	1.1	≤1%	0.48 (0.10)	15 (3)	14	0.129 (0.011)	3.1 (0.3) (0.8)
BON-28-AI	2 (0+2)	123.3***	3.1***	≤1%	0.84 (0.29)	17 (5)	6	0.128 (0.013)	3.0 (0.3) (0.9)
BON-12-A	4 (2+2)	123.9	1.3	≤1%	0.60 (0.15)	13 (3)	37	0.172 (0.008)	4.1 (0.2) (0.8)
BON-26-A	2 (0+2)	124.9	1.9	≤1%	0.63 (0.08)	13 (6)	3	0.139 (0.016)	3.3 (0.4) (0.9)
BON-24-AII.2	3 (1+2)	125.5	2.4	≤2%	0.62 (0.07)	14 (2)	5	0.139 (0.019)	3.3 (0.5) (0.9)
BON-13-AI.1	1 (0+1)	125.8	1.6	≤1%	0.74 (0.17)	16 (5)	10	0.205 (0.023)	4.9 (0.5) (1.0)
BON-33-BI.2	1 (0+1)	129.7**	1.7**	≤1%	0.71 (0.24)	13 (5)	10	0.128 (0.015)	3.0 (0.4) (0.9)

Table 2.1: Details of the coral Sr/Ca records employed in this study.
(*) A previously published late last interglacial coral form Bonaire (Felis et al., 2015). (a) A full assessment of dating different skeletal elements and criteria used to determine less strictly reliable (**) and moderately reliable ages (***) are available from Obert et al. (2016). All other ages are considered strictly reliable (section 2.1.3.5). To calculate the age when multiple determinations of an individual coral existed, the weighted mean and weighted standard error of the sub-samples was used. (b) Powder X-ray diffraction to quantify the calcite content of the coral material. (c) Coral Sr/Ca-SST seasonal relationship of -0.042 mmol/mol per °C was used (Hetzinger et al., 2006) and the ± 1 standard error (s.e.) and combined error (c.e.) considered.

2.1.3.6 Climate model set-up and experimentation

We performed numerical simulations using the coupled general atmosphere-ocean circulation model COSMOS developed originally at the Max Planck Institute for Meteorology, Hamburg, Germany. COSMOS (Jungclaus et al., 2010) is comprised of an atmospheric model ECHAM5, an ocean model MPIOM, and a dynamical vegetation model JSBACH. Further details underpinning the models incorporated into COSMOS can be found in Stepanek and Lohmann (2012) and Felis et al. (2015). Orbital and greenhouse gas parameters identical to those used in the Paleoclimate Modelling Intercomparison Project (Table 2.2) are employed and values evaluated after a spin up of 2500 years. We conduct four equilibrium simulations using 100 pre-industrial and 400 LIG years to evaluate modelled North Atlantic SST seasonality during the pre-industrial, 120, 125 and 130 ka for a 1°x1° gridbox centred at 12.5°N, 68° W. These time-slice experiments supplement COSMOS transient simulations of the LIG SST seasonality utilised in Felis et al. (2015).

Table 2.2: Characteristics of the relevant forcings of carbon dioxide (CO_2), methane (CH_4), nitrous oxide (NO_2) and orbital parameters applied to our time-slice equilibrium simulations, using the coupled atmosphere-ocean general circulation model COSMOS. Experiments are representative of the pre-industrial period (P.I.), 120, 125 and 130 ka (LIG120, LIG125 and LIG130, respectively). The extent of ice sheets is fixed to that of the pre-industrial period.

Experiment	CO_2 (ppm)	CH_4 (ppb)	NO_2 (ppb)	Eccentricity	Obliquity	Precession
PI	280	760	270	0.017	23.446	282.040
LIG120	268	261	261	0.041	22.998	209.040
LIG125	276	263	263	0.040	23.790	127.140
LIG130	257	238	238	0.038	24.246	48.320

2.1.4 Results

2.1.4.1 Skeletal preservation of fossil *Diploria strigosa* corals

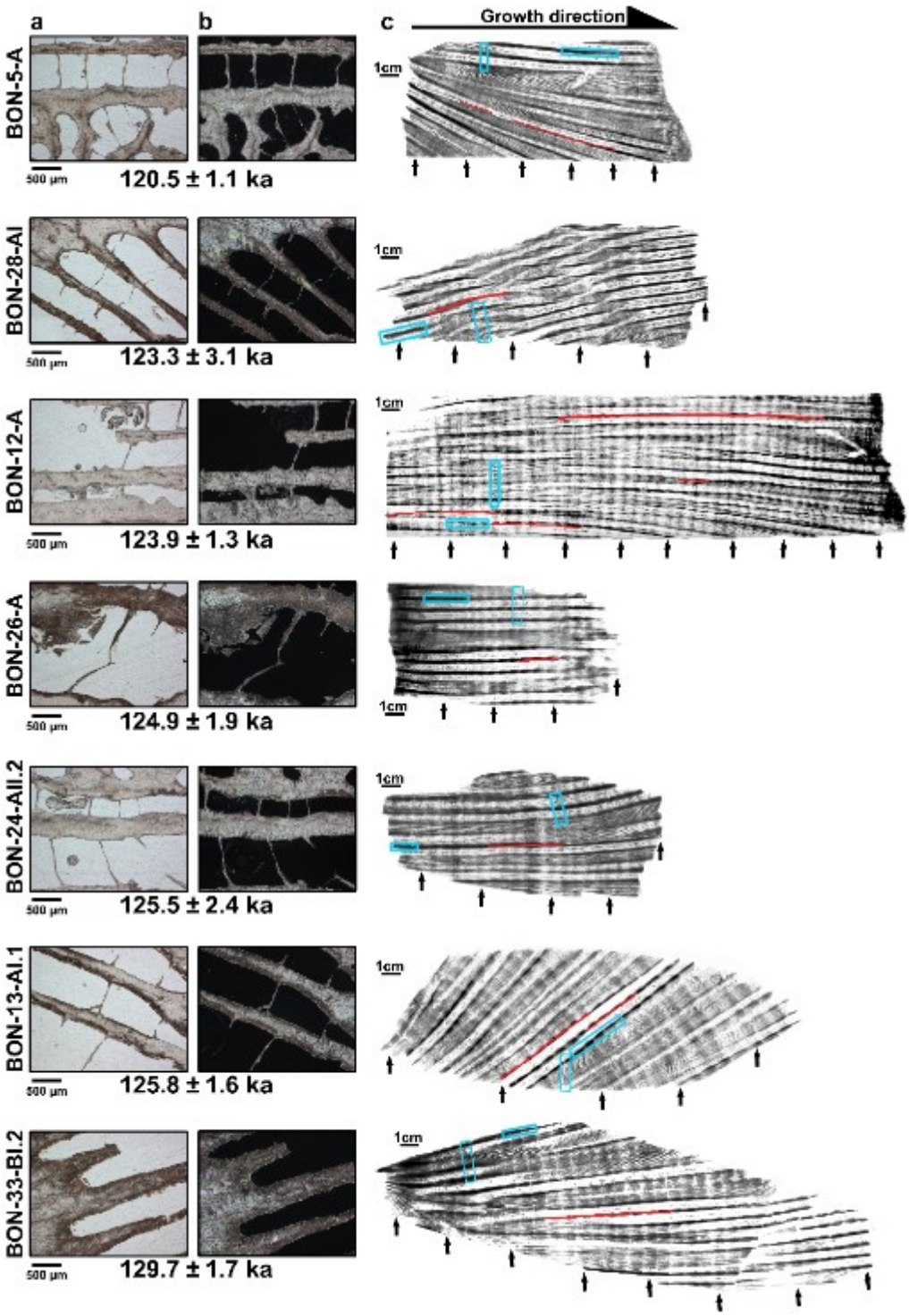

Figure 2.2: Visual assessment of coral slabs arranged according to ^{230}Th/U- ages (descending = older). Thin section images of fossil *Diploria strigosa* colonies using (a) transmitted and (b) cross-polarised light microscopy at x5 magnification (bar = 500 µm). (c) Positive print X-radiographs of coral slabs reveal preserved skeletal elements and density banding in all colonies regardless of age. Red lines denote Sr/Ca analysis sampling paths along theca skeletal elements.

Boxes indicate sampled ^{230}Th/U-dating sections. Black arrows = five-year intervals of annual high-low density band pairs. Bar denotes 1 cm.

Clear and distinct density banding patterns are observed within the X-radiographs of our seven fossil coral colonies (Fig. 2.2c) and are comparable to the annual density-band pairs reported for modern, mid- to late Holocene and late LIG *D. strigosa* corals from Bonaire (Giry et al., 2012; Felis et al., 2015). The X-radiographs indicate that regions of abnormal skeletal density, which typify areas of diagenetic alteration, were avoided. Powder XRD analysis of bulk skeletal material defined the calcite content of six of our seven fossil colonies to be ≤ 1% (Table 2.1). BON-24-AII.2 contained ≤ 2% calcite, which is within acceptable levels for the purposes of our investigations and consistent with other LIG coral palaeoclimatic studies (Felis et al., 2004). Representative thin section images (Fig. 2.2 a-b) revealed that the majority of skeletal elements were free of secondary aragonite cement. On the rare occasion that these were noted, they were found to exist in the porous septum and columellae skeletal elements of the coralline structure and not the theca from which geochemical sampling was targeted. Therefore, we consider our corals well preserved and suitable for palaeoclimatic reconstructions.

2.1.4.2 Coral ^{230}Th/U ages

Following the reliability criteria established by Obert et al. (2016), five of the seven corals have strictly reliable ages (Table 2.1). Although passing all other criteria, the age of coral colony BON-33-BI.2 age is deemed "less strictly reliable" as the age has an (^{234}U/^{238}U) activity ratio equal to 1.1468 within ± 0.008 rather than ± 0.004. In addition, the two ages determined for BON-28-A showed a ^{232}Th content ≥ 1 ng g^{-1}. Thus, we consider the age of this sample "moderately reliable". The majority of ^{230}Th/U-ages cluster around peak LIG conditions (123.3 ± 3.1, 123.9 ± 1.3, 124.9 ± 1.9, 125.5 ± 2.4, 125.8 ± 1.6 ka) while BON-5-A and BON-33-BI.2 grew during the late (120.5 ± 1.1 ka) and early (129.7 ± 1.7 ka) LIG, respectively. Thus our coral Sr/Ca records reflect a broad range of time intervals throughout the LIG.

2.1.4.3 Coral Sr/Ca derived SST time windows during the LIG

Throughout the LIG, we present 85 years of monthly resolved Sr/Ca records from seven fossil corals, representing time windows of between 3 and 37 years (Fig. 2.3). In addition, we make use of a previously published 20 year monthly coral Sr/Ca record from Bonaire (117.7 ± 0.8 ka) (Felis et al., 2015). Annual cycles within the Sr/Ca records are distinct and correspond to the annual density pattern observed in the X-radiographs. Robust internal chronologies were established that facilitate the interpretation of LIG seasonal to inter-annual SST variability. The details underpinning the Sr/Ca records can be found in Table 2.1. Within our Sr/Ca records that

comprise of sampling from multiple theca wall elements within the same colony (BON-12-A and BON-13-A1.1) we detect no anomalous shifts in mean Sr/Ca or reconstructed SST seasonality. Although relationships between growth rates and Sr/Ca ratios have been suggested or other coral species (Goodkin et al., 2007), we found no correlation between *D. strigosa* growth rates and annual mean Sr/Ca or Sr/Ca seasonality values.

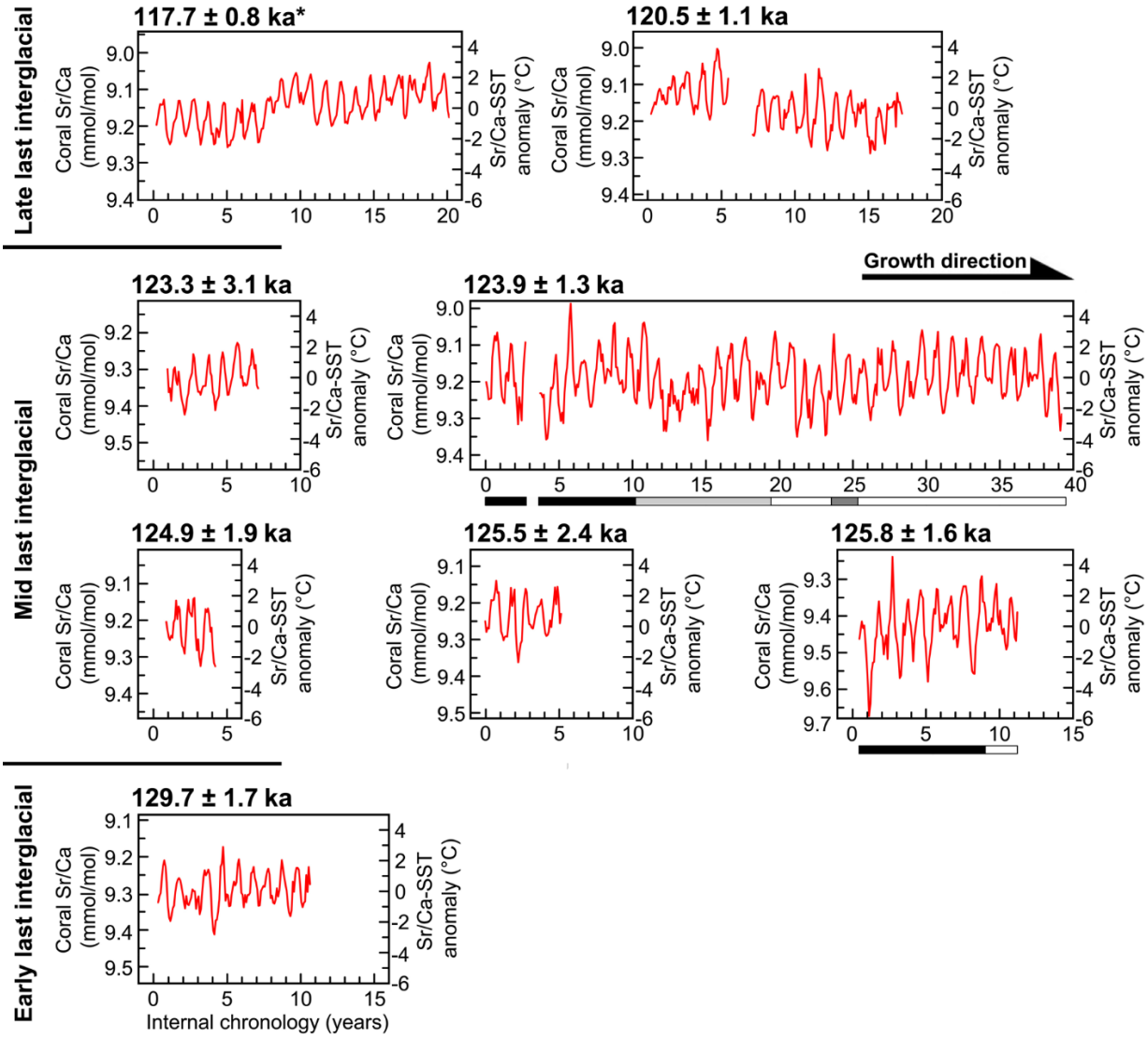

Figure 2.3: Monthly resolved Sr/Ca records from last interglacial Bonaire corals (*Diploria strigosa*), arranged based on ^{230}Th/U-ages for the early, mid- and late interglacial. Associated sea surface temperature (SST) anomalies were calculated using the seasonal Sr/Ca-SST relationship of -0.042 mmol/mol per °C (Hetzinger et al., 2006) for *D. strigosa*. Growth direction is from left to right, older to younger. (*) A coral record from Felis et al. (2015). Records comprised of samples from different overlapping theca walls within a colony are indicated by a horizontal line (greyscale shading = sampled theca).

2.1.4.4 Coral Sr/Ca seasonality throughout the LIG

Mean modern instrumental seasonality of SST surrounding Bonaire is 2.9 ± 0.5 °C (±1 standard deviation, s.d., 1910-2000 AD) (Smith et al., 2008). Employing the seasonal Sr/Ca-SST relationship of -0.042 mmol/mol per °C for *D. strigosa* (Hetzinger et al., 2006), this has been successfully reconstructed using three modern *D. strigosa* colonies from Bonaire, which recorded mean SST seasonality as 2.8 ± 0.4 °C (± 1 s.d.) (Giry et al., 2012). The use of other monthly Sr/Ca-SST calibration slopes (Giry et al., 2012; Xu et al., 2015; von Reumont et al., 2016) alters mainly the absolute amplitude of reconstructed SST seasonality but has only minor effects on the relative SST seasonality estimates exhibited by our specific corals. We note that modern coral-based SST seasonality ranges from 2.4 ± 0.3 to 3.0 ± 0.3 °C (± 1 standard error, s.e.), reflecting inter-colony differences, which are not associated with different sampling resolutions, growth rates or real differences in SST seasonality over the last century. Consequently, our Sr/Ca derived LIG SST seasonality reconstructions implement the s.e. of an individual fossil coral. Although it's not possible to identify the exact palaeo-reef environment (fore or back reef) each coral grew within, we find no evidence such as anomalous growth in our LIG records, which would be indicative of the influence of different reef environments (water depths) on SST seasonality. To address this uncertainty we additionally consider the combined error (c.e.) of Abram et al. (2009) which incorporates differences between the reconstructed mean SST seasonality from three modern Bonaire corals (Giry et al., 2012). The c.e. is derived from the combination (root of the sum of the squares) of 1) the standard deviation (2 s.d.) of the reconstructed mean Sr/Ca seasonality value from three modern corals and 2) the standard error (2 s.e.) surrounding the mean of all Sr/Ca seasonality on record within each fossil coral. We examine individual coral errors relative to the s.d. of Sr/Ca-SST seasonality from the three modern corals. The details underpinning our coral Sr/Ca records (Table 2.1) are consistent with those reported by Giry et al. (2012) and other LIG coral records (Felis et al., 2004; Felis et al., 2015).

Compared to the modern coral reconstructed mean SST seasonality of 2.8 ± 0.4 °C (± 1 s.d.) (Fig. 2.4), we find that our oldest coral at 129.7 ± 1.7 ka records a similar seasonality of 3.0 ± 0.4 °C (± 1 s.e.) during the early LIG. Three of five mid-LIG corals, which contain ≤ 6 years, record a similar to modern SST seasonality of 3.3 ± 0.5 °C (± 1 s.e.), 3.3 ± 0.4 °C (± 1 s.e.) and 3.0 ± 0.3 °C (± 1 s.e.) at 125.5 ± 2.4, 124.9 ± 1.9 and 123.3 ± 3.1 ka, respectively.

However, two coral records at 125.8 ± 1.6 and 123.9 ± 1.3 ka, which contain ≥ 10 years and are considered to be more robust, record significantly higher than modern SST seasonality of 4.9 ± 0.5 (± 1 s.e.) and 4.1 ± 0.2 °C (± 1 s.e.), respectively. The former value is the highest SST seasonality observed in any of the Bonaire coral time windows. Towards the end of LIG, SST seasonality is found to reduce to 3.1 ± 0.3 °C (± 1 s.e.) and 2.6 ± 0.1 °C (± 1 s.e.) at 120.5 ± 1.1 ka and 117.7 ± 0.8 ka, respectively. These late LIG SST seasonality values are similar to modern day.

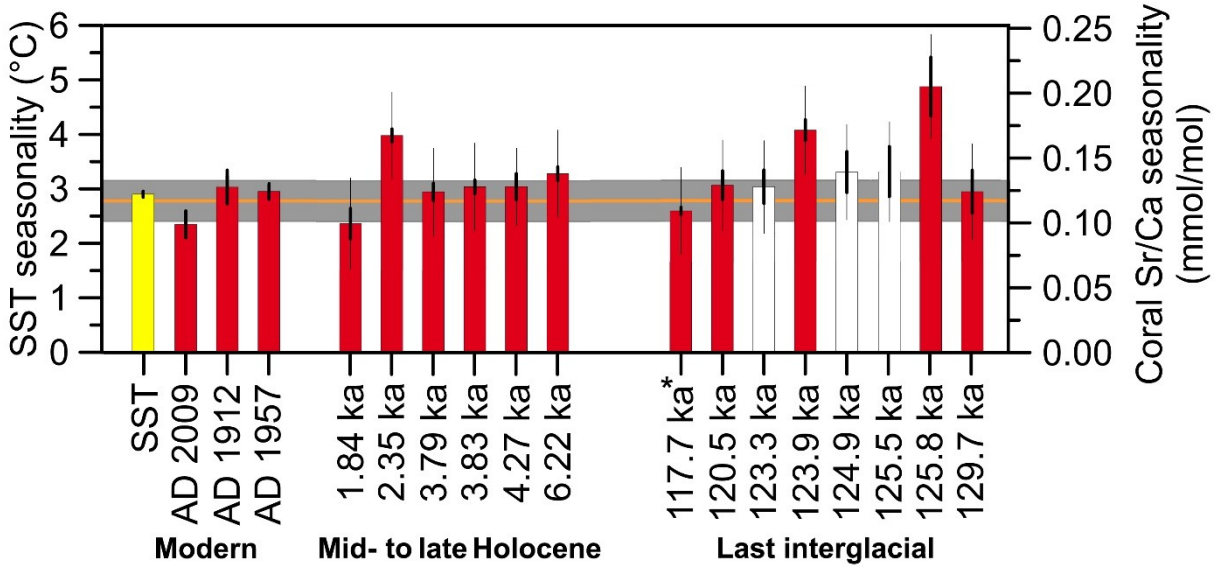

Figure 2.4: Bonaire coral Sr/Ca derived sea surface temperature (SST) seasonality for the last interglacial (LIG) (this study), the end of LIG (*) (Felis et al., 2015), the mid- to late Holocene and modern times (Giry et al., 2012). Less robust LIG records of < 10 years are indicated by white bars. Coral Sr/Ca derived SST seasonality calculated using the seasonal Sr/Ca-SST relationship of -0.042 mmol/mol per °C (Hetzinger et al., 2006). ± 1 standard error and ± 1 combined error, thick and thin vertical lines, respectively. Dark orange horizontal bar with ± 1 standard deviation (light grey shading), shows the reconstructed modern mean SST seasonality based on three modern corals. This is in agreement with the mean instrumental SST seasonality (yellow bar; 1910-2000 AD) for a 2°x2° gridbox centred on 12°N, 68°W (ERSST3vb; Smith et al., 2008).

Without fossil coral records spanning several decades or more, questions regarding our ability to capture and interpret climate evolution during the LIG arise (e.g., Kilbourne et al., 2004). For instance, to what extent can a snapshot of SST seasonality from a coral Sr/Ca time window represent a mean climatic state during the LIG, rather than a short-term excursion? Indeed, within a time window of less than 20 years, how might a single year dominate the interpreted seasonality signal? In order to address these questions, we focus on our two coral time windows that reflect higher than present day seasonality (Fig. 2.4). Firstly, our most robust

record of LIG SST variations comprises of 37 annual cycles from 123.9 ± 1.3 ka. The record of annual seasonality was detrended, and running averages (windows) of various lengths were analysed relative to the standard error (± 1 s.e. and ± 2 s.e.) of the entire record to create hypothetical shorter records of different lengths. Any averaged value within a running window that exceeds the standard error envelope (± 2 s.e.) does not fully represent the seasonality expressed by the entire coral record. We thus consider a record of that length to be more easily influenced by short-term (inter-annual) excursions in reconstructed SST seasonality. Figure 2.5 illustrates that any given running window of < ten years has a value that exceeds ± 2 s.e. of the entire 123.9 ± 1.3 ka record and therefore should be considered unrepresentative. Although this approach is only appropriate to use within this specific record and only for *D. strigosa* corals, it lends support to the rationale behind excluding our 123.3 ± 3.1, 124.9 ± 1.9 and 125.5 ± 2.4 ka records. These records depict SST seasonality similar to modern values while being of ≤ six years in length (Fig. 2.4, denoted by white bars). The moderately reliable age obtained for our 123.3 ± 3.1 ka coral further adds doubt to the interpretation of this record. Our 125.8 ± 1.6 ka record of maximum SST seasonality is supported despite being 10 years in length. Although close examination of this record reveals no reason to do so, randomly excluding the SST seasonality of any year from this record reduces the SST seasonality such that the ± s.e. overlaps with our other mid-LIG record (123.9 ka). Importantly, the mean SST seasonality of our 125.8 ± 1.6 ka record remains above that (± 1 s.e. and c.e.) of the modern average. In summary, the remaining four robust records (at 120.5, 123.9, 125.8 and 129.7 ka), plus the previously published coral from 117.7 ka (Felis et al., 2015), are used to reconstruct the evolution of SST seasonality throughout the LIG. Two of which (123.9 and 125.8 ka) express SST seasonality significantly higher than modern values during the mid-LIG.

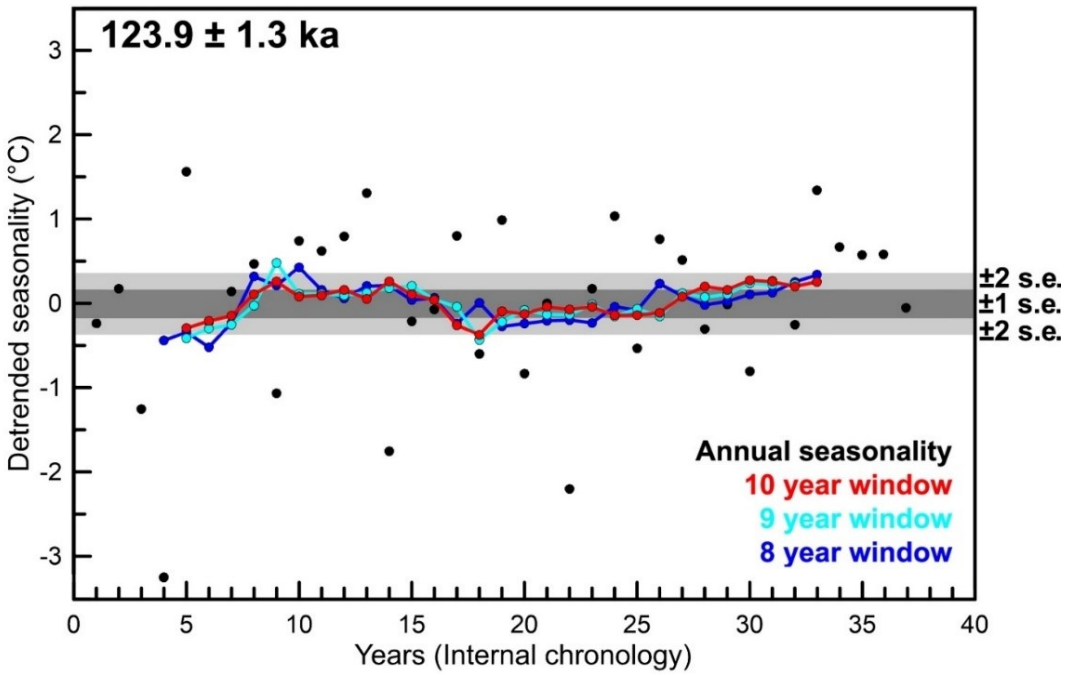

Figure 2.5: Detrended annual sea surface temperature seasonality record for 123.9 ± 1.3 ka (black dots). Running windows of length averaging ten (red), nine (light blue) and eight years (dark blue). ± 1 (dark grey) and 2 (light grey) standard error envelopes from the record mean are displayed.

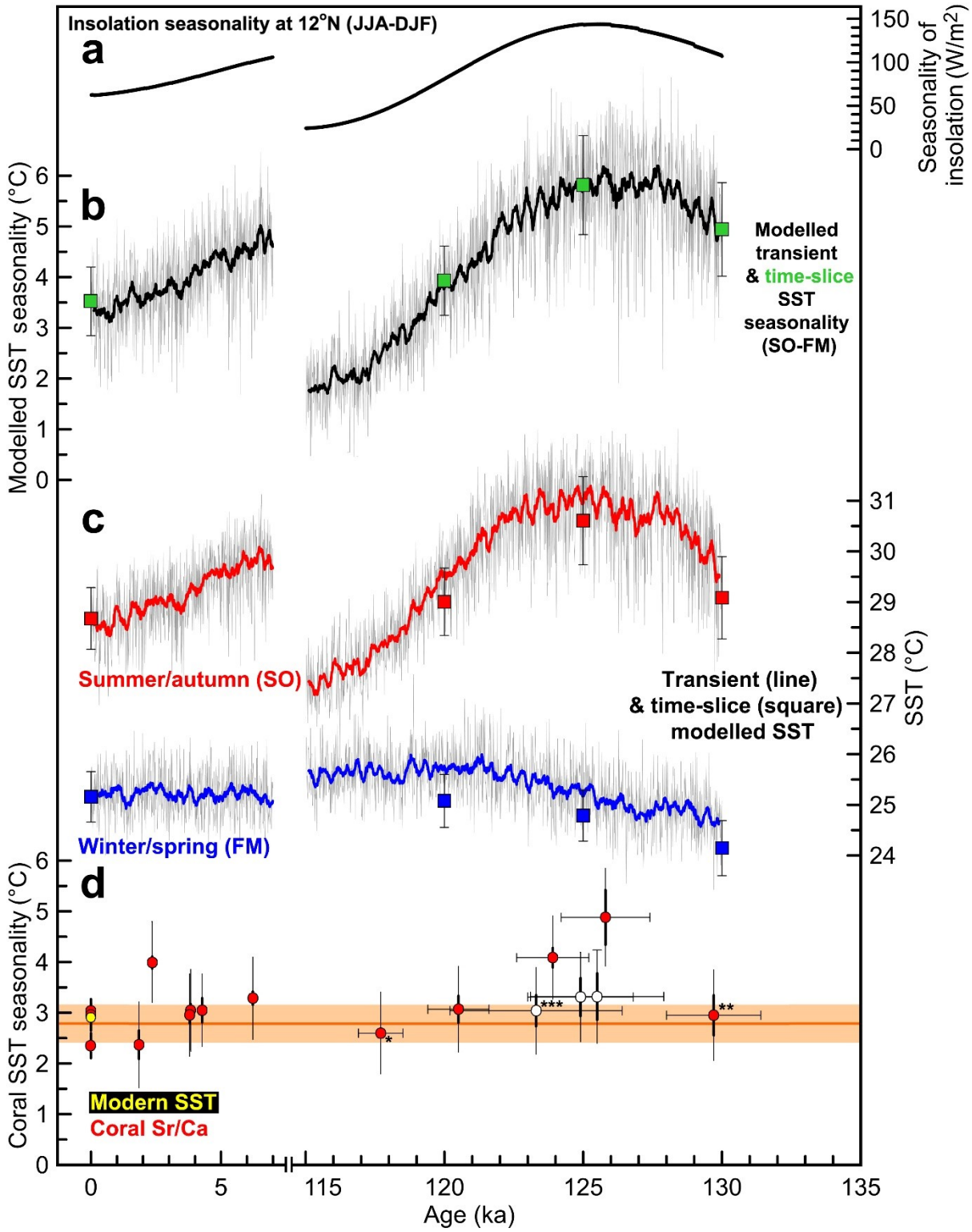

Figure 2.6: Bonaire coral- and model-based sea surface temperature (SST) seasonality throughout the last interglacial (LIG). (a) Seasonality of insolation (June-July-August, JJA minus December-January-February, DJF) at the latitude of Bonaire (12°N) (Berger, 1978). (b) Transient (Felis et al., 2015) and time-slice (squares) simulations of SST seasonality (September-October, SO minus February-March, FM) around Bonaire (1°x1° gridbox centred at 12.5°N, 68° W) using the coupled-atmosphere-ocean general circulation model COSMOS. (c) Transient and time-slice (squares) simulations of Bonaire summer/autumn (SO) and winter/spring (FM) SST. Thick lines (b,c) represents a 21-point running average of the transient

simulation (representing an average of 210 calendar years) and vertical lines around squares represent the ±1 standard deviation (s.d.) of the time-slice simulations. (d) Modern and mid- to late Holocene (Giry et al., 2012), end of LIG (*, Felis et al., 2015) and LIG coral Sr/Ca derived SST seasonality for Bonaire (± 1 standard error = thick vertical lines, ± 1 combined error = thin vertical lines. The three modern corals mean is represented by an orange line with ± 1 s.d. (light orange shading) and agrees with modern instrumental SST seasonality (1910-2000 AD, ERSSTv3b; Smith et al., 2008). Coral Sr/Ca derived SST seasonality calculated using the seasonal Sr/Ca-SST relationship of -0.042 mmol/mol per °C (Hetzinger et al., 2006). White dots denote records of < ten years length. All LIG coral ages are considered strictly reliable (Obert et al., 2016) (section 2.1.3.5), aside from a less strictly reliable (**) and a moderately reliable (***) age. ^{230}Th/U-age uncertainty is reported at 2σ level.

Time-slice equilibrium simulations of pre-industrial, 120, 125 and 130 ka SST seasonality using the coupled atmosphere-ocean general circulation model COSMOS depict a similar trend of 3.5 ± 0.7 °C, 3.9 ± 0.7 °C, 5.8 ± 1.0 °C and 4.9 ± 0.9 °C (± 1 s.d.) (Fig. 2.6b), respectively. These results are in agreement with the composite coral Sr/Ca derived SST seasonality for ~120 and ~125 ka, and indicate that these are representative of the wider tropical and North Atlantic region (Fig. 2.7). Furthermore, our time-slice simulations demonstrate that enhanced mid-LIG SST seasonality in the tropical Atlantic, as indicated by the Bonaire coral Sr/Ca records, was primarily the result of summer warming (Fig. 2.6c)

2.1.4.5 Coral Sr/Ca-SST variability at 124 ka

Of the eight presented coral Sr/Ca records only that of 123.9 ± 1.3 ka, from the mid-LIG, is of sufficient length to potentially capture inter-annual to decadal modes of SST variability (Fig. 2.3). From the 35 continuous years (of 37 years) of this monthly resolved record, we detected quasi-biennial SST variability at 2.7 years with 99% confidence and decadal SST variability at 12.2 years with 95% confidence (Fig. 2.8). Seasonal decomposition of the record reveals that quasi-biennial (2.6 years) SST variability is significant at 95% during December-February (DJF) and June-August (JJA), but is most significant at 99% during March-May (MAM). Quasi-decadal (8.7 years) and decadal (12.3 years) SST variability is only significant (95%) within the DJF record.

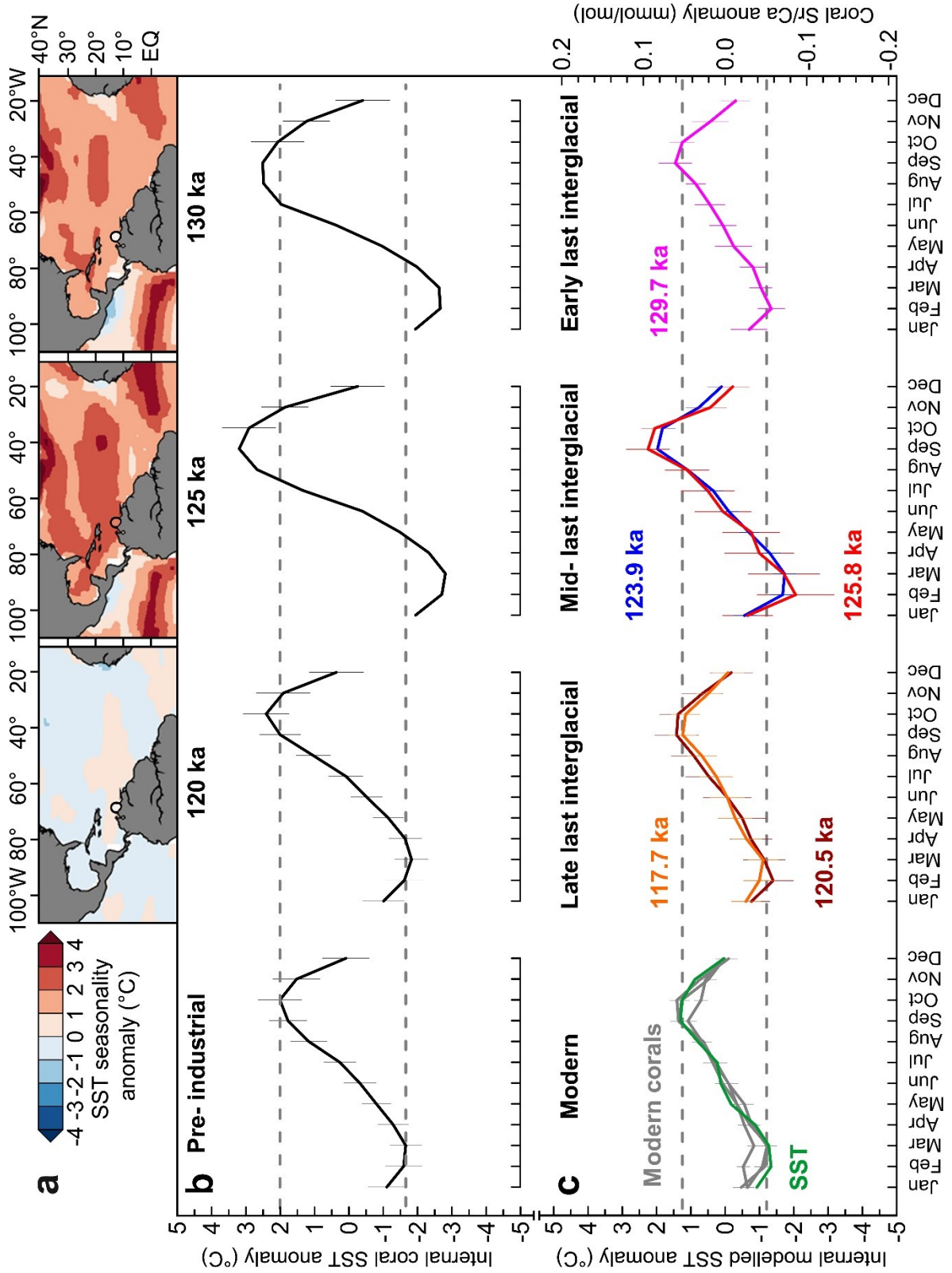

Figure 2.7: Modelled and coral Sr/Ca derived sea surface temperature (SST) seasonality during the last interglacial (LIG). (a) COSMOS climate model time-slice simulations of LIG North Atlantic SST seasonality anomaly relative to a pre-industrial simulation and Bonaire coral Sr/Ca-SST seasonality anomaly (circles) relative to modern SST seasonality (1910-2000 AD, ERSSTv3b, Smith et al., 2008). (b) Simulated SST seasonality around Bonaire (1°x1° gridbox centred at 12.5°N, 68° W) at pre-industrial, 120, 125 and 130 ka (± 1 standard deviation, thin

vertical lines). (c) Modern instrumental SST seasonality (1910-2000 AD, ERSSTv3b, Smith et al., 2008) compared to that derived from three modern, a 117.7, 120.5, 123.9, 125.8 and 129.7 ka coral (± 1 standard error = vertical lines). Horizontal dashed lines denote the pre- industrial and modern analogue for the modelled (b) and coral reconstructed (c) seasonal SST range, respectively. Coral Sr/Ca-SST derived using the seasonal Sr/Ca-SST relationship of -0.042 mmol/mol per °C (Hetzinger et al., 2006). The mean of the Sr/Ca-SST seasonality based on three modern corals successfully reconstructs modern instrumental SST seasonality (1910-2000 AD; Smith et al., 2008).

2.1.5 Discussion

Prior to this study, LIG tropical Atlantic SST seasonality had been characterised by four years of Sr/Ca derived SST from a 127 ka dated *Montastraea faveolata* coral from the Isla de Mona, north-eastern Caribbean (Winter et al., 2003), and 20 years (Felis et al., 2015) from a 118 ka dated *Diploria strigosa* coral from Bonaire. These two single snapshot studies, the first from the mid and the second from the late LIG, report SST seasonality as having been enhanced by 1 °C compared to the present day and within the modern range, respectively. By reconstructing a comprehensive evolution of tropical Atlantic SST seasonality throughout the LIG, we support and build on these two studies that attributed the role of orbital controls on the seasonal insolation cycle as the primary driver of tropical SST seasonality from a single last interglacial time window. Our reconstructed peak SST seasonality of 4.9 ± 0.5 °C (± 1 s.e.) at 125.8 ka, in conjunction with our 123.9 ka record (4.1 ± 0.2 °C), reconstructs mean SST seasonality higher than modern (2.8 ± 0.4 °C, ± 1 s.d.) and likely reflects a period of peak SST seasonality within the Caribbean during the LIG. This assessment is further supported when the combined error is considered (Fig. 2.4 and Fig. 2.6). The combined error (Abram et al., 2009) incorporates modern day inter-colony differences and thus reflects the potential uncertainties in the Sr/Ca-SST calibration, location, water depth (reef habitats) and time intervals associated with differing Sr/Ca-SST seasonality reconstructed from three modern corals (Giry et al., 2012). Although our records of ≤ 6 years window length are unlikely to fully represent SST seasonality for their respective LIG time period, they do provide insights into coral based SST reconstructions. BON-28-A (Table 2.1) (123.3 ka) has a moderately reliable age with relatively large uncertainty (± 3.1 ka), which can potentially place it into the late-LIG for which its reconstructed SST seasonality of 3.0 °C would be plausible. BON-26-A (124.9 ka) and BON-24-AII.2 (125.5 ka) record SST seasonality marginally higher but within error of modern day values. These records illustrate the high degree of variability in reconstructed mid-LIG seasonality and thus the importance of long and continuous records.

2.1.5.1 Forcings on SST seasonality during the LIG

In the Northern Hemisphere, the annual cycle of insolation was significantly more pronounced during the LIG as a result of an enhanced precession cycle, driven by higher obliquity and eccentricity. This coincided with the occurrence of the perihelion in boreal summer (Yin and Berger, 2010). Such an orbital configuration induced stronger seasonal amplitudes of insolation at the latitude of Bonaire (12°N) during the LIG (Fig. 2.6a). In addition to the previously published coral at 117.7 ka (Felis et al., 2015), the Sr/Ca derived SST seasonality from four of our seven new coral time windows, which we consider to be the more robust records (at 120.5, 123.9, 125.8 and 129.7 ka), follow the evolving seasonal cycle of insolation during the LIG (Fig. 2.6a). The significantly higher than present-day SST seasonality at 125.8 and 123.9 ka are in the midst of the LIG and consistent with peak seasonality of insolation at ~125.5 ka (Berger, 1978). The coupled SST-insolation seasonality trend we describe throughout the LIG is similar to the trend observed during the mid- to late Holocene. During the latter period, a notable exception to this trend identified in a 2.3 ka coral is interpreted to reflect a time interval of strengthened ENSO teleconnections to the Caribbean region (Giry et al., 2012; Felis et al., 2015). Importantly however, this does not necessarily imply a strengthening of the ENSO phenomenon in the tropical Pacific at that time (Felis et al., 2015).

Likewise, our climate model (COSMOS) time-slice simulations and the transient simulations (Felis et al., 2015) of LIG SST seasonality are consistent with the coral based results (Fig. 2.6). Figure 2.7a illustrates this modelled SST seasonality trend as representative for the Caribbean and large areas of the tropical North Atlantic. In comparison with the coral records that cluster around 120 and 125 ka, modelled SST seasonality is higher by ~1 to 2 °C, while at 130 ka, a ~2 °C higher seasonality was found. These results are broadly consistent with a ~0.6 °C higher seasonality of the modelled pre-industrial SST compared to the instrumental record (ERSSTv3b; 1910-2000 AD) which, importantly, is in agreement with the reconstructed modern mean coral Sr/Ca-SST seasonality (Fig. 2.6). Regardless of uncertainties surrounding ice sheet sensitivity and vegetation feedback during interglacials, the pre-industrial, 120 and 125 ka SST seasonality simulations are in agreement, within error (± 1 s.d.), with their coral counterparts (Fig. 2.7). The deviation from the coral record at 130 ka is likely a result of the model initialization parameters being unrepresentative of that time. The continued influences of a rapid TII deglaciation event likely saw the presence of larger continental ice sheets and a reorganization of North Atlantic oceanic currents around 130 ka (Govin et al., 2012, and references therein). Of significance to this study is the evolving trend of SST seasonality

throughout the LIG, which is similarly expressed by the coral reconstructions and climate model simulations.

The advantage of the combined coral proxy and modelling approach presented here is the consistency of the results from our coral Sr/Ca records, the time-slice simulations and the transient simulations of Felis et al. (2015). These modelling efforts reveal that the mid-LIG increased SST seasonality in the Caribbean Sea results primarily from summer warming, contrary to the conclusion reached in Winter et al. (2003). Our coral Sr/Ca records and time-slice simulations also further substantiate the transient modelling and hosing experiments (Felis et al., 2015) that demonstrate the insensitivity of tropical SST seasonality to the wider climate instabilities that perturbed the Atlantic realm during the LIG (Sirocko et al., 2005; Blanchon et al., 2009; O'Leary et al., 2013; Galaasen et al., 2014; Mokeddem et al., 2014). In summary, our results affirm the prevailing influence of orbital insolation changes on tropical SST seasonality.

Tropical Pacific SST seasonality has been demonstrated, using single coral time windows, to be in agreement with the orbital configuration influencing seasonality of insolation during MIS 7 (197 ka) (Asami et al., 2013) and MIS 9 (337 - 374 ka) (Kilbourne et al., 2004; Ayling et al., 2006). In conjunction with these studies, tropical SST seasonality during the last three interglacials is observably sensitive to the prevailing orbital configuration and resulting influence on the seasonality of insolation. Our multi-coral approach allows us to demonstrate this for the LIG with greater certainty. Furthermore, multi-coral reconstructions of the evolution of SST seasonality during the LIG contribute to efforts to chart the sequence of events that characterise the LIG, within well-defined age uncertainties (Govin et al., 2015a). For instance, we reconstruct early LIG tropical Atlantic SST seasonality at 130 ka that is similar to modern, implying that modern day SST seasonality at Bonaire was reached relatively rapidly after the onset of the LIG following TII. However, tropical Atlantic corals which date to deglacial and glacial periods are required to further test such assertions.

2.1.5.2 Spectral variability of SST at 123.9 ± 1.3 ka

We detect quasi-biennial (2.6-2.7 years) SST variability at 123.9 ka in the monthly, summer (JJA), spring (MAM) and winter (DJF) coral Sr/Ca based SST records (Fig. 2.8b), which is in agreement with the modern instrumental SST record (Smith et al., 2008). These findings are in accordance with the quasi-biennial behaviour observed within Atlantic SST variability (Dima and Lohmann, 2004) and its influence on a similar quasi-biennial variance seen in tropical Atlantic hurricane activity (Gray, 1984). We also detect a quasi-decadal SST variability of 8.7 years in our 123.9 ka winter record. However, although the underpinning

mechanisms are poorly constrained, the NAO is thought to modulate this ~8 year mode by inducing fluctuations in the easterly trade winds and rainfall in the region of coastal Venezuela (Jury, 2009).

Despite the length of our 123.9 ka record being at the limit of detection of decadal variability, a decadal spectral peak of ~12 years is visually observable throughout all component series, but is only significant in the monthly and DJF SST time series (Fig. 2.8b). While being found in modern instrumental SST records (Deser and Blackmon, 1993) and the Cariaco basin sedimentary records spanning the past ~800 years (Black et al., 1999), our 123.9 ka coral record represents the first evidence of decadal SST variability in the tropical North Atlantic during the LIG. This decadal mode is indicative of the Atlantic SST anomaly tri-pole that influences basin wide air-sea heat fluxes and climatic patterns (Moron et al., 1998). The detection of these SST modes in the southern Caribbean during the LIG suggests a prevailing interconnection with the North Atlantic at that time, perhaps strengthened by orbital forcing. More studies involving multiple sub-annually resolved proxy records of SST are required to further assess the precise relationships between inter-annual to decadal modes of LIG climate variability and corresponding forcing mechanisms.

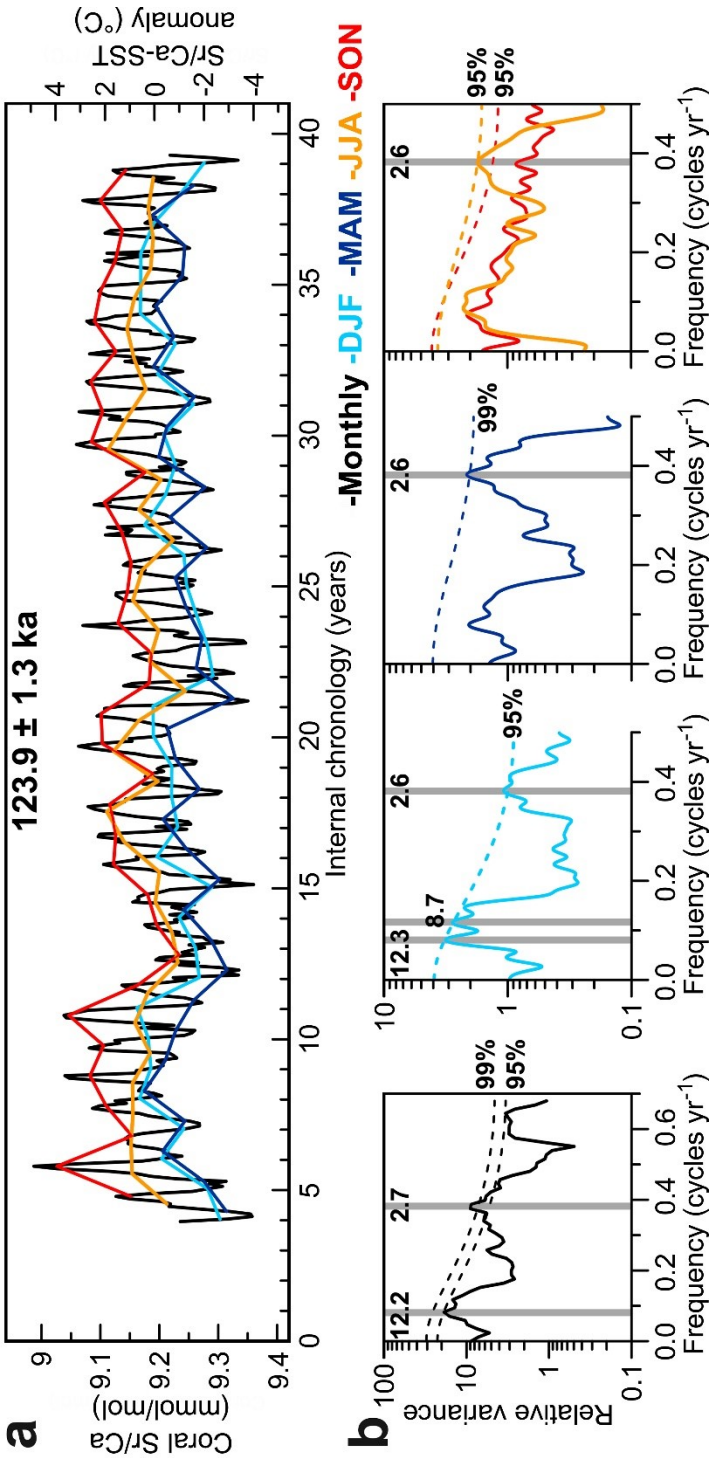

Figure 2.8: Multi-taper spectral analysis of a 35-year monthly resolved coral Sr/Ca proxy record of sea surface temperature (SST) from 124 ka ago. (a) Monthly and seasonally-decomposed time series representing boreal winter (December-January-February, DJF), spring (March-April-May, MAM), summer (June-July-August, JJA) and autumn (September-October-November, SON). Associated SST anomaly derived using a seasonal coral Sr/Ca-relationship of -0.042 mmol/mol per °C for *Diploria strigosa* (Hetzinger et al., 2006). (b) Multi-taper method spectral analysis implementing a red noise null hypothesis (Ghil et al., 2002) on detrended and normalised monthly (with averaged seasonal cycle removed) and seasonally

collated time series. 95% and 99% confidence limits are shown. Vertical grey bars highlight significant periodicities.

2.1.6 Conclusions

Utilizing Sr/Ca measurements of well dated and preserved fossil *Diploria strigosa* corals from the southern Caribbean island of Bonaire; we generated monthly resolved records that reconstruct SST seasonality and variability for various time windows throughout the LIG. These records, along with a previously published one (Felis et al., 2015), total 105 years in length and allow a unique assessment of tropical Atlantic SST seasonality and climate variability during the LIG. Relative to modern instrumental SST records and mid- to late Holocene and modern coral based SST reconstructions we make the following conclusions:

- Our monthly coral Sr/Ca derived SST proxy records reconstruct similar to modern SST seasonality of ~2.9 °C during the early (130 ka) and late LIG (120-118 ka) in the tropical North Atlantic Ocean. However, within the mid-LIG at ~126 ka and ~124 ka we find significantly higher than modern SST seasonality of 4.9 and 4.1 °C, respectively. The reconstructed evolution of SST seasonality is consistent with the evolving amplitude of orbitally induced changes in seasonality of insolation throughout the LIG. This demonstrates the dominance of orbitally controlled changes in the seasonality of insolation on the seasonality of tropical Atlantic SST during the LIG.

- Our climate model simulations are in agreement with the coral Sr/Ca derived SST records of seasonality changes throughout the LIG as a result of orbital forcing and illustrate the representative nature of the reconstructed SST seasonality evolution between 118 and 130 ka for the tropical North Atlantic Ocean. Additionally, our model simulations indicate that reconstructed higher SST seasonality during the mid-LIG was primarily the result of warmer summers.

- In our longest coral record, 35 continuous years from 123.9 ka during the mid-LIG, we detect modes of SST variability. A pattern of quasi-biennial (2.6-2.7 years) SST variability was in existence in the tropical North Atlantic during the mid-LIG. We also find evidence for quasi-decadal (8.7 years) and decadal (~12.2 years) SST variability in the tropical North Atlantic during the mid-LIG. These modes of SST variability are similarly observed in modern instrumental records. Decadal variability is a fundamental feature of North Atlantic SST at the present day. We identify its persistence in this region during a period of the past characterised by warmer than modern conditions and differing orbital configurations.

- The LIG remains an important test-bed for our understanding of climate dynamics, and here we establish that alongside the range of estimates reported for how much warmer the LIG was than today, significant orbitally induced changes occurred in tropical SST seasonality. Recent studies have illustrated that the LIG was a period of notable climatic shifts and instabilities (Felis et al., 2015), however, tropical North Atlantic SST seasonality was relatively stable and evolved in tandem with orbitally driven seasonality of insolation. In light of future changes to climatic boundary conditions, our results point to the important role of orbital insolation forcing on tropical SST seasonality during interglacials warmer than today.

2.1.7 Acknowledgements

We thank the Government of the Island Territory of Bonaire of the former Netherlands Antilles (now Caribbean Netherlands) for research and fieldwork permissions, and E. Beukenboom (STINAPA Bonaire National Parks Foundation) for support. This study was funded by the Deutsche Forschungsgemeinschaft through grants FE 615/3-2, 3-4 to T.F., SCHO 1274/4-4 to D.S. and LO 895/9-4 to G.L. (DFG Priority Programme INTERDYNAMIK - SPP 1266), and FE 615/5-1 to T.F. J.C.O. and D.S. are thankful to K.P. Jochum and M.O. Andreae from the MPI for Chemistry, Mainz, as well as the Max Planck Graduate Center (MPGC) for financial support. J. Pätzold and C. Giry are thanked for field assistance, S. Pape for maintaining and operating of the ICP-OES, C. Vogt for powder X-ray diffraction analysis. G. Wefer, H. Kuhnert, A. Govin and K. DeLong are recognised for their contribution to discussions. T.F. is supported through the DFG-Research Center/Cluster of Excellence ‘The Ocean in the Earth System’ at the University of Bremen. W.B. acknowledges support from GLOMAR (Bremen International Graduate School for Marine Sciences).

2.2 Last interglacial hydroclimate seasonality reconstructed from tropical Atlantic corals

Authors: W. M. Brocas[1], T. Felis[1], Paul Gierz[2], Gerrit Lohmann[2], Martin Werner[2], J. Christina Obert[3], Denis Scholz[3], Martin Kölling[1], Sander R. Scheffers[4]

[1]MARUM - Center for Marine Environmental Sciences, University of Bremen, 28359 Bremen, Germany

[2]Alfred Wegener Institute Helmholtz Centre for Polar and Marine Research, 27570 Bremerhaven, Germany

[3]Institute for Geosciences, Johannes Gutenberg University Mainz, 55099 Mainz, Germany

[4]National Marine Science Centre, Southern Cross University, Lismore, NSW 2480, Australia

Corresponding author:
William M. Brocas, MARUM - Center for Marine Environmental Sciences, University of Bremen, 28359 Bremen, Germany (wbrocas@marum.de) (tel: +4942121865665)

Key Points:

- Last interglacial (LIG) coral $\delta^{18}O$ records are used to reconstruct tropical Atlantic seawater $\delta^{18}O$ ($\delta^{18}O_{seawater}$) seasonality
- Mid-LIG $\delta^{18}O_{seawater}$ seasonality was higher than modern and coral $\delta^{18}O$ leads Sr/Ca records by two months, implying a shift in hydroclimate
- Mid-LIG climate model and coral findings suggest an expansion of the Intertropical Convergence Zone into the South Caribbean Sea

Keywords:
Last interglacial, Tropical Atlantic climate, Hydroclimate seasonality, Coral seawater $\delta^{18}O$ seasonality, Intertropical Convergence Zone

2.2.1 Abstract

The seasonality of hydroclimate during past periods of warmer than modern global temperatures is a critical component for understanding future climate change scenarios. Although partially analogous to these scenarios, the last interglacial (LIG, Marine Isotope Stage 5e, ~127-117 ka) is a popular test-bed. We present coral $\delta^{18}O$ monthly resolved records from multiple Bonaire (southern Caribbean) fossil corals (*Diploria strigosa*) that date to between 130 and 118 ka. These records represent up to 37 years and cover a total of 105 years, offering insights into the seasonality and characteristics of LIG tropical Atlantic hydroclimate. Our coral $\delta^{18}O$ records and available coral Sr/Ca- sea surface temperature (SST) records reveal new insights into the variable relationship between the seasonality of tropical Atlantic seawater $\delta^{18}O$ ($\delta^{18}O_{seawater}$) and SST. Coral $\delta^{18}O$ seasonality is found to coevolve with SST and insolation seasonality throughout the LIG, culminating in significantly higher than modern values at 124 and 126 ka. At 124 ka, we reconstruct a 2-month lead of the coral $\delta^{18}O$ vs. the Sr/Ca-SST annual cycle and increased $\delta^{18}O_{seawater}$ seasonality. A fully-coupled climate model simulates a concomitant increase of southern Caribbean Sea summer precipitation and depletion of summer $\delta^{18}O_{seawater}$. LIG regional hydroclimate differed from today's semiarid climate with a minor rainy season during winter. Cumulatively our coral $\delta^{18}O$, $\delta^{18}O_{seawater}$ and model findings indicate a mid-LIG northward expansion of the South American Intertropical Convergence Zone into the southern Caribbean Sea, highlighting the importance of regional aspects within reconstructions of LIG hydroclimate seasonality.

2.2.2. Introduction

The freshwater budget of the Caribbean is critical for determining the strength of the AMOC and its role in modulating glacial/interglacial climate change (Leduc et al., 2007). The mean position of the tropical Atlantic Intertropical Convergence Zone (ITCZ) has been linked to changes within the tropical hydroclimate of the Caribbean. For instance, sedimentary archives from the Colombian basin have demonstrated the sensitivity of the Caribbean to ITCZ migrations, the consequent impact on AMOC variability (Schmidt and Spero, 2011, and references therein) and its associated influence on extra-tropical climate patterns over glacial/interglacial cycles. On shorter time-scales, the variable supply of precipitated freshwater brought by the annual migration of the ITCZ has various societal impacts, such as droughts (Hastenrath, 1984). How such events might be influenced under future climate change scenarios remains unclear, emphasizing the need for a greater understanding of the constraints and influences upon the ITZC during a variety of climatic background states (Frierson and Hwang, 2012). Although the precise mechanisms underpinning the dynamics of the ITCZ are poorly constrained, and exceptions exist, the ITCZ migrates towards the warming hemisphere (Schneider et al., 2014). Therefore, ITCZ behaviour that differs from present is hypothesised during periods when the orbital configuration promotes the elevation of inter-hemispheric temperature gradients.

The most recent period to have experienced increased seasonality of insolation is the mid-Holocene (~6 ka). Sedimentary records and modelling studies from that time have demonstrated that the ITCZ experienced a northward shift compared to its present mean location at ~5°N (Yarincik et al., 2000; Haug et al., 2001; Yokoyama et al., 2011). Coral studies from the southern Caribbean island of Bonaire (Fig. 2.1) (Giry et al., 2013) and northern South China Sea (Guo et al., 2016), typically reconstruct higher resolution records that have similarly detected the influence of a more northerly positioned ITCZ. In the case of the latter study, this was also associated with a shift in the timing of precipitation (Deng et al., 2009). The last interglacial (LIG, Marine Isotope Stage 5e, ~127-117 ka) is the most recent comparably modern period to have experienced higher than modern seasonality of insolation. This resulted from an orbital configuration that differed from today, characterised by significant increases to the obliquity and eccentricity parameters and a perihelion that occurs in boreal summer as opposed to today's winter. This dominated LIG climate forcing as the planet responded to pronounced increases to seasonality of insolation in the northern hemisphere and inter-hemispheric temperature gradients, whereas annual mean insolation and greenhouse gas concentrations

remained similar to present. In the absence of the anthropogenic emissions projected to influence future climatic change, the LIG provides an opportunity to assess the influence of such changes on natural climate variability. Consequently, the LIG remains an important test-bed for exploring natural climate variability during a time of warmer global temperatures (Lunt et al., 2013).

Although rare, fossil coral material from the LIG can be found preserved upon elevated reef terraces within the tropics. These corals inhabited shallow waters and contain within their skeletal structure monthly resolved proxy records of sea surface properties that offer unique insights into seasonal variability during past time windows. The island of Bonaire is fringed by elevated fossil coral reef terraces and currently experiences a semiarid climate atypical for coastal South America and the Antilles island arcs. For example, Bonaire experiences a comparatively small annual cycle of sea surface salinity (SSS) of ~0.6 psu (Fig. 2.9c) (Carton and Giese, 2008; Zweng et al., 2013), typified by ocean advection of less saline waters in boreal summer (Etter et al., 1987). Much of Bonaire's ~550 mm per year rainfall is convective in nature and falls in boreal winter (Fig. 2.9d) (Martis et al., 2002). As such although Bonaire is not directly affected by the ITCZ, it is uniquely located and sensitive to past ITCZ induced hydroclimate changes. Understanding how the hydroclimate of this southern Caribbean region may have been altered during a period of socially relevant climate change is a primary aim of this study. To achieve this we present coral $\delta^{18}O$ records that allow for the reconstruction of changes to the oxygen isotopic composition of seawater ($\delta^{18}O_{seawater}$) when paired with similarly obtained coral Sr/Ca records (Brocas et al., 2016). This is possible because variations in Sr/Ca act as a proxy for SST, while coral $\delta^{18}O$ variability results from both a SST and $\delta^{18}O_{seawater}$ component (Gagan et al., 1998). By isolating coral $\delta^{18}O_{seawater}$, we aim to examine the seasonal variations of LIG tropical hydroclimate. Increased seasonality of insolation during the mid-LIG has already been demonstrated to result in higher than modern tropical Atlantic sea surface temperature (SST) seasonality, however the affect upon hydroclimate is unknown. Bonaire coral Sr/Ca and $\delta^{18}O$ have previously reconstructed modern, mid- to late Holocene (Giry et al., 2013) and late LIG (Felis et al., 2015) hydroclimate changes and allow LIG findings to be understood in a broader temporal context. We further aim to place high resolution coral proxy findings within the spatial context of the Caribbean and northern South America. As such, we employ fully coupled isotopically enabled climate model simulations to identify the sources that underpin past $\delta^{18}O_{seawater}$ changes and regional hydroclimate patterns.

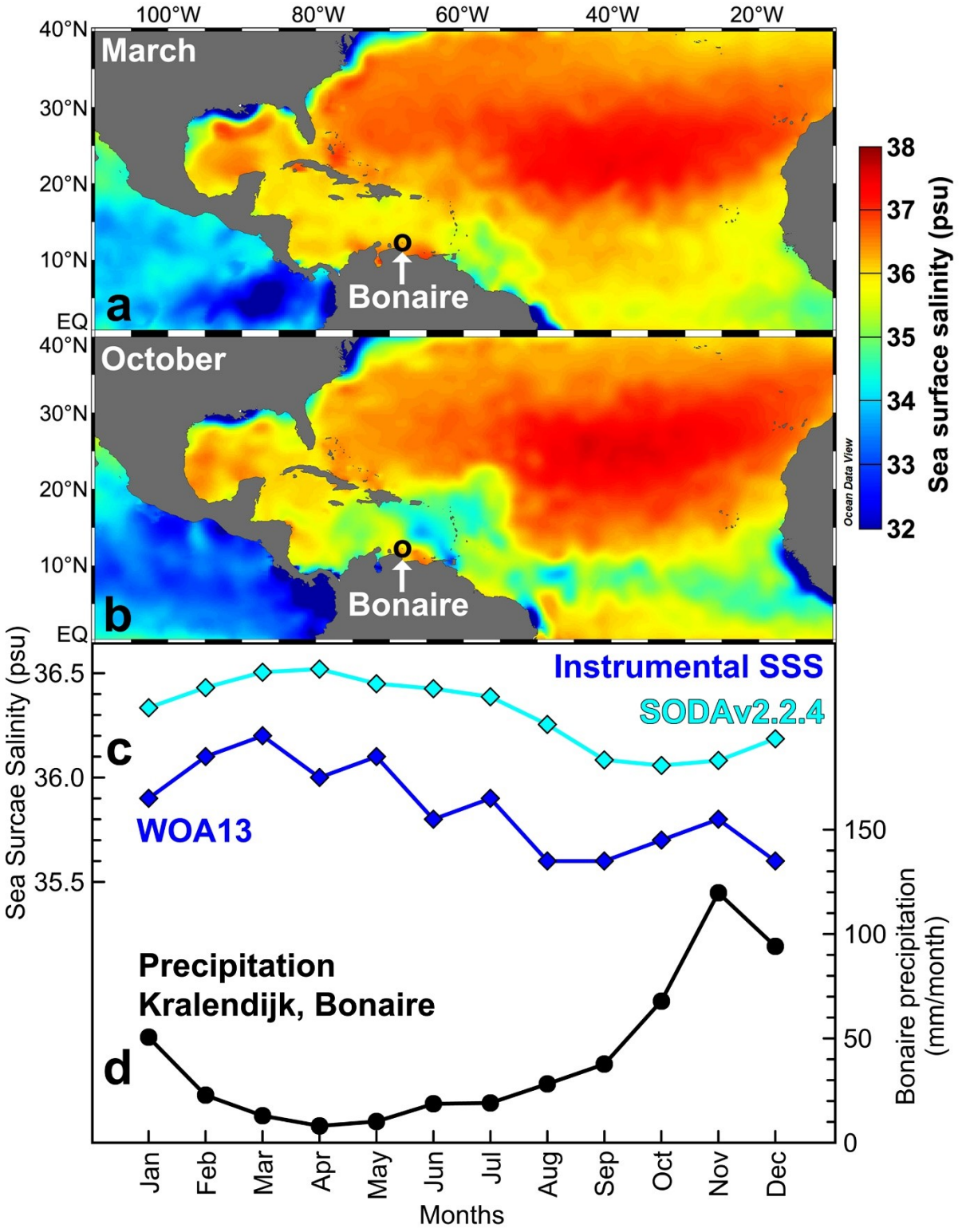

Figure 2.9: Hydroclimate influences upon Bonaire. a) March (winter) and b) October (summer) tropical Atlantic sea surface salinity from the World Ocean Atlas 2013 (WOA13) (Zweng et al., 2013) (Schlitzer, 2015). c) Gridded Instrumental sea surface salinity records from (SODAv2.2.4, light blue) (Carton and Giese, 2008) and (WOA13, dark blue) (Zweng et al., 2013) for a period 1955 to 2012 AD. d) Monthly instrumental precipitation records near our coral sites from Kralendijk weather station on Bonaire (Lawrimore et al., 2011) (1924-51 and 1971-79 AD) are typical for the ABC islands of Aruba, Curaçao and Bonaire.

2.2.3 Materials and Methods

We present seven fossil *Diploria strigosa* (*D. strigosa*) corals from the southern Caribbean island of Bonaire, one the ABC islands that also comprise Aruba and Curaçao (all ~100 km north of Venezuela) (Fig. 2.9), that have been previously described, diagenetically screened and analysed for Sr/Ca (Brocas et al., 2016). These fossil corals were retrieved from a now elevated reef terrace, ^{230}Th/U- dated (Obert et al., 2016) to reveal that they grew during periods throughout the LIG. Additionally, similar Bonaire *D.* strigosa corals have been studied and dated to the end of the LIG (Felis et al., 2015), the mid- to late Holocene and the past century (Giry et al., 2012). As with these studies, we follow the established procedures of Felis et al. (2009; 2015) and Giry et al. (2010; 2013).

2.2.3.1 Coral $\delta^{18}O$ analysis and chronology construction

X-radiographs of sectioned coral slabs confirmed the presence of annual density banding among the coral colonies skeletal elements and the dense thecae walls to be targeted for micro-drilling. A sampling resolution of ~12 per year was achieved using an increment width of 0.4 to 0.5 mm. Stable oxygen isotope ($\delta^{18}O$) measurements were taken from sub-samples of the same coral powder used previously for Sr/Ca analysis (Brocas et al., 2016). A Finnigan MAT 251 mass spectrometer at MARUM (University of Bremen) was used to measure $\delta^{18}O$ in ‰ within ~0.05 mg of micro-drilled coral powder relative to the Vienna peedee belemnite (VPDB). Long term internal reproducibility was better than ±0.07‰ (1σ) based upon ~500 repeat measurements of an internal standard, in accordance with the procedural details outlined in Giry et al. (2010) and Felis et al. (2012). Internal $\delta^{18}O$ chronologies were built based on observable annual density banding and annual Sr/Ca-SST cycles, whereby the average warmest (September-October) and coldest (February-March) months were assigned to the minimum and maximum Sr/Ca value, respectively. The annual cycle SST at Bonaire during the LIG, evidenced by LIG time-slice modelled SST (Brocas et al., 2016), and present-day instrumental records are similar despite the annual cycle of insolation having been more attenuated and symmetrical during the LIG compared to modern (Berger, 1987). Implementing two tie points also allowed direct comparisons to other Bonaire coral records (Giry et al., 2013; Felis et al., 2015) and did not significantly affect reconstructed seasonality. Because the same sample was measured for both Sr/Ca and $\delta^{18}O$, no age uncertainty exists between the observed variations within these records regardless of tie point allocation. Coral records were then linearly interpolated to achieve monthly resolution (Felis et al., 2004; 2009).

2.2.3.2 Assessing LIG $\delta^{18}O_{seawater}$ variability

Coral $\delta^{18}O$ and Sr/Ca seasonality was calculated from monthly resolved records as the difference between the maximum and minimum $\delta^{18}O$ or Sr/Ca value for each year within their respective time series, following the established procedures (Felis et al., 2004, 2015; Giry et al., 2012, 2013; Brocas et al., 2016). A mean seasonality was then calculated from the average of every annual seasonality within a given record. Conversion to SST was done using the established seasonal proxy-SST relationships for tropical Atlantic *D. strigosa* of -0.042 mmol/mol per °C and -0.2‰ per °C for Sr/Ca and $\delta^{18}O$, respectively (Hetzinger et al., 2006; 2016). The use of this Sr/Ca-SST relationship is established at Bonaire (Giry et al., 2012; Felis et al., 2015; Brocas et al., 2016) and is supported by recent calibration studies for *D. strigosa* (Xu et al. ,2015; von Reumont et al., 2016). The error within each coral proxy-SST seasonality estimate is assessed using the ±1 standard error (s.e.) and the ±1 combined error (c.e.) following the definition outlined by Abram et al. (2009), which has been applied to coral SST seasonality estimates by Giry et al. (2012, 2013), Felis et al. (2015) and Brocas et al. (2016). Importantly, the c.e. acknowledges inter-colony differences (Abram et al., 2009) in coral SST seasonality (Felis et al., 2004) associated with differing water depth, location on the reef and time intervals (Felis et al., 2015). Here, the c.e. is calculated by combining (root of the sum of the squares) the (1) ±1 standard deviation (±1 s.d.) of the reconstructed modern mean SST seasonality derived from the three modern corals and (2) the ±1 s.e. of the mean of multiple SST seasonality estimates within each fossil coral (Abram et al., 2009). These fossil coral proxy estimates are then compared to the ±1 s.d. surrounding the three modern coral reconstructed mean SST seasonality.

2.2.3.3 Assessing LIG coral $\delta^{18}O_{seawater}$ seasonality

Coral $\delta^{18}O$ measurements were paired to Sr/Ca records in order to reconstruct seawater $\delta^{18}O$ ($\delta^{18}O_{seawater}$) variations. Typically, to calculate $\delta^{18}O_{seawater}$, the proxy-SST regression slopes are used to convert Sr/Ca and $\delta^{18}O$ into SST and then remove the Sr/Ca derived SST component from the $\delta^{18}O$-SST. Alternatively, changes to $\delta^{18}O_{seawater}$ are calculated and $\delta^{18}O_{seawater}$ records constructed using the methodology of Cahyarini et al. (2008). Subtracting the Sr/Ca-SST seasonality from the $\delta^{18}O$-SST seasonality results in the coral $\delta^{18}O_{seawater}$ seasonality anomaly (Felis et al., 2015), but does not account for temporal offsets between the proxy-SST annual cycles. Following the procedure established by these authors, the error within the $\delta^{18}O_{seawater}$ seasonality anomaly was calculated by combining the ±1 s.e. from each proxy-SST seasonality and comparing it to the reconstructed modern mean $\delta^{18}O_{seawater}$ anomaly based on three modern corals as well as the ±1 s.d. surrounding this value. Additionally we construct

mean annual $\delta^{18}O$, Sr/Ca and $\delta^{18}O_{seawater}$ cycles for each coral by averaging all values of a specific month within their respective records and present them as an anomaly from their individual coral mean. Coral $\delta^{18}O_{seawater}$ seasonality was then calculated by subtracting the minimum from the maximum value within each corals mean annual $\delta^{18}O_{seawater}$ cycle. Alongside the "$\delta^{18}O_{seawater}$ seasonality anomaly", we reconstructed coral "$\delta^{18}O_{seawater}$ seasonality" because it depicts the annual cycle in greater detail, for example, by considering potential temporal offsets between the proxy-SST annual cycles. The significance of the coral $\delta^{18}O_{seawater}$ seasonality was determined by comparing the ±1 s.e. from each record to the ±1 s.d. of the three modern corals. The $\delta^{18}O_{seawater}$ seasonality was evaluated using the analytical error of each proxy-SST seasonality estimate (Cahyarini et al., 2008) rather than the c.e. Alongside the s.e., this was sufficient because it was possible to directly compare $\delta^{18}O_{seawater}$ seasonality with the analytical error averaged from each of the modern corals. The phase relationship between our monthly coral Sr/Ca and $\delta^{18}O$ time series was determined by performing cross - spectral analysis, using AnalySeries©, at the 95% confidence level. In addition to this confidence level, we consider a phase angle uncertainty of ±1 month, which incorporates any potential uncertainty that may have occurred during the monthly interpolation of the Sr/Ca and $\delta^{18}O$ records.

2.2.3.4 LIG climate model simulations

All simulations for this study have been performed using the Earth system model COSMOS (ECHAM5/MPIOM/JSBACH) (Jungclaus et al., 2006). The atmospheric model component ECHAM5 utilises a resolution of T31L19, the ocean component has a resolution of GR30, corresponding to approximately 3.5° × 1.5° laterally, with a higher resolution at the model's poles. Vertically, we use 40 unevenly spaced layers, with higher resolution at the ocean's surface. The model has been previously applied to glacial (Gong et al., 2013) and interglacial conditions (Felis et al., 2015; Pfeiffer and Lohmann, 2016), as well as on warm climate states during the mid-Pliocene (Stepanek and Lohmann, 2012) and those of future scenarios (Gierz et al., 2015). Additionally, the model is enhanced by a stable water isotope diagnostic tool (Werner et al., 2016), consisting of the atmospheric component ECHAM5-WISO (Werner et al., 2011), the dynamic vegetation module JSBACH-WISO (Haese et al., 2012), and the ocean/sea-ice module MPIOM-WISO (Xu et al., 2012). Four equilibrium simulations that represent the pre-industrial period (P.I.), 120, 125 and 130 ka were performed after a model spin-up period of 2500 years using established orbital and greenhouse parameters (Brocas et al., 2016). Each time-slice simulation was then conducted using 200 P.I. and 100

LIG years to evaluate total precipitation, monthly precipitation minus evaporation and $\delta^{18}O_{seawater}$ values in a 1° x 1° grid-box containing Bonaire, centred at 12.5°N, 68°W. Changes from P.I. are evaluated using student t-tests performed at the 95% confidence level. To ensure model findings are representative and consider the sensitive nature of climate at the locality of Bonaire, we also considered all results from adjacent grid-boxes.

2.2.4 Results

2.2.4.1 LIG coral $\delta^{18}O$ seasonality

We present 85 years of LIG coral $\delta^{18}O$ records (Fig. 2.10) which exhibited mean $\delta^{18}O$ seasonality (Fig. 2.11a) that coevolves similarly to Sr/Ca-SST (Fig. 2.11b) seasonality during much of the LIG. For instance, we find higher than modern $\delta^{18}O$ seasonality during the mid-LIG at 123.3 ± 1.3 and 125.8 ± 1.6 ka that coincides with increased seasonality of insolation at that time (Fig. 2.12c). Unlike the LIG Sr/Ca-SST seasonality trend, $\delta^{18}O$ seasonality remains higher than modern during the early LIG at 129.7 ± 1.7 ka. Higher than modern $\delta^{18}O$ seasonality during the early and mid-LIG are statistically significant when considering both the s.e. and c.e. Three of our coral $\delta^{18}O$ records at 125.5 ± 2.4, 124.9 ± 1.9 and 123.3 ± 3.1 ka (denoted by white bars, Fig. 2.11a) contain fewer than the 10 years required to be consider representative of $\delta^{18}O$ seasonality during their respective time intervals (Brocas et al., 2016). Despite this these records were assessed as they demonstrate that the mid-LIG experienced a range of higher than, and comparable to, modern $\delta^{18}O$ seasonality. Reconstructed coral $\delta^{18}O$ seasonality was unaffected by monthly interpolation of raw $\delta^{18}O$ records using either Sr/Ca or $\delta^{18}O$ based chronologies. Furthermore, no significant shifts in mean $\delta^{18}O$ were found within our $\delta^{18}O$ records that might be associated with biological responses to sudden environmental change (Hetzinger et al., 2016), or with records derived from sampling multiple thecae within a colony (Giry et al., 2010). Coral $\delta^{18}O$ seasonality was converted to SST seasonality using the monthly relationship of -0.2‰ per °C (Hetzinger et al., 2006) and derives from the same samples as those used to establish the Sr/Ca- SST of -0.042 mmol/mol per °C. This latter SST relationship has been successfully used to reconstruct modern SST seasonality at Bonaire (Giry et al., 2012) and is in close accordance with recently published calibration slopes (Xu et al., 2015; von Reumont et al., 2016). It is important to note that regardless of the choice of coral Sr/Ca- and $\delta^{18}O$- SST calibration slopes used the relative differences between colonies which form the basis of our findings does not change.

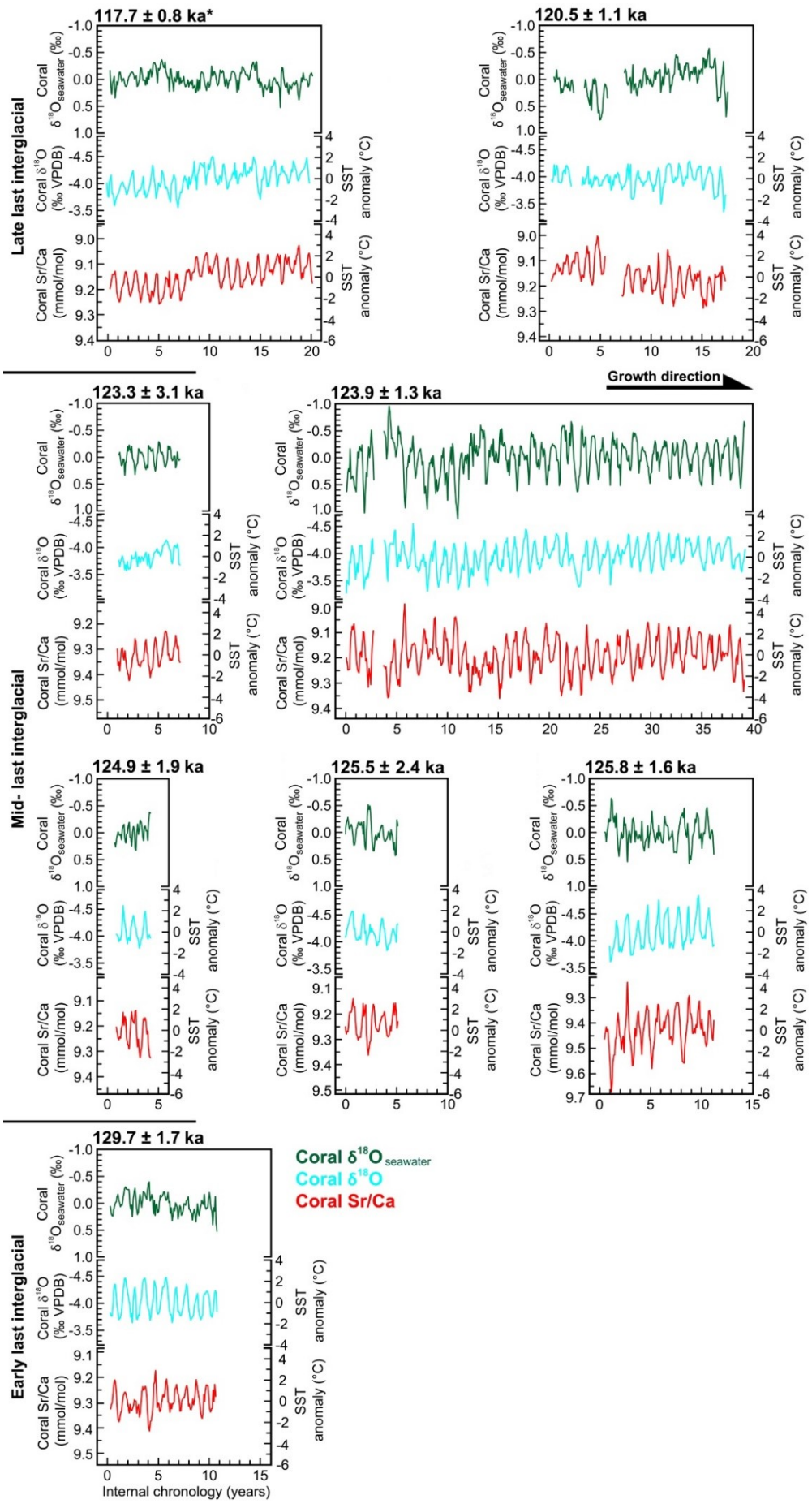
Late last interglacial
Mid- last interglacial
Early last interglacial
117.7 ± 0.8 ka*
120.5 ± 1.1 ka
123.3 ± 3.1 ka
123.9 ± 1.3 ka
124.9 ± 1.9 ka
125.5 ± 2.4 ka
125.8 ± 1.6 ka
129.7 ± 1.7 ka
Growth direction
Coral δ18Oseawater (‰)
Coral δ18O (‰ VPDB)
Coral Sr/Ca (mmol/mol)
SST anomaly (°C)
Coral δ18Oseawater
Coral δ18O
Coral Sr/Ca
Internal chronology (years)

Figure 2.10: Monthly resolved coral $\delta^{18}O$ (light blue), Sr/Ca (red) and $\delta^{18}O_{seawater}$ (green) records from last interglacial (LIG) tropical Atlantic corals. Coral $\delta^{18}O_{seawater}$ records are constructed using the established procedures of Cahyarini et al. (2008). Coral records are grouped according to their $^{230}Th/U$ ages and uncertainty (early, mid- and late LIG) (Brocas et al., 2016). Coral Sr/Ca and $\delta^{18}O$ records are scaled to the same associated sea surface temperatures (SST) using their monthly proxy-SST relationships of -0.042 mmol/mol per °C and -0.2‰ per °C, respectively (Hetzinger et al., 2006). Growth direction is from left to right, older to younger.

2.2.4.2 LIG coral derived $\delta^{18}O_{seawater}$ seasonality

Although coral $\delta^{18}O$ and Sr/Ca-SST seasonality coevolve during the mid- and late LIG (Fig. 2.12a-c), increased coral $\delta^{18}O$ seasonality LIG was not accompanied by increased coral Sr/Ca-SST seasonality during the early LIG, implicating changes in the seasonality of $\delta^{18}O_{seawater}$ at that time. Removing the Sr/Ca-SST seasonality component from $\delta^{18}O$-SST seasonality results in the reconstruction of $\delta^{18}O_{seawater}$ seasonality anomaly during the LIG (Fig. 2.11c). Although a uniquely positive anomaly can be seen at 129.7 ± 1.7 ka, it is not significantly different from the modern $\delta^{18}O_{seawater}$ seasonality anomaly. Likewise, within error of the modern value, the remainder of our LIG time windows express negative $\delta^{18}O_{seawater}$ seasonality anomalies. Although a coral $\delta^{18}O_{seawater}$ seasonality anomaly statistically more negative than modern is found at 123.3 ± 3.1 ka, this record is relatively short (6 years) and unlikely to be representative of that time.

In addition to LIG $\delta^{18}O_{seawater}$ anomaly, monthly averaged annual cycles of $\delta^{18}O_{seawater}$ were constructed and assessed (Cahyarini et al., 2008; Giry et al., 2013) (Fig. 2.13). The seasonality of these cycles was evaluated alongside monthly averaged Sr/Ca-SST and $\delta^{18}O$-SST annual cycles from Bonaire for modern, mid- to late Holocene (Giry et al., 2013) and late LIG time intervals (Felis et al., 2015). Within the LIG, coral $\delta^{18}O_{seawater}$ seasonality is significantly higher, but marginally so, above modern at 125.5 ± 2.4, 123.9 ± 1.3 and 123.3 ± 3.1 ka (Fig. 2.11d). However, of these mid-LIG time windows, only the record of 123.9 ± 1.3 ka was of sufficient length to be considered representative (Brocas et al., 2016) and exhibits a $\delta^{18}O_{seawater}$ seasonality significant above analytical error (Cahyarini et al., 2008) (Fig. 2.13).

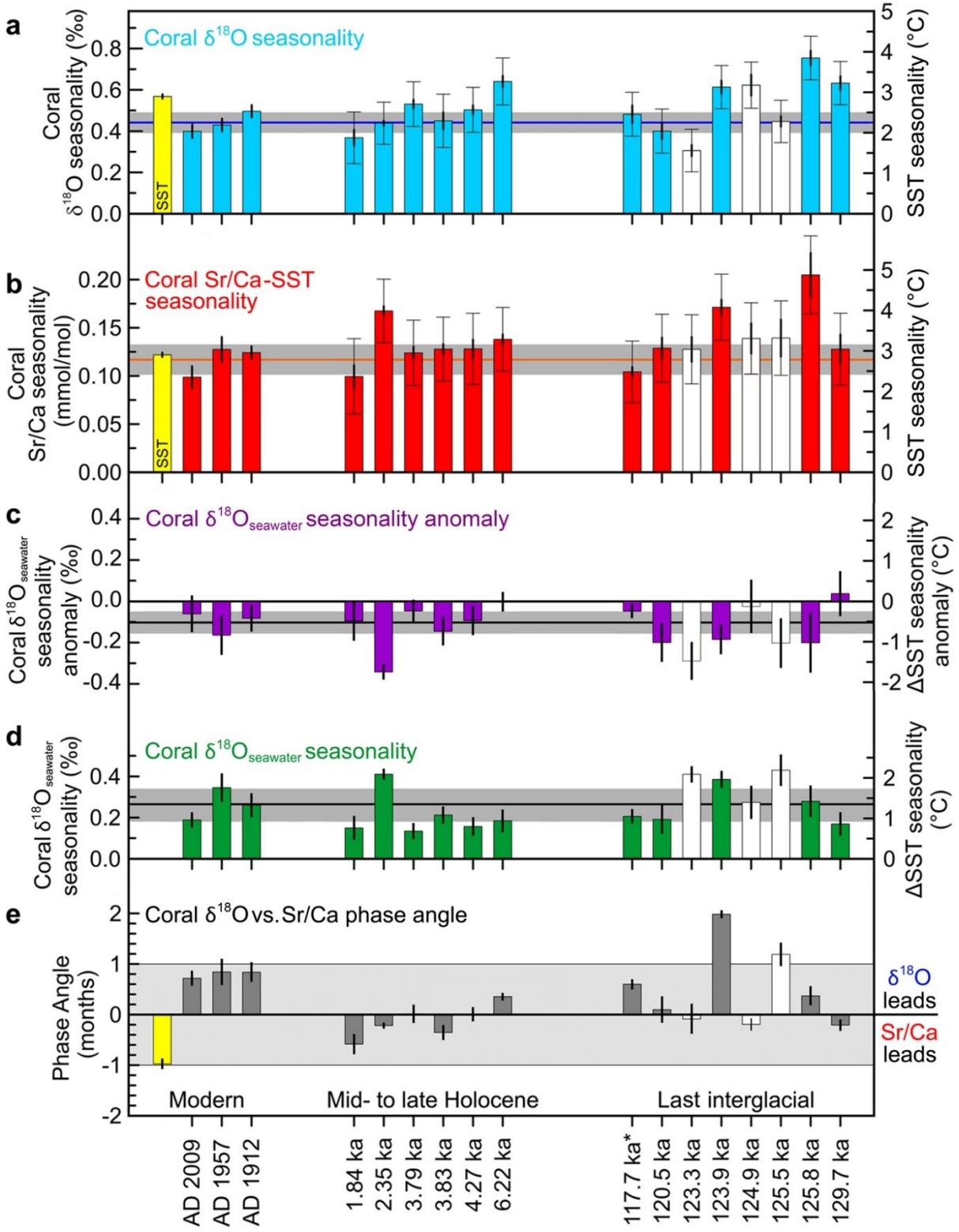

Figure 2.11: Tropical Atlantic coral $\delta^{18}O$, Sr/Ca- sea surface temperature (SST), $\delta^{18}O_{seawater}$ seasonality and phase angle relationships for modern, mid- to late Holocene (Giry et al., 2012, 2013), late last interglacial (LIG) (*) (Felis et al., 2015) and the LIG (this study). (a) Coral $\delta^{18}O$ (light blue) and (b) Sr/Ca (red) (Brocas et al., 2016) derived SST seasonality calculated using the monthly SST relationship of -0.042 mmol/mol per °C and -0.2‰ per °C, respectively (Hetzinger et al., 2006). Uncertainty illustrated using the standard error (±1 s.e. thick vertical black lines) and the combined error (±1 c.e. thin vertical black lines). The dark orange (Sr/Ca)

and blue ($\delta^{18}O$) horizontal bar signifies the average and standard deviation (±1 s.d. light grey shading) of three modern corals. The yellow bar denotes the mean instrumental SST seasonality (ERSST3vb, 1910-2000 AD) (Smith et al., 2008) for a 2° x 2° gridbox centred on 12°N, 68°W. (c) Residual coral $\delta^{18}O_{seawater}$ seasonality anomalies (purple) that result from subtracting the Sr/Ca-SST seasonality from the $\delta^{18}O$-SST (removing the SST contribution to $\delta^{18}O$), using the monthly relationships of Hetzinger et al. (2006). Each coral $\delta^{18}O_{seawater}$ seasonality anomaly error results from combining the ±1 Sr/Ca and ±1 $\delta^{18}O$ seasonality s.e. The reconstructed modern mean $\delta^{18}O_{seawater}$ seasonality anomaly is represented by a dark grey line surrounded by the ±1 s.d. (light grey shading). d) Coral $\delta^{18}O_{seawater}$ seasonality (dark green) calculated from the mean annual cycle of $\delta^{18}O_{seawater}$. The ±1 s.e. of each record (thick vertical lines) is compared to the ±1 s.d. (light grey shading) around the three modern coral mean (horizontal black line). e) The phase angle relationships between our coral Sr/Ca and $\delta^{18}O$ time series (grey bars). Vertical black error lines indicate the 95% confidence interval. The phase angle between Bonaire instrumental SST (ERSSTv3b) (Smith et al., 2008) and precipitation records (Hulme et al., 1998) for 1910-2000 AD is denoted by the yellow bar. A ±1 month grey shaded error bar is included to represent any uncertainty that might arise from the monthly interpolation of coral proxy records. For all graphs, less robust records of fewer than 10 years are denoted by white bars.

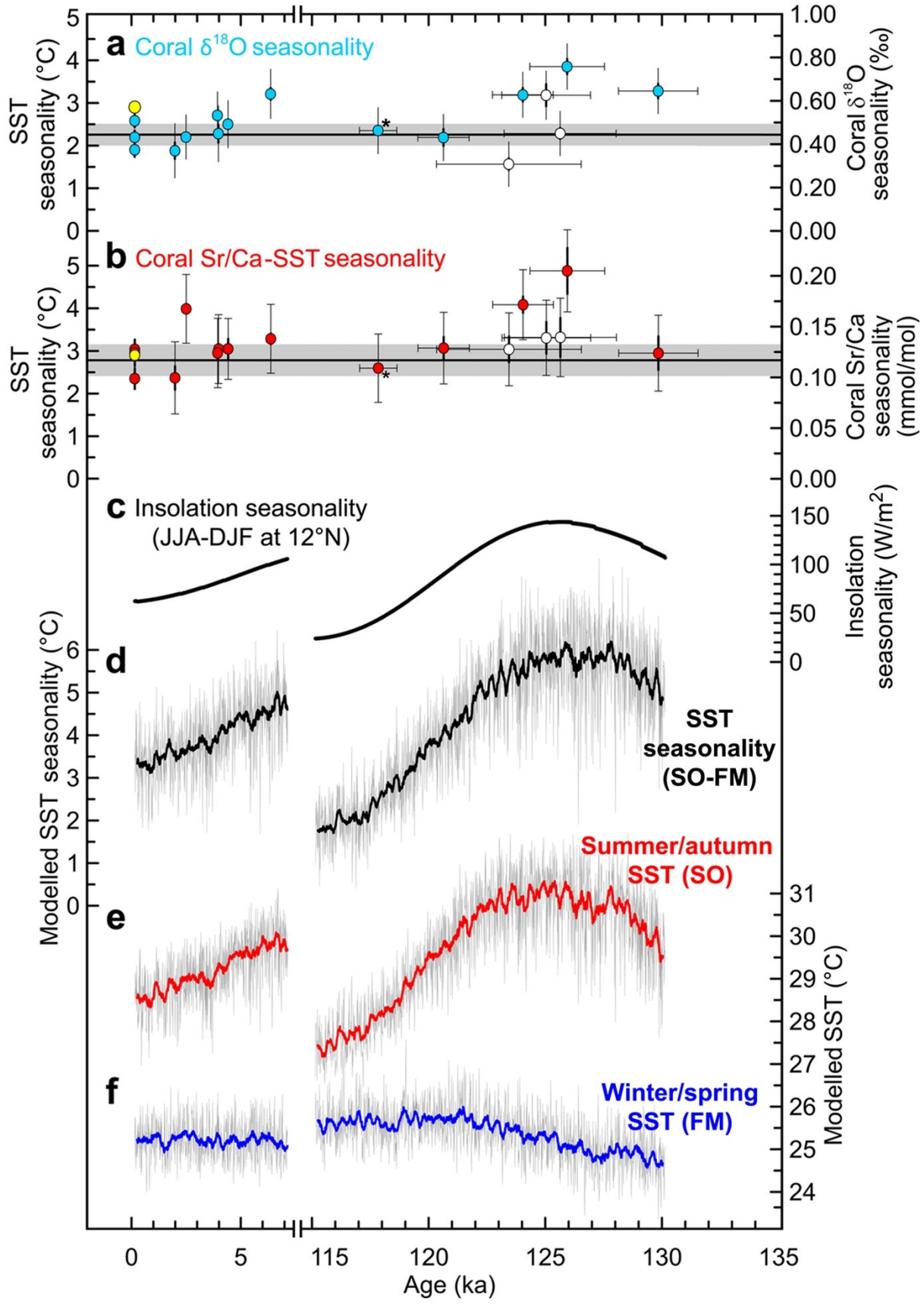

Figure 2.12: Tropical Atlantic reconstructed (coral $\delta^{18}O$, Sr/Ca and model) sea surface temperature (SST) and insolation seasonality. Coral $\delta^{18}O$ (a) and Sr/Ca-SST (b) seasonality for the modern, mid- to late Holocene (Giry et al., 2013), late LIG (*) (Felis et al., 2015) and LIG.

The three modern coral mean is indicated by the horizontal dark line and standard deviation (±1 s.d. grey shading). Standard error (±1 s.e. thick vertical lines) and combined error (±1 c.e. thin vertical lines) indicated. Coral $\delta^{18}O$ and Sr/Ca converted to SST using the proxy-SST relationship of -0.2‰ per °C and -0.042 mmol/mol per °C, respectively (Hetzinger et al., 2006). Records supported by less than 10 years are shown as white circles. Horizontal lines indicate the coral $^{230}Th/U$ age errors (2σ) (Obert et al., 2016; Brocas et al., 2016). The yellow circle denotes modern instrumental SST seasonality (1910-2000 AD, ERSSTv3b) (Smith et al., 2008). c) Seasonality of insolation (June-July-August, JJA, minus December-January-February, DJF) at Bonaire (12°N) (Berger, 1978). d) Modelled SST seasonality (September-October, SO, minus February-March, FM), e) Summer/autumn (September-October) SST and f) winter/spring (February-March) SST modelled using the couple atmospheric-ocean model COSMOS for a 1°x1° gridbox centred at 12.5°N, 68°W (Felis et al., 2015). (d, e, f) Thick lines denote 21 point running average consisting of 210 years.

2.2.2.3 Phase angle between LIG coral $\delta^{18}O$ and Sr/Ca annual cycles

Clear annual cycles of coral $\delta^{18}O$ and Sr/Ca are observed within the paired monthly records (Fig. 2.10) and the monthly averaged annual cycle (Fig. 2.13) for each studied time window, thus the relative timing between these records can be assessed (Fig. 2.11e). The resulting phase angles reveal that there is good agreement between the three modern corals, with $\delta^{18}O$ leading Sr/Ca by ~0.8 of a month (~24 days). However, when the phase relationship between instrumental derived SST (ERSSTv3b) (Smith et al., 2008) and rainfall data (Hulme et al., 1998) is calculated for the period 1910 - 2000 AD (Fig. 2.11e, yellow bar), SST leads precipitation by a month. Although coral proxy measurements are derived from paired samples, we conservatively consider a phase angle uncertainty of ±1 month as a representation of any uncertainty that might arise from monthly interpolation of coral records. During the early LIG our coral record indicates that Sr/Ca marginally leads $\delta^{18}O$. Within the mid-LIG, $\delta^{18}O$ appears to lead or be in phase with Sr/Ca. Late LIG coral records indicate that $\delta^{18}O$ is slightly leading Sr/Ca. However, these phase relationships are indistinguishable from uncertainty. It is within this context that our longest coral record at 123.9 ± 1.3 ka distinctively reveals $\delta^{18}O$ leading Sr/Ca by two months. Visual assessment of the temporal relationship between the 123.9 ka coral Sr/Ca and $\delta^{18}O$ records (Fig. 2.14) illustrates that this lead of $\delta^{18}O$ occurs in both summer and winter.

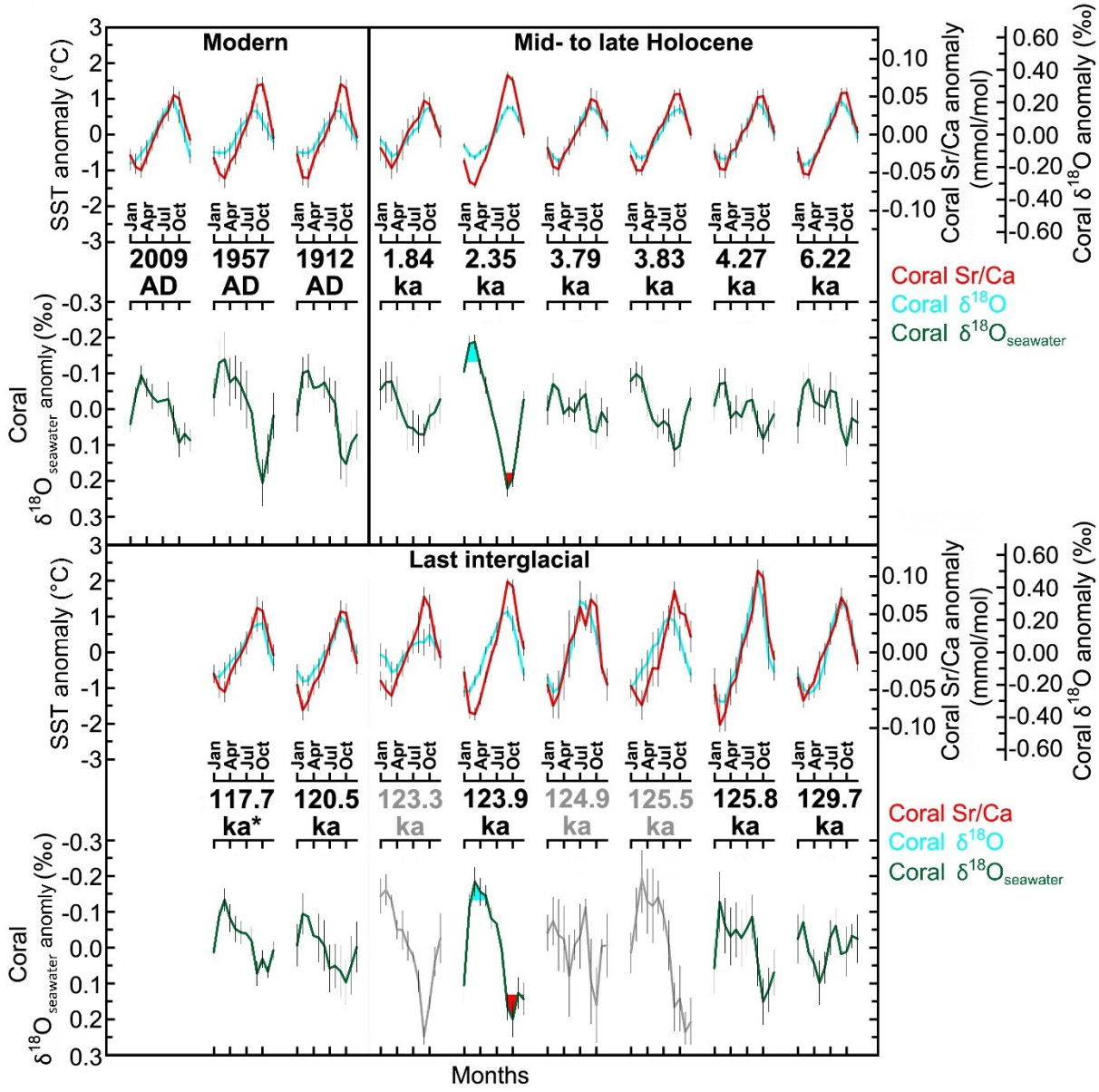

Figure 2.13: Annual averaged cycles of LIG coral Sr/Ca (red), $\delta^{18}O$ (light blue) and $\delta^{18}O_{seawater}$ (green) records constructed from the monthly averaged modern, mid- to late Holocene (Giry et al., 2013), late last interglacial (LIG) (Felis et al., 2015). Coral Sr/Ca and $\delta^{18}O$ converted to sea surface temperature (SST) using the proxy-SST relationship of -0.042 mmol/mol per °C and -0.2‰ per °C, respectively (Hetzinger et al., 2006). Vertical error bars represent the standard error (±1 s.e.) of each month on record. Positive and negative values greater than each corals $\delta^{18}O_{seawater}$ analytical error (Cahyarini et al., 2008) are illustrated by red and blue shading, respectively. Coral $\delta^{18}O_{seawater}$ records comprised of less than 10 years are presented in grey.

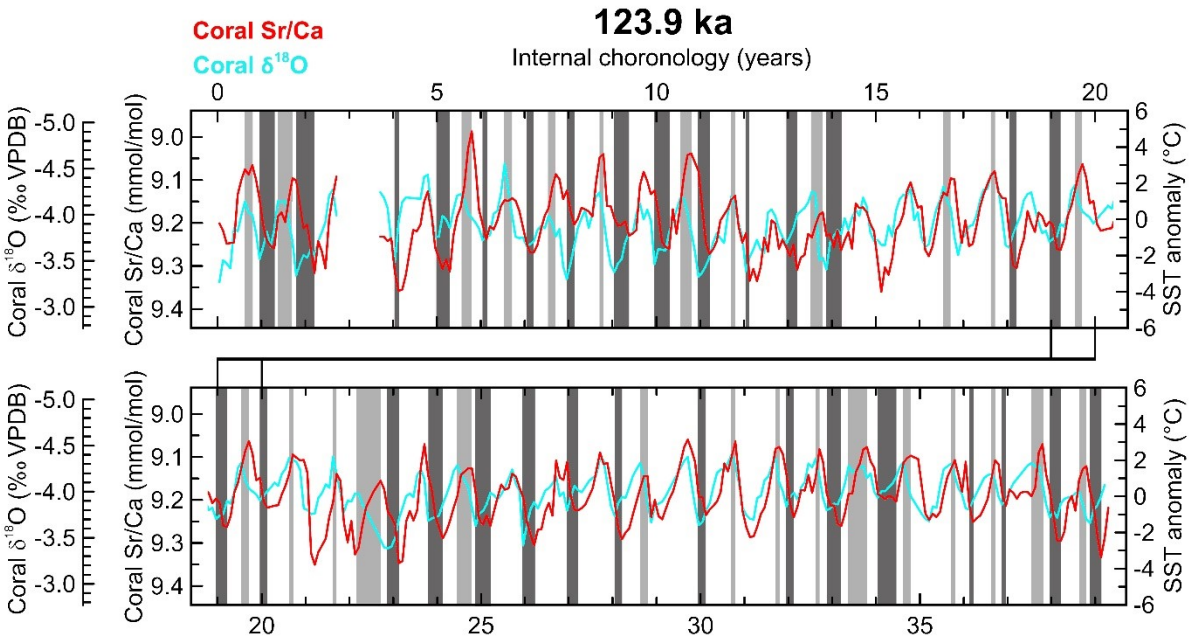

Figure 2.14: Monthly paired coral $\delta^{18}O$ (light blue) and Sr/Ca (red) records (Brocas et al., 2016) $^{230}Th/U$ dated to 123.9 ka (mid-LIG). Records are scaled according to their seasonal proxy-sea surface temperature relationship (Hetzinger et al., 2006). Occasions whereby $\delta^{18}O$ leads Sr/Ca during summer and winter are highlighted in light and dark grey, respectively. For the purposes of clarity, these 37 year records are divided into two sections. Growth direction is from left to right, oldest to youngest.

2.2.2.4 LIG climate model simulations of precipitation and $\delta^{18}O_{seawater}$

Our ECHAM5/MPIOM-WISO simulations allow for the assessment of climatic parameters during P.I., 120, 125 and 130 ka time-slices. Although absolute precipitation values are higher than local instrumental data, P.I. modelled total precipitation exhibits a similar single peak pattern during November (Fig. 2.15a). Precipitation minus evaporation (P-E) was modelled to assess the dominance of evaporation upon sea surface conditions around Bonaire. From January to April, all modelled LIG time-slices simulate P-E values are extremely similar to P.I. and then display a distinct rise from May until November (Fig. 2.15b). This pattern, including biannual peaks, is akin to that found within modern instrumental records (Kalnay et al., 1996). Our 125 and 130 ka time-slices peak during boreal summer P-E ~100 mm/month greater than the P.I. during August and July, respectively, whereas our 120 ka simulated annual P-E cycles are remarkably similar to P.I. The spatial distribution of modelled 125 ka minus P.I. tropical Atlantic total summer (June-July-August, JJA) precipitation anomaly reveals the broad rainfall patterns influencing the region at that time. (Fig. 2.16a) We find increased precipitation within central to southern Caribbean Sea, over northern South America and the tropical Atlantic between 10 and 15°N. Within the oceanic equatorial Atlantic, higher than P.I. precipitation is

accompanied by decreasing values immediately to the south. The $\delta^{18}O_{seawater}$ annual cycle for each of the LIG time-slices reveals an increase in LIG $\delta^{18}O_{seawater}$ seasonality by 0.3 - 0.5 per mill, and mean shifts in $\delta^{18}O_{seawater}$ compared to P.I. (Fig. 2.16c). Notably, the annual cycle of 125 ka $\delta^{18}O_{seawater}$ is similar to P.I. between January and July but indicates reduced values during the latter half of the year. Cumulatively, these modelling results suggest a hydroclimate existed during the mid-LIG at Bonaire, and the wider tropical Atlantic region, that differed significantly from modern.

2.2.5 Discussion

2.2.5.1 LIG coral $\delta^{18}O$ seasonality

Similar to modern mean coral $\delta^{18}O$ seasonality found at 120.5 ka supports the finding of comparably to modern hydroclimate during the late LIG at 117.7 ka (Felis et al., 2015) (Fig. 2.11a, 2.12a). The higher than modern LIG coral $\delta^{18}O$ seasonality can be found at 123.9, 129.7 and peaks at 125.8 ka, broadly coevolving with coral Sr/Ca derived SST seasonality. Aside from a coral at 2.35 ka, a similar relationship can be seen throughout the mid- to late Holocene, with higher than modern $\delta^{18}O$ and insolation seasonality occurring at 6.22 ka (Giry et al., 2013). This coevolution of coral $\delta^{18}O$ and Sr/Ca-SST seasonality reflects the prevailing influence increased seasonality of insolation had upon LIG Caribbean SST seasonality (Brocas et al., 2016) (Fig. 2.12a-c). Coupled transient climate model simulations (COSMOS) suggest that this resulted from warmer summer SST during the mid-LIG (Fig. 2.12e) (Felis et al., 2015; Brocas et al., 2016). Although insolation driven SST changes primarily influenced LIG coral $\delta^{18}O$ seasonality during the mid- and late LIG, during the early LIG (at 129.7 ka) higher coral $\delta^{18}O$ seasonality than modern was not accompanied by higher Sr/Ca-SST seasonality (Fig. 2.11).This would initially imply a more dominant hydroclimate regime, potentially characterised by summer rains.

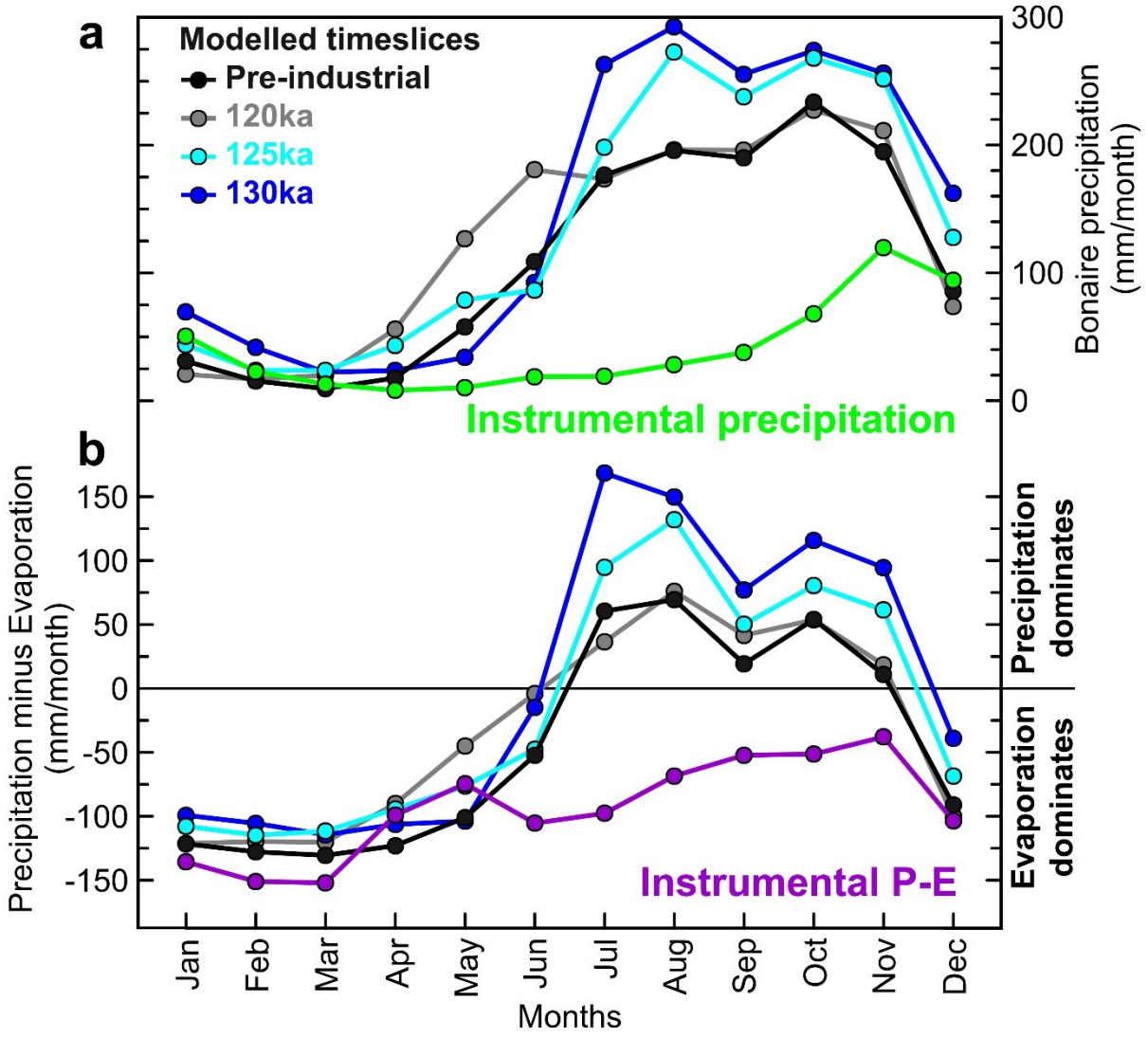

Figure 2.15: Comparisons of annual modern instrumental and modelled last interglacial precipitation cycles. a) Monthly averaged modelled time-slices from ECHAM5/MPIOM-WISO for a 1° x 1° grid box centered during the pre-industrial (black), 120 (grey), 125 (light blue) and 130 ka (dark blue) and instrumental precipitation records from Kralendijk weather station upon Bonaire (green) (Lawrimore et al., 2011) (1924-51 and 1971-79 AD). b) From the same model, precipitation minus evaporation compared to gridded instrumental values within a 2.8° x 2.8°gridbox centred at 67.5°W, 12.5°N 1950-2000 AD (NCAR) (Kalnay et al., 1996). Positive values denote net precipitation at Bonaire.

2.2.5.2 LIG coral derived $\delta^{18}O_{seawater}$ seasonality

Seasonal changes in $\delta^{18}O_{seawater}$ account for differences seen in the reconstructions of coral Sr/Ca-SST and coral $\delta^{18}O$-SST seasonality. Interestingly, we find during the early LIG the only example of a positive coral $\delta^{18}O_{seawater}$ seasonality anomaly value for any LIG period studied at Bonaire (Fig. 2.11c). Although akin to a mid-Holocene coral from 6.22 ka that has been interpreted to reflect hydroclimate cycle effects such as, among others, Bonaire summer

rainfall (Giry et al., 2013; Felis et al., 2015), this value is not significantly above the modern error. At 6.22 ka, and perhaps at 129.7 ka, positive coral $\delta^{18}O_{seawater}$ seasonality anomalies are understood to represent a change from the modern hydroclimate regime, characterised by winter rainfall (Martis et al., 2002), to one dominated by summer rains. An increase in mid-Holocene precipitation during boreal summer occurs because of a more northerly displaced ITCZ (Haug et al., 2001; Giry et al., 2013) and thermodynamically induced processes that result from increased local summer insolation (Schneider et al., 2014). Compared to the present interglacial, the LIG was characterised by a differing orbital configuration that increased seasonality of insolation (Fig. 2.12c) (Berger, 1978), and thus meridional temperature gradients. One could hypothesise that, due to these orbital parameters facilitating the LIG northward migration and/or expansion of the ITCZ, Bonaire coral $\delta^{18}O$ records should reconstruct this influence. However, according to the coral $\delta^{18}O_{seawater}$ seasonality anomaly estimates (Fig 3c), coral $\delta^{18}O_{seawater}$ seasonality did not deviate significantly from modern values during the LIG.

Coral $\delta^{18}O_{seawater}$ seasonality derived from the mean annual $\delta^{18}O_{seawater}$ cycle was found to be higher than modern (Fig. 2.11d) and statistically resolvable (Cahyarini et al., 2008) at 2.35 (Giry et al., 2013) and 123.9 ka (Fig. 2.13), suggesting enhanced and well-defined seasonal hydroclimate regimes at these times. Interestingly, higher than modern $\delta^{18}O_{seawater}$ seasonality is also noted during the mid-LIG at 123.3 and 125.5 ka despite these records consisting of fewer than the 10 years required to be considered representative of their respective time intervals. Despite, a paucity of reliable instrumental SSS records at Bonaire and no modern $\delta^{18}O_{seawater}$ records, a comparatively small annual SSS cycle of ~0.6 psu can be seen within gridded instrumental records (Fig. 2.9c) (Carton and Giese, 2008; Zweng et al., 2013). Broadly instrumental SSS records demonstrate more saline and fresher conditions in March-April and August to October, respectively. However, the modern coral mean annual $\delta^{18}O_{seawater}$ cycles is contrary to this with fresher and more saline conditions in winter (Feb/Mar) and summer (Sep/Oct), respectively. This occurs due to the dominance of coral Sr/Ca-SST upon coral $\delta^{18}O$ using the calibrations of Hetzinger et al. (2006). These uncertainties are reflected by modern Bonaire corals which reconstruct statistically insignificant seasonality of $\delta^{18}O_{seawater}$ (Fig. 2.12) and large inter-colony differences. Indeed, these inter-colony differences prohibit the meaningful conversion of $\delta^{18}O_{seawater}$ to SSS (Giry et al., 2013). Therefore, although the $\delta^{18}O_{seawater}$ seasonality anomaly identified no significant change to the state of the seasonal hydroclimate regime during the LIG (Fig. 2.11c) the higher than modern and statistically robust $\delta^{18}O_{seawater}$ seasonality at 123.9 ka (Fig. 2.11d) is indicative of a well-defined LIG hydroclimate

at that time. Consequently, the timing between LIG coral Sr/Ca and $\delta^{18}O$ is considered within the next section as a third indicator of hydroclimate change.

2.2.5.3 Phase angle between LIG coral $\delta^{18}O$ and Sr/Ca annual cycles

We assessed the relative timing of reconstructed environmental parameters in detail by examining the phase angle relationship between our coral $\delta^{18}O$ and Sr/Ca records. The timing of the annual SST cycle at Bonaire is well-defined with a maximum and minimum in September -October and February-March, respectively (Smith et al., 2008). Simulations reveal that, despite an orbital configuration that differs from present, this remained unchanged during the LIG (Brocas et al., 2016). Moreover, our coral $\delta^{18}O$ records and the Sr/Ca records of Brocas et al. (2016) derive from the same colony samples, and so share an internal chronology. Thus, any resolvable phase difference can be attributed to the influence of hydroclimate. Phase analysis is also independent of the choice of the proxy-SST calibrations used because the relative amplitude between records is not a contributing factor. During the early LIG (at 129.7 ka), when reconstructed $\delta^{18}O_{seawater}$ seasonality anomaly is positive, although not significant, we find no notable phase angle difference between the coral Sr/Ca and coral $\delta^{18}O$ annual cycles. Therefore, if a change in the hydroclimate regime occurred, the timing of the $\delta^{18}O_{seawater}$ annual cycle was not altered from modern. However, at 123.9 ka an extremely distinct 2-month phase lead of the coral $\delta^{18}O$ annual cycle vs. the Sr/Ca annual cycle is found, suggesting less saline conditions occurred in July-August and conditions that are more saline in December-January. This finding is observable, irrespective of season, within much of the 37 years that comprise the coral Sr/Ca and $\delta^{18}O$ records at 123.9 ka (Fig. 2.14). Consequently, our longest mid-LIG coral record displays two (a 2- month phase $\delta^{18}O$ lead and higher than modern coral $\delta^{18}O_{seawater}$ seasonality) out of three indicators of a hydroclimate regime that existed within the southern Caribbean Sea that was distinctly different from today.

2.2.5.4 Climate model simulations of LIG hydroclimate

Our ECHAM5/MPIOM-WISO model simulations can be used to identify changes to, and spatial patterns of, LIG tropical Atlantic hydroclimate which would not be possible with our coral records alone. The modern annual cycles of precipitation (Fig. 2.15a) and P-E (Fig. 2.16b) are successfully modelled by our P.I. time-slices, exhibiting similar temporal patterns as instrumental records. However, absolute P.I. time-slice precipitation and P-E values are increased compared to modern which may be attributed to overlap of the modelled gridbox centred on Bonaire with adjacent regions that have a more precipitation dominated hydroclimate. During the LIG, at 125 and 130 ka, the annual cycle of precipitation displays

higher than P.I. values between July and November as well as a more summer (JJA) orientated distribution of precipitation. Although the pattern of P-E remains much the same as P.I., precipitation increasingly dominates at 125 and 130 ka. These results are indicative of a hydroclimate that differed from modern during the early and mid-LIG. However, considering the temporal proximity of the 130 ka time-slice simulations to the TII deglacial event that saw rapid sea level fluctuations we will not consider these early LIG findings further. The spatial distribution of modelled 125 ka minus P.I. tropical Atlantic summer (JJA) precipitation reveals increased values along northern coastal South America and the Orinoco river basin at 125 ka (Fig. 2.16a). The ITCZ dominates regional precipitation patterns and so our simulation suggest that rainfall was likely intensified in response to ITCZ migratory dynamics. Indeed, between 5 and 15°N increased 125 ka minus P.I. precipitation anomaly is accompanied by decreased values to the south revealing a distinct northward shift of the ITCZ over this oceanic region. Despite no modern instrumental $\delta^{18}O_{seawater}$ records existing for the distinct hydroclimate of Bonaire, our model has previously been demonstrated to successfully simulate $\delta^{18}O_{seawater}$ for other parts of the Caribbean and tropical Atlantic (Werner et al., 2016) and exhibit a temporal pattern akin to modern SSS records (Fig. 2.16b) (Carton and Giese, 2008; Zweng et al., 2013). An increase of 0.3‰ in 125 ka modelled $\delta^{18}O_{seawater}$ seasonality is due to depleted $\delta^{18}O_{seawater}$ between August and December (Fig. 2.16c) and is accompanied by increased modelled boreal summer precipitation at that time.

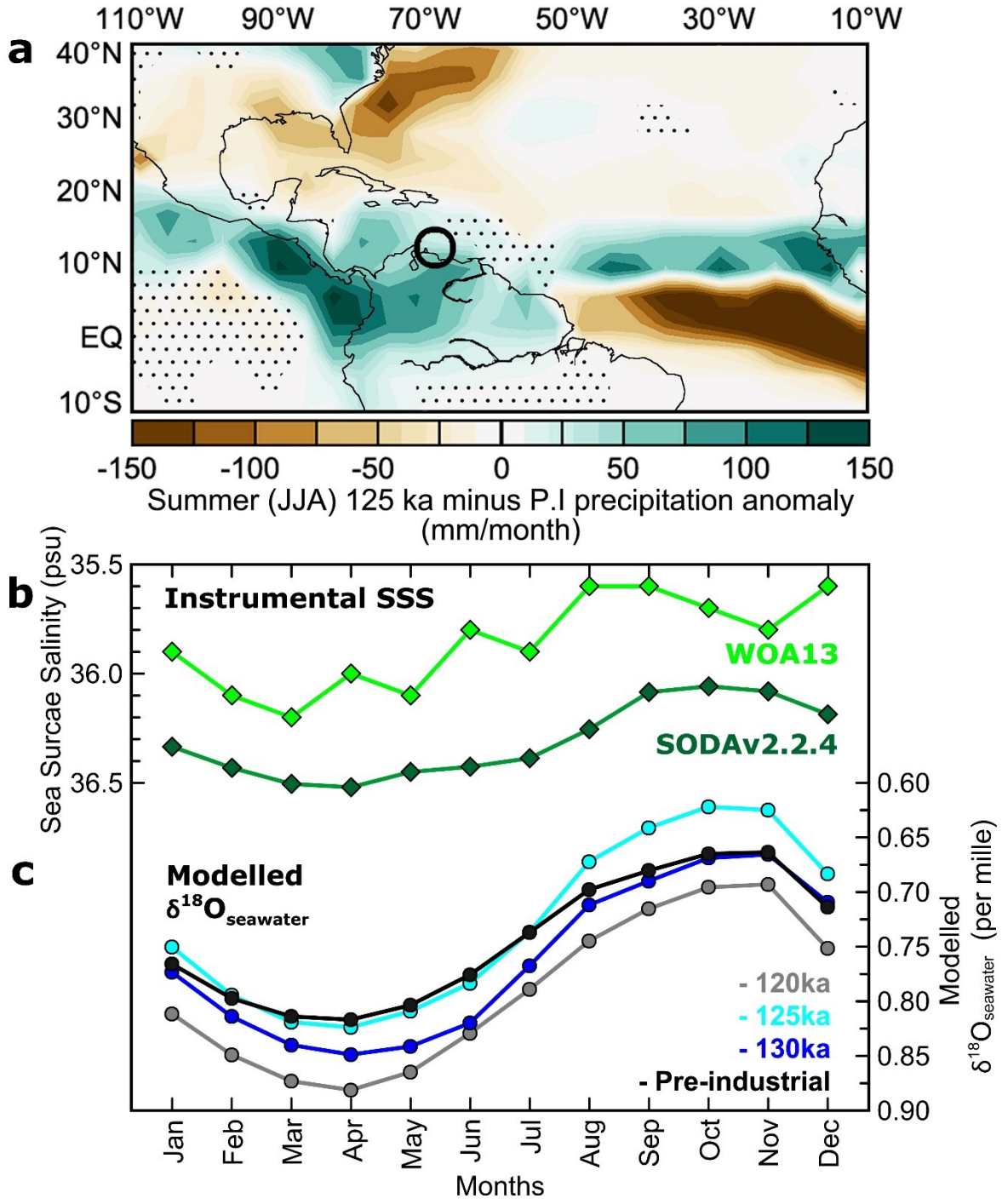

Figure 2.16: Comparison of modern instrumental and last interglacial hydroclimate at and surrounding Bonaire. a) ECHAM5/MPIOM-WISO modelled tropical Atlantic summer (JJA) 125 ka minus pre-industrial (P.I.) precipitation anomaly. Hatching denotes modelled regions statistically identical to the P.I. at the 95% confidence level using a student t-test. Bonaire is found within the circle. b) Instrumental gridded sea surface salinity records from the Simple Ocean Data Assimilation Reanalysis (SODAv2.2.4, light blue) (Carton and Giese, 2008) and the World Ocean Atlas 2013 (WOA13, dark blue) (Zweng et al., 2013) for a period 1955 to 2012 AD. c) ECHAM5/MPIOM-WISO modelled $\delta^{18}O_{seawater}$ for a 1° x 1° grid box centred on Bonaire during the pre-industrial (black), 120 (grey), 125 (light blue) and 130 ka (dark blue) time-slices.

Our model results are indicative of a hydroclimate, and SSS, dominated by boreal summer precipitation rather than oceanic advection during the mid-LIG. Our 125 ka time-slice model and 123.9 ka coral (Fig. 2.11d-e) findings complement one another, together evidencing that the mid-LIG hydroclimate of Bonaire witnessed a northward expansion of ITCZ off the coast of northern South America into the Caribbean Sea. This represent a significant departure for the spatially small region (~200 x 50 km) of hydroclimate the ABC islands currently experiences that is distinct within the southern Caribbean Sea in not receiving ITCZ related precipitation.

2.2.5.5 Other proxy records of LIG southern Caribbean hydroclimate

Sedimentary records from the Cariaco Basin have identified different clay mineral compositions related to the source material originating from various northern Venezuelan rivers during the last glacial/interglacial cycle (Riboulleau et al., 2014). These data indicate that, compared to today, the Cariaco Basin was influenced by a more northerly positioned ITCZ, which increased coastal Venezuelan precipitation during the LIG. A more northerly expanded ITCZ may have also been accompanied by an increase in thermodynamically induced summer rainfall stimulated by the prevailing orbital forcings at that time (Schneider et al., 2014). North easterly trade winds are suppressed by a more northerly positioned ITCZ resulting in a reduction in the eolian derived sedimentary component recorded within the Cariaco basin (Yarincik et al., 2000). Additional evidence from the Colombian Basin reveals that the hydroclimate of the Caribbean Sea likely experienced greater precipitation resulting in less saline sea surface conditions during the LIG (Schmidt and Spero, 2011). However, the hydroclimate signal documented in these Cariaco and Colombian Basin sedimentary records derives primarily from the river catchments of continental northern South America (Colombia and Venezuela) that discharge directly into the southern Caribbean Sea. It is also important to note that at present peak Amazon River freshwater discharge between August and November deviates north upon entering the Caribbean Sea and does not directly influence SSS at Bonaire (Fig. 2.9b) (Chérubin and Richardson, 2007). Consequently, our coral and modelling findings provides direct evidence of a northward expansion of the ITCZ into the Caribbean Sea during the mid-LIG

2.2.6 Conclusions

Our coupled coral $\delta^{18}O$ allow for the reconstruction of tropical Atlantic hydroclimate seasonality during multiple time intervals of the LIG from available Sr/Ca-SST proxy records from the southern Caribbean island of Bonaire. These monthly resolved records are assessed in the context of previous modern, mid- to late Holocene (Giry et al., 2013) and late LIG (Felis et al., 2015) coral reconstructions from the same island. A significantly higher than modern coral $\delta^{18}O$ seasonality during the mid-LIG (124-126 ka) occurred alongside increased SST seasonality at that time, reflecting the coevolution of $\delta^{18}O$ seasonality with Sr/Ca-SST and seasonality of insolation throughout the LIG. At 124 ka, we also reconstruct a 2-month lead of the coral $\delta^{18}O$ annual cycle vs. Sr/Ca-SST and increased $\delta^{18}O_{seawater}$ seasonality. These coral findings are contemporaneous with our model results that similarly suggest a boreal summer precipitation dominated hydroclimate during the mid-LIG. Together our coral and climate model-based findings provide evidence for a mid-LIG northward expansion of the South American Intertropical Convergence Zone (ITCZ) into the southern Caribbean Sea. A scenario distinctly different from the hydroclimate regime found at Bonaire today. Our study supports the broad spatial coherence of ITCZ migratory dynamics during the mid-LIG, and highlights the importance of regional aspects in proxy and model estimates of hydroclimate seasonality during the LIG.

2.2.7 Acknowledgments

The Government of the Island Territory of Bonaire of the former Netherlands Antilles (now the Caribbean Netherlands) are thanked for research and fieldwork permissions, and E. Beukenboom (STINAPA Bonaire National Parks Foundation) for support. The Deutsche Forschungsgemeinschaft funded this study through grants FE 615/3-2, 3-4 to T.F., SCHO 1274/4-4 to D.S. and LO 895/9-4 to G.L. (DFG Priority Programme INTERDYNAMIK - SPP 1266), and FE 615/5-1 to T.F. J. Pätzold and C. Giry are thanked for field assistance, S. Pape for maintaining and operating of the ICP-OES, as well as M. Segl for stable isotope analysis. We acknowledge G. Wefer, H. Kuhnert and M. Martinez for their contribution to discussions. T.F. is supported through the DFG-Research Center/Cluster of Excellence ‘The Ocean in the Earth System’ at the University of Bremen. W.B. acknowledges support from GLOMAR (Bremen International Graduate School for Marine Sciences). All coral data used in this study can be obtained from www.pangaea.de.

2.3 Corals evidence mid-last interglacial tropical Atlantic cooling and freshening

Authors: W. M. Brocas[1], T. Felis[1]

[1]MARUM - Center for Marine Environmental Sciences, University of Bremen, 28359 Bremen, Germany.

Corresponding author: William M. Brocas (wbrocas@marum.de)

Key Points (3x140 characters):

- Mid-last interglacial coral Sr/Ca reconstructs ~2.0 °C colder than modern sea surface temperatures
- Paired coral $\delta^{18}O$ allowed $\delta^{18}O_{seawater}$ to be isolated, revealing a fresher mid-LIG due to increase ocean advection of equatorial surface waters
- Coral Sr/Ca and $\delta^{18}O$ records complement sedimentary records of last interglacial tropical Atlantic temperature and hydroclimate change

Keywords:
last interglacial, coral Sr/Ca, coral $\delta^{18}O$, coral $\delta^{18}O$ seawater, tropical Atlantic, temperature, hydroclimate

2.3.1 Abstract

The last interglacial (LIG, Marine Isotope Stage 5e, 127-117 ka) experienced globally warmer than modern temperatures and profound regional differences occurred relevant to the assessment of future climate change scenarios. Tropical Atlantic sea surface temperatures (SST) and hydroclimate are intrinsic to the spatiotemporal climatic evolution of such societally relevant periods. Eight monthly resolved coral Sr/Ca reconstruct mean annual SST and are paired with $\delta^{18}O$ records to reveal $\delta^{18}O_{seawater}$ changes throughout the LIG tropical Atlantic. ~2.0 °C colder SST and less saline than modern surface waters are found at ~125 ka. Despite proxy specific uncertainties our coral findings agree with contemporaneous tropical Atlantic sedimentary records, together indicating enhanced mid-LIG ocean advection of colder and fresher equatorial Atlantic waters. Modern like SST and salinities were then reconstructed from ~124 ka into the late LIG suggesting the arrival of a northward expanded boreal summer intertropical convergence zone, dampening ocean advection.

2.3.2 Introduction

The last interglacial (LIG, Marine Isotope Stage (MIS 5e), 127-117 ka) represents a time period partially analogous to the natural climate evolution expected for the present interglacial. LIG reconstructions have yielded a range from no significant change to ~2 °C warmer than pre-industrial (P.I.) global temperatures (CLIMAP Project Members et al., 1984; Turney and Jones, 2010; McKay et al. 2011; Otto-Bliesner et al., 2013). This is comparable to future climate change projections which rely on robust quantification of environmental parameters during society relevant time periods, such as the LIG. Importantly, the LIG differed from present due to an orbital configuration that promoted the seasonality of insolation globally (Berger, 1978) and regional difference, such as pronounced warming in the extra-tropics (> 23.5 °N- 23.5 °S) (Capron et al., 2014). Although the LIG is not considered a perfect global analog, insights can be gained into the regional response to, and the drivers behind, feedback mechanisms involved with future climate change scenarios (*Tzedakis et al.,* 2012). Such insights further the understanding of LIG climatic spatiotemporal evolution and so aids the contextualization of anthropogenic influences upon modern and future climates. Critical to the planets distribution of heat, the AMOC modulates glacial/interglacial climate change and its dynamics are partly governed by the heat and freshwater budget of the Caribbean Sea and tropical Atlantic (Leduc et al., 2007).

The current understanding of LIG tropical Atlantic annual SST derives from foraminifera assemblage transfer functions, Mg/Ca and $U^{k'}_{37}$ proxies. While Mg/Ca-SST and $\delta^{18}O$ records can be coupled to infer $\delta^{18}O_{seawater}$ changes, there is currently a paucity of records portraying tropical Atlantic hydroclimate change. Fossil coral Sr/Ca records are used to reconstruct sea surface temperatures (SST) and can be combined with coral $\delta^{18}O$ records to yield $\delta^{18}O_{seawater}$ values indicative of past hydroclimate changes (*Gagan et al.,* 1998). Such coral records are often dated using $^{230}Th/U$- dating techniques (*Obert et al.,* 2016) with well constrained uncertainties, allowing paleoclimatic insights to be gained independent of the orbital tuning methods that typically underpin sedimentary records. Additionally, the growth structure of tropical corals facilitates the generation of internally consistent records, portraying the response to climatic variability at sub-seasonal to centennial resolution. This resolution allows mean annual Sr/Ca-SST and $\delta^{18}O_{sewater}$ values to be calculated from tens to hundreds of individual measurements without seasonal bias. These attributes complement sedimentary records which typically explore broader variability from single measurements on centennial to millennial timescales. Additionally, the interpretation of specific sedimentary records is often complicated by the assumption of globally synchronous LIG warmth, insufficient sampling

resolution, seasonal bias, temporal averaging, proxy calibrations and age uncertainties (Leduc et al., 2017; Hoffman et al., 2017). In order to address such proxy-specific uncertainties, commonalities are sought between coral and sedimentary palaeoclimate records with the aim of better constraining LIG spatiotemporal temperature and hydroclimate change. Previously fossil corals have reconstructed higher than modern tropical Atlantic sea surface temperature and $\delta^{18}O_{seawater}$ seasonality during the LIG (Felis et al., 2015; Brocas et al., 2016; Brocas et al., submitted). These changes coincided with higher seasonality of insolation values and were indicative of intertropical convergence zone (ITZC) dynamics at that time. However, it is unknown whether the mean annual conditions of the tropical Atlantic were altered in response.

2.3.3 Materials and Methods

2.3.3.1 Coral material and its environmental setting

Fossil *Diploria strigosa* (*D. Strigosa*) colonies were recovered from the southern Caribbean island of Bonaire (Caribbean Netherlands, 12 °10'N, 68 °18'W) (Fig. 18). This open ocean setting is located 100 km north of Venezuela and is currently characterised by a semiarid climate, receiving ~550 mm of rainfall per year. Easterly trade winds that comprise the Caribbean low level jet (CLLJ) prevail throughout the year ensuring a close connection between this region and the north Atlantic subtropical high. The CLLJ drives the oceanic currents that supply tropical Atlantic waters to the Caribbean where they warm, become more saline, and eventually feed into the Gulf Stream (Fig. 18). Eight fossil *D. strigosa* colonies have been dated using coral ^{230}Th/U dating techniques to between 117.7 and 129.7 ka (Felis et al., 2015; Obert et al., 2016). Consistent with well-established methodologies and techniques (Giry et al. 2010, 2013; Felis et al., 2009), fossil *D. strigosa* colonies were sectioned parallel to growth, analysed for diagenesis (X-ray and power XRD) and micro-sampled for paired Sr/Ca geochemistry and $\delta^{18}O$ and isotopic analysis. Micro-sampling the dense thecae element within the skeletal structure of *D. strigosa* allows for the generation of monthly resolved records of sea surface properties in which the coral grew. Such techniques have previously been applied to generate Bonaire coral Sr/Ca and $\delta^{18}O$ records representing the mid- to late Holocene (Giry et al., 2012, 2013) and LIG (Felis et al., 2015, Brocas et al., 2016). Mean annual Sr/Ca, $\delta^{18}O$ and $\delta^{18}O_{seawater}$ of these eight LIG fossil *D. strigosa* colonies were calculated by averaging the monthly interpolated record value for each year, and then averaged these for the entire record. Coral Sr/Ca proxies' sea surface temperatures (SST) and we used the annual relationship of -0.066 (Hetzinger et al., 2006), -0.084 (Gagan et al., 2012) and -0.140 mmol/mol per ^{o}C (Felis et al., 2009). These three calibration slopes were used in the absence of a conclusive calibration for

annual Sr/Ca-SST for tropical Atlantic *D. strigosa*. This approach mitigates potential calibration uncertainties, as demonstrated with *Isopora* corals (Felis et al., 2014). The annual Sr/Ca-SST relationship of -0.066 was reported in the same study as the established monthly resolved *D. strigosa* relationship of -0.042 mmol/mol per ºC (Hetzinger et al., 2006; von Reumont et al., 2016; Xu et al. 2015; Brocas et al., 2016). The annual calibration slopes of -0.084 (Gagan et al., 2012) and -0.140 mmol/mol per ºC (Felis et al., 2009) derive from the annual rescaling of seasonal SST calibrations and an mean annual calibration, respectively, for the better studied *Porites* spp. coral. Coral $\delta^{18}O$ contains components related to SST and the $\delta^{18}O$ content of seawater ($\delta^{18}O_{seawater}$) allowing coral $\delta^{18}O_{seawater}$ to be calculated by subtracting the coral Sr/Ca-SST component from the coral $\delta^{18}O$-SST signal (Cahyarini et al., 2008). We used the coral $\delta^{18}O$-SST annual relationship of -0.196 ‰ per °C (Hetzinger et al., 2006) which is similar to the *Porites* spp. coral $\delta^{18}O$-SST calibration slope of -0.220 ‰ per °C (Felis et al., 2009, Gagan et al., 2012). Coral mean annual Sr/Ca-SST anomalies were calculated from modern (coral ΔSST) by subtracting the mean of three modern colony (Giry et al., 2012). Individual fossil mean annual coral Sr/Ca-SST, $\delta^{18}O$ and $\delta^{18}O_{seawater}$ values were assessed using the combined error (c.e.) (Abram et al., 2009) which incorporates uncertainties associated with the observed differences between the mean annual values of three modern corals (Giry et al., 2012). This represents uncertainties associated with corals potentially inhabiting differing palaeo-reef environments (water depths), time intervals and locations. The c.e. is calculated by combining (root of the sum of the squares) the (1) ±1 standard deviation (±1 s.d.) of the reconstructed modern mean SST seasonality derived from the three modern corals and (2) the ±1 standard error (s.e.) of the mean of multiple SST seasonality estimates within each fossil coral (Abram et al., 2009). Additionally all mean annual values were assessed relative to the ±1 s.d. of the three modern corals.

2.3.3.2 Comparing LIG coral Sr/Ca and $\delta^{18}O_{seawater}$ to sedimentary records

We compiled tropical Atlantic (0-35 °N, 100-30 °W) sedimentary records that reportedly reconstruct LIG annual SST and derive from sedimentary foraminifera assemblage transfer functions, $U^{k'}_{37}$ and Mg/Ca proxy records. LIG SST anomalies (sedimentary ΔSST) have been previously complied and defined by Turney and Jones, (2010), McKay et al. (2011) and (Hoffman et al., 2017) using different methodologies that best addressed specific research questions and uncertainties (supplementary figure 2.20). Our study defined sedimentary ΔSST within sedimentary record by subtracting the most recent from the nearest reconstructed annual SST to 125.8 ka. Foraminifera assemblage derived ΔSST results from the peak SST of a three

point running average over MIS 5e interval being subtracted from core top values, as per CLIMAP Project Members et al. (1984). Annual foraminifera assemblage SST records often derive from the averaged LIG summer and winter records (unless specified the boreal season is always referred to). However, this results in a seasonal bias which we corrected for by subtracting from the sedimentary ΔSST the difference between a) the average of summer (JJA, June-July-August) and winter (DFJ, December-January-February) SST and b) the annual average SST, using ERSSTv3b (1910-2000 AD) (Smith et al., 2008).

2.3.4 Results and discussion

2.3.4.1 Mid-LIG coral Sr/Ca- and sedimentary SST anomalies

Higher mean annual coral Sr/Ca are reconstructed by three of five mid-LIG corals, however only one of these corals, dated to 125.8 ka, is significantly higher than the three modern coral mean (Fig. 2.17b) (Giry et al., 2012). This coral shares a similar age to a coral dated at 125.5 ka and so these mean annual coral Sr/Ca-SST are averaged. In order to address potential calibration uncertainties we consider a variety of published Sr/Ca-SST calibration slopes from Hetzinger et al. (2006), Gagan et al. (2012) and Felis et al. (2009) that yield a significantly colder than modern peak mid-LIG coral ΔSST of 4.0, 3.1 and 1.9 °C, respectively. We favour the latter calibration of Felis et al. (2009) due to its utility in reconstructing last deglacial meridional SST changes within the Great Barrier Reef. Whereas coral annual ΔSST reconstruction are comparable to tropical Atlantic Last Glacial Maximum sedimentary reconstruction (ranging from 2.5 (Schmidt and Spero, 2011) to 4.8 °C (Ziegler et al., 2008)) using Hetzinger et al. (2006) and Gagan et al. (2012) Sr/Ca-SST calibration values. Importantly our findings remains significant regardless of the specific coral Sr/Ca-SST calibration used.

Consequently, we report a mid-LIG SST ~2.0 °C colder than modern, a value plausible within the thermal tolerance of *D. strigosa* corals if the modern mean annual SST (ERSSTv3b, 1910-2000 AD, Smith et al. (2008)) and the Sr/Ca-SST seasonality (Brocas et al., 2016) at Bonaire are considered. Therefore, these corals inhabited waters between 23 and 28°C, a range slightly lower than that for modern optimal survival, 25-29 °C (Fricke and Meischner, 1985), but higher than the lowest adaptable thermal tolerance of 18 °C (Stoddart, 1969). These coral grew at ~0.7 cm/yr, a typical rate for LIG *D. strigosa* (Brocas et al., 2016), indicating no systematic influence of mean annual growth rates upon Sr/Ca and $\delta^{18}O$ (supplementary figure 2.23). Our coral findings assume that the LIG Sr and $\delta^{18}O$ content of LIG seawater was similar to modern despite the occurrence of fluctuations associated with

continental ice volume and sea level changes on glacial-interglacial time scales (*Stoll et al.,* 1999, *Waelbroeck et al.,* 2002). Although previous studies have corrected for such fluctuations (*Kilbourne et al*., 2004; *Asami et al*., 2013; *Felis et al*., 2012, 2014), we find our findings are not significantly altered regardless of a range of relative sea level estimates considered (*Kopp et al*., 2009; *Dutton and Lambeck*, 2012; *O'Leary et al*., 2013).

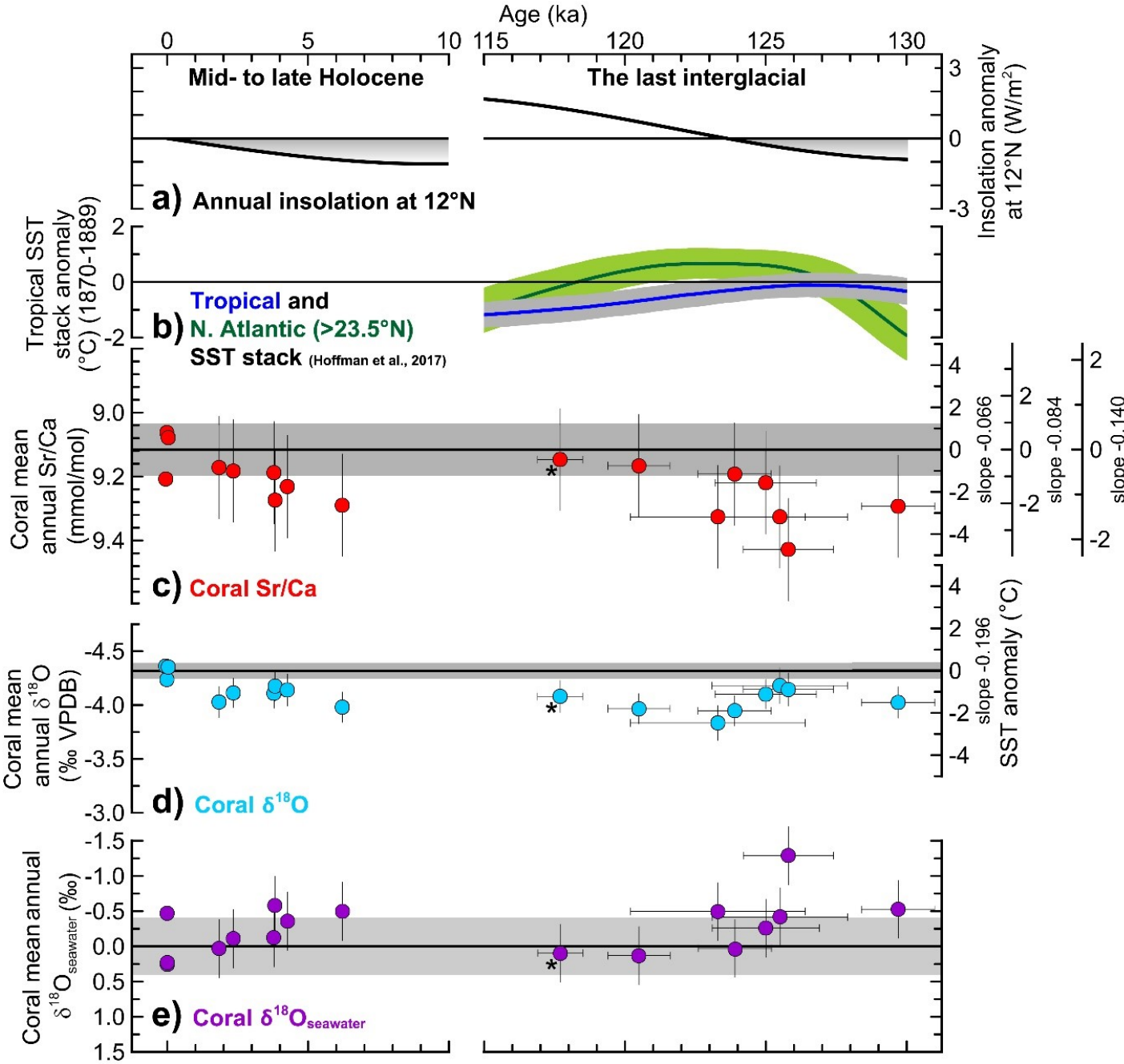

Figure 2.17: Coral- and sedimentary stack- reconstructions of Atlantic mean annual sea surface temperatures (SST) and $\delta^{18}O_{seawater}$ during the mid- to late Holocene and last interglacial (LIG). a) Mean annual insolation negative anomaly from present (grey shading) at Bonaire (12 °N) (Berger, 1978). b) LIG tropical (23.5 °N-23.5 °S) and extra-tropical north Atlantic (>23.5 °N) (thick blue and green line, respectively) mean annual SST stack anomaly from 1870-1889 HadISST1.1 (Hoffman et al., 2017) with ±2 standard deviation (s.d. grey and light green

shading, respectively). c, d and e) Modern, mid- to late Holocene (Giry et al., 2012), late LIG (*, Felis et al., 2012) and LIG (this study) mean annual coral Sr/Ca, $\delta^{18}O$ and $\delta^{18}O_{seawater}$. Vertical lines illustrates the ±1 combined error. Three coral modern mean is indicated by the thick black line with the ±1 s.d. (grey shading). LIG coral Sr/Ca-SST anomaly from the three modern coral average is calculated using the annual Sr/Ca-SST relationship of -0.066, -0084 and -0.140 mmol/mol per °C from Hetzinger et al. (2006), Gagan et al. (2012) and Felis et al. (2009), respectively. Coral annual $\delta^{18}O$-SST relationship of -0.196 ‰ per °C (Hetzinger et al., 2006) was used. Coral annual $\delta^{18}O_{seawater}$ was calculated using the coral Sr/Ca and $\delta^{18}O$ relationships of Hetzinger et al. (2006). Horizontal lines indicate ^{230}Th/U-age uncertainty at 2σ level (Obert et al., 2016).

Our reconstruction of ~2.0 °C colder mid-LIG coral mean Sr/Ca-SST derives from 180 monthly interpolated measurements (15 years) and supports single measurement foraminifera assemblage transfer function derived topical Atlantic ΔSST (supplementary figures 2.20 and 2.22). Tropical Atlantic foraminifera assemblage transfer function records are potentially influenced by surface water calibration cold biases resulting from the assumption of comparable thermal structure between P.I. and the Last Glacial Maximum (Telford et al., 2003). However, this assumption remains valid while no indication of altered subsurface- surface thermal relationships is known during the LIG. Correcting for the seasonal bias of averaged winter and summer foraminifera assemblage (CLIMAP Project Members et al., 1984) derived SST using ERSSTv3b (1910-2000 AD) (Smith et al., 2008) yields similar values of ±0.1 - 0.3 °C as those reported by Hoffman et al. (2017). Furthermore, many of these records lack a definitive age model, inhibiting further spatiotemporal interpretations of LIG SST. However, annual sedimentary ΔSST reconstructed by $U^{k'}_{37}$ and Mg/Ca are typically 0.5 to 1.5 °C warmer than other records, especially within the Caribbean Sea. The Colombian Basin Mg/Ca record (Schmidt et al, 2004) reconstructs SST at low temporal resolution and may well reflect a summer SST bias (Schmidt and Spero, 2011). Similarly, the Cariaco Basin $U^{k'}_{37}$ record reflects a tendency towards warmer spring-summer SST as a result of higher unsaturation ratios within this upwelling influenced site (Hebert and Schuffert, 2000) (Supplementary figure 2.22, record no.4 and 6, respectively). Although both records are excluded from the sedimentary ΔSST compilations of Turney and Jones (2010) and Hoffman et al. (2017), we include them here for illustrative purposes. Gulf of Mexico (GOM) Foraminifera assemblage (CLIMAP Project Members et al., 1984) and Mg/Ca (Ziegler et al., 2008) annually derived ΔSST reconstructions, indicate a 1.4 °C cooling and 1.9 °C warming, respectively. This reflects Mg/Ca-SST likely sensitivity towards an expanded summer Atlantic Warm Pool and a strengthened Loop Current which drew in warmer summer Caribbean waters during the mid-LIG (Ziegler et al., 2008; Nürnberg et al., 2008).

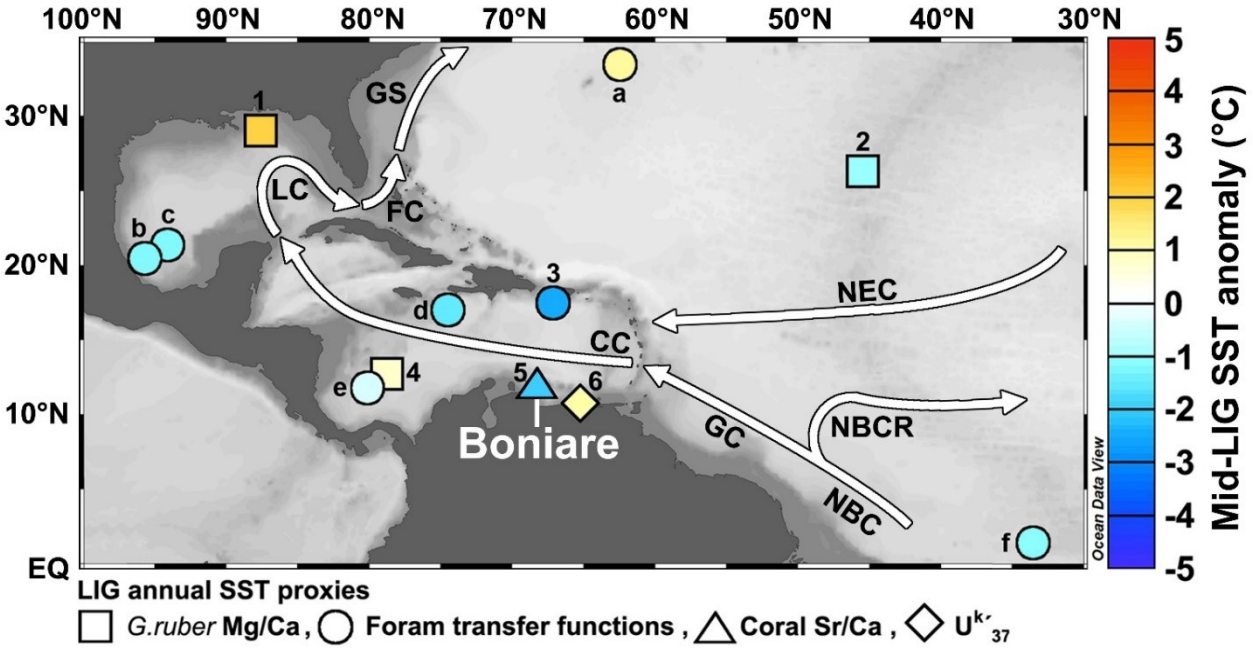

Figure 2.18: Compilation of tropical Atlantic mid-LIG SST anomalies reconstructions derived from $U^{k'}_{37}$ (diamond), Mg/Ca (numbered squares) and foraminifera assemblage transfer functions (lettered circles) sedimentary proxy records. The location of Bonaire and our coral Sr/Ca derived SST anomaly (triangle, 5) is indicated. (Schlitzer, 2015). Dominant ocean currents of the Gulf Stream (GS), Florida Current (FC), Loop Current (LC), Caribbean Current (CC), Guiana Current (GC), North Equatorial Current (NEC), North Brazil Current (NBC) and its July to December retroflection (NBCR) are illustrated.

Despite the different methodologies used, our compilation of sedimentary ΔSST agrees with those of other authors (Fig. 2, Supplementary figure S1). Colder than modern mid-LIG coral Sr/Ca and foraminifera assemblage derived ΔSST reconstructions during the (Fig. 1c) appear to be an extension of colder equatorial Atlantic ΔSST (Fig. 2, record f). Furthermore, our coral Sr/Ca-SST findings agree with the tropical mean annual SST stack generated by *Hoffman et al.* (*2017*) (Fig. 1b) which reconstructed colder than P.I. (HadISST1.1 1870-1889) and would report still colder mid LIG ΔSST if referenced to modern times. These findings occurred during a period of insignificantly lower than modern tropical annual insolation and atmospheric greenhouse gas concentrations were similar to P.I. (*Langebroek and Nisancioglu,* 2014). Thus it is unlikely these drivers of LIG climate change contributed to our findings, however minimum coral mean Sr/Ca-SST values do coincide with increased coral Sr/Ca-SST and insolation seasonality (Fig. 3a) (*Brocas et al.,* 2016). Therefore, colder than modern coral Sr/Ca-SST must result from winter (MAM, March-April-May) SST that were colder than summer (SOM, September-October-November) SST were warmer. Modern and late-Holocene winter (MAM) tropical Atlantic SST are closely related to

the strength of the easterly CLLJ that drives oceanic waters into the Caribbean (*Wang et al*., 2007; *Würtzel et al.,* 2013). Consequently, our mid-LIG coral Sr/Ca-SST results reflect increased ocean advection of colder surface waters from the equatorial Atlantic into the Caribbean Sea. This likely resulted from orbitally induced increased AMOC strength which warmed the northern hemisphere, sustained warmer European summer temperatures and lead to strong but variable Greenland ice sheet melt at that time (*Sánchez Goñi et al.,* 2013; *Capron et al.,* 2014). In regards to the spatiotemporal evolution of tropical Atlantic SST, the finding of comparably modern mean annual coral Sr/Ca-SST at 129.7 ka suggests modern like SST were reached shortly after the contemporaneous Termination II deglacial event. This was followed by a cooling leading to our reconstruction of lower than modern coral mean annual Sr/Ca-SST at 125.8 ka. An abrupt (within ~1 ka) warming to modern like SST occurred thereafter and coincides with tropical annual insolation reaching higher than modern values (Fig. 1a). However, while a similar the non-significant relationship between annual insolation and coral Sr/Ca-SST was seen within the mid- to late Holocene (*Giry et al.,* 2012), modern like late LIG coral Sr/Ca-SST coincides with higher than modern LIG annual insolation values. This, and the overall magnitude of change, further demonstrates that local annual insolation did not primarily control annual coral Sr/Ca-SST during the LIG.

Comparisons of mid-LIG climate simulations, using well established LIG initialization parameters, have been unable to reach a consensus regarding tropical Atlantic SST anomalies from P.I. during the mid-LIG (*Lunt et al., 2013*). Such modelling efforts have recently simulated ~0.5 °C colder than (*McKay et al.,* 2011), ~0.5 °C warmer than (*Nikolova et al*., 2013; *Otto-Bliesner et al.*, *2013*) and similar to (*Pedersen et al.,* 2016) P.I. mid-LIG Caribbean SST, respectively. Interestingly, our compilation of coral Sr/Ca-SST and sedimentary derived ΔSST agrees with the *Otto-Bliesner et al.* (*2013*) simulation that reveal a thin coastal strip of ~0.5 °C colder than P.I waters extending from the equatorial Atlantic along northern coastal Brazil and Venezuela. Despite uncertainties, both our mean annual coral Sr/Ca-SST and sedimentary SST records within the tropical Atlantic reconstruct a broad tendency toward warmest SST during the late-LIG (Supplementary figure S2 and S3). This is contrary to, and consistent with, the tropical (23.5 °N - 23.4 °S) and extratropical north Atlantic (>23.5°N) SST stack, respectively, at that time (*Hoffman et al., 2017*). Ultimately, our the temporal evolution of our coral Sr/Ca-SST findings agree with the tropical and North Atlantic tendency towards peak late LIG SST (*Capron et al*., 2014), while specifically, ~2.0

°C colder than modern SST akin to the equatorial and south Atlantic are reconstructed at ~125ka.

2.3.4.2 LIG tropical Atlantic hydroclimate change

Comparably modern mid-LIG mean annual coral $\delta^{18}O$ values are found, at 125.8 and 125.5 ka, and progressively enrich into the late LIG (Fig. 2.17d). This differs from our coral Sr/Ca findings and highlights the influence of coral $\delta^{18}O_{seawater}$ as a marker for hydroclimate changes during the LIG. We find lower mean annual coral $\delta^{18}O_{seawater}$ during the early and mid-LIG, however, only at 125.8 ka is this significantly lower than modern (Giry et al., 2013) (Fig. 19b). This leads a tendency from the mid- towards higher, modern like, $\delta^{18}O_{seawater}$ values into the late LIG, akin to an insignificant tendency found between the mid- Holocene and modern times (Giry et al., 2013). However, significantly lower than modern day mean annual coral $\delta^{18}O_{seawater}$ at 125.8 ka was not accompanied by other coral indicators of hydroclimate change such as those reported at 123.9 Ka (Brocas et al., submitted). Here, a 2-month lead of coral $\delta^{18}O$ vs. Sr/Ca (Fig. 2.19c) and increased coral $\delta^{18}O_{seawater}$ seasonality was found (Fig. 2.19d) and coincided with higher than modern mid-LIG simulated tropical Atlantic precipitation (Nikolova et al., 2012; Pedersen et al., 2016; Brocas et al., submitted). This indicated that at 123.9 ka the hydroclimate of Bonaire was predominately characterised by summer precipitation rather than ocean advection, with most precipitation in winter, as it is today. Such hydroclimate perturbations coincided with a peak in higher than modern LIG seasonality of isolation (Fig. 2.19a.) and evidence an intensification and expansion of the summer ITCZ into the southern Caribbean Sea at that time. Conversely, we find modern like mean annual coral $\delta^{18}O_{seawater}$ values at 123.9 ka suggesting SSS were not altered in response to summer ITCZ expansion. However, lower than modern $\delta^{18}O_{seawater}$ are reported within a late LIG Colombian basin sedimentary record (Fig. 2.19e) (Schmidt and Spero, 2011) in response to increased ITCZ induced summer precipitation, demonstrating regional sensitivities within the southern Caribbean Sea.

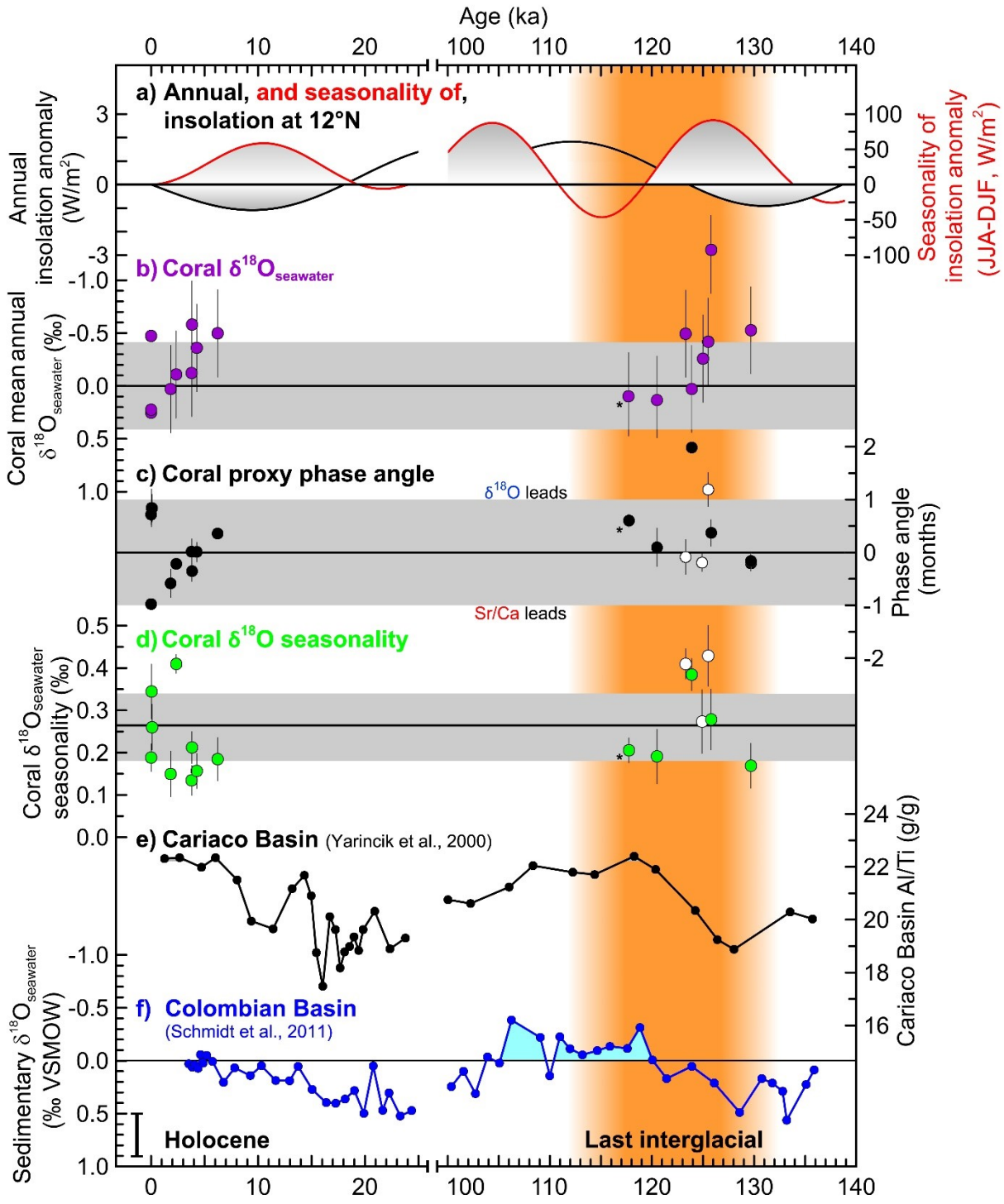

Figure 2.19: Coral $\delta^{18}O_{seawater}$ and sedimentary evidence for hydroclimate changes from present upon the tropical Atlantic. a) Annual (black line) and seasonality of (red line, June-July-August minus December-January-February) insolation at 12°N, grey shading illustrates positive and negative anomalies from present values (Berger, 1978). b) Bonaire coral mean annual $\delta^{18}O_{seawater}$ reconstructed for the mid- to late Holocene (Giry et al., 2013), late last interglacial (LIG) (*, Felis et al., 2012) and LIG (this study). c) Bonaire coral phase angle relationship between paired Sr/Ca and $\delta^{18}O$ records (Brocas et al. submitted). Black horizontal lines indicate 95% confidence interval. Arbitrary ±1 month shading is indicated to account for potential interpolation uncertainties. d) Bonaire coral $\delta^{18}O_{seawater}$ seasonality derived from the

climatology of $\delta^{18}O_{seawater}$ records (Brocas et al. submitted). (c, d) Potentially unrepresentative records comprised of fewer than 10 years are indicate by white circles. (b, d) Coral $\delta^{18}O_{seawater}$ seasonality and mean $\delta^{18}O_{seawater}$ is estimated using the Sr/Ca- and $\delta^{18}O$- SST seasonal relationship of -0.042 mmol/mol per ºC and -0.196 ‰ per °C, respectively. Vertical black lines indicate the ±1 combined error. The three modern coral average is depicted by the horizontal black line surrounded by the ±1 standard deviation (light grey shading). e) Cariaco Basin sedimentary record of Al/Ti ratios indicative of eolian transported dust particles. Higher values indicate reduced eolian input as a result of a more northerly displaced ITCZ. f) Sedimentary record of reconstructed $\delta^{18}O_{seawater}$ during the Holocene and LIG from ODP hole 999A (12°N, 78°W, Colombian basin) (Schmidt et al. 2011). Fresher than mid-Holocene values are indicated by light blue shading. The black bracket (bottom left) signifies the ± 1σ propagated error for this $\delta^{18}O_{seawater}$ record.

Our significantly lower coral mean annual Sr/Ca-SST and $\delta^{18}O_{seawater}$ at 125.8 ka findings indicate enhanced ocean advection, due to a strengthen AMOC and the Guiana Current, of colder and fresher than modern Atlantic surface waters into the southern Caribbean Sea at that time. ITCZ and AMOC dynamics are closely coupled, such that a strengthened AMOC evidences increased interhemispheric extratropical temperature gradients that are conducive to the northward expansion/migration of the ITCZ (Schneider et al., 2014). The transition from 125.8 ka toward modern like temperatures and salinities at 123.9 ka is consistent with a progressive expansion of the ITZC into the southern Caribbean during that period (Brocas et al., submitted). This was also likely accompanied by increased thermodynamically induced local summer rainfall due to increased seasonality of insolation at that time (Fig. 2.19a). Furthermore, easterly trade winds that promote surface heat loss, vertical mixing and drive oceanic currents were likely diminished, suppressing the advection of colder and fresher oceanic waters into the Caribbean Sea. This scenario agrees with the reconstruction of increased sedimentary Al/Ti within the Cariaco Basin, indicative of reduced eolian derived sedimentary material and wind fields during a northerly migration of the ITCZ at that time (Fig. 2.19d) (Yarincik et al., 2000). Additionally, a return to modern like SST and SSS may have been influenced by the gradual intensification of the North Brazil Current summer-fall retroflection between 125 and 115 ka that diverted colder and less saline oceanic and Amazon waters away from the Caribbean Sea (Govin et al., 2015b). Thus our mean annual coral $\delta^{18}O_{seawater}$ records contribute to the paucity of records that reconstruct the spatiotemporal evolution of tropical Atlantic hydroclimate during the LIG.

2.3.5 Conclusions

Our tropical Atlantic corals reconstruct comparably modern mean annual Sr/Ca-SST during much of the LIG, however these were interrupted by ~ 2.0 °C colder than modern SST

at ~125 ka. This was likely in response to winter temperatures being colder than summer temperatures were warmer at that time. Our coral records are independent from and support colder than modern mid-LIG SST reconstructions derived from foraminifera transfer functions, indicating regional commonalities despite of proxy specific uncertainties. Together these reconstructions characterise colder than modern mid-LIG tropical Atlantic SST while north Atlantic SST were warmer. This is indicative of increased ocean advection into the tropical Atlantic due to strengthened AMOC at that time. Furthermore, annual coral Sr/Ca-SST records are used to isolate SST from paired $\delta^{18}O$ records allowing LIG hydroclimate change to be deciphered. We find lower than modern coral annual $\delta^{18}O_{sewater}$, and thus fresher SSS, accompanied colder SST further indicating increased ocean advection at 125.8 ka. We find modern like mean annual Sr/Ca-SST and $\delta^{18}O_{sewater}$ accompanied a coral dated to 123.9 ka which, alongside contemporaneous climate simulation, demonstrated the existence of a hydroclimate at that time which differed from present, due to the expansion of the summer ITCZ into the southern Caribbean Sea (Brocas et al., submitted). This suggests an abrupt transition occurred between 125.8 and 123.9 ka as the progressive influence of a northward expanding summer ITCZ served to dampen trade winds and ocean advection. We illustrate the utility of our mean annual coral Sr/Ca-SST and $\delta^{18}O_{seawater}$ records to further constrain the spatiotemporal evolution of LIG tropical Atlantic during this period of societal relevant climate change.

2.3.6 Acknowledgments

We thank the Government of the Island Territory of Bonaire of the former Netherlands Antilles (now Caribbean Netherlands) for research and fieldwork permissions, and E. Beukenboom (STINAPA Bonaire National Parks Foundation) for support. This study was funded through grants FE 615/3-2, 3-4 to T.F., SCHO 1274/4-4 to D.S. and LO 895/9-4 to G.L. (DFG Priority Programme INTERDYNAMIK - SPP 1266), and FE 615/5-1 to T.F by the Deutsche Forschungsgemeinschaft. We thank J. Pätzold and C. Giry for field assistance, S. Pape for maintaining and operating of the ICP-OES, as well as M. Segl for stable isotope analysis. G. Wefer, H. Kuhnert, M. Martinez and D. De Vleeschouwer are acknowledged for their contribution to discussions. T.F. is supported through the DFG-Research Center/Cluster of Excellence ‘The Ocean in the Earth System’ at the University of Bremen. W.B. acknowledges support from GLOMAR (Bremen International Graduate School for Marine Sciences).

2.3.7 Supporting Information

This supplementary material contains additional figures pertinent to the study of last interglacial (LIG) sea surface temperatures (SST) using fossil coral material.

Figure 2.20 illustrates our compilation of tropical Atlantic mid-last interglacial (LIG) SST anomalies derived from sedimentary records and coral Sr/Ca-SST with previously published compilations. Although these compilation address proxy-specific uncertainties using a variety of different methodologies they yield comparable results. In doing so we highlight the context in which our coral Sr/Ca and $\delta^{18}O$ records are significant to the interpretation of LIG SST.

Figure 2.21 demonstrates our mean annual coral-Sr/Ca-SST record alongside the local annual insolation and the full sedimentary Mg/Ca, foraminifera assemblage transfer functions and $U^{k'}_{47}$ records for the tropical Atlantic. This highlights the context of coral Sr/Ca reconstructed mid-LIG cooling in light of other regional reconstructions and their proxy specific resolution and seasonal uncertainties. These sedimentary records possess age models for the LIG

Figure 2.23 depicts LIG tropical Atlantic annual SST reconstructed using foraminifera assemblage transfer functions. These records do not process age models and, with expectation of one north Atlantic record, show colder than modern annual SST during the LIG. Our mid-LIG mean annual coral Sr/Ca-SST at 125.8 ka agrees with these records.

Figure 2.24 Mean annual coral Sr/Ca-SST, $\delta^{18}O$ and growth rates are presented illustrating no temperature dependent growth relationship between our proxy records.

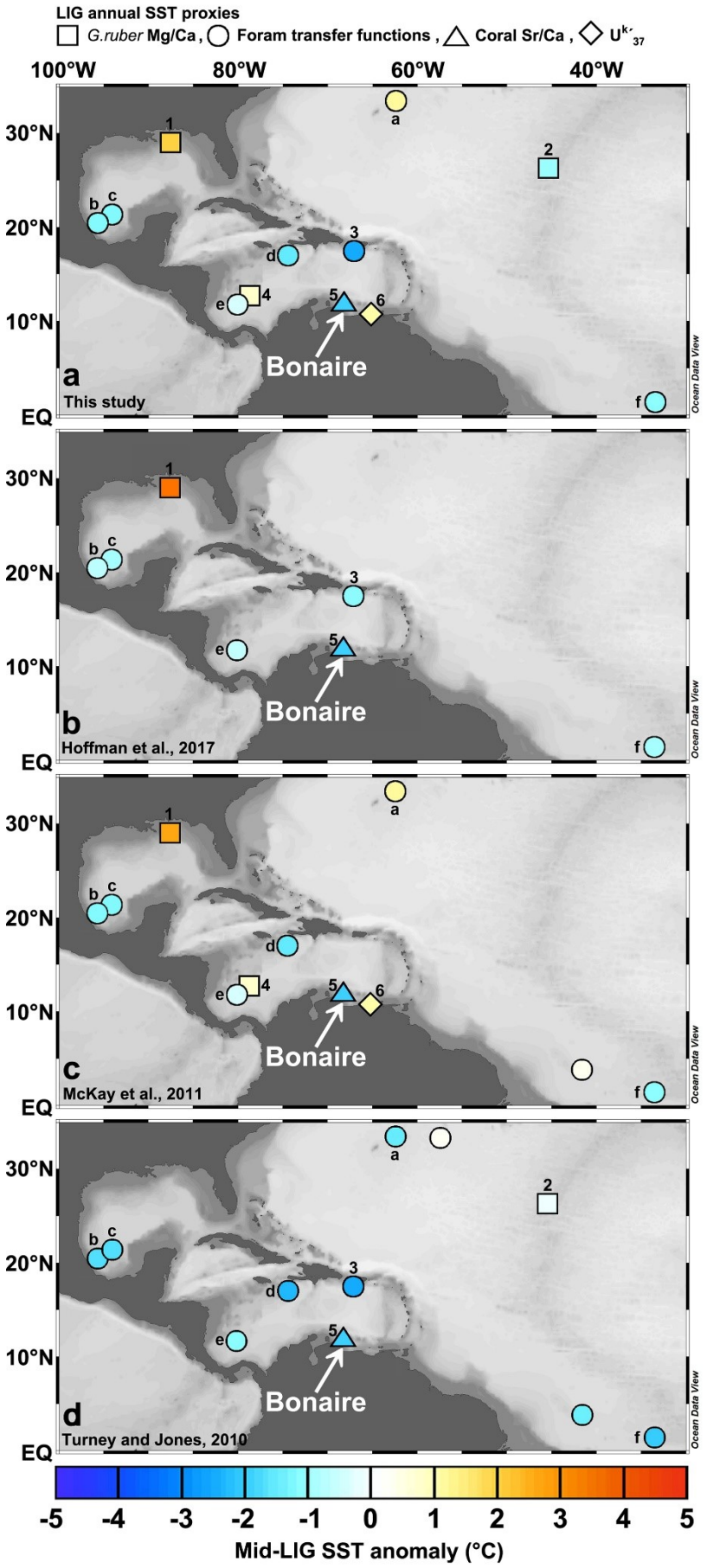
LIG annual SST proxies
G.ruber Mg/Ca , Foram transfer functions , Coral Sr/Ca , U^k'37
100°W
80°W
60°W
40°W
30°N
20°N
10°N
EQ
Bonaire
a
This study
b
Hoffman et al., 2017
c
McKay et al., 2011
d
Turney and Jones, 2010
Ocean Data View
-5 -4 -3 -2 -1 0 1 2 3 4 5
Mid-LIG SST anomaly (°C)

Figure 2.20

Figure 2.20: Tropical Atlantic last interglacial (LIG) SST anomalies complied for a) this study, b) Hoffman et al. (2017), c) McKay et al. (2011) and d) Turney and Jones, (2010). LIG SST reconstruction derived from, $U^{k'}_{37}$ (diamond), G.ruber Mg/Ca (numbered squares) and foraminifera assemblage transfer functions (numbered circles) proxies. Turney and Jones, (2010) derived sedimentary ΔSST by averaging reconstructed SST over the MIS 5e isotopic plateau and subtracting the average SST within the nearest 2° x 2° gridded instrumental data series (1961 - 1990 AD). Whereas McKay et al. (2011) defined sedimentary ΔSST as the average SST of 5 ka centred on peak LIG SST minus the average SST between 0 and 5 ka. Furthermore, McKay et al. (2011) and Hoffman et al. (2017) only considered sedimentary records with a resolution less than 3 and 4 ka, respectively, on their published age models. Hoffman et al. (2017) calculated ΔSST for each proxy record with reference to the HadISST1.1 1870-1889, based on this periods SST being closest within this database to the pre-industrial (P.I.). The location of Bonaire and our mid-LIG coral Sr/Ca-SST finding is illustrated (triangle, 5) (Schlitzer, 2015).

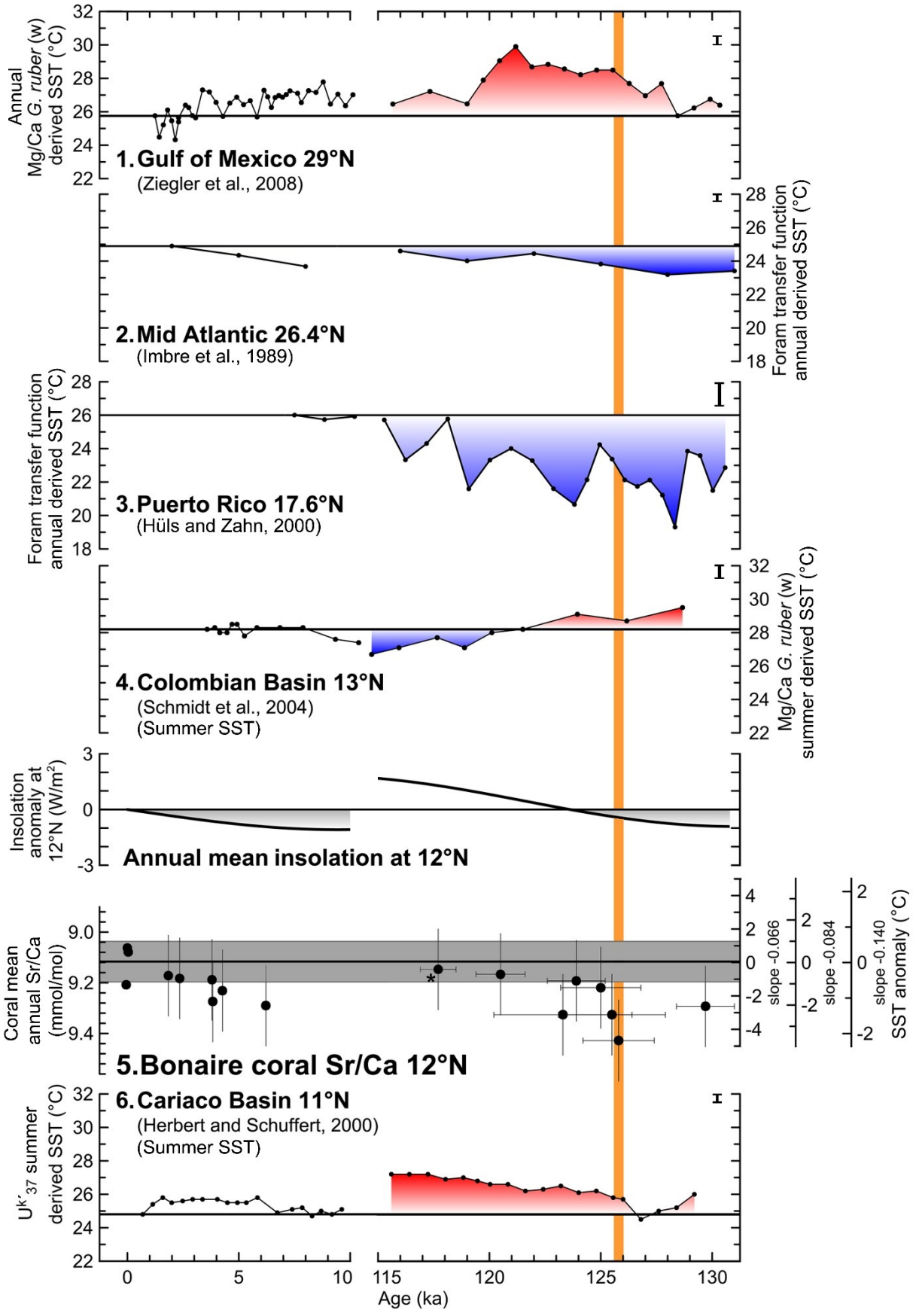
Annual Mg/Ca G. ruber (w) derived SST (°C)
1. Gulf of Mexico 29°N
(Ziegler et al., 2008)
Foram transfer function annual derived SST (°C)
2. Mid Atlantic 26.4°N
(Imbre et al., 1989)
Foram transfer function annual derived SST (°C)
3. Puerto Rico 17.6°N
(Hüls and Zahn, 2000)
Mg/Ca G. ruber (w) summer derived SST (°C)
4. Colombian Basin 13°N
(Schmidt et al., 2004)
(Summer SST)
Insolation anomaly at 12°N (W/m²)
Annual mean insolation at 12°N
Coral mean annual Sr/Ca (mmol/mol)
slope -0.066
slope -0.084
slope -0.140
SST anomaly (°C)
5. Bonaire coral Sr/Ca 12°N
6. Cariaco Basin 11°N
(Herbert and Schuffert, 2000)
(Summer SST)
Uk'37 summer derived SST (°C)
Age (ka)

Figure 2.21

Figure 2.21: Coral Sr/Ca and sedimentary records that reconstruct annual (records 2, 3 and 5) and summer (records 1, 4 and 6) sea surface temperatures (SST) during the mid- to late Holocene and last interglacial (LIG). Record 5 illustrates Bonaire (12°N, 68°W) coral mean annual Sr/Ca-SST for modern, the mid- to late Holocene (Giry et al., 2012), the late last interglacial (*, Felis et al., 2012) and LIG (this study). Coral Sr/Ca derived SST anomaly from the three modern coral average is calculated using the annual Sr/Ca-SST relationship of -0.042, -0084 and -0,140 mmol/mol per °C from Hetzinger et al. (2006), Gagan et al. (2012) and Felis et al. (2009), respectively. The coral ±1 combined error is indicated by vertical lines while the thick black horizontal line denotes the three modern coral average and surrounding ±1 standard deviation (light grey shading). Coral colonies are dated using ^{230}Th/U techniques with the age uncertainty (±2σ) depicted by horizontal lines (Obert et al., 2016). Mean annual insolation anomaly from present received at 12°N is illustrated above (Berger, 1978). Sedimentary records derived from Mg/Ca G.ruber (w) (records 1 and 4), foraminifera transfer functions (records 2 and 4) and $U^{k'}_{47}$ (record 6) proxies are illustrated for the western tropical Atlantic (0° - 35°N x 100° - 30°W). These records are numbered according to latitude and correspond to figure S1. When during the LIG these records are warmer or colder than the most recently reconstructed SST is illustrated by red and blue shading, respectively. The reported ±1 standard deviation is depicted in the top right of each record. Vertical orange shading indicates the date ascribed to our coldest dwelling coral at 125.8ka. Sedimentary records 4 and 6 likely reflect summer rather than annual SST (Schmidt et al., 2011 and Herbert and Schuffert, 2000, respectively).

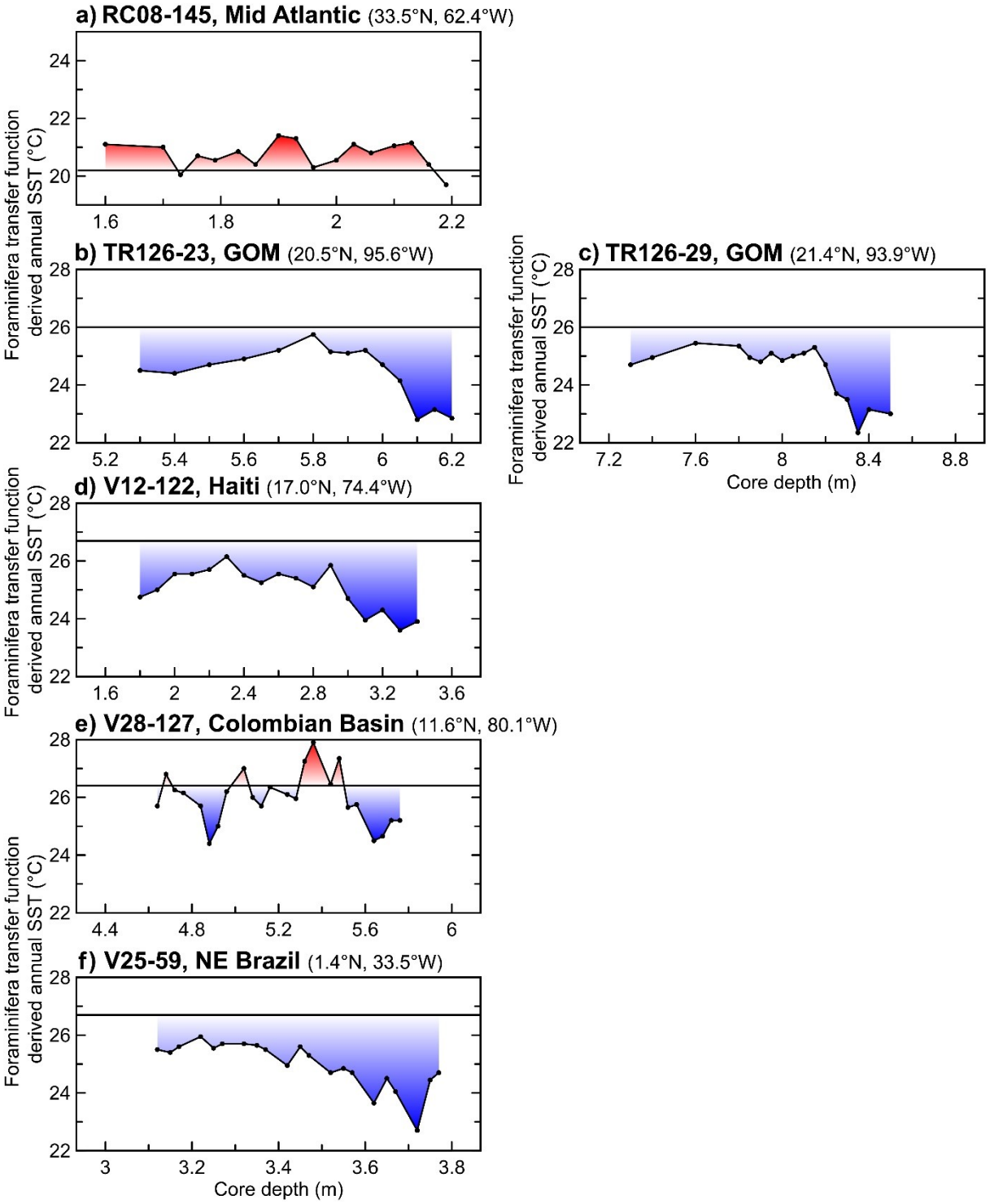

Figure 2.22: Last interglacial foraminifera assemblage transfer functions derived SST for the tropical Atlantic. Horizontal dark lines illustrates the core top value with red and blue shading indicates warmer and colder departures from this, respectively. All records originate from CLIMAP Project Members, (1984).

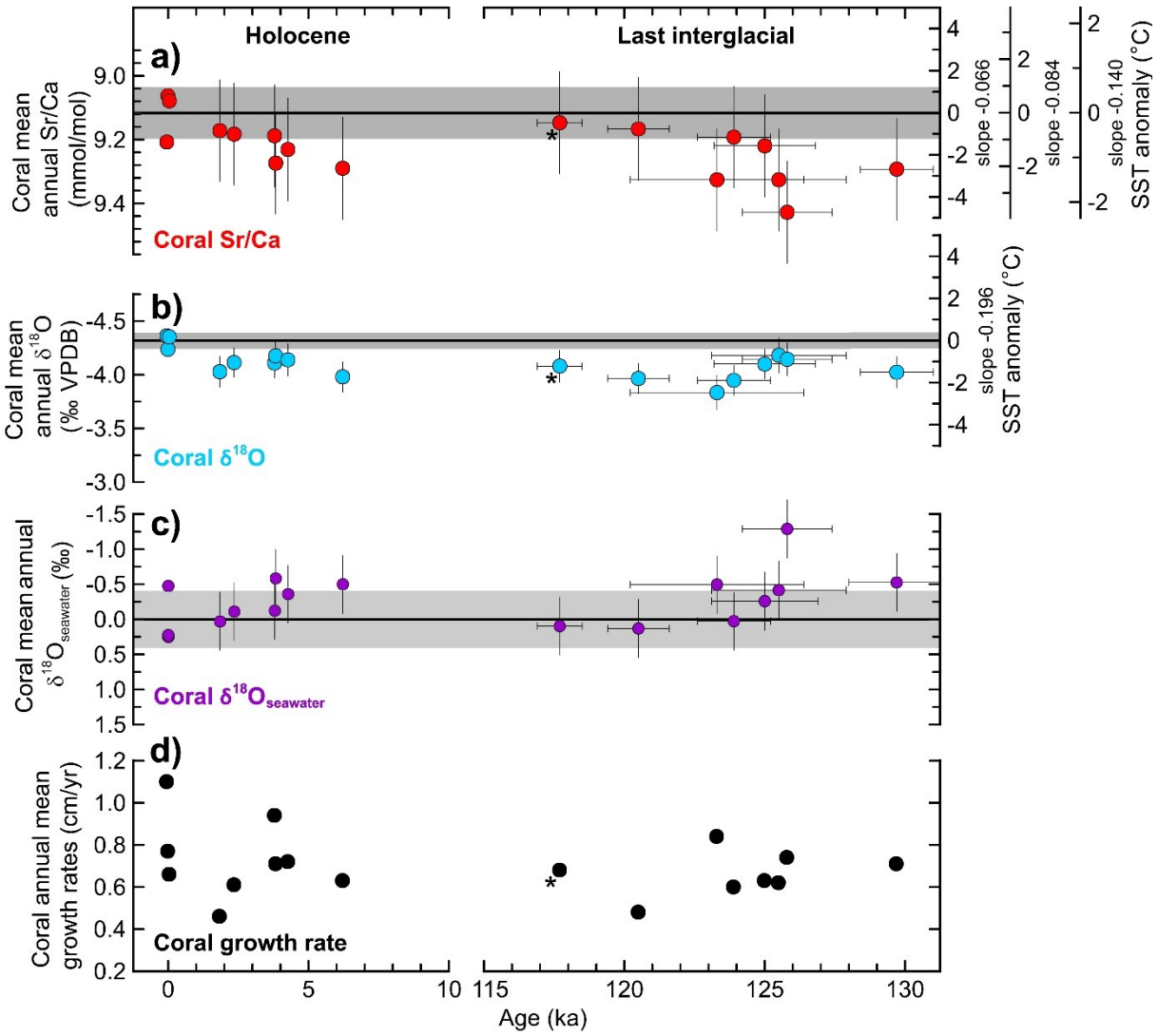

Figure 2.23: Tropical Atlantic mean annual coral (a) Sr/Ca-SST, (b) $\delta^{18}O$ and (c) $\delta^{18}O_{seawater}$ compared to their respective d) annual average growth rates. Mean annual coral Sr/Ca, $\delta^{18}O$, $\delta^{18}O_{seawater}$ and growth rates represent modern, mid- to late Holocene (Giry et al., 2012), the late LIG (*, Felis et al., 2015) and the LIG (this study) time windows. a, b, c) Vertical lines illustrates the ± 1 combined error. Three coral modern mean is indicated by the black lines with ± 1 standard deviation (grey shading). Horizontal lines indicate $^{230}Th/U$-age uncertainty at 2σ level (Obert et al., 2016). a) Coral Sr/Ca derived SST anomaly from the three modern coral average is calculated using the annual Sr/Ca-SST relationship of -0.066, -0084 and -0.140 mmol/mol per °C from Hetzinger et al. (2006), Gagan et al. (2012) and Felis et al. (2009), respectively. b) Coral annual $\delta^{18}O$-SST relationship of -0.196 ‰ per °C (Hetzinger et al., 2006). c) Coral $\delta^{18}O_{seawater}$ calculated using mean annual the proxy-SST relationships of (Hetzinger et al., 2006). Mean annual coral growth are calculated using the mean averaged distance between successive annual Sr/Ca peaks.

3.0 Summary and conclusions

Contained within the skeletal structure of *D. strigosa* are records of the seawater properties these corals inhabited. Coral records have been used to confidently reconstruct characteristics of modern tropical Atlantic instrumental climate records (Kuhnert et al., 2005; Hetzinger et al., 2006). Judicious sampling strategies have been applied to the skeletal structure of *D. strigosa* found upon the southern Caribbean island of Bonaire (Giry et al., 2010). Live, coastal deposits and elevated reef terraces *D. strigosa* coral material has been established as a reliable source of modern, mid- to late Holocene (Giry et al., 2012, 2013) and early LIG (Felis et al, 2015) SST and hydroclimate records, respectively. Building upon the example set by these studies, the first goal of this thesis is to ascertain the potential for similar records to be obtained from multiple fossil coral material that has been ^{230}Th/U dated to distinct time intervals throughout the LIG (Obert et al., 2016). This presents a unique opportunity to assess sub seasonal to multi-decadal SST and hydroclimate variability at a location sensitive to multiple climate phenomena. The insights gained are intrinsically linked to the evolution of tropical Atlantic climate during a period relevant to the study of future climate change. The following paragraphs summarise the key findings and the conclusions that can be draw from the manuscripts presented within thesis.

Manuscript I details the first study of multiple monthly resolved Tropical Atlantic *D. strigosa* coral Sr/Ca records that proxy SST seasonality and variability throughout the LIG. From these records is can be concluded that SST seasonality similar to modern during the early and late while higher than modern SST seasonality occurred within two separate mid-LIG records. These coral Sr/Ca-SST findings are representative of the wider tropical Atlantic realm and increase SST seasonality as demonstrated by a similar evolution of SST seasonality depicted within contemporaneous climate model simulations. LIG insolation seasonality was higher than modern during the mid-LIG and concluded to have been the primary driver of tropical Atlantic SST seasonality at that time. This is significant within the LIG as a period that experienced broader global climate instability and change. The longest presented Sr/Ca-SST record of 37 years detects decadal SST variability for the first time during the mid-LIG which had only previously been seen within instrumental SST records. Thus it is demonstrated that Atlantic climate phenomena and the southern Caribbean Sea were closely linked during a period of significance to the validation of climate models.

Manuscript II examines multiple monthly resolved *D. strigosa* coral $\delta^{18}O$ that were measured on the same samples as the Sr/Ca-SST records of manuscript I. Coral $\delta^{18}O$ records contain a $\delta^{18}O_{seawater}$ component and a SST signal that was removed using the Sr/Ca-SST records described in manuscript I. This study further demonstrates the utility of isolating coral $\delta^{18}O_{seawater}$ as an indicator of Bonaire hydroclimate seasonality for multiple occasions throughout the LIG. Higher than modern mid-LIG coral $\delta^{18}O$ seasonality was reconstructed alongside Sr/Ca-SST during a period of higher than modern insolation seasonality. Additionally, a unique two month lead of coral $\delta^{18}O$ vs. Sr/Ca-SST annual cycle was also detected demonstrating that a temporal hydroclimate shift occurred during the mid-LIG at that differed from modern. New isotopically enabled coupled climate model simulations of that time reveal increased precipitation and depleted $\delta^{18}O_{seawater}$ during summer within much of the southern Caribbean Sea. Together these coral $\delta^{18}O_{seawater}$ and model findings provide the first direct evidence that the ITCZ migrated northward beyond the northern coastline of South America and into the Caribbean Sea during the mid-LIG. Consequently, southern Caribbean Sea hydroclimate is demonstrably sensitive to the isolation forcing mechanisms that dominated the LIG. This resulted in a shift as summer rainfall became more influential to hydroclimate, in contrast to the ocean advection regime of present, with peak rainfall in winter.

Manuscript III differs from the previous studies by utilising these LIG monthly resolved coral Sr/Ca-SST, $\delta^{18}O$ and $\delta^{18}O_{seawater}$ records to assess mean annual SST and hydroclimate changes. These records reveal ~2 °C colder and fresher than modern tropical Atlantic surface waters at ~126 ka. Proxy specific uncertainties were assessed and agreement found between mean annual coral Sr/Ca-SST and sedimentary foraminifera transfer function records that similarly derive colder than modern mid-LIG SST. These characteristics of the Caribbean Sea are significant to the modulation of ocean currents, such as the AMOC, and climate patterns that influence extra-tropical climate. This is indicative of colder and fresher than modern Atlantic waters entered the Caribbean Sea as a result of enhanced ocean advection. Mean annual SST and $\delta^{18}O_{seawater}$ then reconstruct a transition to modern-like sea surface condition at 124 ka that are maintained into the late LIG. This coincided with the northward migration of the ITCZ into the Caribbean Sea at 124 ka and a return to modern-like ocean advection.

In conclusion Bonaire *D. strigosa* palaeoclimate records further define the spatiotemporal evolution and variability of tropical Atlantic SST and hydroclimate during LIG. The 85 years of *D. strigosa* monthly resolved Sr/Ca-SST, $\delta^{18}O$ and $\delta^{18}O_{seawater}$ records presented herein contribute significantly to the current paucity of LIG tropical Atlantic palaeoclimate records. Insights are provided into distinct features of high frequency, sub-seasonal to decadal climate variability unavailable to, and independent from, sedimentary records that typically explore LIG palaeoclimate. Bonaire *D. strigosa* results lead to the conclusion that modern-like SST and hydroclimate were reached rapidly after the TII deglacial event at ~130ka. In response to mid-LIG orbital controls on tropical seasonality of insolation, coral Sr/Ca-SST seasonality was higher than modern during the mid-LIG at ~126 ka and 124 ka. This is in agreement with mid-LIG climate model simulations that support the conclusion that this was a feature of the topical Atlantic at that time. *D. strigosa* reconstructs colder and less saline than modern surface waters at 126 ka, in agreement with available sedimentary records, supporting the conclusion of a connection between Bonaire and Atlantic AMOC dynamics at that time. At 124 ka, $\delta^{18}O_{seawater}$ seasonality was higher than modern and accompanied by a shift in hydroclimate regime. Modelling simulations reveal this to be indicative of increased summer precipitation at that time. Together these findings characterises the northward expansion of the ITCZ into the Caribbean Sea and its sensitivity to orbital controls during the mid-LIG. However, coral findings also revealed that at 124 ka these changes did not alter mean annual SST and SSS at Bonaire from modern. Additionally, quasi-biennial and decadal coral Sr/Ca-SST variability is detected supporting the conclusion that this feature of modern Atlantic instrumental climate records is natural and existed during the mid-LIG. During the late LIG, as seasonality of insolation and the ITCZ returned to modern-like behaviour so too did Bonaire seasonality of, and mean annual, SST and hydroclimate. Thus, *D. strigosa* characterises late LIG tropical Atlantic palaeoclimate as indistinguishable from modern. Interestingly, it can be concluded that the above described evolution of SST and hydroclimate occurred regardless of the numerous climate instabilities documented throughout the LIG within the extra-tropical Atlantic.

These conclusions have implications for the assessment of climate phenomena during a period of higher than modern global temperatures and well defined orbital controls. The agreement found between coral-based reconstructions and model simulations of tropical Atlantic SST and hydroclimate seasonality reinforces the conclusion that the LIG is a suitable test-bed for future climate change projections.

4.0 Outlook for future research

The manuscripts presented within this thesis raise a variety of worthwhile research questions that future studies could potentially address.

Primarily, this thesis encourages the future use of monthly resolved coral records despite the labour intensive precise micro-sampling techniques required to extract robust palaeoclimate records from the delicate thecae of LIG coral material. Monthly resolved records that comprise of 12 or more samples should be aimed for in order to confidently capture the high frequency climate variability induced by phenomena such at the ITCZ, ENSO and NAO (Quinn et al., 1996). Due to the strong relationship these phenomena have with SST and hydroclimate seasonality, the findings of this thesis would not have been possible using a lower sampling resolution. Sub-seasonally resolved records are recommended as they aid in the detection of potential vital effects and can be more readily used to test the biological processes behind the incorporation of geochemical signatures into the aragonite skeletons of corals. Furthermore, this thesis demonstrates the benefit to future studies of comparing with modern climate allegories, represented by multiple modern specimens, that allow uncertainties such as vital effects and unknown palaeo reef habitats to be better addressed.

The advantages gained by a multi-fossil coral approach to tropical palaeoclimatic investigations are evident from the presented studies. This is especially true as demonstrated by the variety of characteristics of spatiotemporal evolution of SST and hydroclimate seasonality found throughout the LIG. Constructing multiple time windows of coral palaeoclimate records in the aim of covering a significant periods of time is still relatively rare in the literature. For example, prior to this study the only previous multi-coral LIG study was of ENSO variability within the west Pacific (Tudhope et al., 2001). This thesis further demonstrates the complementary nature of combined coral and climate model studies as a worthwhile approach for future studies to identify the influence of regional climate phenomena. Furthermore, significant regional differences within the Caribbean are highlighted and should be considered in future tropical Atlantic palaeoclimatic studies.

Although the approach taken favours the use of the coral Sr/Ca and $\delta^{18}O$ to SST calibrations of Hetzinger et al. (2006), it also ensures that the findings are significant regardless of this choice. However, while the Sr/Ca-SST calibration from Guadeloupe is well-established and recommended within the tropical Atlantic paleoclimate, future investigations should aim for a definitive Bonaire $\delta^{18}O$-SST calibration based on multi-decadal records. This

is required to better reflect the distinct hydroclimate of the ABC islands that at present differs from the rest of the Caribbean Sea and have been demonstrated to have shifted during the LIG

Due to the rarity of well-preserved coral material, no studies from interglacial periods prior to the LIG exist within the tropical Atlantic. Future studies could build on the framework provided within this thesis to examine coral material cemented to other Bonaire reef terraces that likely represent sea level highstand and thus interglacial periods older than the LIG. Manuscript I is in agreement with examples from the Pacific Ocean using *Porites* spp. that demonstrate the significance of insolation forcing upon the seasonality of coral palaeoclimate records dated to 197.2 ka (MIS 7, Asami et al., 2013) and 337 - 374 ka (MIS 9, Ayling et al., 2006). Indeed, Ayling et al. (2006) utilise this relationship to constrain the larger ^{230}Th/U dating uncertainties associated with MIS 9 coral based paleoclimatic study. Therefore such a principle could also be applied to tropical Atlantic coral studies prior to the LIG. Coral material from 370 - 420 ka (MIS 11) would offer insights from another interglacial also considered analogous to future climate projection of a warmer global temperatures. Consequently, future Bonaire coral studies would seek to characterise influences upon tropical climate variability under numerous background states.

This thesis demonstrates the sensitivity of coral $\delta^{18}O_{seawater}$ records from Bonaire and tropical Atlantic climate simulations to the northward migration of the ITZC during the mid-LIG, a time of higher insolation seasonality. Similar records from the Antilles island arc could ascertain the northerly influence of the ITCZ, whereas coral material from the Atlantic coastline of South America could potentially demonstrate the southern extent of the ITCZ during boreal winter. Indeed, while it is documented that the SAMS was intensified during the LIG due to insolation forcing (Govin et al., 2015b), coastal records independent of continental influences are required to fully constrain ITCZ spatially. Thus, future research could determining if ITCZ induced precipitation within the tropical Atlantic expanded and/or intensified north and south of the equator. Furthermore, coral records are shown to contribute to the growing body of proxy evidence that characterises tropical mid-LIG annually averaged surface waters as colder than modern. This has important implications for further study of the spatiotemporal evolution of extra-tropical LIG temperatures and modelling studies that currently offer no consensus on mid-LIG tropical Atlantic SST. Finally, tropical Atlantic. For example, although coral records and model simulations have demonstrated board agreement in response to LIG seasonality of insolation changes, further study is required to ascertain the differences seen between reconstructions of mean annual climate states.

5.0 Bibliography

1. Abram, N. J., H. V. McGregor, M. K. Gagan, W. S. Hantoro, and B. W. Suwargadi (2009), Oscillations in the southern extent of the Indo-Pacific Warm Pool during the mid-Holocene, Quat. Sci. Rev., 28(25 - 26), 2794-2803, doi:10.1016/j.quascirev.2009.07.006.

2. Andersen, M., C. Stirling, B. Zimmermann, and A. Halliday (2010), Precise determination of the open ocean $^{234}U/^{238}U$ composition, Geochem. Geophys. Geosyst., 11(12), doi:10.1029/2010GC003318.

3. Andrade, C. A., E. D. Barton, and C. N. Mooers (2003), Evidence for an eastward flow along the Central and South American Caribbean Coast, J. Geophy. Res-Oceans, 108(C6), doi:10.1029/2002JC001549.

4. Asami, R., T. Felis, P. Deschamps, K. Hanawa, Y. Iryu, E. Bard, N. Durand, and M. Murayama (2009), Evidence for tropical South Pacific climate change during the Younger Dryas and the Bølling–Allerød from geochemical records of fossil Tahiti corals, Earth Planet. Sci. Lett., 288(1), 96-107, doi:10.1016/j.epsl.2009.09.011.

5. Asami, R., Y. Iryu, K. Hanawa, T. Miwa, P. Holden, R. Shinjo, and G. Paulay (2013), MIS 7 interglacial sea-surface temperature and salinity reconstructions from a southwestern subtropical Pacific coral, Quat. Res., 80(3), 575-585, doi:10.1016/j.yqres.2013.09.002.

6. Ayling, B. F., M. T. McCulloch, M. K. Gagan, C. H. Stirling, M. B. Andersen, and S. G. Blake (2006), Sr/Ca and $\delta^{18}O$ seasonality in a *Porites* coral from the MIS 9 (339 - 303 ka) interglacial, Earth Planet. Sci. Lett., 248(1), 462-475, doi:10.1016/j.epsl.2006.06.009.

7. Bak, R. P., G. Nieuwland, and E. H. Meesters (2005), Coral reef crisis in deep and shallow reefs: 30 years of constancy and change in reefs of Curacao and Bonaire, Coral Reefs, 24(3), 475-479, doi:10.1007/s00338-005-0009-1.

8. Bakker, P., E. Stone, S. Charbit, M. Gröger, U. Krebs-Kanzow, S. Ritz, V. Varma, V. Khon, D. Lunt, and U. Mikolajewicz (2013), Last interglacial temperature evolution-a model inter-comparison, Clim. Past, 9(2), 605, doi:10.5194/cp-9-605-2013.

9. Barnett, P. T. (1991), The interaction of multiple timescales in the tropical climate system, J. Climate, 4, 269-285, doi:10.1175/1520-04421991004.

10. Beck, J. W., R. L. Edwards, E. Ito, F. W. Taylor, J. Recy, F. Rougerie, P. Joannot, and C. Henin (1992), Sea-surface temperature from coral skeletal strontium/calcium ratios, Science, 257(5070), 644-647, doi:10.1126/science.257.5070.644.

11. Berger, A., L. (1978), Long-term variations of caloric insolation resulting from the earth's orbital elements, Quat. Res., 9(2), 139-167, doi:10.1016/0033-5894(78)90064-9.

12. Black, D. E., L. C. Peterson, J. T. Overpeck, A. Kaplan, M. N. Evans, and M. Kashgarian (1999), Eight centuries of north Atlantic ocean atmosphere variability, Science, 286(5445), 1709-1713, doi:10.1126/science.286.5445.1709.

13. Black, D. E., M. A. Abahazi, R. C. Thunell, A. Kaplan, E. J. Tappa, and L. C. Peterson (2007), An 8-century tropical Atlantic SST record from the Cariaco Basin: Baseline variability, twentieth-century warming, and Atlantic hurricane frequency, Paleoceanography, 22(4), doi:10.1029/2007PA001427.

14. Blanchon, P., A. Eisenhauer, J. Fietzke, and V. Liebetrau (2009), Rapid sea-level rise and reef back-stepping at the close of the last interglacial highstand, Nature, 458(7240), 881-884, doi:10.1038/nature07933.

15. de Buisonjé, P. H., (1974), Neogene and Quaternary geology of Aruba, Curaçao and Bonaire. PhD thesis, Universiteit Utrecht, The Netherlands.

16. Braconnot, P., S. P. Harrison, M. Kageyama, P. J. Bartlein, V. Masson-Delmotte, A. Abe-Ouchi, B. Otto-Bliesner, and Y. Zhao (2012), Evaluation of climate models using palaeoclimatic data, Nature Clim. Change, 2(6), 417-424. doi:10.1038/NCLIMATE1456.

17. Bradley, R. S. (2015), Chapter 14 - Corals, in Paleoclimatology (Third Edition), edited by R. S. Bradley, pp. 499-516, San Diego, Academic Press.

18. Broccoli, A. J., K. A. Dahl, and R. J. Stouffer (2006), Response of the ITCZ to Northern Hemisphere cooling, Geophys. Res. Lett., 33(1), doi:10.1029/2005GL024546.

19. Budd, A. F., F. Hironobu, N. D. Smith, and N. Knowlton (2012), Taxonomic classification of the reef coral family Mussidae (Cnidaria: Anthozoa: Scleractinia), Zool. J. Linn. Soc., 166(3), 465-529, doi:10.1111/j.1096-3642.2012.00855.x.

20. Cahyarini, S. Y., M. Pfeiffer, O. Timm, W. Dullo, and D. G. Schönberg (2008), Reconstructing seawater $\delta^{18}O$ from paired coral $\delta^{18}O$ and Sr/Ca ratios: Methods, error analysis and problems, with examples from Tahiti (French Polynesia) and Timor (Indonesia), Geochim. Cosmochim. Acta, 72(12), 2841-2853, doi:10.1016/j.gca.2008.04.005.

21. Capron, E., A. Govin, E. J. Stone, V. Masson-Delmotte, S. Mulitza, B. Otto-Bliesner, T. L. Rasmussen, L. C. Sime, C. Waelbroeck, and E. W. Wolff (2014), Temporal and spatial structure of multi-millennial temperature changes at high latitudes during the Last Interglacial, Quat. Sci. Rev., 103, 116-133, doi:10.1016/j.quascirev.2014.06.031.

22. Cardinal, D., B. Hamelin, E. Bard, and J. Pätzold (2001), Sr/Ca, U/Ca and $\delta^{18}O$ records in recent massive corals from Bermuda: relationships with sea surface temperature, Chem. Geol., 176(1), 213-233, doi:10.1016/S0009-2541(00)00396-X.

23. Carton, J. A. and B. S. Giese (2008), A reanalysis of ocean climate using Simple Ocean Data Assimilation (SODA), Mon. Weather Rev., 136(8), 2999-3017, doi:10.1175/2007MWR1978.1.

24. Carr, A. S., M. D. Bateman, D. L. Roberts, C. V. Murray-Wallace, Z. Jacobs, and P. J. Holmes (2010), The last interglacial sea-level high stand on the southern Cape coastline of South Africa, Quatern. Res., 73(2), 351-363, doi:10.1016/j.yqres.2009.08.006.

25. Chang, P., Y. Fang, R. Saravanan, L. Ji, and H. Seidel (2006), The cause of the fragile relationship between the Pacific El Nino and the Atlantic Nino, Nature, 443(7109), 324, doi:10.1038/nature05053.

26. Chang, P., L. Ji, and H. Li (1997), A decadal climate variation in the tropical Atlantic Ocean from thermodynamic air-sea interactions, Nature, 385(6616), 516, doi:10.1038/385516a0.

27. Chérubin, L. and P. L. Richardson (2007), Caribbean current variability and the influence of the Amazon and Orinoco freshwater plumes**,** Deep Sea Res. Part I Oceanogr. Res. Pap., 54(9), 1451-1473, doi:10.1016/j.dsr.2007.04.021.

28. Chiang, J. C., Y. Kushnir, and A. Giannini (2002), Deconstructing Atlantic Intertropical Convergence Zone variability: Influence of the local cross-equatorial sea surface temperature gradient and remote forcing from the eastern equatorial Pacific, J. Geophy. Res-Atmos., 107(D1), doi:10.1029/2000JD000307.

29. Choukri, A., O. K. Hakam, J. L. Reyss, and J. C. Plaziat (2007), Radiochemical data obtained by α spectrometry on unrecrystallized fossil coral samples from the Egyptian shoreline of the north-western Red Sea, Radiat. Meas., 42(2), 271-280, doi:10.1016/j.radmeas.2006.12.005.

30. Clement, A. C., R. Seager, and M. Cane (1999), Orbital controls on the El Niño/Southern Oscillation and the tropical climate, Paleoceanography, 14(4), 441-456, doi:10.1029/1999PA900013.

31. CLIMAP (1984), The Last Interglacial Ocean, Quat. Res., 21, 123-224, doi:10.1016/0033-5894(84)90098-X.

32. Climate Prediction Center of the National Oceanic and Atmospheric Administration (NOAA) (http://www.cpc.ncep.noaa.gov/data/indices)

33. Cohen, A. L., S. R. Smith, M. S. McCartney, and J. v. Etten (2004), How brain corals record climate: an integration of skeletal structure, growth and chemistry of *Diploria labyrinthiformis* from Bermuda, Marine Ecology, 271, 147-158, doi:10.3354/meps271147.

34. Corrège, T., M. K. Gagan, J. W. Beck, and G. S. Burr (2004), Interdecadal variation in the extent of South Pacific tropical waters during the Younger Dryas event, Nature, 428(6986), 927, doi:10.1038/nature02506.

35. Corrège, T. (2006), Sea surface temperature and salinity reconstruction from coral geochemical tracers, Palaeogeogr., Palaeoclimatol., Palaeoecol., 232(2–4), 408-428, doi:10.1016/j.palaeo.2005.10.014.

36. Cutler, K., R. Edwards, F. Taylor, H. Cheng, J. Adkins, C. Gallup, P. Cutler, G. Burr, and A. Bloom (2003), Rapid sea-level fall and deep-ocean temperature change since the last interglacial period, Earth Planet. Sci. Lett., 206(3), 253-271, doi:10.1016/S0012-821X(02)01107-X.

37. Czaja, A. (2004), Why Is North Tropical Atlantic SST Variability Stronger in Boreal Spring?, J. Climate, 17(15), 3017-3025, doi:10.1175/1520-0442(2004)017<3017:WINTAS>2.0.CO;2.

38. Dahl-Jensen, D., M. Albert, A. Aldahan, N. Azuma, D. Balslev-Clausen, M. Baumgartner, A. Berggren, M. Bigler, T. Binder, and T. Blunier (2013), Eemian interglacial reconstructed from a Greenland folded ice core, Nature, 493(7433), 489, doi:10.1038/nature11789.

39. Dai, A., J. C. Fyfe, S. Xie, and X. Dai (2015), Decadal modulation of global surface temperature by internal climate variability, Nat. Clim. Change, 5(6), 555-559, doi:10.1038/nclimate2605.

40. Dana, J. (1846), Zoophytes. Volumen VII of the United States Exploring Expedition during the years 1838, 1839, 1840, 1841, 1842, under the command of Charles Wilkes, USN, Lea & Blanchard, Philadelphia.

41. De La Rocha, C. L. and D. J. DePaolo (2000), Isotopic evidence for variations in the marine calcium cycle over the Cenozoic, Science, 289(5482), 1176-1178, doi:10.1126/science.289.5482.1176.

42. DeCarlo, T. M., G. A. Gaetani, A. L. Cohen, G. L. Foster, A. E. Alpert, and J. A. Stewart (2016), Coral Sr-U thermometry, Paleoceanography, 31(6), 626-638, doi:10.1002/2015PA002908.

43. DeLong, K. L., J. A. Flannery, C. R. Maupin, R. Z. Poore, and T. M. Quinn (2011), A coral Sr/Ca calibration and replication study of two massive corals from the Gulf of Mexico, Palaeogeogr., Palaeoclimatol., Palaeoecol., 307(1–4), 117-128, doi:10.1016/j.palaeo.2011.05.005.

44. DeLong, K. L., T. M. Quinn, F. W. Taylor, K. Lin, and C. Shen (2012), Sea surface temperature variability in the southwest tropical Pacific since AD 1649, Nat. Clim. Change, 2(11), 799, doi:10.1038/nclimate1583.

45. DeLong, K. L., T. M. Quinn, F. W. Taylor, C. Shen, and K. Lin (2013), Improving coral-base paleoclimate reconstructions by replicating 350years of coral Sr/Ca variations, Palaeogeogr., Palaeoclimatol., Palaeoecol., 373, 6-24, doi:10.1016/j.palaeo.2012.08.019.

46. Dendy, S., J. Austermann, J. R. Creveling, and J. X. Mitrovica (2017), Sensitivity of Last Interglacial sea-level high stands to ice sheet configuration during Marine Isotope Stage 6, Quaternary Sci. Rev., 171, 234-244, doi:10.1016/j.quascirev.2017.06.013.

47. Deng, W., G. Wei, X. Li, K. Yu, J. Zhao, W. Sun, and Y. Liu (2009), Paleoprecipitation record from coral Sr/Ca and $\delta^{18}O$ during the mid Holocene in the northern South China Sea, The Holocene, 19(6), 811-821, doi:10.1177/0959683609337355.

48. Deser, C. and M. L. Blackmon (1993), Surface Climate Variations over the North Atlantic Ocean during Winter: 1900-1989, J. Climate, 6(9), 1743-1753, doi:10.1175/1520-0442(1993)006<1743:SCVOTN>2.0.CO;2.

49. Dima, M., and G. Lohmann (2004), Fundamental and derived modes of climate variability: concept and application to inter-annual time-scales, Tellus A, 56(3), 229-249, doi:10.1111/j.1600-0870.2004.00059.x.

50. Dima, M., G. Lohmann, and N. Rimbu (2015), Possible North Atlantic origin for changes in ENSO properties during the 1970s, Clim. Dyn., 44(3-4), 925-935, doi:10.1007/s00382-014-2173-x.

51. Dutton, A., A. E. Carlson, A. J. Long, G. A. Milne, P. U. Clark, R. DeConto, B. P. Horton, S. Rahmstorf, and M. E. Raymo (2015), Sea-level rise due to polar ice-sheet mass loss during past warm periods, Science, 349(6244), 4019, doi:10.1126/science.aaa4019.

52. Dutton, A. and K. Lambeck (2012), Ice volume and sea level during the last interglacial, Science, 337(6091), 216-219, doi:10.1126/science.1205749.

53. Druffel, E. R. (1997), Geochemistry of corals: proxies of past ocean chemistry, ocean circulation, and climate, Proc. Natl. Acad. Sci., U.S.A., 94(16), 8354-8361, doi:10.1073/pnas.94.16.8354.

54. Dunbar, R. B., G. M. Wellington, M. W. Colgan, and P. W. Glynn (1994), Eastern Pacific sea surface temperature since 1600 AD: The $\delta^{18}O$ record of climate variability in Galápagos corals, Paleoceanography, 9(2), 291-315, doi:10.1029/93PA03501.

55. Elsner, J. B., K. Liu, and B. Kocher (2000), Spatial variations in major US hurricane activity: Statistics and a physical mechanism, J. Clim., 13(13), 2293-2305, doi:10.1175/1520-0442(2000)013<2293:SVIMUS>2.0.CO;2.

56. Emiliani, C., J. H. Hudson, E. A. Shinn, and R. Y. George (1978), Oxygen and carbon isotopic growth record in a reef coral from the Florida keys and a deep-sea coral from blake plateau, Science, 202(4368), 627-629, doi:10.1126/science.202.4368.627.

57. Enfield, D. B. and D. A. Mayer (1997), Tropical Atlantic sea surface temperature variability and its relation to El Niño-Southern Oscillation, J. Geophy. Res-Oceans, 102(C1), 929-945, doi:10.1029/96JC03296.

58. Enfield, D.B., A. M. Mestas-Nunez and P.J. Trimble, (2001): The Atlantic multi-decadal oscillation and it's relation to rainfall and river flows in the continental U.S. Geophys. Res. Lett., Vol. 28, 2077-2080.

59. Engel, M., H. Brückner, V. Wennrich, A. Scheffers, D. Kelletat, A. Vött, F. Schäbitz, G. Daut, T. Willershäuser, and S. M. May (2010), Coastal stratigraphies of eastern Bonaire (Netherlands Antilles): New insights into the palaeo-tsunami history of the southern Caribbean, Sediment. Geol., 231(1–2), 14-30, doi:10.1016/j.sedgeo.2010.08.002.

60. Engel, M., H. Brückner, K. Messenzehl, P. Frenzel, S. M. May, A. Scheffers, S. Scheffers, V. Wennrich, and D. Kelletat (2012), Shoreline changes and high-energy wave impacts at the leeward coast of Bonaire (Netherlands Antilles), Earth, planets and space, 64(10), 9, doi:10.5047/eps.2011.08.011.

61. Epstein, S., R. Buchsbaum, H. A. Lowenstam, and H. C. Urey (1953), Revised carbonate-water isotopic temperature scale, Geol. Soc. of Am. Bull., 64(11), 1315-1326, doi:10.1130/0016-7606(1953)64(1315:RCITS)2.0.CO;2.

62. Etter, P. C., P. J. Lamb, and D. H. Portis (1987), Heat and freshwater budgets of the Caribbean Sea with revised estimates for the Central American Seas, J. Phys. Oceanogr., 17(8), 1232-1248, doi:10.1175/1520-0485(1987)017<1232:HAFBOT>2.0.CO;2.

63. Fairbanks, R. G. and R. E. Dodge (1979), Annual periodicity of the $^{18}O^{16}O$ and $^{13}C^{12}C$ ratios in the coral Montastrea annularis, Geochim. Cosmochim. Acta, 43(7), 1009-1020, doi:10.1016/0016-7037(79)90090-5.

64. Felis, T., J. Pätzold, and Y. Loya (2003), Mean oxygen-isotope signatures in *Porites spp*. corals: inter-colony variability and correction for extension-rate effects, Coral Reefs, 22(4), 328-336, doi:10.1007/s00338-003-0324-3.

65. Felis, T., G. Lohmann, H. Kuhnert, S. J. Lorenz, D. Scholz, J. Pätzold, A. S. Al-Rousan, and M. S. Al-Moghrabi (2004), Increased seasonality in Middle East temperatures during the last interglacial period, Nature, 429(6988), 164-168, doi:10.1038/nature02546.

66. Felis, T., A. Suzuki, H. Kuhnert, M. Dima, G. Lohmann, and H. Kawahata (2009), Subtropical coral reveals abrupt early-twentieth-century freshening in the western North Pacific Ocean, Geology, 37(6), 527-530, doi:10.1130/G25581A.1.

67. Felis, T., U. Merkel, R. Asami, P. Deschamps, E. C. Hathorne, M. Kölling, E. Bard, G. Cabioch, N. Durand, M. Prange, M. Schulz, S. Y. Cahyarini, and M. Pfeiffer (2012), Pronounced inter-annual variability in tropical South Pacific temperatures during Heinrich Stadial 1, Nat. Commun., 3, 965, doi:10.1038/ncomms1973.

68. Felis, T., H. V. McGregor, B. K. Linsley, A. W. Tudhope, M. K. Gagan, A. Suzuki, M. Inoue, A. L. Thomas, T. M. Esat, W. G. Thompson, M. Tiwari, D. C. Potts, M. Mudelsee, Y. Yokoyama, and J. M. Webster (2014), Intensification of the meridional temperature gradient in the Great Barrier Reef following the Last Glacial Maximum. Nat. Commun., 5, 4102, doi:10.1038/ncomms5102.

69. Felis, T., C. Giry, D. Scholz, G. Lohmann, M. Pfeiffer, J. Pätzold, M. Kölling, and S. R. Scheffers (2015), Tropical Atlantic temperature seasonality at the end of the last interglacial, Nat. Commun., 6, 6159, doi:10.1038/ncomms7159.

70. Ffield, A. (2005), North Brazil Current rings viewed by TRMM Microwave Imager SST and the influence of the Amazon Plume, Deep Sea Res. Part I Oceanogr. Res. Pap., 52(1), 137-160, doi:10.1016/j.dsr.2004.05.013.

71. Fricke, H. And D. Meischner (1985), Depth Limits of Bermudan Scleractinian Corals - a Submersible Survey, Mar. Biol., 88(2), 175-187, doi:10.1007/BF00397165.

72. Frierson, D. M. and Y. Hwang (2012), Extratropical influence on ITCZ shifts in slab ocean simulations of global warming, J. Climate., 25(2), 720-733, doi:10.1175/JCLI-D-11-00116.1.

73. Gagan, M. K., L. K. Ayliffe, D. Hopley, J. A. Cali, G. E. Mortimer, J. Chappell, M. T. McCulloch, and M. J. Head (1998), Temperature and Surface-Ocean Water Balance of the Mid-Holocene Tropical Western Pacific, Science, 279(5353), 1014-1018, doi:10.1126/science.279.5353.1014.

74. Gagan, M., L. Ayliffe, J. W. Beck, J. Cole, E. Druffel, R. B. Dunbar, and D. Schrag (2000), New views of tropical paleoclimates from corals, Quaternary Sci. Rev., 19(1), 45-64, doi:10.1016/S0277-3791(99)00054-2.

75. Gagan, M., G. Dunbar, and A. Suzuki (2012) The effect of skeletal mass accumulation in Porites on coral Sr/Ca and paleothermometry, Paleoceanography, 27, PA1203, 27(PA1203), doi:10.1029/2011PA002215.

76. Galaasen, E. V., U. S. Ninnemann, N. Irvali, H. F. Kleiven, Y. Rosenthal, C. Kissel, and D. A. Hodell (2014), Rapid Reductions in North Atlantic Deep Water During the Peak of the Last Interglacial Period, Science, 343(6175), 1129-1132, doi:10.1126/science.1248667.

77. Gallup, C. D., R. L. Edwards, and R. G. Johnson (1994), The timing of high sea levels over the past 200,000 years, Science, 263(5148), 796-799, doi:10.1126/science.263.5148.796.

78. Galy, A., N. S. Belshaw, L. Halicz, and R. K. O'Nions (2001), High-precision measurement of magnesium isotopes by multiple-collector inductively coupled plasma mass spectrometry, Int. J. Mass. Spectrom., 208(1), 89-98, doi:10.1016/S1387-3806(01)00380-3.

79. Ghil, M., M. Allen, M. Dettinger, K. Ide, D. Kondrashov, M. Mann, A. W. Robertson, A. Saunders, Y. Tian, and F. Varadi (2002), Advanced spectral methods for climatic time series, Rev. Geophys., 40(1), 3-1-3-41, doi:10.1029/2000RG000092.

80. Giannini, A., Y. Kushnir, and M. Cane A. (2000), Interannual Variability of Caribbean Rainfall, ENSO, and the Atlantic Ocean*, J. Climate, 13(2), 297, doi:10.1175/1520-0442(2000)013<0297:IVOCRE>2.0.CO;2.

81. Gierz, P., G. Lohmann, and W. Wei (2015), Response of Atlantic overturning to future warming in a coupled atmosphere-ocean-ice sheet model, Geophys. Res. Lett., 42(16), 6811-6818, doi:10.1002/2015GL065276.

82. Giry, C., T. Felis, M. Kölling, and S. Scheffers (2010), Geochemistry and skeletal structure of *Diploria strigosa*, implications for coral-based climate reconstruction, Palaeogeogr., Palaeoclimatol., Palaeoecol., 298(3 - 4), 378-387, doi:10.1016/j.palaeo.2010.10.022.

83. Giry, C., T. Felis, M. Kölling, D. Scholz, W. Wei, G. Lohmann, and S. Scheffers (2012), Mid- to late Holocene changes in tropical Atlantic temperature seasonality and inter-annual to multi-decadal variability documented in southern Caribbean corals, Earth Planet. Sci. Lett., 331-332, 187-200, doi:10.1016/j.epsl.2012.03.019.

84. Giry, C., Felis, T., Kölling, M., Wei, W., Lohmann, G., and Scheffers, S. (2013), Controls of Caribbean surface hydrology during the mid- to late Holocene: insights from monthly resolved coral records, Clim. Past, 9, 841-858, doi:10.5194/cp-9-841-2013.

85. Gong, X., G. Knorr, G. Lohmann, and X. Zhang (2013), Dependence of abrupt Atlantic meridional ocean circulation changes on climate background states, Geophys. Res. Lett., 40(14), 3698-3704, doi:10.1002/grl.50701.

86. Goodkin, N. F., K. A. Hughen, A. L. Cohen, and S. R. Smith (2005), Record of Little Ice Age sea surface temperatures at Bermuda using a growth-dependent calibration of coral Sr/Ca, Paleoceanography, 20(4), doi:10.1029/2005PA001140.

87. Goodkin, N. F., K. A. Hughen, and A. L. Cohen (2007), A multicoral calibration method to approximate a universal equation relating Sr/Ca and growth rate to sea surface temperature, Paleoceanography, 22(1), doi:10.1029/2006PA001312.

88. Govin, A., Braconnot, P., Capron, E., Cortijo, E., Duplessy, J.-C., Jansen, E., Labeyrie, L., Landais, A., Marti, O., Michel, E., Mosquet, E., Risebrobakken, B., Swingedouw, D., and Waelbroeck, C (2012), Persistent influence of ice sheet melting on high northern latitude climate during the early Last Interglacial, Clim. Past, 8, 483-507, doi:10.5194/cp-8-483-2012.

89. Govin, A., E. Capron, P. Tzedakis, S. Verheyden, B. Ghaleb, C. Hillaire-Marcel, G. St-Onge, J. Stoner, F. Bassinot, and L. Bazin (2015a), Sequence of events from the onset to the demise of the Last Interglacial: Evaluating strengths and limitations of chronologies used in climatic archives, Quaternary Sci. Rev., 129, 1-36, doi:10.1016/j.quascirev.2015.09.018.

90. Govin, A., B. Blazey, M. Prange, and A. Paul (2015b), What Ends an Interglacial? Feedbacks Between Tropical Rainfall, Atlantic Climate and Ice Sheets During the Last Interglacial, in Integrated Analysis of Interglacial Climate Dynamics (INTERDYNAMIC), edited by Anonymous, pp. 25-30, Springer.

91. Guo, Y., W. Deng, X. Chen, G. Wei, K. Yu, and J. Zhao (2016), Saltier sea surface water conditions recorded by multiple mid-Holocene corals in the northern South China Sea, J. Geophys. Res-Oceans., 121(8), 6323-6330, doi:10.1002/2016JC012034.

92. Grant, K., E. Rohling, C. B. Ramsey, H. Cheng, R. Edwards, F. Florindo, D. Heslop, F. Marra, A. Roberts, and M. E. Tamisiea (2014), Sea-level variability over five glacial cycles, Nat. commun., 5, doi:10.1038/ncomms6076.

93. Gray, W. M. (1984), Atlantic Seasonal Hurricane Frequency. Part I: El Nino and 30 mb Quasi-Biennial Oscillation Influences, Mon. Weather. Rev., 112(9), 1649-1668, doi:10.1175/1520-0493(1984)112<1649:ASHFPI>2.0.CO;2.

94. Haese, B., M. Werner, and G. Lohmann (2012), Stable water isotopes in the coupled atmosphere-land surface model ECHAM5-JSBACH, Geosci. Model Dev., 6, 3375-3418, doi:10.5194/gmd-6-1463-2013.

95. Haug, G. H. and R. Tiedemann (1998), Effect of the formation of the Isthmus of Panama on Atlantic Ocean thermohaline circulation, Nature, 393(6686), 673-676, doi:10.1038/31447.

96. Haug, G. H., K. A. Hughen, D. M. Sigman, L. C. Peterson, and U. Röhl (2001), Southward Migration of the Intertropical Convergence Zone Through the Holocene, Science, 293(5533), 1304-1308, doi:10.1126/science.1059725.

97. Hastenrath, S. (1984), Inter-annual variability and annual cycle: Mechanisms of circulation and climate in the tropical Atlantic sector, Mon. Weather Rev., 112(6), 1097-1107, doi:10.1175/1520-0493(1984)112<1097:IVAACM>2.0.CO;2.

98. Hathorne, E. C., A. Gagnon, T. Felis, J. Adkins, R. Asami, W. Boer, N. Caillon, D. Case, K. M. Cobb, E. Douville, P. deMenocal, A. Eisenhauer, D. Garbe-Schönberg, W. Geibert, S. Goldstein, Hughen K., M. Inoue, H. Kawahata, M. Kölling, F. L. Cornec, B. K. Linsley, H. V. McGregor, P. Montagna, I. S. Nurhati, T. M. Quinn, J. Raddatz, H. Rebaubier, L. Robinson, A. Sadekov, R. Sherrell, D. Sinclair, A. W. Tudhope, G. Wei, H. Wong, H. C. Wu, and C. You (2013), Interlaboratory study for coral Sr/Ca and other element/Ca ratio measurements, Geochem. Geophys. Geosyst., 14(9), 3730-3750, doi:10.1002/ggge.20230.

99. Herbert, T. D. and J. D. Schuffert (2000), 16. Alkenone unsaturation estimates of sea-surface temperatures at site 1002 over a full glacial cycle, Proc. Ocean Drill. Program Sci. Results, 165, 239-247.

100. Hendy, E., M. Gagan, J. Lough, M. McCulloch, and P. DeMenocal (2007), Impact of skeletal dissolution and secondary aragonite on trace element and isotopic climate proxies in Porites corals, Paleoceanography, 22(4), doi:10.1029/2007PA001462.

101. Hernández-Guerra, A. and T. M. Joyce (2000), Water masses and circulation in the surface layers of the Caribbean at 66°W, Geophys. Res. Lett., 27(21), 3497-3500, doi:10.1029/1999GL011230.

102. Hetzinger, S., M. Pfeiffer, W. Dullo, E. Ruprecht, and D. Garbe-Schönberg (2006), Sr/Ca and $\delta^{18}O$ in a fast-growing *Diploria strigosa* coral: Evaluation of a new climate archive for the tropical Atlantic, Geochem. Geophys. Geosyst., 7(10), Q10002, doi:10.1029/2006GC001347.

103. Hetzinger, S., M. Pfeiffer, W. Dullo, N. Keenlyside, M. Latif, and J. Zinke (2008), Caribbean coral tracks Atlantic Multidecadal Oscillation and past hurricane activity, Geology, 36(1), 11-14, doi:10.1130/G24321A.1

104. Hetzinger, S., M. Pfeiffer, W. Dullo, D. Garbe-Schönberg, and J. Halfar (2010), Rapid 20th century warming in the Caribbean and impact of remote forcing on climate in the northern tropical Atlantic as recorded in a Guadeloupe coral, Palaeogeogr., Palaeoclimatol., Palaeoecol., 296(1 - 2), 111-124, doi:10.1016/j.palaeo.2010.06.019.

105. Hetzinger, S., M. Pfeiffer, W. C. Dullo, J. Zinke, and D. Garbe-Schonberg (2016), A change in coral extension rates and stable isotopes after El Nino-induced coral bleaching and regional stress events, Sci. Rep., 6, 32879, doi:10.1038/srep32879.

106. Hodell, D. A., G. A. Mead, and P. A. Mueller (1990), Variation in the strontium isotopic composition of seawater (8 Ma to present) : Implications for chemical weathering rates and dissolved fluxes to the oceans, Chemical Geology: Isotope Geoscience section, 80(4), 291-307, doi:10.1016/0168-9622(90)90011-Z.

107. Hodell, D., C. Charles, and F. Sierro (2001), Late Pleistocene evolution of the ocean's carbonate system, Earth Planet. Sci. Lett., 192(2), 109-124, doi:10.1016/S0012-821X(01)00430-7.

108. Hoffman, J. S., P. U. Clark, A. C. Parnell, and F. He (2017), Regional and global sea-surface temperatures during the last interglaciation, Science, 355(6322), 276-279, doi:10.1126/science.aai8464.

109. Hughen, K. A., D. P. Schrag, S. B. Jacobsen, and W. Hantoro (1999), El Niño during the Last Interglacial Period recorded by a fossil coral from Indonesia, Geophys. Res. Lett., 26(20), 3129-3132, doi:10.1029/1999GL006062Huang, P. (2016), Time-varying response of ENSO-induced tropical Pacific rainfall to global warming in CMIP5 models. Part I: multimodel ensemble results, J. Clim., 29(16), 5763-5778, doi:10.1175/JCLI-D-16-0058.1.

110. Huang, P. and S. Xie (2015), Mechanisms of change in ENSO-induced tropical Pacific rainfall variability in a warming climate, Nat. Geosci., 8(12), 922, doi:10.1038/ngeo2571.

111. Huang, P. (2016), Time-varying response of ENSO-induced tropical Pacific rainfall to global warming in CMIP5 models. Part I: multimodel ensemble results, J. Clim., 29(16), 5763-5778, doi:10.1175/JCLI-D-16-0058.1.

112. Hulme, M., T. J. Osborn, and T. C. Johns (1998), Precipitation sensitivity to global warming: Comparison of observations with HadCM2 simulations, Geophys. Res. Lett., 25(17), 3379-3382, doi:10.1029/98GL02562.

113. Hüls, M. and R. Zahn (2000), Millennial-scale sea surface temperature variability in the western tropical North Atlantic from planktonic foraminiferal census counts, Paleoceanography 15(6), 659-678, doi:10.1029/1999PA000462.

114. Hurrell, J. W. (1995), Decadal trends in the North Atlantic Oscillation: regional temperatures and precipitation, Science, 269(5224), 676-678, doi:10.1126/science.269.5224.676.

115. Imbrie, J., A. McIntyre, and A. Mix (1989), Oceanic response to orbital forcing in the late Quaternary: Observational and experimental strategies, in Climate and Geo-sciences, edited by Anonymous, pp. 121-164, Springer.

116. IPCC, (2013), The Physical Science Basis. Contribution of Working Group I to the Fifth Assessment Report of the Intergovernmental Panel on Climate Change. Cambridge University Press, Cambridge, United Kingdom and New York, NY, USA. doi:10.1017/CBO9781107415324.

117. Jiménez-Amat, P. and R. Zahn (2015), Offset timing of climate oscillations during the last two glacial-interglacial transitions connected with large-scale freshwater perturbation, Paleoceanography, 30(6), 768-788, doi:10.1002/2014PA002710.

118. Johns, W. E., T. L. Townsend, D. M. Fratantoni, and W. D. Wilson (2002), On the Atlantic inflow to the Caribbean Sea. Deep Sea Res. Part I Oceanogr. Res. Pap., 49(2), 211-243, doi:10.1016/S0967-0637(01)00041-3.

119. Jouzel, J., V. Masson-Delmotte, O. Cattani, G. Dreyfus, S. Falourd, G. Hoffmann, B. Minster, J. Nouet, J. M. Barnola, J. Chappellaz, H. Fischer, J. C. Gallet, S. Johnsen, M. Leuenberger, L. Loulergue, D. Luethi, H. Oerter, F. Parrenin, G. Raisbeck, D. Raynaud, A. Schilt, J. Schwander, E. Selmo, R. Souchez, R. Spahni, B. Stauffer, J. P. Steffensen, B. Stenni, T. F. Stocker, J. L. Tison, M. Werner, and E. W. Wolff (2007), Orbital and millennial Antarctic climate variability over the past 800,000 years, Science, 317(5839), 793-796, doi: 10.1126/science.1141038.

120. Jungclaus, J., N. Keenlyside, M. Botzet, H. Haak, J. Luo, M. Latif, J. Marotzke, U. Mikolajewicz, and E. Roeckner (2006), Ocean circulation and tropical variability in the coupled model ECHAM5/MPI-OM, J. Clim., 19(16), 3952-3972, doi:10.1175/JCLI3827.1.

121. Jungclaus, J., S. Lorenz, C. Timmreck, C. Reick, V. Brovkin, K. Six, J. Segschneider, M. Giorgetta, T. Crowley, and J. Pongratz (2010), Climate and carbon-cycle variability over the last millennium, Clim. Past, 6, 723-737, doi:10.5194/cp-6- 723-2010.

122. Jury, M., B. A. Malmgren, and A. Winter (2007), Subregional precipitation climate of the Caribbean and relationships with ENSO and NAO, J. Geophys. Res-Atmos., 112(D16), doi:10.1029/2006JD007541.

123. Jury, M. R. (2009), A quasi-decadal cycle in Caribbean climate, J. Geophys. Res. Atmos., (1984 - 2012), 114(D13), doi:10.1029/2009JD011741.

124. Kalnay, E., M. Kanamitsu, R. Kistler, W. Collins, D. Deaven, L. Gandin, M. Iredell, S. Saha, G. White, and J. Woollen (1996), The NCEP/NCAR 40-year reanalysis project, Bull. Am. Meteorol. Soc., 77(3), 437-471, doi:10.1175/1520-0477(1996)077<0437:TNYRP>2.0.CO;2.

125. Kaplan, A., Y. Kushnir, and M. A. Cane (2000), Reduced space optimal interpolation of historical marine sea level pressure: 1854–1992, J. Clim., 13(16), 2987-3002, doi:10.1175/1520-0442(2000)013<2987:RSOIOH>2.0.CO;2.

126. Karl, T. R., A. Arguez, B. Huang, J. H. Lawrimore, J. R. McMahon, M. J. Menne, T. C. Peterson, R. S. Vose, and H. Zhang (2015), Possible artifacts of data biases in the recent global surface warming hiatus, Science, 348(6242), 1469-1472, doi:10.1126/science.aaa5632.

127. Kerr, R.A. (2000). A North Atlantic Climate Pacemaker for the Centuries. Science, 288, 1984-1985. doi: 10.1126/science.288.5473.1984.

128. Kerr, R. A. (2014), Atlantic Current Can Shut Down for Centuries, Disrupting Climate, Science, 343(6173), 831-831, doi:10.1126/science.343.6173.831.

129. Kilbourne, K. H., T. M. Quinn, and F. W. Taylor (2004), A fossil coral perspective on western tropical Pacific climate ~350 ka, Paleoceanography, 19(1), doi:10.1029/2003PA000944.

130. Kilbourne, K. H., T. M. Quinn, R. Webb, T. Guilderson, J. Nyberg, and A. Winter (2008), Paleoclimate proxy perspective on Caribbean climate since the year 1751: Evidence of cooler temperatures and multidecadal variability, Paleoceanography, 23(3), PA3220, doi:10.1029/2008PA001598.

131. Kilbourne, K. H., M. A. Alexander, and J. A. Nye (2014), A low latitude paleoclimate perspective on Atlantic multidecadal variability, J. Mar. Syst., 133, 4-13, doi:10.1016/j.jmarsys.2013.09.004.

132. Kim, K. H. and D. J. Lee (1999), Distribution and depositional environments of coralline lithofacies in uplifted Pleistocene coral reefs of Bonaire, Netherlands Antilles, J. Korean Phys. Soc., 15(2), 115-133.

133. Kim, S. T., W. Cai, F. Jin, A. Santoso, L. Wu, E. Guilyardi, and S. An (2014), Response of El Niño sea surface temperature variability to greenhouse warming, Nat. Clim. Change, 4(9), 786, doi:10.1038/nclimate2326.

134. Kinsman, D. J. and H. D. Holland (1969), The co-precipitation of cations with CaCO3—IV. The co-precipitation of Sr2 with aragonite between 16° and 96° C, Geochim. Cosmochim. Acta, 33(1), 1-17, doi:10.1016/0016-7037(69)90089-1.

135. Knight, J. R., C. K. Folland, and A. A. Scaife (2006), Climate impacts of the Atlantic multidecadal oscillation, Geophys. Res. Lett., 33(17), doi:10.1029/2006GL026242.

136. Knutson, D. W., R. W. Buddemeier, and S. V. Smith (1972), Coral chronometers: seasonal growth bands in reef corals, Science, 177(4045), 270-272, doi:10.1126/science.177.4045.270.

137. Kopp, R. E., F. J. Simons, J. X. Mitrovica, A. C. Maloof, and M. Oppenheimer (2009), Probabilistic assessment of sea level during the last interglacial stage, Nature 462(7275), 863-867, doi:10.1038/nature08686.

138. Kuhnert, H., T. Crüger, and J. Pätzold (2005), NAO signature in a Bermuda coral Sr/Ca record, Geochem. Geophys. Geosyst., 6(4), Q04004, doi:10.1029/2004GC000786.

139. Kukla, G. J., A. C. Clement, M. A. Cane, J. E. Gavin, and S. E. Zebiak (2002), Last interglacial and early glacial ENSO, Quatern. Res., 58(1), 27-31, doi:10.1006/qres.2002.2327.

140. Kushnir, Y., W. A. Robinson, P. Chang, and A. W. Robertson (2006), The physical basis for predicting Atlantic sector seasonal-to-interannual climate variability, J. Clim., 19(23), 5949-5970, doi:doi.org/10.1175/JCLI3943.1.

141. Langebroek, P. M. and Nisancioglu, K. H. (2014) Simulating last interglacial climate with NorESM: role of insolation and greenhouse gases in the timing of peak warmth, Clim. Past 10, 1305-1318, doi:10.5194/cp-10-1305-2014.

142. Latif, M., C. Böning, J. Willebrand, A. Biastoch, J. Dengg, N. Keenlyside, U. Schweckendiek, and G. Madec (2006a), Is the thermohaline circulation changing? J. Clim., 19(18), 4631-4637, doi:10.1175/JCLI3876.1.

143. Latif, M., M. Collins, H. Pohlmann, and N. Keenlyside (2006b), A review of predictability studies of Atlantic sector climate on decadal time scales, J. Clim., 19(23), 5971-5987, doi:10.1175/JCLI3945.1.

144. Lawrimore, J. H., M. J. Menne, B. E. Gleason, C. N. Williams, D. B. Wuertz, R. S. Vose, and J. Rennie (2011), An overview of the Global Historical Climatology Network monthly mean temperature data set, version 3, J. Geophys. Res-Atmos., 116(D19), doi:10.1029/2011JD016187.

145. Leduc, G., L. Vidal, K. Tachikawa, F. Rostek, C. Sonzogni, L. Beaufort, and E. Bard (2007), Moisture transport across Central America as a positive feedback on abrupt climatic changes, Nature, 445(7130), 908-911, doi:10.1038/nature05578.

146. Leduc, G., R. Schneider, J. Kim, and G. Lohmann (2010), Holocene and Eemian sea surface temperature trends as revealed by alkenone and Mg/Ca paleothermometry, Quat. Sci. Rev. 29(7), 989-1004, doi:10.1016/j.quascirev.2010.01.004.

147. Lear, C. H., H. Elderfield, and P. Wilson (2003), A Cenozoic seawater Sr/Ca record from benthic foraminiferal calcite and its application in determining global weathering fluxes, Earth Planet. Sci. Lett., 208(1), 69-84, doi:10.1016/S0012-821X(02)01156-1.

148. LeGrande, A. N. and G. A. Schmidt (2006), Global gridded data set of the oxygen isotopic composition in seawater, Geophys. Res. Lett., 33(12), doi:10.1029/2006GL026011.

149. Linsley, B. K., G. M. Wellington, and D. P. Schrag (2000), Decadal sea surface temperature variability in the subtropical South Pacific from 1726 to 1997 A.D, Science, 290(5494), 1145-1148, doi:10.1126/science.290.5494.1145.

150. Linsley, B., G. Wellington, D. Schrag, L. Ren, M. Salinger, and A. Tudhope (2004), Geochemical evidence from corals for changes in the amplitude and spatial pattern of South Pacific interdecadal climate variability over the last 300 years, Clim. Dyn., 22(1), 1-11, doi:10.1007/s00382-003-0364-y.

151. Lisiecki, L. E. and M. E. Raymo (2005), A Pliocene-Pleistocene stack of 57 globally distributed benthic $\delta^{18}O$ records, Paleoceanography, 20(1), PA1003, doi:10.1029/2004PA001071.

152. Locarnini, R.A., Mishonov, A.V., Antonov, J.I., Boyer, T.P., Garcia, H.E., Baranova, O.K., Zweng, M.M., Paver, C.R., Reagan, J.R., Johnson, D.R., Hamilton, M., Seidov, D (2013). World Ocean Atlas 2013. In: Levitus, S. (Ed.), Mishonov, A. (Technical Ed.), Temperature, vol. 1. NOAA Atlas NESDIS 73, 40 pp.

153. Lough, J. M. (2004), A strategy to improve the contribution of coral data to high-resolution paleoclimatology, Palaeogeogr., Palaeoclimatol., Palaeoecol., 204(1), 115-143, doi:10.1016/S0031-0182(03)00727-2.

154. Loulergue, L., A. Schilt, R. Spahni, V. Masson-Delmotte, T. Blunier, B. Lemieux, J. Barnola, D. Raynaud, T. F. Stocker, and J. Chappellaz (2008), Orbital and millennial-scale features of atmospheric CH_4 over the past 800,000 years, Nature, 453(7193), 383-386, doi:10.1038/nature06950.

155. Lunt, D. J., A. Abe-Ouchi, P. Bakker, A. Berger, P. Braconnot, S. Charbit, N. Fischer, N. Herold, J. H. Jungclaus, V. C. Khon, U. Krebs-Kanzow, P. M. Langebroek, G. Lohmann, K. H. Nisancioglu, B. Otto-Bliesner, W. Park, M. Pfeiffer, S. J. Phipps, M. Prange, R. Rachmayani, H. Renssen, N. Rosenbloom, B. Schneider, E. J. Stone, K. Takahashi, W. Wei, Q. Yin, and Z. S. Zhang (2013), A multi-model assessment of last interglacial temperatures, Clim. Past, 9(2), 699-717, doi:10.5194/cp-9-699-2013.

156. Luthi, D., M. Le Floch, B. Bereiter, T. Blunier, J. Barnola, U. Siegenthaler, D. Raynaud, J. Jouzel, H. Fischer, K. Kawamura, and T. F. Stocker (2008), High-resolution carbon dioxide concentration record 650,000-800,000 years before present, Nature, 453(7193), 379-382, doi:10.1038/nature06949.

157. Mann, M. E. and J. M. Lees (1996), Robust estimation of background noise and signal detection in climatic time series, Clim. Change, 33(3), 409-445, doi:10.1007/BF00142586.

158. Martis, A., G. J. van Oldenborgh, and G. Burgers (2002), Predicting rainfall in the Dutch Caribbean- more than El Nino?, Int. J. Climatol., 22(10), 1219-1234, doi:10.1002/joc.779.

159. Maupin, C. R., T. M. Quinn, and R. B. Halley (2008), Extracting a climate signal from the skeletal geochemistry of the Caribbean coral *Siderastrea siderea*, Geochem. Geophys. Geosyst., 9(12), doi:10.1029/2008GC002106.

160. Masson-Delmotte, V., D. Buiron, A. Ekaykin, M. Frezzotti, H. Gallée, J. Jouzel, G. Krinner, A. Landais, H. Motoyama, and H. Oerter (2011), A comparison of the present and last interglacial periods in six Antarctic ice cores, Clim. Past, 7(2), 397-423, doi:10.5194/cp-7-397-2011.

161. McConnaughey, T. (1989), ^{13}C and ^{18}O isotopic disequilibrium in biological carbonates: I. Patterns, Geochim. Cosmochim. Acta, 53(1), 151-162, doi:10.1016/0016-7037(89)90282-2.

162. McCulloch, M. T., M. K. Gagan, G. E. Mortimer, A. R. Chivas, and P. J. Isdale (1994), A high-resolution Sr/Ca and δ18O coral record from the Great Barrier Reef, Australia, and the 1982–1983 El Niño, Geochim. Cosmochim. Acta, 58(12), 2747-2754, doi:10.1016/0016-7037(94)90142-2.

163. McCulloch, M. T., A. W. Tudhope, T. M. Esat, G. E. Mortimer, J. Chappell, B. Pillans, A. R. Chivas, and A. Omura (1999), Coral Record of Equatorial Sea-Surface Temperatures During the Penultimate Deglaciation at Huon Peninsula, Science, 283(5399), 202-204, doi:10.1126/science.283.5399.202.

164. McCulloch, M. T. and T. Esat (2000), The coral record of last interglacial sea levels and sea surface temperatures, Chem. Geol., 169(1–2), 107-129, doi:10.1016/S0009-2541(00)00260-6.

165. McKay, N. P., J. T. Overpeck, and B. L. Otto-Bliesner (2011), The role of ocean thermal expansion in Last Interglacial sea level rise, Geophys. Res. Lett., 38(14), L14605, doi:10.1029/2011GL048280.

166. Mokeddem, Z., J. F. McManus, and D. W. Oppo (2014), Oceanographic dynamics and the end of the last interglacial in the subpolar North Atlantic, Proc. Natl. Acad. Sci., 111(31), 11263-11268, doi:10.1073/pnas.1322103111.

167. Montaggioni, L. F. and C. J. Braithwaite (2009), Quaternary coral reef systems: history, development processes and controlling factors, vol. 5, Elsevier.

168. Montoya, M., H. von Storch, and T. J. Crowley (2000), Climate Simulation for 125 kyr BP with a Coupled Ocean-Atmosphere General Circulation Model, J. Climate, 13(6), 1057-1072, doi:10.1175/1520-0442(2000)013<1057:CSFKBW>2.0.CO;2.

169. Moron, V., R. Vautard, and M. Ghil (1998), Trends, interdecadal and inter-annual oscillations in global sea-surface temperatures, Clim. Dyn., 14(7-8), 545-569, doi:10.1007/s003820050241.

170. Muhs, D. R., K. R. Simmons, and B. Steinke (2002), Timing and warmth of the Last Interglacial period: new U-series evidence from Hawaii and Bermuda and a new fossil compilation for North America, Quaternary Sci. Rev., 21(12), 1355-1383, doi:10.1016/S0277-3791(01)00114-7.

171. Nikolova, I., Q. Yin, A. Berger, U. K. Singh, and M. Karami (2013), The last interglacial (Eemian) climate simulated by LOVECLIM and CCSM3, Clim. Past 9(4), 1789-1806, doi:10.5194/cp-9-1789-2013.

172. Nürnberg, D., M. Ziegler, C. Karas, R. Tiedemann, and M. W. Schmidt (2008), Interacting Loop Current variability and Mississippi River discharge over the past 400 kyr, Earth Planet. Sci. Lett. 272(1), 278-289, doi:10.1016/j.epsl.2008.04.051.

173. Obert, J. C., D. Scholz, T. Felis, W. M. Brocas, K. P. Jochum, and M. O. Andreae (2016), ^{230}Th/U dating of Last interglacial brain corals from Bonaire (southern Caribbean) using bulk and theca wall material, Geochim. Cosmochim. Acta, 178, 20-40, doi:10.1016/j.gca.2016.01.011.

174. O'Leary, M. J., P. J. Hearty, W. G. Thompson, M. E. Raymo, J. X. Mitrovica, and J. M. Webster (2013), Ice sheet collapse following a prolonged period of stable sea level during the last interglacial, Nat. Geosci., 6(9), 796-800, doi:10.1038/ngeo1890.

175. Otto-Bliesner, B. L., N. Rosenbloom, E. J. Stone, N. P. McKay, D. J. Lunt, E. C. Brady, and J. T. Overpeck (2013), How warm was the last interglacial? New model-data comparisons, Philos. Trans. A. Math. Phys. Eng. Sci., 371, 20130097, doi:10.1098/rsta.2013.0097.

176. Pedersen, R. A., P. L. Langen, and B. M. Vinther (2016), The last interglacial climate: comparing direct and indirect impacts of insolation changes, Clim. Dyn. 1-17, doi:10.1007/s00382-016-3274-5.

177. Pfeiffer, M., O. Timm, W. Dullo, and D. Garbe-Schönberg (2006), Paired coral Sr/Ca and $\delta^{18}O$ records from the Chagos Archipelago: Late twentieth century warming affects rainfall variability in the tropical Indian Ocean, Geology, 34(12), 1069-1072, doi:10.1130/G23162A.1.

178. Pfeiffer, M. and G. Lohmann (2016), Greenland Ice Sheet influence on Last Interglacial climate: global sensitivity studies performed with an atmosphere - ocean general circulation model, Clim. Past, 12, 1313-1338, doi:10.5194/cp-12-1313-2016.

179. Pol, K., V. Masson-Delmotte, O. Cattani, M. Debret, S. Falourd, J. Jouzel, A. Landais, B. Minster, M. Mudelsee, M. Schulz, and B. Stenni (2014), Climate variability features of the last interglacial in the East Antarctic EPICA Dome C ice core, Geophys. Res. Lett., 41(11), 4004-4012, doi:10.1002/2014GL059561.

180. Pollock, A., P. van Beynen, K. DeLong, V. Polyak, Y. Asmerom, and P. Reeder (2016), A mid-Holocene paleoprecipitation record from Belize, Palaeogeogr., Palaeoclimatol., Palaeoecol., 463, 103-111, doi:10.1016/j.palaeo.2016.09.021.

181. Quinn, T. M., F. W. Taylor, T. J. Crowley, and S. M. Link (1996), Evaluation of sampling resolution in coral stable isotope records: A case study using records from New Caledonia and Tarawa, Paleoceanography, 11(5), 529-542, doi:10.1029/96PA01859.

182. Reimer, P. J., E. Bard, A. Bayliss, J. W. Beck, P. G. Blackwell, C. B. Ramsey, C. E. Buck, H. Cheng, R. L. Edwards, and M. Friedrich (2013), IntCal13 and Marine13 radiocarbon age calibration curves 0–50,000 years cal BP, Radiocarbon, 55(4), 1869-1887, doi:10.2458/azu_js_rc.55.16947.

183. Ren, L., B. K. Linsley, G. M. Wellington, D. P. Schrag, and O. Hoegh-Guldberg (2003), Deconvolving the $\delta^{18}O$ seawater component from subseasonal coral $\delta^{18}O$ and Sr/Ca at Rarotonga in the southwestern subtropical Pacific for the period 1726 to 1997, Geochim. Cosmochim. Acta, 67(9), 1609-1621, doi:10.1016/S0016-7037(02)00917-1.

184. von Reumont, J., S. Hetzinger, D. Garbe-Schönberg, C. Manfrino, and W. Dullo (2016), Impact of warming events on reef-scale temperature variability as captured in two Little Cayman coral Sr/Ca records, Geochem. Geophys. Geosyst., doi:10.1002/2015GC006194.

185. Riboulleau, A., V. Bout-Roumazeilles, and N. Tribovillard (2014), Controls on detrital sedimentation in the Cariaco Basin during the last climatic cycle: insight from clay minerals, Quat. Sci. Rev., 94, 62-73, doi:10.1016/j.quascirev.2014.04.023.

186. Richey, J. N., R. Z. Poore, B. P. Flower, T. M. Quinn, and D. J. Hollander (2009), Regionally coherent little ice age cooling in the Atlantic warm pool, Geophys. Res. Lett., 36(21), doi:10.1029/2009GL040445.

187. Robson, J., P. Ortega, and R. Sutton (2016), A reversal of climatic trends in the North Atlantic since 2005, Nat. Geosci., 9(7), 513-517, doi:10.1038/ngeo2727.

188. Rohling, E. J. (2007), Oxygen isotope composition of seawater, Encyclopedia of Quaternary Science, vol. 3, edited by Anonymous , pp. 1748-1756, Elsevier Amsterdam.

189. Rohling, E. J., K. Grant, C. Hemleben, M. Siddall, B. Hoogakker, M. Bolshaw, and M. Kucera (2008), High rates of sea-level rise during the last interglacial period, Nat. Geosci., 1(1), 38-42, doi:10.1038/ngeo.2007.28.

190. Sánchez-Goñi, M. F., P. Bakker, S. Desprat, A. E. Carlson, C. J. Van Meerbeeck, O. Peyron, F. Naughton, W. J. Fletcher, F. Eynaud, and L. Rossignol (2012), European climate optimum and enhanced Greenland melt during the Last Interglacial, Geology, 40(7), 627-630, doi:10.1130/G32908.1.

191. Scheffers, A. M., M. Engel, S. M. May, S. R. Scheffers, R. Joannes-Boyau, E. Hänssler, K. Kennedy, D. Kelletat, H. Brückner, and A. Vött (2014), Potential and limits of combining studies of coarse-and fine-grained sediments for the coastal event history of a Caribbean carbonate environment, Geological Society, London, Special Publications, 388(1), 503-531, doi:doi.org/10.1144/SP388.4.

192. Schlitzer, R., Ocean Data View, (2015). (Available online at http://odv.awi.de)

193. Schmidt, M., W., H. J. Spero, and D. Lea W. (2004), Links between salinity variation in the Caribbean and North Atlantic thermohaline circulation, Nature, 42(6979), 160-163, doi:10.1038/nature02346.

194. Schmidt, M. W., M. J. Vautravers, and H. J. Spero (2006), Western Caribbean sea surface temperatures during the late Quaternary, Geochem. Geophys. Geosyst., 7(2), doi:10.1029/2005GC000957.

195. Schmidt, M. W. and H. J. Spero (2011), Meridional shifts in the marine ITCZ and the tropical hydrologic cycle over the last three glacial cycles, Paleoceanography, 26(1), doi:10.1029/2010PA001976.

196. Schneider, T., T. Bischoff, and G. H. Haug (2014), Migrations and dynamics of the intertropical convergence zone, Nature, 513(7516), 45-53, doi:10.1038/nature13636.

197. Scholz, D. and A. Mangini (2007), How precise are U-series coral ages? Geochim. Cosmochim. Acta, 71(8), 1935-1948, doi:10.1016/j.gca.2007.01.016.

198. Scholz, D. and D. Hoffmann (2008), 230Th/U-dating of fossil corals and speleothems, Quat. Sci. J, 57, 52.

199. Schrag, D. P. (1999), Rapid analysis of high-precision Sr/Ca ratios in corals and other marine carbonates, Paleoceanography, 14(2), 97-102, doi:10.1029/1998PA900025.

200. Servain, J. (1991), Simple climatic indices for the tropical Atlantic Ocean and some applications, J. Geophy. Res-Oceans, 96(C8), 15137-15146, doi:10.1029/91JC01046.

201. Servain, J., G. Clauzet, and I. C. Wainer (2003), Modes of tropical Atlantic climate variability observed by PIRATA, Geophys. Res. Lett., 30(5), doi:10.1029/2002GL015124.

202. Serreze, M. C. and R. G. Barry (2011), Processes and impacts of Arctic amplification: A research synthesis, Global Planet. Change, 77(1), 85-96, doi:10.1016/j.gloplacha.2011.03.004.

203. Shaffer, G., M. Huber, R. Rondanelli, and J. O. Pepke Pedersen (2016), Deep time evidence for climate sensitivity increase with warming, Geophys. Res. Lett., 43(12), 6538-6545, doi:10.1002/2016GL069243.

204. Sirocko, F., K. Seelos, K. Schaber, B. Rein, F. Dreher, M. Diehl, R. Lehne, K. Jäger, M. Krbetschek, and D. Degering (2005), A late Eemian aridity pulse in central Europe during the last glacial inception, Nature, 436(7052), 833-836, doi:10.1038/nature03905.

205. Smith, D. M., R. Eade, N. J. Dunstone, D. Fereday, J. M. Murphy, H. Pohlmann, and A. A. Scaife (2010), Skilful multi-year predictions of Atlantic hurricane frequency, Nat. Geosci., 3(12), 846, doi:10.1038/ngeo1004.

206. Smith, J. M., T. M. Quinn, K. P. Helmle, and R. B. Halley (2006), Reproducibility of geochemical and climatic signals in the Atlantic coral *Montastraea faveolata*, Paleoceanography, 21(1), doi:10.1029/2005PA001187.

207. Smith, S. V., R. W. Buddemeier, R. C. Redalje, and J. E. Houck (1979), Strontium-calcium thermometry in coral skeletons, Science, 204(4391), 404-407, doi:10.1126/science.204.4391.404.

208. Smith, T. M., R. W. Reynolds, T. C. Peterson, and J. Lawrimore (2008), Improvements to NOAA's Historical Merged Land - Ocean Surface Temperature Analysis (1880 - 2006), J. Clim., 21(10), 2283-2296, doi:10.1175/2007JCLI2100.1.

209. Sommer, B., P. L. Harrison, L. Brooks, and S. R. Scheffers (2011), Coral community decline at Bonaire, southern Caribbean, Bull. Mar. Sci., 87(3), 541-565, doi:10.5343/bms.2010.1046.

210. Spahni, R., J. Chappellaz, T. F. Stocker, L. Loulergue, G. Hausammann, K. Kawamura, J. Flückiger, J. Schwander, D. Raynaud, V. Masson-Delmotte, and J. Jouzel (2005), Atmospheric Methane and Nitrous Oxide of the Late Pleistocene from Antarctic Ice Cores, Science, 310(5752), 1317-1321, doi:10.1126/science.1120132.

211. Speed, R. and H. Cheng (2004), Evolution of marine terraces and sea level in the last interglacial, Cave Hill, Barbados, Geol. Soc. of Am. Bull., 116(1-2), 219-232, doi:10.1130/B25167.1.

212. Stepanek, C. and G. Lohmann (2012), Modelling mid-Pliocene climate with COSMOS, Geosci. Model Dev., 5, 1221-1243, doi:10.5194/gmd-5-1221-2012.

213. Stirling, C., T. Esat, M. McCulloch, and K. Lambeck (1995), High-precision U-series dating of corals from Western Australia and implications for the timing and duration of the Last Interglacial, Earth Planet. Sci. Lett., 135(1-4), 115-130, doi:10.1016/0012-821X(95)00152-3.

214. Stirling, C., T. Esat, K. Lambeck, and M. McCulloch (1998), Timing and duration of the Last Interglacial: evidence for a restricted interval of widespread coral reef growth, Earth Planet. Sci. Lett., 160(3), 745-762, doi:doi:10.1016/S0012-821X(98)00125-3.

215. Stirling, C. H. and M. B. Andersen (2009), Uranium-series dating of fossil coral reefs: extending the sea-level record beyond the last glacial cycle, Earth Planet. Sci. Lett., 284(3), 269-283, doi:10.1016/j.epsl.2009.04.045.

216. Stoddart, D. R. (1969), Ecology and morphology of recent coral reefs, Biological Reviews, 44(4), 433-498, doi:10.1111/j.1469-185X.1969.tb00609.x.

217. Stoll, H. M. and D. P. Schrag (1998), Effects of Quaternary sea level cycles on strontium in seawater, Geochim. Cosmochim. Acta, 62(7), 1107-1118, doi:10.1016/S0016-7037(98)00042-8.

218. Stoll, H. M., D. P. Schrag, and S. C. Clemens (1999), Are seawater Sr/Ca variations preserved in Quaternary foraminifera? Geochim. Cosmochim. Acta, 63(21), 3535-3547, doi:10.1016/S0016-7037(99)00129-5.

219. Sutton, R. T., S. P. Jewson, and D. P. Rowell (2000), The Elements of Climate Variability in the Tropical Atlantic Region, J. Climate, 13(18), 3261-3284, doi:10.1175/1520-0442(2000)013<3261:TEOCVI>2.0.CO;2.

220. Suzuki, A., M. K. Gagan, P. De Deckker, A. Omura, I. Yukino, and H. Kawahata (2001), Last interglacial coral record of enhanced insolation seasonality and seawater ^{18}O enrichment in the Ryukyu Islands, northwest Pacific, Geophys. Res. Lett., 28(19), 3685-3688, doi:10.1029/2001GL013482.

221. Swart, P., H. Elderfield, and M. Greaves (2002), A high-resolution calibration of Sr/Ca thermometry using the Caribbean coral Montastraea annularis, Geochem. Geophys. Geosyst., 3(11), 1-11, doi:10.1029/2002GC000306.

222. Taylor, G. T., F. E. Muller-Karger, R. C. Thunell, M. I. Scranton, Y. Astor, R. Varela, L. T. Ghinaglia, L. Lorenzoni, K. A. Fanning, S. Hameed, and O. Doherty (2012), Ecosystem responses in the southern Caribbean Sea to global climate change, Proc. Natl. Acad. Sci. U. S. A., 109(47), 19315-19320, doi:10.1073/pnas.1207514109.

223. Telford, R., C. Li, and M. Kucera (2013), Mismatch between the depth habitat of planktonic foraminifera and the calibration depth of SST transfer functions may bias reconstructions, Clim. Past 9(2), 859-870, doi:10.5194/cp-9-859-2013.

224. Tourre, Y. M., B. Rajagopalan, and Y. Kushnir (1999), Dominant patterns of climate variability in the Atlantic Ocean during the last 136 years, J. Clim., 12(8), 2285-2299, doi:10.1175/1520-0442(1999)012<2285:DPOCVI>2.0.CO;2.

225. Tudhope, A. W., C. P. Chilcott, M. T. McCulloch, E. R. Cook, J. Chappell, R. M. Ellam, D. W. Lea, J. M. Lough, and G. B. Shimmield (2001), Variability in the El Niño-Southern Oscillation Through a Glacial-Interglacial Cycle, Science, 291(5508), 1511-1517, doi:10.1126/science.1057969.

226. Turney, C. S. M. and R. T. Jones (2010), Does the Agulhas Current amplify global temperatures during super-interglacials? J. Quaternary Sci., 25(6), 839-843, doi:10.1002/jqs.1423.

227. Tzedakis, P., E. Wolff, L. Skinner, V. Brovkin, D. Hodell, J. F. McManus, and D. Raynaud (2012), Can we predict the duration of an interglacial? Clim. Past, 8(5), 1473-1485, doi:10.5194/cp-8-1473-2012.

228. Urey, H. C. (1947), The thermodynamic properties of isotopic substances, Journal of the Chemical Society (Resumed), 562-581.

229. Waelbroeck, C., L. Labeyrie, E. Michel, J. C. Duplessy, J. McManus, K. Lambeck, E. Balbon, and M. Labracherie (2002), Sea-level and deep water temperature changes derived from benthic foraminifera isotopic records, Quat. Sci. Rev., 21(1), 295-305, doi:10.1016/S0277-3791(01)00101-9.

230. Waliser, D. E. and C. Gautier (1993), A satellite-derived climatology of the ITCZ, J. Clim., 6(11), 2162-2174, doi:10.1175/1520-0442(1993)006<2162:ASDCOT>2.0.CO;2.

231. Wan, X., P. Chang, R. Saravanan, R. Zhang, and M. W. Schmidt (2009), On the interpretation of Caribbean paleo-temperature reconstructions during the Younger Dryas, Geophys. Res. Lett. 36(2), doi:10.1029/2008GL035805.

232. Wang, C. (2007), Variability of the Caribbean low-level jet and its relations to climate, Clim. Dyn., 29(4), 411-422, doi:10.1007/s00382-007-0243-z.

233. Wang, C., S. Lee, and D. B. Enfield (2008), Atlantic Warm Pool acting as a link between Atlantic Multi-decadal Oscillation and Atlantic tropical cyclone activity, Geochem. Geophys. Geosyst., 9(5), Q05V03, doi:10.1029/2007GC001809.

234. Watanabe, T., A. Winter, and T. Oba (2001), Seasonal changes in sea surface temperature and salinity during the Little Ice Age in the Caribbean Sea deduced from Mg/Ca and $^{18}O/^{16}O$ ratios in corals, Mar. Geol., 173(1–4), 21-35, doi:10.1016/S0025-3227(00)00166-3.

235. Weber, J. N. and P. M. Woodhead (1972), Temperature dependence of oxygen-18 concentration in reef coral carbonates, J. Geophy. Res., 77(3), 463-473, doi:10.1029/JC077i003p00463.

236. Wendel, J. (2014), Last interglacial period experienced highly variable climate, EOS, Trans. Am. Geophys. Union, 95(41), 376-376, doi:10.1002/2014EO410009.

237. Werner, M., B. Haese, X. Xu, X. Zhang, M. Butzin, and G. Lohmann (2016), Glacial - interglacial changes in $H_2{}^{18}O$, HDO and deuterium excess - results from the fully coupled ECHAM5/MPI-OM Earth system model, Geosci. Model Dev., 9(2), 647-670, doi:10.5194/gmd-9-647-2016.

238. Werner, M., P. M. Langebroek, T. Carlsen, M. Herold, and G. Lohmann (2011), Stable water isotopes in the ECHAM5 general circulation model: Toward high-resolution isotope modeling on a global scale, J. Geophys. Res-Atmos., 116(D15), doi:10.1029/2011JD015681.

239. Winter, A., A. Paul, J. Nyberg, T. Oba, J. Lundberg, D. Schrag, and B. Taggart (2003), Orbital control of low-latitude seasonality during the Eemian, Geophys. Res. Lett., 30(4), 1163, doi:10.1029/2002GL016275.

240. Woodruff, S. D., S. J. Worley, S. J. Lubker, Z. Ji, J. Eric Freeman, D. I. Berry, P. Brohan, E. C. Kent, R. W. Reynolds, and S. R. Smith (2011), ICOADS Release 2.5: extensions and enhancements to the surface marine meteorological archive, Int. J. Climatol., 31(7), 951-967.

241. Wurtzel, J. B., D. E. Black, R. C. Thunell, L. C. Peterson, E. J. Tappa, and S. Rahman (2013), Mechanisms of southern Caribbean SST variability over the last two millennia, Geophys. Res. Lett. 40(22), 5954-5958, doi:10.1002/2013GL058458.

242. Wüst, G. (1963), On the stratification and the circulation in the cold water sphere of the Antillean-Caribbean basins, An abstract, Deep-Sea Res. Oceanogr. Abstr., 10(3), doi:10.1016/0011-7471(63)90354-1.

243. Xie, S. and J. A. Carton (2004), Tropical Atlantic variability: Patterns, mechanisms, and impacts, Earth's Climate, 121-142, doi:10.1029/147GM07.

244. Xu, Y., S. Pearson, and K. H. Kilbourne (2015), Assessing coral Sr/Ca - SST calibration techniques using the species *Diploria strigosa*, Palaeogeogr., Palaeoclimatol., Palaeoecol., 440, 353-362, doi:10.1016/j.palaeo.2015.09.016.

245. Yarincik, K., R. Murray, and L. Peterson (2000), Climatically sensitive eolian and hemipelagic deposition in the Cariaco Basin, Venezuela, over the past 578,000 years: Results from Al/Ti and K/Al, Paleoceanography, 15(2), 210-228, doi:10.1029/1999PA900048.

246. Yin, Q. Z. and A. Berger (2010), Insolation and CO_2 contribution to the interglacial climate before and after the Mid-Brunhes Event, Nature Geosci., 3(4), 243-246, doi:10.1038/ngeo771.

247. Yokoyama, Y., A. Suzuki, F. Siringan, Y. Maeda, A. Abe-Ouchi, R. Ohgaito, H. Kawahata, and H. Matsuzaki (2011), Mid-Holocene palaeoceanography of the northern South China Sea using coupled fossil-modern coral and atmosphere-ocean GCM model, Geophys. Res. Lett., 38(8), doi:10.1029/2010GL044231.

248. Yu, J., H. Elderfield, Z. Jin, P. Tomascak, and E. J. Rohling (2014), Controls on Sr/Ca in benthic foraminifera and implications for seawater Sr/Ca during the late Pleistocene, Quaternary Sci. Rev., 98, 1-6, doi:10.1016/j.quascirev.2014.05.018.

249. Zazo, C., J. L. Goy, C. Hillaire-Marcel, C. J. Dabrio, J. A. GonzÃ¡lez-Delgado, A. Cabero, T. BardajÃ, B. Ghaleb, and V. Soler (2010), Sea level changes during the last and present interglacials in Sal Island (Cape Verde archipelago), Global Planet. Change, 72(4), 302-317, doi:10.1016/j.gloplacha.2010.01.006.

250. Zhang, D., R. Msadek, M. J. McPhaden, and T. Delworth (2011), Multidecadal variability of the North Brazil Current and its connection to the Atlantic meridional overturning circulation, J. Geophy. Res-Oceans, 116(C4), doi:10.1029/2010JC006812.

251. Zhang, R. (2017), On the Persistence and Coherence of Subpolar Sea Surface Temperature and Salinity Anomalies Associated with the Atlantic Multidecadal Variability, Geophys. Res. Lett., 44, doi:10.1002/2017GL074342.

252. Ziegler, M., D. Nürnberg, C. Karas, R. Tiedemann, and L. J. Lourens (2008), Persistent summer expansion of the Atlantic Warm Pool during glacial abrupt cold events, Nat. Geosci. 1(9), 601-605, doi:10.1038/ngeo277.

253. Zinke, J., W. Dullo, G. Heiss, and A. Eisenhauer (2004), ENSO and Indian Ocean subtropical dipole variability is recorded in a coral record off southwest Madagascar for the period 1659 to 1995, Earth Planet. Sci. Lett., 228(1), 177-194, doi:10.1016/j.epsl.2004.09.028.

254. Zweng, M.M, J.R. Reagan, J.I. Antonov, R.A. Locarnini, A.V. Mishonov, T.P. Boyer, H.E. Garcia, O.K. Baranova, D.R. Johnson, D.Seidov, M.M. Biddle (2013), World Ocean Atlas 2013, Volume 2: Salinity. S. Levitus, Ed., A. Mishonov Technical Ed.; NOAA Atlas NESDIS 74, 39 pp.